Circuit Theory of Charge Transport in Mesoscopic Conductors

Inauguraldissertation
zur
Erlangung der Würde eines Doktors der Philosophie
vorgelegt der
Philosophisch-Naturwissenschaftlichen Fakultät
der Universität Basel
von

Mihajlo Vanević
aus Belgrad (Serbia)

Basel, 2008.

Genehmigt von der Philosophisch-Naturwissenschaftlichen Fakultät
auf Antrag von

Prof. Dr. Christoph Bruder

Prof. Dr. Wolfgang Belzig

Prof. Dr. Markus Büttiker

Basel, 19. Februar 2008.

Prof. Dr. Hans-Peter Hauri
Dekan

Acknowledgements

First of all, I would like to thank Prof. Wolfgang Belzig and Prof. Christoph Bruder for accepting me as a PhD student and giving me the opportunity to work in the exciting field of full counting statistics. Without persistent interaction with them, the work presented in this Thesis could not have been performed. I am indebted to Wolfgang for introducing me to the field, offering interesting research topics, and discussing the ongoing issues. I am grateful to Christoph for valuable discussions and critical comments which significantly improved my understanding of the subject. I thank both of them for their strong support throughout my PhD studies both in scientific and non-scientific matters. I am also grateful to Prof. Yuli V. Nazarov for giving me the opportunity to spend a month as a visitor in his group at Technical University of Delft. I really enjoyed his professionalism, deep thinking, and sharp comments, which were both enlightening and stimulating to me. I must stress his availability for discussions: we discussed on a daily basis, and each time his comments and remarks were important for further progress. From this collaboration emerged the understanding of elementary events in the voltage-driven mesoscopic junctions (Chapter VII).

The Condensed Matter Theory Group at the University of Basel, headed by Prof. Daniel Loss and Prof. Christoph Bruder, has provided a hard-working but pleasant atmosphere during my stay. I thank to all of the group members. I benefited a lot from the journal clubs and theory seminars in which the first-class results were presented on various topics: spintronics, quantum computation, cold atoms, nanoelectromechanical systems, etc. I also acknowledge many fruitful discussions with the members of the Quantum Transport Group at the University of Konstanz.

I am also grateful to Prof. Christian Schönenberger and his experimental Nano-Electronics group at the University of Basel for organizing Monday morning meetings together with theoreticians. This was an unique opportunity for me to learn about experimental techniques and results and to appreciate the art of device fabrication and modelling.

I would like to express my deepest gratitude to all my physics teachers who developed my interest in physics and guided me in the right direction. I am especially obliged to my first physics teacher Mrs. Vera Radovanović, my high-school teachers Ms. Nataša Čaluković and Prof. Irena Knežević, and the professor of solid state physics and my diploma thesis advisor Prof. Zoran Radović. I also had a privilege to study in Mathematical High School in Belgrade, the unique school specialized in mathematics, physics, and computer science. This school had a crucial impact on my education and development of my scientific attitude.

Separate chapters of this Thesis were proof-read by Dimitrije Stepanenko, Verena Körting, and Björn Trauzettel. I am grateful for the feedback.

I would like to thank Prof. Markus Büttiker for co-refereeing this Thesis and Prof. Daniel Loss for chairing the defense.

Finally, I warmly thank Milica Popović, my parents Milanka and Slobodan, and my brother Dušan for their love and support.

Summary

This Thesis is devoted to the circuit theory of mesoscopic transport. The emphasis is put on its extension which provides a method to obtain the complete statistics of the transferred charge. To accomplish this task, several topics have to be combined: a mathematical description of the charge transfer statistics, the scattering approach to mesoscopic transport, and the nonequilibrium Keldysh-Green's function technique. Although the underlying theory is rather complex, the circuit-theory rules which are obtained at the end are in fact very simple. They resemble Kirchhoff's laws for conventional macroscopic conductors, with currents and voltages replaced by their mesoscopic counterparts. An important difference is that the mesoscopic "currents" and "voltages" acquire matrix structure, and that the "current"-"voltage" relation is in general nonlinear. The matrix structure originates from the Keldysh-Green's function formalism which is needed to account for the many-body quantum state of the electrons in the system. The circuit theory is applicable to multiterminal mesoscopic structures with terminals of different types, e.g., normal metals, superconductors, and ferromagnets. The junctions within the structure can be different also, e.g., transparent quantum point contacts, tunnel barriers, disordered interfaces, diffusive wires, etc.

The Thesis is organized as follows. In Chapter I, we provide introductory information on noise. We discuss early experiments on noise in vacuum tubes and the Schottky result which relates the spectral density of current fluctuations and the average current. We summarize some important results on noise in mesoscopic conductors which can be obtained within circuit theory. Chapters II and III are devoted to theoretical prerequisites needed for the circuit theory. In Chapter II, we define the notion of the cumulant generating function and its relation to statistically independent processes. In Chapter III, we introduce the scattering approach to mesoscopic transport and the method of Keldysh-Green's functions. The circuit theory is presented in Chapter IV focusing on the extension which provides complete information on the charge transfer statistics. The method is illustrated by calculation of the transmission distribution in 2-terminal junctions, and by studying current cross correlations in a superconductor-beam splitter geometry. In Chapters V – VII we apply the general template of the circuit theory and obtain the charge transfer statistics in several physical systems of interest: a cavity coupled to a superconductor and a normal terminal, several junctions in series, and a voltage driven mesoscopic junction. The knowledge of the charge transfer statistics enables us to identify the elementary charge transfer processes in these systems. The conclusion is given in Chapter VIII.

Contents

CHAPTER I

Charge fluctuations in electrical conductors

§ 1. Noise in vacuum tubes

The current $I(t)$ in electrical conductors fluctuates due to the stochastic nature of electron emission and transport. These fluctuations constitute a stochastic process with $I(t)$ being a random variable at each instant of time. An ensemble of identical physical systems prepared in the same macroscopic state at the initial time t_0 will result in different realizations of the current $I(t)$. The quantity measured experimentally is the average value $\langle I(t)\rangle$ where $\langle\cdots\rangle$ denotes statistical averaging. The averaging is present in any measuring device which interacts with the system during a finite measurement time. In the ideal case, the back action of the classical measurement apparatus on the system is negligible. The measurement time should be small with respect to the characteristic time scale on which the statistics of $I(t)$ changes due to the time evolution of the system, but large enough to provide sufficient sampling of $I(t)$. In this case the time averaging during the measurement is the same as the statistical averaging of $I(t)$ over the corresponding probability distribution. This assumption, called the ergodic hypothesis, is inherent in statistical physics [1].

Current fluctuations can be characterized by the correlation function

$$\langle \Delta I(t+\tau)\Delta I(t)\rangle\,, \tag{1.1}$$

where $\Delta I(t) = I(t) - \langle I(t)\rangle$ is the deviation of the current with respect to the average value.[1)] In the stationary state, the average current does not depend on time, while the correlation function depends only on the time difference τ and not on the overall time shift t. In this case the correlation function is an even function of τ: $\langle \Delta I(t+\tau)\Delta I(t)\rangle = \langle \Delta I(t-\tau)\Delta I(t)\rangle$. It is convenient to analyze current fluctuations in the frequency domain, in terms of the Fourier transform $S_I(\nu)$ of the correlation function:

$$\langle \Delta I(t+\tau)\Delta I(t)\rangle = \int_{-\infty}^{\infty} d\nu\; S_I(\nu)\; e^{-i2\pi\nu\tau}. \tag{1.2}$$

The Fourier transform $S_I(\nu)$ is real and even function of frequency, $S_I(\nu) = S_I(-\nu)$. For $\tau = 0$ we obtain

$$\left\langle [\Delta I(t)]^2\right\rangle = \langle I^2\rangle - \langle I\rangle^2 = \int_{-\infty}^{\infty} d\nu\; S_I(\nu) = 2\int_0^{\infty} d\nu\; S_I(\nu). \tag{1.3}$$

Therefore, $S_I(\nu)$ represents the spectral density of current fluctuations at any instant of time. [Equation (1.3) is independent of t.]

[1)] Here we assume that the system is classical. The correlation function for a quantum system is defined as a symmetrized product $(1/2)\langle \Delta\hat{I}(t+\tau)\Delta\hat{I}(t) + \Delta\hat{I}(t)\Delta\hat{I}(t+\tau)\rangle$ where $\hat{I}(t)$ is the current operator and the average is taken with respect to a quantum state.

The first theoretical study of current fluctuations in vacuum tubes was carried out by Schottky in 1918 [2]. The assumption used by Schottky is that the electron transfer events are rare and uncorrelated, in which case the total number of transmitted electrons is distributed according to the Poisson distribution

$$\mathcal{P}(N) = \frac{\langle N\rangle^N}{N!}\, e^{-\langle N\rangle}. \tag{1.4}$$

Schottky found that the spectral density of current fluctuations is independent of frequency in a wide frequency range and is proportional to the unit charge e and the mean electric current $\langle I\rangle$:

$$S_I = |e\langle I\rangle|. \tag{1.5}$$

In this case the current fluctuations at different times are uncorrelated (white noise). The variance of current fluctuations is proportional to the average current and the bandwidth, $\langle I^2\rangle - \langle I\rangle^2 = 2|e\langle I\rangle|\Delta\nu$. Here $\Delta\nu$ includes the positive frequencies only.

An immediate consequence of the Schottky's formula, Eq. (1.5), is the possibility to measure the electron charge by measuring the average current and the dissipated power which is proportional to $\langle I^2\rangle$. This is an altogether different and independent approach than the one used by Millikan in the oil-drop experiment [3]. The first noise measurements in vacuum tubes have been performed by Hartmann in 1921 [4] (see also [5]). In these experiments Hartmann observed the existence of fluctuations and obtained values of e of the right order of magnitude. In an improved setup, Hull and Williams obtained the correct value of e with accuracy of a few percents [6, 7]. Further measurements reduced the error to less than one percent [8, 9].

Already these early experiments showed that the noise in vacuum tubes is affected by the parameters of the system, such as the anode voltage and the frequency of the detection circuit. The agreement with the Schottky theory is achieved only at large enough anode voltages when the anode current saturates. In this case there is no space charge accumulated in the tube. This results in a linear decrease of the potential between the electrodes with all electrons emitted by the cathode being collected at the anode. At lower anode voltages, the space charge piles up in the vicinity of cathode, where the emitted electrons are attracted back by the ionized atoms. As a result, not all emitted electrons reach the anode and the noise is suppressed below the Schottky value.

Concerning the frequency dependence, all experiments which confirmed the result of Schottky have been performed at frequencies above 100kHz [6–9]. In an early experiment by Johnson [5], the frequency has been varied in the range 8Hz – 6kHz. Johnson found a noise result that was modified 0.7 – 100 times with respect to the Schottky value, depending on the frequency and the material of the cathode. In general, as the frequency is decreased, the noise spectral density increases as $S_I \propto 1/\nu^\alpha$ $(0 < \alpha < 2)$ which is known as the flicker or $1/f$ noise [10]. Johnson attributed the effect to irregular temporal changes in the cathode emissivity which cause the emission of electrons to deviate from a strictly random one. At higher frequencies these changes are not effective and the electron emission is random.

§ 2. Thermal noise

In contrast to the noise in vacuum tubes which is proportional to the average current, there exists another type of electrical noise which is present even in conductors in thermal equilibrium with no voltage applied and no current flowing. This noise has been experimentally observed by Johnson [11] and explained theoretically by Nyquist [12] and is called thermal or Johnson-Nyquist noise. The source of this noise is thermal fluctuation of the potential difference across a conductor. Since there is no net charge transfer, these fluctuations have a vanishing mean but non-zero variance. The spectral densities of the thermal current and voltage fluctuations are given by [1]

$$S_I^{\mathrm{eq}}(\nu) = 2G(\nu)\left(\frac{h\nu}{2} + \frac{h\nu}{e^{h\nu/k_BT_e}-1}\right) \tag{2.1a}$$

$$S_V^{\mathrm{eq}}(\nu) = 2R(\nu)\left(\frac{h\nu}{2} + \frac{h\nu}{e^{h\nu/k_BT_e}-1}\right). \tag{2.1b}$$

Here T_e is the temperature of the conductor, $G(\nu) = \mathrm{Re}[1/Z(\nu)]$ is the conductance, $R(\nu) = \mathrm{Re}[Z(\nu)]$ is the resistance, and $Z(\nu)$ is the impedance. At room temperature and frequencies up to a few terahertz, $h|\nu|/k_BT_e \ll 1$, the quantum effects are negligible and the spectrum of thermal fluctuations reduces to

$$S_I^{\mathrm{eq}}(\nu) = 2k_BT_eG(\nu), \qquad S_V^{\mathrm{eq}}(\nu) = 2k_BT_eR(\nu). \tag{2.2}$$

For example, in a conductor which consists of an ohmic resistance R_0 and an inductance L_0 in series, the spectral density of current fluctuations is given by $S_I^{\mathrm{eq}}(\nu) = 2k_BT_eR_0/[R_0^2 + (2\pi L_0\nu)^2]$. From Eq. (1.3) we obtain $L_0\langle I^2\rangle/2 = k_BT_e/2$, i.e., the current fluctuates in such a way that the average energy stored in the system equals the thermal energy quantum. Similarly, for the conductor which consists of an ohmic resistance R_0 and a capacitance C_0 in parallel, voltage fluctuations are given by $C_0\langle V^2\rangle/2 = k_BT_e/2$, which is the average energy stored in the capacitor. From the engineering point of view, identifying the sources of noise and modelling the noise propagation in electronic circuits is important in order to ensure the stability of operation and the quality of the output signal [13]. In practical circuit analysis, it is convenient to model the thermal noise generated in a resistor by replacing the noisy resistor with an ideal noiseless one in series with a noisy voltage source, or, in parallel with a noisy current source (Fig. 1). Ideal capacitors and inductors do

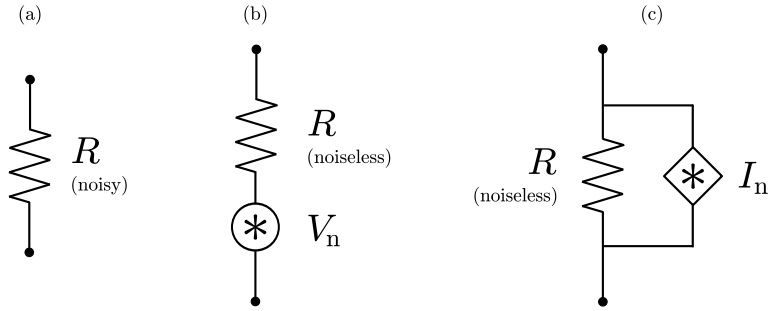

Fig. 1: **Equivalent circuits for thermal noise generated in a resistor.** *A realistic resistor which generates thermal noise (a) can be replaced by an ideal one which is noiseless in series with a noisy voltage source (b) or in parallel with a noisy current source (c). The noise sources have white spectral densities given by* $S_{V_n}^{\mathrm{eq}} = 2k_BT_eR$ *and* $S_{I_n}^{\mathrm{eq}} = 2k_BT_eR^{-1}$. *Noise sources of different resistors in a circuit are uncorrelated.*

not generate thermal noise but do affect the noise propagation through the circuit. Current and voltage fluctuations at the output are calculated assuming that different thermal noise sources are uncorrelated.

The general quantum mechanical theory of thermal fluctuations has been formulated by Callen and Welton [14]. According to this theory, Eqs. (2.1) are just a special case of a much more general relationship between thermal fluctuations of macroscopic quantities and the dissipative response of the system upon the corresponding perturbations. More details on this important result are given in § 25 in the Appendix.

§ 3. Noise in mesoscopic conductors

The advancements in microfabrication technology and experimental techniques over the last two decades opened a new field of research in physics – the field of mesoscopic transport [15, 16]. Mesoscopic conductors are fabricated typically by electrostatic confinement of a 2-dimensional electron gas (2DEG) on a semiconductor chip, with linear dimensions so small that quantum effects are pronounced. The characteristic length scales of these systems are the coherence length l_ϕ, the energy relaxation length $l_{\rm in}$, the elastic mean free path l, the Fermi wavelength λ_F, the atomic Bohr radius a_0, and the sample size L. At low temperatures, typically from 50mK to 4K, these structures enter the mesoscopic regime with the length scales fulfilling

$$a_0 \ll \lambda_F \lesssim l < L < l_\phi \lesssim l_{\rm in}. \tag{3.1}$$

The Fermi wavelength in metals is in the range $\lambda_F = 3 - 10$Å, i.e., of the order of the atomic radius, which makes them difficult to bring into this regime. In the following we briefly describe the most important effects which are visible already in the conductance, and then discuss more recent studies of the current fluctuations in mesoscopic conductors.

The phase coherence of mesoscopic conductors makes the quantum effects pronounced. The most notable effects are the conductance quantization, the Aharonov-Bohm oscillations of conductance, the weak localization correction, and the universal conductance fluctuations. The conductance quantization, first observed experimentally by van Wees *et al.* [17] and Wharam *et al.* [18], is the effect due to strong lateral confinement of the electronic wave functions in a narrow constrictions of the width comparable to the Fermi wavelength. As the width of the constriction is increased, new transversal modes become propagating and the conductance increases in steps of $G_Q = 2e^2/h$ (in spin-degenerate system). The effects of the contact geometry on the accuracy of conductance quantization have been studied theoretically in [19, 20]. The Aharonov-Bohm effect [21] is the interference effect between electronic wave functions traversing two branches of a mesoscopic ring-like structure threaded by a magnetic flux. The phase difference acquired by the electron propagating along the two arms of the ring in the presence of the external vector potential $\boldsymbol{A}$ is given by $\Delta\varphi = \varphi_0 + (e/\hbar)\oint \boldsymbol{A}\cdot d\boldsymbol{l} = \varphi_0 + 2\pi\Phi/\Phi_0$. Here φ_0 is the phase difference in the absence of the field, Φ is the magnetic flux through the ring, and $\Phi_0 = h/e$ is the flux quantum. The transmission probability through the system is given by $T = T_1 + T_2 + 2\sqrt{T_1 T_2}\cos(\varphi_0 + 2\pi\Phi/\Phi_0)$, with $T_{1,2}$ being the transmission probabilities of individual arms which we assumed to be single-channel conductors. Therefore, the conductance oscillates as a function of external flux Φ with period Φ_0. The Aharonov-Bohm oscillations were observed in small metallic rings of diameter

$d \approx 200 - 800$nm and width $W \approx 40$nm by Webb *et al.* [22] and in rings fabricated on semiconductor heterostructures by Timp *et al.* [23].

Weak localization is the effect of enhanced backscattering in coherent disordered conductors due to constructive interference of time-reversed paths [15]. An external magnetic field perpendicular to the sample breaks time reversal symmetry and suppresses weak localization. Therefore, the weak localization manifests itself as decrease of conductance of the order $G_Q = 2e^2/h$ in coherent samples at zero magnetic field. The effect is also visible in the samples of linear dimensions larger than the phase coherence length, $l_\phi < L$. In this case the *conductivity* decreases by $\Delta\sigma = (2e^2/h)l_\phi/W$ for a wire of width $W \ll l_\phi$ and by $\Delta\sigma = (2e^2/\pi h)\ln(l_\phi/l)$ for a 2-dimensional sample. The effect is suppressed by a magnetic field of the order $B_c = h/(el_\phi^2)$ which corresponds to one flux quantum through the largest coherent loop of area l_ϕ^2. For a wire geometry, the magnetic field B_c which destroys the weak localization is larger, $B_c = h/(eWl_\phi)$. For $W \sim 40$nm and $l_\phi \sim 1\mu$m this field is of order $B_c \sim 0.1$T.

Universal conductance fluctuations [24,25] are characteristic to coherent samples, in which case the transmission depends on microscopic positions of scatterers due to interference effects. Different samples of the same geometry inevitably have a different microscopic configuration of scatterers, which causes random conductance fluctuations from one sample to another, with the standard deviation of the order $\Delta G \sim G_Q$ independent of the average conductance $\langle G \rangle$. The effect can be studied experimentally in the same sample by changing the phase shifts by applying a magnetic field or by changing the Fermi wavelength by using gates to modify the electron density. For samples larger than the phase coherence length, the conductance fluctuations are reduced due to uncorrelated contributions of independent phase-coherent parts. The reduction factor for a wire of length L and width W ($W \ll l_\phi \ll L$) is given by $(l_\phi/L)^{3/2}$.

The field of research of current fluctuations in mesoscopic conductors is very broad. The results on noise have been reviewed by Blanter and Büttiker [26, 27]. We also mention previous reviews on noise by de Jong and Beenakker [28] and Reznikov *et al.* [29]. The Keldysh approach to noise in Luttinger liquids and the relation between noise and entanglement are discussed by Martin [30]. The book by Kogan [31] covers a broad range of topics, including noise in superconductors and a thorough discussion of $1/f$ noise. The experimental progress in measuring higher-order current correlations is discussed by Reulet [32]. In the following we present just a small selection of theoretical and experimental results.

The current noise power $S_I(\nu = 0)$ in a coherent mesoscopic junction between two terminals is given by [33–35]

$$S_I = \frac{2e^2}{h} \sum_n \int d\mathcal{E}\ \{T_n[f_1(1-f_1) + f_2(1-f_2)] + T_n(1-T_n)(f_1-f_2)^2\}. \qquad (3.2)$$

Here $f_{1,2}(\mathcal{E})$ are the electron occupation numbers in the terminals and $\{T_n\}$ are the transmission probabilities of the junction. In thermal equilibrium the distributions f_i are given by the Fermi functions $f_i(\mathcal{E}) = [e^{(\mathcal{E}-\mu_i)/k_BT_e} + 1]^{-1}$ with μ_i being the chemical potentials and T_e the electronic temperature. The energy integration in Eq. (3.2) can be performed explicitly if the transmission probabilities T_n do not depend on energy in the energy range set by the applied voltage and temperature.

After integration, the current noise power reduces to

$$S_I = \frac{2e^2}{h} \sum_n \left\{ T_n \, 2k_B T_e + T_n(1-T_n) \, \left[eV \coth\left(\frac{eV}{2k_B T_e}\right) - 2k_B T_e \right] \right\}, \qquad (3.3)$$

where V is the bias voltage ($\mu_2 = \mu_1 + eV$). At high temperatures, $k_B T_e \gg eV$, thermal fluctuations are the dominant source of noise and S_I reduces to the Johnson-Nyquist expressions given by Eq. (2.2). At temperatures much smaller then the applied bias, $k_B T_e \ll eV$, thermal fluctuations of electron occupation numbers in the leads give a negligible contribution with respect to the noise generated by the partitioning of the incoming stream of electrons at the junction. The noise in this case is due to the stochastic nature of the charge *transport* (shot noise). The shot noise power is given by

$$S_I^{\text{shot}} = \frac{2e^2}{h} |eV| \sum_n T_n(1-T_n). \qquad (3.4)$$

This result, obtained by Büttiker [33], is the multi-channel generalization of the single-channel formulas of Khlus [36], Lesovik [37], and Yurke and Kochanski [38].

A convenient way to quantify the shot noise in the system is to compare it to the noise of the rare and uncorrelated electron transfers given by the Schottky formula, Eq. (1.5). The ratio of the two is called Fano factor [39] and is given by

$$F = \frac{S_I^{\text{shot}}}{|e\langle I\rangle|} = \frac{\sum_n T_n(1-T_n)}{\sum_n T_n}. \qquad (3.5)$$

Therefore, the noise is suppressed with respect to the Schottky value, which reflects the way the electron stream is partitioned at the contact. For a tunnel junction with low transmission probabilities $T_n \ll 1$ in all channels, the noise coincides with the Schottky value, $F = 1$. For a completely open contact, $T_n = 1$, all emitted electrons are transferred. In this case both emission and transport are noiseless which results in $F = 0$. The noise suppression in quantum point contacts has been studied experimentally in [40–42]. At intermediate junction transparencies, the suppression of the shot noise depends on the distribution of transmission channels. This information is beyond reach of the conductance measurements which reveal the average transmission only.

In some cases transport properties of coherent conductors are universal, i.e., do not depend on details like the geometry of the sample or the microscopic distribution of impurities [43–45]. Examples include diffusive conductors and chaotic cavities with a large number of transport channels. The transmission distributions in these cases can be obtained using random matrix theory [46].

The transmission distribution of diffusive wires has been obtained by Dorokhov [47, 48] and Mello and Pichard [49]. Using this distribution, a $F = 1/3$ suppression of the noise has been predicted in the coherent case [50]. Interestingly, the same suppression is obtained in incoherent diffusive wires [51] shorter than the electron-electron and electron-phonon scattering lengths, $l_\phi \ll L \ll l_{ee}, l_{e-\text{ph}}$, using the semiclassical Boltzmann-Langevin approach [52, 53]. This suppression occurs also in arrays of many tunnel junctions in series [52], and in arrays of many chaotic cavities connected with arbitrary contacts [54]. However, the enhanced value $F = \sqrt{3}/4$ has been found in wires longer than the electron-electron scattering length but shorter than the electron-phonon length, $l_{ee} \ll L \ll l_{e-\text{ph}}$ [55–57]. This result is also universal, i.e., it is valid not only for quasi one-dimensional diffusive wires but for arbitrary

geometries, as shown by Sukhorukov and Loss [44,45]. The difference between these two regimes can be understood by considering the electronic distribution function $f(\mathcal{E},x)$ at a distance x from the left lead along the wire. For $L \ll l_{e-\mathrm{ph}}$ the electrons exhibit only elastic scattering at impurities or energy-conserving electron-electron collisions. Therefore, the total energy of electronic subsystem *within the wire* is conserved. The distribution $f(\mathcal{E},x)$ has to fulfill the current and the energy conservation conditions, $I_1 + I_2 = 0$ and $I_{Q1} + I_{Q2} = 0$, with the charge and the heat currents given by

$$eI_1 = \int_0^\infty d\mathcal{E}\; G_1(f_1 - f), \qquad eI_2 = \int_0^\infty d\mathcal{E}\; G_2(f - f_2), \tag{3.6}$$

and

$$e^2 I_{Q1} = \int_0^\infty d\mathcal{E}\; \mathcal{E}\; G_1(f_1 - f), \qquad e^2 I_{Q2} = \int_0^\infty d\mathcal{E}\; \mathcal{E}\; G_2(f - f_2). \tag{3.7}$$

Here $f_i(\mathcal{E}) = [e^{(\mathcal{E}-\mu_i)/k_BT_e} + 1]^{-1}$ are the Fermi distributions in the leads, the bias voltage V is taken into account by the shift of the chemical potential $\mu_2 = \mu_1 + eV$, $G_{1,2}$ are the conductances of the junction left and right from the point x, and T_e is the electronic temperature in the leads equal to the lattice temperature. For $L \ll l_{ee}, l_{e-\mathrm{ph}}$, the total energy of each injected electron is conserved within the wire. Therefore, the current and energy conservations hold for each energy slice, which gives

$$f(\mathcal{E},x) = \frac{G_1 f_1(\mathcal{E}) + G_2 f_2(\mathcal{E})}{G_1 + G_2}. \tag{3.8}$$

Taking into account that $G_1 \propto 1/x$ and $G_2 \propto 1/(L-x)$ we obtain $f(x) = f_1 + (x/L)(f_2 - f_1)$. The distribution $f(\mathcal{E})$ is a nonequilibrium one, with two steps at $\mathcal{E} = \mu_1$ and $\mathcal{E} = \mu_2$. On the other hand, for $l_{ee} \ll L \ll l_{e-\mathrm{ph}}$ the electrons which traverse the wire exhibit many electron-electron collisions which thermalize the electron subsystem. Now the distribution $f(\mathcal{E},x)$ is given by the Fermi distribution with effective chemical potential $\mu(x)$ and the effective electronic temperature $T_e^*(x)$ which characterize the local equilibrium. From the current conservation we obtain

$$\mu(x) = \frac{G_1\mu_1 + G_2\mu_2}{G_1 + G_2}, \tag{3.9}$$

i.e., $\mu(x) = \mu_1 + (x/L)eV$. The energy conservation gives[2)]

$$[k_BT_e^*(x)]^2 = (k_BT_e)^2 + \frac{3}{\pi^2}\frac{G_1G_2}{(G_1+G_2)^2}(eV)^2, \tag{3.10}$$

i.e., $k_BT_e^*(x) = [(k_BT_e)^2 + (3/\pi^2)(eV)^2x(L-x)/L^2]^{1/2}$. Therefore, the effective electronic temperature is larger than the lattice temperature. This is the so-called "hot electron" regime. Since the electronic subsystem is in local equilibrium, we can apply the model of noisy resistors described in § 2 to calculate the total noise. We divide the wire into a large number N of resistors with resistance $R_1 = R/N$, where R is the total resistance. Each resistor contains a fluctuating voltage source V_i in series, with the spectral density given by $S_{V_i} = 2k_BT_{ei}^*R_1$. The total current through the system is given by $I = (V_1 + \cdots + V_N)/R$. Taking into account that thermal fluctuations of voltages at different resistors are independent, we find $S_I = (S_{V_1} + \cdots + S_{V_N})/R^2 = (2k_B/R)(T_{e1}^* + \cdots + T_{eN}^*)/N$. In the continuous limit we

[2)] The integration in Eq. (3.7) can be performed using the Sommerfeld asymptotic expansion $\int_0^\infty dz\; g(z)/(e^{z-\alpha}+1) \approx \int_0^\alpha g(z)dz + (\pi^2/6)g'(\alpha) + (7\pi^4/360)g'''(\alpha) + \cdots$, which is valid for $\alpha \gg 1$ (see §58 in Ref. [1]).

obtain $S_I = (2/R)L^{-1}\int_0^L k_B T_e^*(x)dx$. At low lattice temperature in the leads, the first term in Eq. (3.10) can be neglected and we find $S_I = (\sqrt{3}/4)|e\langle I\rangle|$. Therefore, the noise in the hot electron regime is due to thermal voltage fluctuations across the wire. Unlike the usual thermal noise which is current-independent, in this case thermal noise does depend on the current because of voltage dependence of the effective temperature induced by heating.

The suppression of noise in diffusive wires has been studied experimentally by several authors [58–60]. The value $F = 1/3$ has been found in short wires and a value close to $F = \sqrt{3}/4$ in long ones, in agreement with theoretical predictions. In diffusive wires of length much larger than the electron-phonon scattering length, $L \gg l_{e-\mathrm{ph}}$, the shot noise vanishes[3)] as $S_I^{\mathrm{shot}}/|e\langle I\rangle| \propto l_{e-\mathrm{ph}}/L$ [50,56,57,61,62]. This happens because the electrons are thermalized by phonons to the lattice temperature T_e. Therefore, macroscopic conductors exhibit current-independent thermal noise and no shot noise. The shot noise as a function of the wire length is schematically shown in Fig. 2.

The sample-to-sample fluctuations of the shot noise power in coherent diffusive wires have been studied by de Jong and Beenakker [63]. These noise fluctuations are also universal, i.e., independent of the length and geometry of the conductor. The weak localization correction of the average noise power was also obtained. Both the average shot noise power and the sample-to-sample fluctuations vanish for a conductor much larger than the electron-phonon scattering length.

The transmission distribution in a chaotic cavity coupled to the leads by quantum point contacts supporting the same number of transport channels, $N_1 = N_2 \gg 1$, has been obtained by Baranger and Mello [64] and Jalabert *et al.* [65]. The transmission distribution in the more general case of asymmetric coupling $N_1 \neq N_2$ has been obtained by Nazarov [66] (see also [46]). Using this distribution, the suppression of shot noise $F = N_1N_2/(N_1+N_2)^2$ is obtained. For the symmetric coupling $N_1 = N_2$ the suppression is $F = 1/4$. The same suppression has been obtained by Blanter and Sukhorukov [67] using the semiclassical theory with no phase coherence. The analysis of Ref. [67] also shows how the universality of chaotic transport is broken as the openings of the contacts are increased, in which case direct transmission from one contact to another becomes possible.

In the following we outline the derivation of the noise suppression in a chaotic cavity using the discrete circuit representation of the system. This is a simple example of the circuit theory of mesoscopic transport, which is discussed in more detail in Chapter IV. The electronic distribution function $f(\mathcal{E})$ inside the cavity does not depend on position and direction of propagation due to the chaotic dynamics which provides good isotropization. In the absence of electron-electron and electron-phonon scattering, the distribution $f(\mathcal{E})$ is the nonequilibrium one given by Eq. (3.8) with $G_{1,2} = (2e^2/h)N_{1,2}$ being the conductances of the contacts. Since the cavity is an additional electron reservoir, the fluctuations at different contacts are independent. Therefore, the current noise power through the system is given by $R^2S_I = R_1^2S_{I_1} + R_2^2S_{I_2}$, where $R = R_1 + R_2$ and R_i and S_{I_i} are the resistances and current noise powers of individual contacts. From Eq. (3.2) we obtain $S_{I_i} = [G_i/(G_1+G_2)]|e\langle I\rangle|$ at $T_e = 0$ in the reservoirs. The total current noise power is given by $S_I = F|e\langle I\rangle|$ with the Fano factor $F = G_1G_2/(G_1+G_2)^2 = N_1N_2/(N_1+N_2)^2$. The effect of electron heating in

[3)] Reference [57] predicts a different dependence $S_I^{\mathrm{shot}}/|e\langle I\rangle| \propto L^{-2/5}$.

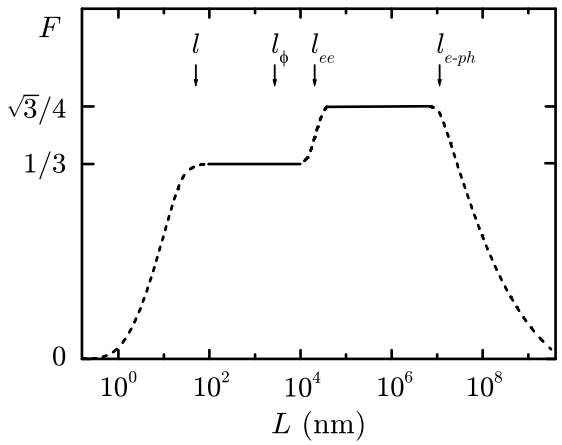

Fig. 2: **Shot noise power suppression in a diffusive wire as a function of length.** *(The figure is adapted from Ref. [59].) The orders of magnitude of the length scales l, l_ϕ, l_{ee}, and $l_{e-\mathrm{ph}}$ are indicated by arrows. Shot noise is present both in coherent and in incoherent conductors smaller than the electron-phonon scattering length. Macroscopic conductors larger than the electron-phonon scattering length do not exhibit shot noise. Solid lines represent theoretical predictions and dashed lines are the interpolations expected in the crossover regions. For $l_\phi \ll L \ll l_{ee}$, the electronic subsystem in the wire is out of equilibrium with the two-step distribution function given by Eq.* (3.8)*. For $l_{ee} \ll L \ll l_{e-\mathrm{ph}}$ the electrons in the wire are in local equilibrium characterized by the Fermi distribution function with the local chemical potential and the local effective temperature given by Eqs.* (3.9) *and* (3.10)*. Notice that the effective temperature depends on the applied bias and is increased with respect to the lattice temperature. This is the so-called "hot electron" regime.*

the cavity ($l_{ee} \ll L \ll l_{e-\mathrm{ph}}$) can be analyzed similarly. Electron-electron interactions bring the electrons in the cavity in local thermal equilibrium. In this case the distribution $f(\mathcal{E})$ in the cavity is a Fermi function with the chemical potential μ and the effective temperature T_e^* given by Eqs. (3.9) and (3.10). From Eq. (3.2) we obtain the current noise powers at contacts $S_{I_i} = G_i k_B T_e^*$, at $T_e = 0$ in the reservoirs. Using that the fluctuations at the contacts are independent, we obtain the total current noise power $S_I = F|e\langle I\rangle|$ with the Fano factor $F = (\sqrt{3}/\pi)\sqrt{N_1 N_2}/(N_1 + N_2)$ which is increased with respect to the noninteracting case [28]. For a symmetric cavity $F \approx 0.276$ which corresponds to an increase of about 10%, much smaller than the heating-induced increase in diffusive wires (about 30%, see Fig. 2).

Shot noise in chaotic cavities has been studied experimentally by Oberholzer *et al.* [68] for different sizes of cavities and openings of the contacts. The results for smaller cavities with large contact openings show no electron heating because the dwell time is smaller than the electron-electron collision time. However, electron heating becomes important in larger cavities with smaller contact openings, in agreement with theoretical predictions. The shot noise of several cavities in series has been studied both theoretically and experimentally in [69]. The results are in agreement with the semiclassical model which takes into account the "cavity noise" and show clear deviations from the one-dimensional model of scattering in the chain of barriers with no cavities present [52]. The difference is that the electron which enters the cavity can exhibit the next scattering event at either cavity contact due

to randomization of the direction of propagation. On the other hand, in the absence of the cavity, the next scattering event happens at the adjacent barrier in chain. Although both models give the same suppression $F = 1/3$ in the limit of large chains, they differ for the chains of finite size. Recently, the transmission distribution of an array of cavities is series has been obtained quantum mechanically [54]. The noise suppression using this distribution coincides with the result of [69].

The transmission distribution of a strongly disordered interface with impurities arranged at a length scale comparable or smaller than the Fermi wavelength, $L \lesssim \lambda_F$, has been obtained by Schep and Bauer [70]. This distribution results in a noise suppression given by $F = 1/2$. Interestingly, the same distribution is obtained in the case of two tunnel junctions in series [52, 71].

Shot noise can be used to study the crossover from stochastic to deterministic transport. Stochastic transport occurs, e.g., in a cavity with an electron dwell time larger than the Ehrenfest time needed for the wave packet to spread over the cavity [72–74]. In this case the Fano factor is given by Eq. (3.5). If the electron dwell time is much smaller than the Ehrenfest time, then the wave packet stays localized and the electrons are transferred as classical particles. The classical particle is either transmitted or reflected with unit probability and the Fano factor vanishes. The crossover from stochastic to deterministic transport in a cavity has been studied experimentally by Oberholzer *et al.* [75]. The electron dwell time is varied by changing the openings of the contacts. As the dwell time is decreased, the Fano factor is suppressed below the value $F = 1/4$ for the stochastic transport in a symmetric cavity. The stochastic-to-deterministic crossover in the charge transfer statistics has been studied theoretically in [76].

An interesting application of the shot noise is the observation of fractional charges $e^* = e/3$ and $e^* = e/5$ in experiments in the quantum Hall regime [77–79], see also [29]. These experiments confirmed that the current is carried by quasiparticles of fractional charge, in agreement with theoretical predictions of Lauglin [80] and Kane and Fisher [81].

Another example in which shot noise is used to identify the effective charge involved in elementary transport processes is in normal-metal/superconductor junctions. In this case the charges are transferred in pairs at subgap temperatures and bias voltages due to the Andreev process [82]. Since there are no quasiparticle states in the superconductor at energies below the gap, the electron which is incident from the normal metal couples with another one below the Fermi level and both enter the superconductor as a Cooper pair, with the hole being reflected in the normal metal (Andreev reflection). The scattering approach has been extended to take into account superconducting terminals in [83] and the shot noise has been obtained in [84] (see also [46]). At low temperatures and bias voltages much smaller than the superconducting gap ($k_B T_e \ll eV \ll |\Delta|$) the conductance and the shot noise power of the normal-metal/superconductor junction are given by

$$G = \frac{4e^2}{h} \sum_n R_n^A, \tag{3.11}$$

and

$$S_I^{\rm shot} = \frac{8|e^3 V|}{h} \sum_n R_n^A (1 - R_n^A), \tag{3.12}$$

where $R_n^A = T_n^2/(2-T_n)^2$ is the coefficient of the Andreev reflection in the nth transport channel. The Fano factor in this case is given by

$$F = \frac{S_I^{\rm shot}}{|e\langle I\rangle|} = \frac{2\sum_n R_n^A(1-R_n^A)}{\sum_n R_n^A}. \tag{3.13}$$

Equation (3.12) is the multichannel extension of the single channel result of Khlus [36]. For the completely open junction $T_n = 1$, all incident electrons are Andreev reflected ($R_n^A = 1$) and the conductance is doubled with respect to the normal state case. However, the transport is noiseless and the Fano factor vanishes. In the tunnel limit, at low Andreev reflection probabilities $R_n^A \ll 1$, the charge transfer events are rare but the shot noise is doubled with respect to the Poisson value. This is a signature of the doubled effective charge involved in elementary transport events. At intermediate transparencies, the shot noise power is related to the distribution of transmission eigenvalues of the junction. We emphasize that Eqs. (3.11) and (3.12) hold for the coherent junction. Using the distributions of transmission eigenchannels $\rho(T)$ of a diffusive wire, chaotic cavity, and strongly disordered interface, we can calculate the conductances and the Fano factors in the case in which one lead is superconducting. The results are summarized in a table given below.

	$\rho(T)/\tilde{G}_N$	G_{NS}/G_N	F_N	F_S
diffusive wire	$\frac{1}{2T\sqrt{1-T}}$	1	1/3	2/3
chaotic cavity	$\frac{2}{\pi\sqrt{T(1-T)}}$	$2(2-\sqrt{2}) \approx 1.17$	1/4	$(1+\sqrt{2})/4 \approx 0.604$
disordered interface	$\frac{1}{\pi T^{3/2}\sqrt{1-T}}$	$1/\sqrt{2}$	1/2	3/4

Here G_N (G_{NS}) and F_N (F_{NS}) refer to the normal (superconducting) state and $\tilde{G}_N = G_N/G_Q$. The values for the chaotic cavity are given for the case of symmetric coupling to the leads. The results for disordered interface coincide with the ones for a double tunnel junction. We observe that the changes in conductance and Fano factor due to the presence of a superconducting lead are not generic, with the twofold increase achieved only in special cases. The conductance of a diffusive wire in contact with a superconductor is the same as in the normal state, whereas for the cavity it is slightly enhanced and for the disordered interface it is decreased with respect to the normal state value. On the other hand, the Fano factors are increased with respect to the normal-state case. A twofold increase is obtained for a diffusive wire, while for the disordered interface the increase is by a factor of 1.5. The Fano factor of a cavity in contact with a superconductor is more than two times larger than in the normal state ($F_S/F_N \approx 2.4$).

The doubling of shot noise in a diffusive normal metal/ superconductor junction has been experimentally observed in [85,86]. The results are in excellent agreement with the semiclassical theory of noise in the incoherent regime [87] at voltages both below and above the gap. The noise in a coherent diffusive normal metal/ superconductor junction with a tunnel barrier at the interface has been measured in [88] for bias voltages both below and above the gap. The noise above the gap is Poissonian and below the gap is doubled, which is the signature of the charge doubling in the crossover from the normal to the Andreev transport. More recently, noise measurements have been performed in a cavity coupled to a superconducting lead

with relatively high transparency of the contacts [89]. The measured Fano factor is more than two times larger than in the normal state, in agreement with theoretical predictions.

The effects of phase coherence on the conductance in diffusive normal metal/superconductor junctions have been studied theoretically by Nazarov and Stoof [90]. The effects of coherence on noise and higher-order current correlators have been studied by Belzig and Nazarov [91] and Samuelsson *et al.* [92]. The result is that all transport properties exhibit reentrant behavior: they are the same in the completely coherent ($L \ll \xi_N$) and the completely incoherent ($L \gg \xi_N$) regime. Here $\xi_N = \sqrt{\hbar D/\max(k_B T_e, |eV|)}$ is the length scale on which the proximity-induced superconducting correlations between the electrons in diffusive normal metal survive and $D = v_F l/3$ is the diffusion constant. However, in the intermediate regime $L \sim \xi_N$ the coherence does affect the transport: both the conductance and noise are increased by about 10%. The effect in a chaotic cavity coupled to a superconductor has been studied in [93].

So far we have discussed noise in normal and superconducting mesoscopic junctions with a dc voltage applied. An ac voltage drive couples electron states of different energies which results in so-called photon-assisted effects visible in noise and higher even-order current correlators. The effect is not present in the conductance in the linear regime with transmission probabilities independent of energy. The first theoretical study of photon-assisted noise in a quantum point contact with both dc and ac voltages applied was done by Lesovik and Levitov [94]. The shot noise power is a piecewise linear function of the dc voltage bias with kinks which correspond to integer multiples of the driving frequency and slopes which depend on the shape of the ac voltage component. The scattering theory of photon-assisted noise has been developed by Pedersen and Büttiker [95]. An interpretation of the noise and current cross-correlations in terms of excited electron-hole pairs has been given by Rychkov *et al.* [96] for the case of an ac drive of low amplitude $|eV_0| \ll \hbar\omega$, where ω is the driving frequency. In this case at most one electron-hole pair can be created per period. The elementary transport events in the full range of driving voltages have been identified in [97] and are discussed in detail in Chapter VII. Photon-assisted noise has been observed experimentally in normal coherent conductors [42, 98] and in diffusive normal metal – superconductor junctions [99].

We conclude this paragraph by a brief account of experimental progress in measuring higher-order current correlators. For example, the zero-frequency component of the third-order current correlator $\langle \Delta I(t+\tau_1+\tau_2)\Delta I(t+\tau_1)\Delta I(t)\rangle_{\omega_1=\omega_2=0}$ is proportional to the third moment $\langle(\Delta N)^3\rangle$ of the number of charges N transmitted within the measurement time t_0. In the voltage-biased normal-state junction the third moment is given by $\langle(\Delta N)^3\rangle = (2t_0/h)eV\sum_n T_n(1-T_n)$ for $|eV| \ll k_B T_e$, and by $\langle(\Delta N)^3\rangle = (2t_0/h)[6k_B T_e \sum_n T_n^2(1-T_n) + eV\sum_n T_n(1-T_n)(1-2T_n)]$ for $|eV| \gg k_B T_e$. Therefore, unlike the noise which is at high temperatures dominated by Johnson-Nyquist noise, the thermal fluctuations do not contribute to the third-order current correlator at high temperatures. The third-order current correlator is proportional to the current and carries information on the distribution of transmission channels both at temperatures much lower and much higher than the bias. Low bias measurements are preferable because the junction is in the linear regime and the effects of electron heating are decreased. On the other hand, low bias gives a low output signal. Also, accurate measurements of the higher-order current correlators

are increasingly more difficult. The first measurement of the third-order current correlator in a tunnel junction was done by Reulet *et al.* [100], see also [32]. In this experiment the junction was neither in the voltage- nor in the current-bias regime with results deviating from the ideal theoretical model due to fluctuations induced in the environment [101–103]. In a more recent experiment [104] the environmental effects are suppressed with the results being in agreement with the Poisson statistics of rare electron transport across the tunnel junction, $\langle(\Delta N)^3\rangle = \langle N\rangle$.

CHAPTER II

Elements of probability theory

In this chapter we define the characteristic and cumulant generating functions for a set of random variables in terms of the joint probability distribution and review their basic properties. The concept of cumulant generating function is particularly important because in many cases it can be obtained much easier and more directly than the characteristic function or the probability distribution. The reason for this lies in the fact that independent random variables give additive contributions to the joint cumulant generating function. Therefore, the analysis of composite processes reduces to the analysis of independent elementary ones, which is, in general, a much simpler task. We illustrate this approach in § 6 by constructing the binomial and Pascal distributions starting from the elementary processes. To make a better connection with the rest of the Thesis, we do this using the toy-model of electron transport across a scatterer, although any other stochastic process (like, e.g., tossing a coin) could serve the purpose equally well. In § 7 and § 8 we illustrate how the analysis of elementary events can be used to obtain multiparticle and multiterminal transfer statistics.

In some situations it may be difficult to recognize what are the independent elementary processes, while it may still be possible to obtain the generating function for the composite process. In this case the elementary processes can be identified from the decomposition of the total generating function, which often provides additional physical understanding. In § 9 we illustrate this situation by studying the statistics of the total number of particles in the ideal classical and quantum gases in thermal equilibrium.

§ 4. Moments and cumulants

Let $x_1, \ldots, x_n$ be real and continuous random variables characterized by the joint probability density function $f(x_1, \ldots, x_n)$. An alternative way to characterize the set of random variables is to use the characteristic function which is defined by

$$\begin{aligned} \phi(\chi_1, \ldots, \chi_n) &= \left\langle e^{\sum_{\alpha=1}^{n} i\chi_\alpha x_\alpha} \right\rangle \\ &\equiv \int dx_1 \cdots dx_n \; f(x_1, \ldots, x_n) \; e^{\sum_{\alpha=1}^{n} i\chi_\alpha x_\alpha}. \end{aligned} \tag{4.1}$$

The normalization of the probability distribution implies $\phi(\chi = 0) = 1$. If the characteristic function is known, the probability density can be obtained by the inverse Fourier transformation

$$f(x_1, \ldots, x_n) = \int \frac{d\chi_1}{2\pi} \cdots \frac{d\chi_n}{2\pi} \; \phi(\chi_1, \ldots, \chi_n) \; e^{-\sum_{\alpha=1}^{n} i\chi_\alpha x_\alpha}. \tag{4.2}$$

A more direct insight into the properties of the probability distribution can be gained through the moments $\mathcal{M}_{\alpha_1 \ldots \alpha_m}$ of the distribution, which are defined as the averages

$$\mathcal{M}_{\alpha_1 \ldots \alpha_m} = \langle x_{\alpha_1} \cdots x_{\alpha_m} \rangle \,. \tag{4.3}$$

Here the indices α_k assume values from the set $\{1, \ldots, n\}$ and can be mutually equal. The different moments can be obtained by taking the derivatives of the characteristic function:

$$\mathcal{M}_{\alpha_1 \ldots \alpha_m} = \left[\partial_{i\chi_{\alpha_1}} \cdots \partial_{i\chi_{\alpha_m}} \, \phi(\chi_1, \ldots, \chi_n)\right]_{\chi=0} . \tag{4.4}$$

The expression for the characteristic function in terms of the moments is obtained by the series expansion of Eq. (4.1):

$$\phi(\chi_1, \ldots, \chi_n) = 1 + \sum_{m=1}^{\infty} \frac{i^m}{m!} \sum_{\alpha_1, \ldots, \alpha_m = 1}^{n} \mathcal{M}_{\alpha_1 \ldots \alpha_m} \, \chi_{\alpha_1} \cdots \chi_{\alpha_m}. \tag{4.5}$$

Equation (4.5) implicitly assumes that the real numbers $\mathcal{M}_{\alpha_1 \ldots \alpha_m}$ constitute moments of a well-defined probability measure and that such measure is unique. The question under what conditions a set of real numbers constitutes moments of a probability measure is known as *the moment problem*. It turns out that, in general, the probability measure *is not determined uniquely* by its moments. In § 26 we summarize the results on existence and uniqueness of probability measure and provide further references on the subject.

Another useful characterization of the probability distribution is by the cumulant generating function $\mathcal{S}(\chi_1, \ldots, \chi_n)$ which is defined by $\mathcal{S} = \ln \phi$, i.e.,

$$e^{\mathcal{S}(\chi_1, \ldots, \chi_n)} = \left\langle e^{\sum_{\alpha=1}^{n} i\chi_\alpha x_\alpha} \right\rangle . \tag{4.6}$$

The normalization of the probability distribution implies $\mathcal{S}(\chi = 0) = 0$. If the cumulant generating function is known, the probability density can be obtained from Eq. (4.2). The cumulants $\mathcal{C}_{\alpha_1 \ldots \alpha_m}$ are defined as derivatives of $\mathcal{S}$:

$$\mathcal{C}_{\alpha_1 \ldots \alpha_m} = \left[\partial_{i\chi_{\alpha_1}} \cdots \partial_{i\chi_{\alpha_m}} \mathcal{S}(\chi_1, \ldots, \chi_n)\right]_{\chi=0} . \tag{4.7}$$

If the cumulants are known, then $\mathcal{S}$ is given by the series expansion

$$\mathcal{S}(\chi_1, \ldots, \chi_n) = \sum_{m=1}^{\infty} \frac{i^m}{m!} \sum_{\alpha_1, \ldots, \alpha_m = 1}^{n} \mathcal{C}_{\alpha_1 \ldots \alpha_m} \, \chi_{\alpha_1} \cdots \chi_{\alpha_m}. \tag{4.8}$$

Similarly as before, here we assume that the set of cumulants $\mathcal{C}_{\alpha_1 \ldots \alpha_m}$ corresponds to a well-defined and unique probability measure.

An important property of the cumulants is that $\mathcal{C}_{\alpha_1 \ldots \alpha_m} = 0$ if the set of different random variables $x_{\alpha_1}, \ldots, x_{\alpha_m}$ can be split into two statistically independent subsets. For example, let us assume that the subsets $x_{\alpha_1}, \ldots, x_{\alpha_k}$ and $x_{\alpha_{k+1}}, \ldots, x_{\alpha_m}$ are statistically independent for some k ($1 \leq k \leq m-1$). In this case the joint probability density and the characteristic function factorize,

$$f(x_{\alpha_1}, \ldots, x_{\alpha_m}) = f(x_{\alpha_1}, \ldots, x_{\alpha_k}) \, f(x_{\alpha_{k+1}}, \ldots, x_{\alpha_m}) \tag{4.9}$$

and

$$\phi(\chi_{\alpha_1}, \ldots, \chi_{\alpha_m}) = \phi(\chi_{\alpha_1}, \ldots, \chi_{\alpha_k}) \, \phi(\chi_{\alpha_{k+1}}, \ldots, \chi_{\alpha_m}), \tag{4.10}$$

while the cumulant generating function is the sum

$$\mathcal{S}(\chi_{\alpha_1}, \ldots, \chi_{\alpha_m}) = \mathcal{S}(\chi_{\alpha_1}, \ldots, \chi_{\alpha_k}) + \mathcal{S}(\chi_{\alpha_{k+1}}, \ldots, \chi_{\alpha_m}). \tag{4.11}$$

From Eqs. (4.7) and (4.11) we obtain $\mathcal{C}_{\alpha_1 \ldots \alpha_m} = 0$. If all variables $x_{\alpha_1}, \ldots, x_{\alpha_m}$ are independent, the probability density and the characteristic function factorize completely, and the cumulant generating function is the sum of the contributions of the individual variables.

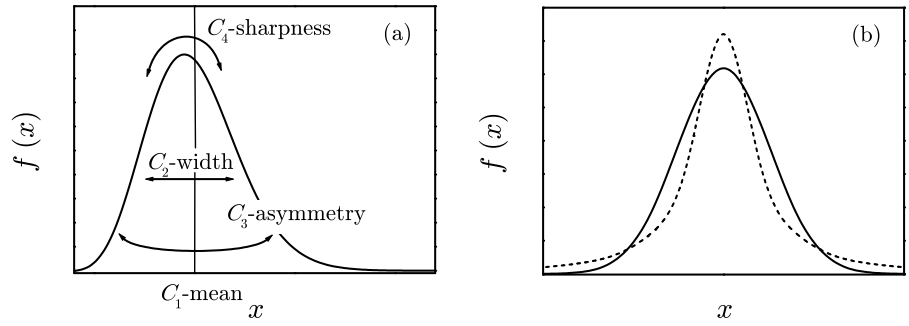

Fig. 3: *The interpretation of the first four cumulants [panel (a)]: The first cumulant is equal to the mean of the probability distribution. The second cumulant is equal to the variance and characterizes the width of distribution. The third cumulant is related to the asymmetry of distribution and is positive (negative) when the long tail is at large (small) values [$\mathcal{C}_3 > 0$ for the case shown in panel (a)]. For symmetric distributions $\mathcal{C}_3 = 0$ [panel (b)]. The fourth cumulant is related to the sharpness of distribution, parametrized by the kurtosis excess $\gamma_2 = \mathcal{C}_4/\mathcal{C}_2^2$. The normal distribution has zero excess, $\gamma_2 = 0$. A positive excess signifies that the distribution of a continuous random variable is more peaked at the center and has fatter tails [dashed curve in panel (b)] with respect to the normal distribution with the same mean and variance [solid curve in panel (b)].*

In the following we focus on a single random variable x. From Eqs. (4.5) and (4.8) we obtain relations which express the higher-order cumulants $\mathcal{C}_n = [\partial_{i\chi}^n \mathcal{S}(\chi)]_{\chi=0}$ in terms of central moments:

$$\begin{aligned} \mathcal{C}_1 &= \langle x \rangle \,, \\ \mathcal{C}_2 &= \mathcal{M}'_2, \\ \mathcal{C}_3 &= \mathcal{M}'_3, \\ \mathcal{C}_4 &= \mathcal{M}'_4 - 3\mathcal{M}'^2_2, \\ \mathcal{C}_5 &= \mathcal{M}'_5 - 10\mathcal{M}'_2\mathcal{M}'_3, \end{aligned} \tag{4.12}$$

where $\mathcal{M}'_n = \langle (x - \langle x \rangle)^n \rangle$. The interpretation of the first four cumulants is depicted in Fig. 3. The first cumulant is equal to the mean value of the probability distribution. The second cumulant is equal to the variance and characterizes the width of the distribution, i.e., the dispersion of the random variable. The third cumulant is related to the so-called skewness, $\gamma_1 = \mathcal{C}_3/\mathcal{C}_2^{3/2}$, which measures the asymmetry of the probability distribution. It is positive (negative) when the long tail of distribution is at large (small) values, and vanishes for probability distributions which are symmetric around the mean value. The fourth cumulant is related to the kurtosis excess defined by $\gamma_2 = \mathcal{C}_4/\mathcal{C}_2^2$. The kurtosis excess vanishes for the normal distribution. For distributions with the same mean and variance, a positive kurtosis excess signifies that the distribution is more peaked at the center and has fatter tails [dashed curve in Fig. 3(b)].

The above definitions are given for continuous random variables. For the case of discrete random variables all formulas remain the same, with the joint probability

density given by

$$f(x_1,\ldots,x_n)=\sum_{N_1,\ldots,N_n}\mathcal{P}(N_1,\ldots,N_n)\;\delta(x_1-N_1)\cdots\delta(x_n-N_n). \tag{4.13}$$

Here $\mathcal{P}(N_1,\ldots,N_n)$ is the joint probability distribution and the summations are performed over the discrete values N_α of the corresponding variables. From Eq. (4.1) we obtain the characteristic function for a set of discrete random variables

$$\phi(\chi_1,\ldots,\chi_n)=\sum_{N_1,\ldots,N_n}\mathcal{P}(N_1,\ldots,N_n)\;e^{\sum_{\alpha=1}^{n}i\chi_\alpha N_\alpha}, \tag{4.14}$$

and similar for the cumulant generating function $\mathcal{S}$. In the applications we encounter in this Thesis, the random variables x_α represent the number of charges which enter the terminal α of a mesoscopic sample within the measurement time. Therefore, N_α are discrete and can assume positive or negative integer values only. In this case ϕ and $\mathcal{S}$ are 2π-periodic functions of the arguments, and the joint probability distribution is given by

$$\mathcal{P}(N_1,\ldots,N_n)=\int_{-\pi}^{\pi}\frac{d\chi_1}{2\pi}\cdots\frac{d\chi_n}{2\pi}\;e^{\mathcal{S}(\chi_1,\ldots,\chi_n)}e^{-\sum_{\alpha=1}^{n}i\chi_\alpha N_\alpha}. \tag{4.15}$$

§ 5. Functions of random variables. Central limit theorem

Let us consider a random variable $y=g(x_1,\ldots,x_n)$ which is a function of the set of random variables $x_1,\ldots,x_n$ with the joint probability density $f(x_1,\ldots,x_n)$. The probability density $f(y)$ for the variable y can be obtained from the requirement that the averages $\langle h(y)\rangle_{f(y)}$ with respect to y and $\langle h[g(x_1,\ldots,x_n)]\rangle_{f(x_1,\ldots,x_n)}$ with respect to $(x_1,\ldots,x_n)$ coincide for an arbitrary function h. From this requirement we obtain

$$f(y)=\int dx_1\cdots dx_n\;f(x_1,\ldots,x_n)\;\delta[y-g(x_1,\ldots,x_n)]. \tag{5.1}$$

In the case of a single random variable x, the above formula reduces to

$$f(y)=\int dx\;f(x)\;\delta[y-g(x)]=\sum_i\frac{1}{|g'(x_i)|}f(x_i), \tag{5.2}$$

where the summation goes over all simple roots x_i of $g(x)=y$.

A particulary important example is the special case $y=x_1+\cdots+x_n$ in which the cumulant generating function $\mathcal{S}(\chi)$ of y is simply related to the cumulant generating function $\mathcal{S}(\chi_1,\ldots,\chi_n)$ of $(x_1,\ldots,x_n)$. By choosing $h(y)=e^{i\chi y}$ we obtain

$$e^{\mathcal{S}(\chi)}=\left\langle e^{i\chi y}\right\rangle_{f(y)}=\left\langle e^{i\chi(x_1+\cdots+x_n)}\right\rangle_{f(x_1,\ldots,x_n)}=e^{\mathcal{S}(\chi_1=\chi,\ldots,\chi_n=\chi)}. \tag{5.3}$$

Therefore, the cumulant generating function for a sum of random variables is obtained by putting all counting fields χ_α equal:

$$\mathcal{S}(\chi)=\mathcal{S}(\chi_1=\chi,\ldots,\chi_n=\chi). \tag{5.4}$$

In the special case of independent random variables x_α with probability densities $f_\alpha(x_\alpha)$ and generating functions $\mathcal{S}_\alpha(\chi_\alpha)$, Eq. (5.4) reduces to the sum of contributions of individual variables

$$\mathcal{S}(\chi)=\mathcal{S}_1(\chi)+\cdots+\mathcal{S}_n(\chi). \tag{5.5}$$

In this case the higher-order cumulants are also additive. From Eq. (5.1) we obtain that the probability density of y is the convolution of the densities of individual variables,

$$f(y) = \int dx_1 \cdots dx_{n-1}\; f_1(x_1) \cdots f_{n-1}(x_{n-1}) f_n(x_n), \tag{5.6}$$

where $x_n = y - x_1 - \cdots - x_{n-1}$. For discrete random variables $N = N_1 + \cdots + N_n$ the similar expression holds in terms of probability distributions,

$$\mathcal{P}(N) = \sum_{N_1,\ldots,N_{n-1}} \mathcal{P}_1(N_1) \cdots \mathcal{P}_{n-1}(N_{n-1}) \mathcal{P}_n(N_n), \tag{5.7}$$

with $N_n = N - N_1 - \cdots - N_{n-1}$.

The central limit theorem states that an important universal limit is reached for a sum of a large number of independent variables. Here we formulate the theorem for equally distributed variables, while in the more general form the theorem holds also for random variables which may have different distributions. Let $\{x_\alpha\}$ be a sequence of equally distributed independent random variables with finite mean $m = \langle x_\alpha \rangle$ and dispersion $\sigma = \sqrt{\langle (x_\alpha - m)^2 \rangle}$. Let $y_n = x_1 + \cdots + x_n$ denote the n-th partial sum of the random variables x_α. The central limit theorem states that the random variable $z_n = (y_n - nm)/(\sigma\sqrt{n})$ is asymptotically normal for $n \to \infty$, with the probability density $f(z) = 1/\sqrt{2\pi}\; e^{-z^2/2}$. To prove the theorem we calculate the characteristic function $\phi(\chi)$ which corresponds to $f(z_n)$ for large n. Using that x_α are independent and equally distributed we obtain

$$\begin{aligned} \phi(\chi) &= \lim_{n\to\infty} \left\langle e^{\sum_{\alpha=1}^n i\chi(x_\alpha - m)/\sigma\sqrt{n}} \right\rangle = \lim_{n\to\infty} \left\langle e^{i\chi(x_1-m)/\sigma\sqrt{n}} \right\rangle^n \\ &= \lim_{n\to\infty} [1 - \chi^2/2n + o(1/n)]^n = e^{-\chi^2/2}, \end{aligned} \tag{5.8}$$

which is the characteristic function of the normal distribution.

§ 6. Basic probability distributions

In this paragraph we study a single discrete random variable and review the basic probability distributions such as binomial, Poisson, and Pascal. To introduce these distributions we consider a mesoscopic system depicted in Fig. 4 which consists of the electron source at the left lead and the barrier of transmission T in the central region. The source emits uncorrelated electrons, each having the same probability T to be transmitted to the right. The probability distribution of the total number of electrons N which enter the right lead is binomial and given by

$$\mathcal{P}(N) = \binom{M}{N} T^N (1-T)^{M-N} \tag{6.1}$$

for $N = 0, \ldots, M$ and $\mathcal{P}(N) = 0$ otherwise. Here M is the number of emitted electrons within the measurement time and $\binom{M}{N} = M!/[N!(M-N)!]$ is the number of ways to choose N electrons which are transmitted among M emitted. The corresponding cumulant generating function $\mathcal{S}(\chi)$ is defined by $e^{\mathcal{S}(\chi)} = \langle e^{i\chi N} \rangle$. After taking the average by using Eq. (6.1) we obtain

$$\mathcal{S}(\chi) = M \ln[1 + T(e^{i\chi} - 1)]. \tag{6.2}$$

The first four cumulants $\mathcal{C}_n = [\partial_{i\chi}^n \mathcal{S}(\chi)]_{\chi=0}$ of the binomial distribution are given by

$$\mathcal{C}_1 = M\,T, \qquad\qquad \mathcal{C}_2 = M\,T(1-T),$$

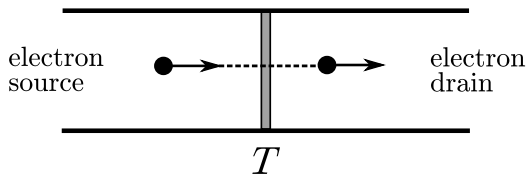

Fig. 4: *A simple model of electron transport. The electron source at the left lead emits uncorrelated electrons. At constant voltage bias, the total number of emitted electrons within the measurement time is fixed. The electrons are independently transmitted to the drain with probability T. The statistics of the number N of transmitted electrons is binomial. For a large number of emitted electrons and rare transfer events $T \ll 1$, the statistics of N is Poissonian.*

$$\mathcal{C}_3 = M\,T(1-T)(1-2T), \qquad \mathcal{C}_4 = M\,T(1-T)[1-6T(1-T)]. \tag{6.3}$$

Now let us consider the limit of low transparency $T \ll 1$ and a large number of emitted electrons $M \gg 1$, such that the product MT stays finite. In this case the cumulant generating function reduces to

$$\mathcal{S}(\chi) = \langle N\rangle(e^{i\chi}-1), \tag{6.4}$$

which corresponds to the Poisson probability distribution

$$\mathcal{P}(N) = \frac{\langle N\rangle^N}{N!}\, e^{-\langle N\rangle} \tag{6.5}$$

with $\langle N\rangle = MT$ and $N = 0, 1, 2, \ldots$. The Poisson distribution describes the process of rare uncorrelated electron transfer events. From Eq. (6.4) follows that all cumulants of the Poisson distribution are the same and equal to the average value, $\mathcal{C}_n = \langle N\rangle$.

It is instructive to approach the problem on the level of elementary transfer processes. The total number of transmitted electrons is given by $N = N_1 + \cdots + N_M$, where $N_\alpha = 0, 1$ is the number of electrons transmitted in a single attempt. Since the attempts are uncorrelated, the random variables N_α are independent and the total cumulant generating function is the sum of contributions of different attempts [see Eq. (5.5)]. Because all attempts are equivalent, we have $\mathcal{S}(\chi) = M\mathcal{S}_1(\chi)$. The cumulant generating function $\mathcal{S}_1$ for a single attempt is given by $e^{\mathcal{S}_1(\chi)} = \left\langle e^{i\chi N_1}\right\rangle = Te^{i\chi 1} + (1-T)e^{i\chi 0} = 1 + T(e^{i\chi}-1)$, and we recover Eq. (6.2). The elementary processes could be inferred from Eq. (6.2) immediately, by noting that $\mathcal{S}(\chi)$ is the sum of M well-defined generating functions. This illustrates an important point: If we know the cumulant generating function for the whole process, then we can identify the underlying elementary processes by decomposing it into a sum of simpler generating functions. The constitutive generating functions may differ since the elementary processes do not have to be equivalent, in general.

The central limit theorem applied to the decomposition $N = N_1 + \cdots + N_M$ states that the binomial and Poisson probability distributions given by Eqs. (6.1) and (6.5) approach the normal distribution for a large number of attempts M. More precisely, for the random variable N with binomial distribution, the random variable z defined by $z = (N - MT)/\sqrt{MT(1-T)}$ is asymptotically normal for large M such that $MT, M(1-T) \gg 1$. Similarly, the random variable $z = (N - \langle N\rangle)/\sqrt{\langle N\rangle}$ is asymptotically normal for large $\langle N\rangle$, where N is a random variable with Poisson distribution.

In the previous examples we considered the case of an electron source at the left lead with a positive number of electrons N transferred from left to right. For the case of a 'hole source' in the left lead, the electrons are transferred in opposite direction, which corresponds to $N < 0$. The cumulant generating functions for this case are given by Eqs. (6.2) and (6.4) with $e^{i\chi}$ replaced by $e^{-i\chi}$. Therefore, the sign of χ is related to direction of charge transfer.

So far we have discussed the case in which the number of attempts M is constant, and the number of transmitted electrons N fluctuates. Physically, this corresponds to the voltage-biased junction with $M = eVt_0/\pi$, where e is the electron charge, V is the bias voltage, and t_0 is the preset measurement time. The transmitted charge is, of course, related to the current. The higher-order cumulants of charge transferred can be obtained by measuring higher-order correlations of current fluctuations.

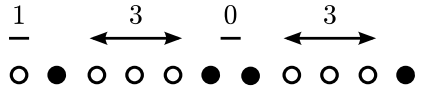

Fig. 5: *Decomposition of the number of attempts M needed to transfer N electrons into a series of attempts needed to transfer the single one. Open (filled) dots represent reflection (transmission) events. The numbers indicate reflection events between two successive transmissions. The statistics of M is Pascal.*

In the case of current bias, the situation is the opposite: the current is kept constant and the voltage fluctuates. In a simple model this corresponds to a constat number of electrons N transmitted within the measurement time and a fluctuating number of attempts M needed. The probability distribution $\mathcal{P}(M)$ can be obtained by considering elementary processes which consist of a series of attempts needed to transfer a single electron. Let the random variables M'_α denote the numbers of reflections between successive transmissions of $\alpha - 1$ and α electrons, as shown in Fig. 5. For N electrons transmitted, the total number of reflections is given by $M' = M'_1 + \cdots M'_N$, with the total number of attempts $M = M' + N$. The random variables M'_α are independent and equally distributed with $\mathcal{P}(M'_\alpha) = R^{M'_\alpha}T$, which describes M'_α successive reflections and transmission in the next attempt. The cumulant generating function for M' is given by

$$\mathcal{S}'(\chi) = N \ln \left\langle e^{i\chi M'_1} \right\rangle = N \ln \left(\frac{T}{1 - Re^{i\chi}} \right). \tag{6.6}$$

The corresponding probability distribution is called the Pascal (or negative binomial, waiting time) distribution and reads

$$\mathcal{P}(M') = \binom{M' + N - 1}{N - 1} T^N R^{M'} \tag{6.7}$$

for $M' \geq 0$ and $\mathcal{P}(M') = 0$ otherwise. The distribution of the total number of attempts M ($M \geq N$) is given by

$$\mathcal{P}(M) = \binom{M - 1}{N - 1} T^N R^{M-N}. \tag{6.8}$$

In this Thesis we focus on current fluctuations in the voltage-biased junction. For a discussion of voltage fluctuations in a current-biased junction we refer to [101–103].

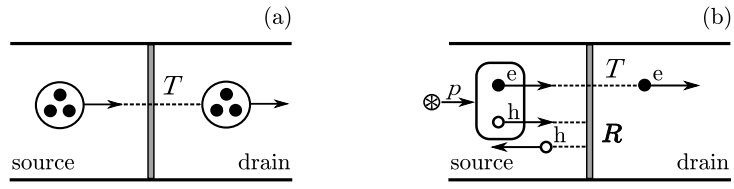

Fig. 6: *Panel (a): Unidirectional multiparticle transfer processes. Charges are transmitted in groups of n with probability T. The signature of n-particle unidirectional transport is $2\pi/n$ periodicity of the cumulant generating function, or the ratio $\mathcal{C}_2/\mathcal{C}_1 = n$ in the limit of rare transfer events ($T \ll 1$). Panel (b): A bidirectional 2-particle transfer process. Electron-hole pairs are created by an external perturbation with probability p and move towards the scatterer. Charge transport occurs if one particle is transmitted and the other is reflected. For $p = 1$ the electrons and holes contribute separately and the statistics of the transmitted charges is of single-particle type. For intermediate p, the statistics can not be decomposed into independent contributions of electrons and holes.*

§ 7. Multiparticle transfer processes

Let us consider the charge transfer process which consists of M attempts, such that in each attempt a cluster of m particles can be transmitted with probability p_m ($\sum_{m=-\infty}^{\infty} p_m = 1$). Depending on the sign of m, transfer can occur in either direction. The cumulant generating function $\mathcal{S}_1$ for a single attempt is given by $e^{\mathcal{S}_1(\chi)} = \langle e^{i\chi m}\rangle = \sum_m p_m e^{im\chi}$. For M attempts we obtain

$$\mathcal{S}(\chi) = M \ln\left(\sum_{m=-\infty}^{\infty} p_m\, e^{im\chi}\right). \tag{7.1}$$

In the following we analyze two important special cases of Eq. (7.1).

Let us consider the case depicted in Fig. 6(a), in which only n-particle transfers occur, $p_m = T\delta_{mn}$. In this case Eq. (7.1) reduces to

$$\mathcal{S}(\chi) = M \ln[1 + T(e^{in\chi} - 1)]. \tag{7.2}$$

The corresponding probability distribution is given by

$$\mathcal{P}(N) = \binom{M}{k} T^k (1-T)^{M-k} \tag{7.3}$$

for $N = kn$ ($k = 0, \ldots, M$) and $\mathcal{P}(N) = 0$ otherwise. As expected, the particles are transferred in multiples of n, with a binomial distribution of the number k of transmitted clusters. The signature of *unidirectional* n-particle transfers is the $2\pi/n$ periodicity of the cumulant generating function. The higher-order cumulants of N are given by

$$\begin{aligned} &\mathcal{C}_1 = nM\,T, && \mathcal{C}_2 = n^2 M\,T(1-T),\\ &\mathcal{C}_3 = n^3 M\,T(1-T)(1-2T), && \mathcal{C}_4 = n^4 M\,T(1-T)[1-6T(1-T)]. \end{aligned} \tag{7.4}$$

Therefore, the existence of unidirectional n-particle processes can also be inferred from the ratio $\mathcal{C}_2/\mathcal{C}_1 = n$ in the limit $T \ll 1$ of rare transport events. Unidirectional two-particle charge transfers occur in relatively transparent superconductor-normal metal junctions at subgap voltages and low temperatures. In this case the mechanism of charge transport is given by the Andreev process: an electron in the normal metal couples with another one of the opposite spin, and both enter the superconductor as a Cooper pair.

In the following we consider a different situation depicted in Fig. 6(b) in which charges are transferred in both directions. Due to an external time-dependent drive, electron-hole (e–h) pairs are created in the left lead with probability p. The total number of attempts for e–h pair creation during the measurement time is denoted by M. We assume that both particles move towards the scatterer and are transmitted (reflected) independently from each other with probability T ($R = 1 - T$). We are interested in the statistics of the number of transmitted charges N to the right within the measurement time. As before, the analysis can be reduced to independent attempts, in which $m = 1, 0, -1$ charges can be transferred. In the course of an attempt, the charge $m = \pm 1$ is transferred with probability $p_{\pm 1} = pTR$, which corresponds to e–h pair generation, electron (hole) transmission and the hole (electron) reflection. On the other hand, no charges are transferred ($m = 0$) either if the e–h pair is not created, or, if the pair is created and both particles are transmitted. This happens with probability $p_0 = (1 - p) + p(T^2 + R^2)$. Therefore, the cumulant generating function given by Eq. (7.1) reduces to

$$\mathcal{S}(\chi) = M \ln[1 + pTR(e^{i\chi} + e^{-i\chi} - 2)]. \tag{7.5}$$

Since electrons and holes are transmitted with equal probabilities, the average transmitted charge and all odd-order cumulants vanish, $\mathcal{C}_{2n+1} = 0$. However, the signatures of charge fluctuations caused by bidirectional transport can be seen in the even-order cumulants, with the lowest two given by

$$\mathcal{C}_2 = 2M\ pTR, \qquad \mathcal{C}_4 = 2M\ pTR(1 - 6pTR). \tag{7.6}$$

For $p = 1$, e–h pairs are always created and the cumulant generating function decomposes into independent contributions of electrons and holes, $\mathcal{S}_1(\chi) = \ln[1 + T(e^{i\chi} - 1)] + \ln[1 + T(e^{-i\chi} - 1)]$. This corresponds to independent binomial electron and hole transmission events. Similarly, for $pTR \ll 1$ the charge transfer events are rare and we have $\mathcal{S}_1(\chi) \approx pTR(e^{i\chi} - 1) + pTR(e^{-i\chi} - 1)$. The statistics is again decomposed into single-particle electron and hole transfers. For intermediate values of pTR, the elementary processes are of two-particle type and cannot be split into separate electron and hole contributions.

The probability distribution for the total charge transferred can be obtained from Eqs. (4.15) and (7.5):

$$\begin{aligned}
\mathcal{P}(N) &= \int_{-\pi}^{\pi} \frac{d\chi}{2\pi}\ \left[1 + \gamma(e^{i\chi/2} - e^{-i\chi/2})^2\right]^M e^{-i\chi N} \\
&= \int_{-\pi}^{\pi} \frac{d\chi}{2\pi}\ \sum_{n=0}^{M} \binom{M}{n} \gamma^n (e^{i\chi/2} - e^{-i\chi/2})^{2n}\ e^{-i\chi N} \\
&= \sum_{n=0}^{M} \sum_{m=0}^{2n} \binom{M}{n} \binom{2n}{m} (-1)^m \gamma^n \delta_{n-m,N}.
\end{aligned} \tag{7.7}$$

Here we assume that the number of attempts M is integer and introduce $\gamma \equiv pTR$ ($0 \le \gamma \le 1/4$) for brevity. For $|N| > M$ the probability $\mathcal{P}(N)$ vanishes, while for $|N| \le M$ we have

$$\mathcal{P}(N) = (-1)^N \sum_{n=|N|}^{M} \binom{M}{n} \binom{2n}{n - N} (-\gamma)^n. \tag{7.8}$$

This sum can be expressed in terms of the hypergeometric function ${}_2F_1$ [105], and we obtain

$$\mathcal{P}(N) = \binom{M}{|N|} \gamma^{|N|}\, {}_2F_1\left(\frac{2|N|+1}{2}, |N|-M, 2|N|+1, 4\gamma\right) \tag{7.9}$$

for $|N| = 0, \ldots, M$ and $\mathcal{P}(N) = 0$ otherwise. For noninteger M, the summation over n in Eq. (7.7) goes to infinity, and we find

$$\begin{aligned}\mathcal{P}(N) =& \frac{\Gamma(M+1)}{|N|!\,\Gamma(M+1-|N|)}\,\frac{\sin(M\pi)}{\sin[(M-|N|)\pi]}(-\gamma)^{|N|} \\ &\times {}_2F_1\left(\frac{2|N|+1}{2}, |N|-M, 2|N|+1, 4\gamma\right)\end{aligned} \tag{7.10}$$

for $|N| \le M$ and $\mathcal{P}(N) = 0$ otherwise. As already discussed, the probability distribution $\mathcal{P}(N)$ is symmetric with respect to $N = 0$ and has vanishing odd-order cumulants. The kurtosis excess of $\mathcal{P}(N)$ is positive for $0 < pTR < 1/6$ and negative for $1/6 < pTR < 1/4$ [Eq. (7.6)]. Bidirectional processes of this type are created by time-dependent bias voltage, with probabilities which depend on the shape of the driving (Chapter VII).

§ 8. Multiterminal geometry

In the following we study the system depicted in Fig. 7, in which e–h pairs are created with probability p and are directed towards the scatterer which has transmission probability T. After traversing the scatterer, particles enter one of the leads with probability $\tilde{g}_{1,2}$ without reflection ($\tilde{g}_1 + \tilde{g}_2 = 1$). We are interested in the statistics of transmitted charge in the terminals within the measurement time. The total number of attempts for the e–h pair creation is M.

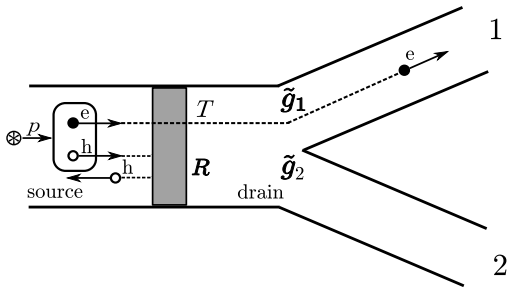

Fig. 7: *An example of a multiterminal geometry. The e–h pair is created with probability p and directed towards the scatterer of transmission T. After traversing the scatterer, particles enter the outgoing terminals 1 or 2 with probabilities $\tilde{g}_{1,2}$, without reflection ($\tilde{g}_1 + \tilde{g}_2 = 1$).*

Let (N_1', N_2') denote the charge transmitted into the corresponding terminals in a single attempt. The possible outcomes and their probabilities are listed in the following table:

N_1'	N_2'	$\mathcal{P}(N_1', N_2')$
0	0	$(1-p) + pR^2 + pT^2(\tilde{g}_1^2 + \tilde{g}_2^2)$
± 1	0	$pTR\tilde{g}_1$
0	± 1	$pTR\tilde{g}_2$
± 1	∓ 1	$pT^2\tilde{g}_1\tilde{g}_2$

For example, no charge is transferred into the terminals if the pair is not created in the first place (probability $1-p$), or, if the pair is created and both particles are reflected (probability pR^2), or, if the pair is created and both particles are transmitted into the same outgoing terminal [probability $pT^2(\tilde{g}_1^2+\tilde{g}_2^2)$]. Similarly, $\mathcal{P}(+1,-1) = pT^2\tilde{g}_1\tilde{g}_2$ describes the creation of the e–h pair (probability p), and transmission of both particles with the electron entering lead 1 and the hole entering lead 2 (probability $T^2\tilde{g}_1\tilde{g}_2$). The cumulant generating function $\mathcal{S}'(\chi_1,\chi_2)$ for the single attempt is given by

$$e^{\mathcal{S}'(\chi_1,\chi_2)} = \langle e^{i\chi_1 N_1'} e^{i\chi_2 N_2'}\rangle = \sum_{N_1',N_2'} \mathcal{P}(N_1',N_2')\; e^{i\chi_1 N_1'} e^{i\chi_2 N_2'}. \tag{8.1}$$

Using the probabilities $\mathcal{P}(N_1',N_2')$ given in the table, we obtain

$$\begin{aligned}\mathcal{S}'(\chi_1,\chi_2) = \ln[&1-p+pR^2+pT^2(\tilde{g}_1^2+\tilde{g}_2^2)\\ &+pTR\tilde{g}_1(e^{i\chi_1}+e^{-i\chi_1})+pTR\tilde{g}_2(e^{i\chi_2}+e^{-i\chi_2})\\ &+pT^2\tilde{g}_1\tilde{g}_2(e^{i\chi_1}e^{-i\chi_2}+e^{-i\chi_1}e^{i\chi_2})].\end{aligned} \tag{8.2}$$

Here we note that the electron (hole) transfers are described by terms in which the counting field χ enters with positive (negative) sign. The cumulant generating function for the transmitted charge (N_1,N_2) after M attempts is given by $\mathcal{S}(\chi_1,\chi_2) = M\mathcal{S}'(\chi_1,\chi_2)$. The cumulant generating function for the total charge $N=N_1+N_2$ which enters any of the two terminals is given by $\mathcal{S}(\chi)=\mathcal{S}(\chi,\chi)$ [see Eq. (5.4)] and we recover Eq. (7.5) for the two-terminal case.

§ 9. Example: Particle number statistics in equilibrium

In the following we provide yet another illustration of the mathematical concepts introduced in the previous paragraphs. We obtain the statistics of equilibrium particle number fluctuations in ideal classical and quantum gases described by the grand canonical ensemble. For the classical Boltzmann and quantum Fermi gas, the statistics can be readily interpreted in terms of elementary single-particle exchange processes with the reservoir. On the other hand, in the case of the Bose gas multiparticle exchange processes occur.

Let us consider a quantum system of constant volume V being part of the larger system at temperature T_e which serves as the heat and particle reservoir. The system is described by a Hamiltonian $\hat{H}$ which conserves the number of particles, $[\hat{H},\hat{N}]=0$. The state of the system is given by the grand canonical ensemble $\hat{\rho} = e^{\beta\Omega_{\rm td}}\, e^{-\beta(\hat{H}-\mu\hat{N})}$, where $\Omega_{\rm td}(\mu,T_e,V) = -T_e \ln {\rm Tr}(e^{-\beta(\hat{H}-\mu\hat{N})})$ is the grand thermodynamic potential. The number of particles N in the system fluctuates due to exchange of particles with the reservoir. It is easy to verify that the higher-order moments of the particle number are given by

$$\langle \hat{N}^n\rangle = e^{\beta\Omega_{\rm td}(\mu)}\, \frac{\partial^n}{\partial(i\chi)^n}\Big|_{\chi=0}\, e^{-\beta\Omega_{\rm td}(\mu+i\chi T_e)}. \tag{9.1}$$

From Eq. (4.4) we obtain that the cumulant generating function of the particle number statistics is given by the thermodynamic potential

$$\mathcal{S}(\chi) = -\beta\Omega_{\rm td}(\mu+i\chi T_e) + \beta\Omega_{\rm td}(\mu). \tag{9.2}$$

The last term in Eq. (9.2) ensures the normalization $\mathcal{S}(\chi=0)=0$ of the particle number distribution and has no effect on the higher-order cumulants of the particle

number statistics. Equation (9.2) is valid also for a classical system in the grand canonical ensemble.

In the following we obtain the particle number statistics of the ideal classical and quantum gases in equilibrium. The grand thermodynamic potential of the classical Boltzmann gas is given by $\Omega_{\rm td}^{(cl)} = -T_e e^{\beta\mu} V/\lambda_{T_e}^3$ [106], where $\lambda_{T_e} = \sqrt{2\pi\hbar^2/mk_BT_e}$ is the thermal wavelength. The average number of particles in the system is $\langle N\rangle = -(\partial\Omega_{\rm td}/\partial\mu)_{T_e,V} = e^{\beta\mu}V/\lambda_{T_e}^3$. From Eq. (9.2) we obtain $\mathcal{S}^{(cl)}(\chi) = \langle N\rangle(e^{i\chi}-1)$. Therefore, the particle number statistics of the classical gas in thermal equilibrium is Poissoninan, with the probability distribution $\mathcal{P}^{(cl)}(N) = \langle N\rangle^N e^{-\langle N\rangle}/N!$ (see § 6). All cumulants of the particle number are the same and equal to the average value, $\mathcal{C}_1^{(cl)} = \mathcal{C}_2^{(cl)} = \cdots = \langle N\rangle$. To obtain a physical interpretation of this result we rewrite $\mathcal{S}^{(cl)}(\chi) = \sum_{\boldsymbol{p}} \langle n_{\boldsymbol{p}}\rangle(e^{i\chi}-1)$, where the momentum $\boldsymbol{p}$ labels single-particle states of energy $\mathcal{E}_{\boldsymbol{p}} = \boldsymbol{p}^2/2m$ and $\langle n_{\boldsymbol{p}}\rangle = e^{-\beta(\mathcal{E}_{\boldsymbol{p}}-\mu)}$ are the average occupation numbers. This decomposition shows that the statistics of the total number of particles $N = \sum_{\boldsymbol{p}} n_{\boldsymbol{p}}$ consists of the independent population of the single-particle levels via one-particle transfers from the reservoir. The statistics of the population of the single-particle levels is also Poissonian.

Now we consider quantum systems. The grand thermodynamic potential of the ideal quantum gas is given by

$$\Omega_{\rm td}^{(B,F)} = \pm T_e \sum_{\boldsymbol{p}} \ln(1 \mp e^{-\beta(\mathcal{E}_{\boldsymbol{p}}-\mu)}), \tag{9.3}$$

where the upper and lower signs correspond to bosons and fermions, respectively.[4)] From Eq. (9.2) we obtain

$$\mathcal{S}^{(B,F)}(\chi) = \mp \sum_{\boldsymbol{p}} \ln[1 \mp n_{\boldsymbol{p}}^{\mp}(e^{i\chi}-1)], \tag{9.4}$$

with $n_{\boldsymbol{p}}^{\mp} = [e^{\beta(\mathcal{E}_{\boldsymbol{p}}-\mu)} \mp 1]^{-1}$ being the corresponding average occupation numbers. Equation (9.4) can be readily interpreted in terms of elementary processes. For the Fermi gas, the population of the single-particle levels follows from $\mathcal{S}_{\boldsymbol{p}}^{(F)}(\chi) = \ln[1+n_{\boldsymbol{p}}^{+}(e^{i\chi}-1)]$. Therefore, the single-particle states can accommodate maximally one electron and are occupied with probabilities $n_{\boldsymbol{p}}^{+}$, independently from each other. The particle transfers between the system and the reservoir are of the single-particle type. For the Bose gas, the population of single-particle levels follows from $\mathcal{S}_{\boldsymbol{p}}^{(B)}(\chi) = -\ln[1-n_{\boldsymbol{p}}^{-}(e^{i\chi}-1)] = \ln[r_{\boldsymbol{p}}/(1-t_{\boldsymbol{p}}e^{i\chi})]$, where $t_{\boldsymbol{p}} = e^{-\beta(\mathcal{E}_{\boldsymbol{p}}-\mu)}$ and $r_{\boldsymbol{p}} = 1-t_{\boldsymbol{p}}$. Like before, the single-particle levels are populated independently, but now can accommodate any number of particles, $n_{\boldsymbol{p}} \geq 0$. The statistics of occupation numbers is negative binomial and is given by $\mathcal{P}(n_{\boldsymbol{p}}) = t_{\boldsymbol{p}}^{n_{\boldsymbol{p}}} r_{\boldsymbol{p}}$ [c.f. with Eqs. (6.6) and (6.7)]. We can rewrite $\mathcal{S}_{\boldsymbol{p}}^{(B)}$ in the form $\mathcal{S}_{\boldsymbol{p}}^{(B)}(\chi) = \ln(r_{\boldsymbol{p}} + t_{\boldsymbol{p}}r_{\boldsymbol{p}}e^{i\chi} + t_{\boldsymbol{p}}^2 r_{\boldsymbol{p}}e^{2i\chi} + t_{\boldsymbol{p}}^3 r_{\boldsymbol{p}}e^{3i\chi} + \cdots)$. This shows that the level is occupied through a single multiparticle transfer process from the reservoir (§ 7). Bosons emitted from the reservoir bunch into the level as long as they are absorbed (with $t_{\boldsymbol{p}}$ being the probability of absorption). The bunching process stops when the next boson is reflected.

The statistics of the total number of particles can be obtained by performing the summations over the single-particle states in Eqs. (9.3) and (9.4). For the grand thermodynamic potential we obtain $\Omega_{\rm td}^{(B,F)} = -(T_eV/\lambda_{T_e}^3)G_{5/2}^{\pm}(e^{\beta\mu})$, where $G_s^{\pm}(z) =$

[4)] For simplicity we neglect the spin degeneracy.

$\sum_{n=1}^{\infty}(\pm 1)^{n+1}z^n/n^s$ is the polylogarithm function. The average particle number in the system is $\langle N\rangle = (V/\lambda_{T_e}^3)G_{3/2}^{\pm}(e^{\beta\mu})$. The cumulant generating function is given by

$$\mathcal{S}^{(B,F)}(\chi) = \frac{V}{\lambda_{T_e}^3}\left[G_{5/2}^{\pm}(e^{\beta\mu+i\chi}) - G_{5/2}^{\pm}(e^{\beta\mu})\right]. \tag{9.5}$$

For high temperatures ($e^{\beta\mu} \ll 1$) all results approach the classical limit. At low temperatures at which the thermal wavelength becomes comparable to the average interparticle distance, quantum correlations due to the Bose and Fermi nature of the particles become important, and the total particle number statistics is no longer Poissonian. For example, the second cumulant is given by $\mathcal{C}_2^{(B,F)} = (V/\lambda_{T_e}^3)G_{1/2}^{\pm}(e^{\beta\mu}) \approx \langle N\rangle[1 \pm (1/2\sqrt{2})\lambda_{T_e}^3\langle N\rangle/V]$, where the expansion in the last step holds for small quantum corrections $\lambda_{T_e}^3 \ll V/\langle N\rangle$. For the same average number of particles, the equilibrium fluctuations satisfy $\mathcal{C}_2^{(F)} < \mathcal{C}_2^{(cl)} < \mathcal{C}_2^{(B)}$.[5] The total probability distribution function $\mathcal{P}(N)$ can be obtained from Eq. (4.15).

The cumulant generating function for the Bose gas can be rewritten as $\mathcal{S}^{(B)}(\chi) = \sum_{n=1}^{\infty}\mathcal{S}_n^{(B)}(\chi)$, where $\mathcal{S}_n^{(B)}(\chi) = M_n(e^{in\chi}-1)$ and $M_n = e^{n\beta\mu}V/n^{5/2}\lambda_{T_e}^3$. Each term $\mathcal{S}_n^{(B)}(\chi)$ corresponds to an n-particle transfer process with the probability distribution function given by

$$\mathcal{P}_n(N) = \begin{cases} M_n^k e^{-M_n}/k!, & \text{for } N = kn,\ k = 0,1,\ldots \\ 0, & \text{otherwise,} \end{cases} \tag{9.6}$$

and the mean value $\langle N\rangle_n = nM_n$. Therefore, the equilibrium particle number fluctuations in the ideal Bose gas consist of independent Poisson n-particle transfer processes between the system and environment. These processes include simultaneous many-particle transfers to different single-particle states. The total particle number distribution is given by the convolution $\mathcal{P}(N) = \sum_{\{N_n\}}\prod_{n=1}^{\infty}\mathcal{P}_n(N_n)$, where $N = \sum_n N_n$ (see § 5). In the classical limit only single-particle transfers remain, $\mathcal{P}(N) = \mathcal{P}_1(N)$.

The concept of particle-number statistics has been used to study trapped ultracold atomic Fermi gases in the crossover regime from weak (BCS) to strong (BEC) attractive interaction. For a discussion we refer to [107] and the references therein.

[5] The results for the Bose gas are valid for temperatures above the critical temperature of Bose-Einstein condensation. Approaching the critical temperature, the fluctuations $\mathcal{C}_2^{(B)}$ diverge. However, any interaction, no matter how weak, will render these fluctuations finite [1].

CHAPTER III

Introduction to mesoscopic transport

§ 10. Scattering formalism

In this section we briefly describe the scattering approach to mesoscopic transport introduced by Landauer [108, 109] and further developed by Imry [110] and Büttiker [34, 111, 112]. We start with the formulation of the scattering problem in § 10.1 and define the scattering matrix and scattering states for a coherent 2-terminal junction. In § 10.2 we show that the scattering matrix is unitary and discuss its properties for a system with and without time reversal symmetry. We outline the generalizations of 2-terminal scattering theory to multiterminal geometries in § 10.3, with the possibility of including superconducting leads and dephasing. In § 10.4 we apply the scattering theory and derive the famous Landauer formula for conductance. In § 10.5 we obtain the general expression for noise in 2-terminal coherent conductors, focusing on the nonequilibrium contribution which carries additional information on the charge transfer statistics and the transmission distribution of the junction. Finally, in § 10.6 we discuss the role of phase averaging due to finite voltage and temperature, as well as the phase self-averaging in conductors with many transport channels. We show how phase averaging restores Ohm's law of adding resistances in series and leads to universality of transport properties in multichannel diffusive conductors [113].

§ **10.1. Scattering matrix and scattering states.** Let us consider a 2-terminal coherent junction which consists of a central scattering region connected to macroscopic electron reservoirs via ballistic leads, as depicted in Fig. 8. We assume elastic spin-independent scattering in the junction while inelastic processes provide the equilibration in the reservoirs. For simplicity, we consider a single-electron problem and assume that the electron propagation along the leads is free, i.e., that the confining potential does not depend on z.[6)] The electron wave functions in the leads are given by

$$\phi^{\pm}_{\alpha\mathcal{E}n}(\boldsymbol{r}) = \frac{1}{\sqrt{v_{\alpha n}}}\, e^{\pm ip_{\alpha n}z}\chi_{\alpha n}(x,y), \tag{10.1}$$

where $\alpha = L, R$ labels the leads, $p_{\alpha n} = \sqrt{2m(\mathcal{E} - \mathcal{E}_{\perp\alpha n})}$ is the longitudinal momentum, $\mathcal{E}$ is the electron energy with respect to the bottom of the conduction band and $\mathcal{E}_{\perp\alpha n}$ are the energies of the transversal modes $\chi_{\alpha n}(x,y)$ labeled by mode index n. The wave functions are orthogonal

$$\int d\boldsymbol{r}\; \phi^{k'*}_{\alpha\mathcal{E}'n'}\, \phi^{k''}_{\alpha\mathcal{E}''n''} = \delta_{k'k''}\delta_{n'n''}\, 2\pi\delta(\mathcal{E}' - \mathcal{E}''), \tag{10.2}$$

[6)] This assumption can be relaxed by using the adiabatic approximation in which the width of the leads $d(z)$ changes slowly with z, $|\partial d/\partial z| \ll 1$.

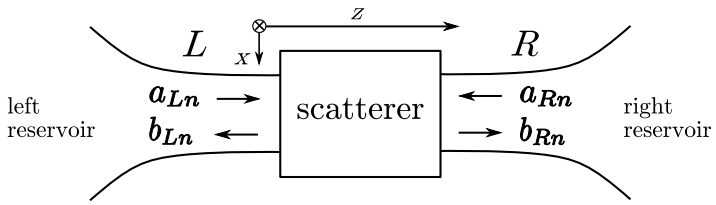

Fig. 8: **Schematic representation of a mesoscopic conductor.** *The conductor is divided into the central scattering region and the ballistic leads (L and R) connected to the reservoirs by reflectionless contacts. The scattering matrix relates the amplitudes $b_{L,R}$ of the outgoing waves and the amplitudes $a_{L,R}$ of the incoming waves.*

with $k', k'' = \{+, -\}$, and normalized to the unit particle flux over the cross-section

$$\frac{-i}{2m}\int dxdy\,[\phi^{\pm *}_{\alpha\mathcal{E}n}(\partial_z\phi^{\pm}_{\alpha\mathcal{E}n}) - (\partial_z\phi^{\pm *}_{\alpha\mathcal{E}n})\phi^{\pm}_{\alpha\mathcal{E}n}] = \pm 1. \tag{10.3}$$

The number of transversal modes is finite and given by $\mathcal{E}_{\perp n} < \mathcal{E}$, with the explicit form of the modes and their energies being dependent on the details of the lateral confining potential. For hard-wall leads of rectangular cross section $L_x \times L_y$, transversal modes are given by $\chi_{n_x,n_y}(x,y) = (4/L_xL_y)^{1/2}\sin(q_{n_x}x)\sin(q_{n_y}y)$, where $q_{n_{x,y}} = \pi n_{x,y}/L_{x,y}$ and $\mathcal{E}_{\perp n_x n_y} = (q^2_{n_x} + q^2_{n_y})/2m$. For a junction patterned on a 2DEG, the confinement in y-direction is much stronger than the one in x-direction, which results in a large spacing between the energies of y-modes. Therefore, for the voltages and temperatures of interest, only one y-mode is populated, and the problem reduces effectively to a 2-dimensional one.

An arbitrary eigenstate of energy $\mathcal{E}$ can be expanded over the basis set of functions in the leads

$$\psi_{\mathcal{E}}(\boldsymbol{r}) = \begin{cases} \sum_n a_{L\mathcal{E}n}\phi^{+}_{L\mathcal{E}n} + \sum_n b_{L\mathcal{E}n}\phi^{-}_{L\mathcal{E}n}, & z \in L, \\ \sum_n a_{R\mathcal{E}n}\phi^{-}_{R\mathcal{E}n} + \sum_n b_{R\mathcal{E}n}\phi^{+}_{R\mathcal{E}n}, & z \in R, \end{cases} \tag{10.4}$$

where $a_{L,R}$ and $b_{L,R}$ are the amplitudes of the incoming and outgoing states with respect to the scatterer, Fig. 8. The precise form of the eigenstate in the scattering region is in general very complicated and depends on the details of the scatterer. The incoming and outgoing amplitudes are related by a linear transformation [114] which can be obtained, in principle, by matching the solution in the middle region with the solutions at the leads given by Eq. (10.4). This linear dependence is usually expressed in terms of the energy-dependent scattering matrix $\boldsymbol{S} = \boldsymbol{S}(\mathcal{E})$ defined by

$$\boldsymbol{b} = \boldsymbol{S}\boldsymbol{a}, \tag{10.5}$$

where

$$\boldsymbol{a} = (a_{L1}, \ldots, a_{LN_L}, a_{R1}, \ldots, a_{RN_R})^T, \tag{10.6a}$$

$$\boldsymbol{b} = (b_{L1}, \ldots, b_{LN_L}, b_{R1}, \ldots, b_{RN_R})^T, \tag{10.6b}$$

with $N_{L,R} = N_{L,R}(\mathcal{E})$ being the number of modes in the leads. In the block-matrix notation

$$\boldsymbol{S} = \begin{pmatrix} \boldsymbol{r}_{N_L\times N_L} & \boldsymbol{t}'_{N_L\times N_R} \\ \boldsymbol{t}_{N_R\times N_L} & \boldsymbol{r}'_{N_R\times N_R} \end{pmatrix} \tag{10.7}$$

where subscripts indicate the dimensions of matrices.

It is useful to define the so called scattering states which are characterized by a single wave in the mode n incoming from the left (right): $a_{Ln} = 1$, $a_{Lm\neq n} = 0$, and $a_{Rm} = 0$ ($a_{Rn} = 1$, $a_{Rm\neq n} = 0$, and $a_{Lm} = 0$), for all m. From Eqs. (10.4) and (10.5) we find that the left and right scattering states are given by

$$\psi_{L\mathcal{E}n}(\boldsymbol{r}) = \begin{cases} \phi^+_{L\mathcal{E}n} + \sum_m r_{mn}\phi^-_{L\mathcal{E}m}, & z \in L, \\ \sum_m t_{mn}\phi^+_{R\mathcal{E}m}, & z \in R, \end{cases} \tag{10.8a}$$

and

$$\psi_{R\mathcal{E}n}(\boldsymbol{r}) = \begin{cases} \phi^-_{R\mathcal{E}n} + \sum_m r'_{mn}\phi^+_{R\mathcal{E}m}, & z \in R, \\ \sum_m t'_{mn}\phi^-_{L\mathcal{E}m}, & z \in L. \end{cases} \tag{10.8b}$$

The matrix elements $r_{mn}(\mathcal{E})$ [$t_{mn}(\mathcal{E})$] are the probability amplitudes for the incoming state $\phi^+_{L\mathcal{E}n}$ from the left to be reflected (transmitted) into the outgoing state $\phi^-_{L\mathcal{E}m}$ ($\phi^+_{R\mathcal{E}m}$). Similarly, $r'_{mn}(\mathcal{E})$ [$t'_{mn}(\mathcal{E})$] are the amplitudes of the reflection (transmission) for the state $\phi^-_{R\mathcal{E}n}$ incoming from the right.

§ **10.2. Unitarity of the scattering matrix.** The unitarity of the scattering matrix follows from current conservation, which holds in the stationary state when there is no charge accumulation in the scattering region. For a general eigenstate given by Eq. (10.4), the incoming (outgoing) particle flux is proportional to $\sum_n |a_{Ln}|^2 + \sum_m |a_{Rm}|^2 = \boldsymbol{a}^\dagger\boldsymbol{a}$ ($\sum_n |b_{Ln}|^2 + \sum_m |b_{Rm}|^2 = \boldsymbol{b}^\dagger\boldsymbol{b}$). From current conservation and Eq. (10.5) we find that $\boldsymbol{b}^\dagger\boldsymbol{b} = \boldsymbol{a}^\dagger\boldsymbol{S}^\dagger\boldsymbol{S}\boldsymbol{a} = \boldsymbol{a}^\dagger\boldsymbol{a}$ for arbitrary amplitudes $\boldsymbol{a}$, which proves the unitarity of the $\boldsymbol{S}$-matrix:

$$\boldsymbol{S}\boldsymbol{S}^\dagger = \boldsymbol{S}^\dagger\boldsymbol{S} = \boldsymbol{1}. \tag{10.9}$$

In block matrix form we obtain

$$\boldsymbol{r}\boldsymbol{r}^\dagger + \boldsymbol{t}'\boldsymbol{t}'^\dagger = \boldsymbol{r}^\dagger\boldsymbol{r} + \boldsymbol{t}^\dagger\boldsymbol{t} = \boldsymbol{1}_{N_L}, \tag{10.10a}$$

$$\boldsymbol{r}'\boldsymbol{r}'^\dagger + \boldsymbol{t}\boldsymbol{t}^\dagger = \boldsymbol{t}'^\dagger\boldsymbol{t}' + \boldsymbol{r}'^\dagger\boldsymbol{r}' = \boldsymbol{1}_{N_R}, \tag{10.10b}$$

$$\boldsymbol{r}\boldsymbol{t}^\dagger + \boldsymbol{t}'\boldsymbol{r}'^\dagger = \boldsymbol{r}^\dagger\boldsymbol{t}' + \boldsymbol{t}^\dagger\boldsymbol{r}' = \boldsymbol{0}_{N_L\times N_R}. \tag{10.10c}$$

Further properties of the $\boldsymbol{S}$-matrix can be obtained by analyzing the transformation of the Hamiltonian under time reversal.[7)] In the presence of a time-independent external magnetic field $\boldsymbol{B} = \operatorname{rot}\boldsymbol{A}$, the Hamiltonian in the leads is given by $\hat{H}_{\boldsymbol{B}} = (1/2m)[\hat{\boldsymbol{p}} - (e/c)\boldsymbol{A}(\boldsymbol{r})]^2 + V(\boldsymbol{r})$, where $V(\boldsymbol{r})$ is the electrostatic confining potential, $\boldsymbol{A}(\boldsymbol{r})$ is the vector potential, and $\hat{\boldsymbol{p}} = -i\nabla$. An eigenstate $\psi_{\mathcal{E}}$ satisfies the Schrödinger equation in the leads

$$\hat{H}_{\boldsymbol{B}}\,\psi_{\mathcal{E}}(\boldsymbol{r}) = \mathcal{E}\psi_{\mathcal{E}}(\boldsymbol{r}), \tag{10.11}$$

with the incoming ($\boldsymbol{a}$) and the outgoing ($\boldsymbol{b}$) amplitudes related by

$$\boldsymbol{b} = \boldsymbol{S}_{\boldsymbol{B}}\boldsymbol{a}. \tag{10.12}$$

[7)] The operator of time reversal $\hat{\mathcal{J}}$ is antilinear, $\hat{\mathcal{J}}(\alpha|\psi\rangle + \beta|\phi\rangle) = \alpha^*\hat{\mathcal{J}}|\psi\rangle + \beta^*\hat{\mathcal{J}}|\phi\rangle$, hermitian, and involutive $\hat{\mathcal{J}} = \hat{\mathcal{J}}^\dagger = \hat{\mathcal{J}}^{-1}$ [115]. The action on the coordinate (momentum) basis is given by $\hat{\mathcal{J}}|\boldsymbol{r}\rangle = |\boldsymbol{r}\rangle$ ($\hat{\mathcal{J}}|\boldsymbol{p}\rangle = |-\boldsymbol{p}\rangle$). In the coordinate (momentum) representation we have $\hat{\mathcal{J}}\psi(\boldsymbol{r}) = \psi^*(\boldsymbol{r})$ [$\hat{\mathcal{J}}\psi(\boldsymbol{p}) = \psi^*(-\boldsymbol{p})$]. The basic set of observables transforms according to $\hat{\mathcal{J}}\hat{\boldsymbol{r}}\hat{\mathcal{J}} = \hat{\boldsymbol{r}}$ and $\hat{\mathcal{J}}\hat{\boldsymbol{p}}\hat{\mathcal{J}} = -\hat{\boldsymbol{p}}$.

Applying the time reversal operation[8] $\hat{\mathcal{J}}$ on Eq. (10.11), we obtain that $\psi^*_{\mathcal{E}}(\boldsymbol{r}) = \hat{\mathcal{J}}\psi_{\mathcal{E}}(\boldsymbol{r})$ is the eigenstate of the Hamiltonian $\hat{H}_{-\boldsymbol{B}} = \hat{\mathcal{J}}\hat{H}_{\boldsymbol{B}}\hat{\mathcal{J}}$. Time reversal changes the direction of propagation, i.e., the incoming and the outgoing amplitudes of $\psi^*_{\mathcal{E}}$ are given by $\boldsymbol{b}^*$ and $\boldsymbol{a}^*$, respectively, with

$$\boldsymbol{a}^* = \boldsymbol{S}_{-\boldsymbol{B}}\boldsymbol{b}^*. \tag{10.13}$$

From Eqs. (10.9), (10.12), and (10.13) we obtain that the $\boldsymbol{S}$-matrix in the presence of a magnetic field satisfies

$$\boldsymbol{S}_{-\boldsymbol{B}} = \boldsymbol{S}^T_{\boldsymbol{B}}. \tag{10.14}$$

For $\boldsymbol{B} = 0$ the system is invariant under time reversal, $[\hat{H}_{\boldsymbol{B}=0}, \hat{\mathcal{J}}] = 0$, and the $\boldsymbol{S}$-matrix is symmetric

$$\boldsymbol{S}_{\boldsymbol{B}=0} = \boldsymbol{S}^T_{\boldsymbol{B}=0}. \tag{10.15}$$

§ **10.3. Generalizations.** The scattering approach introduced in the previous sections has been formulated for a coherent 2-terminal normal junction with spin-independent scattering. However, these assumptions can be relaxed, i.e., the theory can be generalized for a multiterminal geometry [111, 116] with one or more superconducting reservoirs [83, 117, 118]. The loss of phase coherence can be modeled by fictitious voltage probes which act as dephasing terminals [50, 53, 119, 120] (for an alternative model of dephasing, the so called dephasing stub, see [121]). The details of these generalizations are beyond the scope of this Thesis, and we refer the reader to the literature [26, 28, 30, 46] for a more elaborate discussion.

§ **10.4. Landauer formula.** In § 10.1 we introduced the scattering approach using a single-electron picture. This is clearly an oversimplification because many electrons can populate transversal modes in the leads simultaneously and the effect of the Pauli principle has to be taken into account even in the noninteracting case. The most efficient way to do this is by introducing field operators using the single-particle basis given by Eq. (10.1). The field operators in the Heisenberg picture are given by

$$\hat{\psi}_L(\boldsymbol{r}, t) = \int \frac{d\mathcal{E}}{2\pi}\, e^{-i\mathcal{E}t} \sum_{n=1}^{N_L(\mathcal{E})} \left(\hat{a}_{L\mathcal{E}n}\phi^+_{L\mathcal{E}n}(\boldsymbol{r}) + \hat{b}_{L\mathcal{E}n}\phi^-_{L\mathcal{E}n}(\boldsymbol{r})\right), \tag{10.16a}$$

$$\hat{\psi}_R(\boldsymbol{r}, t) = \int \frac{d\mathcal{E}}{2\pi}\, e^{-i\mathcal{E}t} \sum_{n=1}^{N_R(\mathcal{E})} \left(\hat{a}_{R\mathcal{E}n}\phi^-_{R\mathcal{E}n}(\boldsymbol{r}) + \hat{b}_{R\mathcal{E}n}\phi^+_{R\mathcal{E}n}(\boldsymbol{r})\right). \tag{10.16b}$$

Here $\hat{a}_\alpha$ ($\hat{b}_\alpha$) are the annihilation operators of the incoming (outgoing) states in lead α which satisfy the usual anticommutation relations

$$\{\hat{a}_{\alpha\mathcal{E}'n'}, \hat{a}^\dagger_{\alpha\mathcal{E}''n''}\} = \delta_{n'n''}\, 2\pi\delta(\mathcal{E}' - \mathcal{E}''), \tag{10.17a}$$

$$\{\hat{a}_{\alpha\mathcal{E}'n'}, \hat{a}_{\alpha\mathcal{E}''n''}\} = \{\hat{a}^\dagger_{\alpha\mathcal{E}'n'}, \hat{a}^\dagger_{\alpha\mathcal{E}''n''}\} = 0 \tag{10.17b}$$

(and similar for $\hat{b}_\alpha$). Elastic scattering is characterized by the $\boldsymbol{S}$-matrix which relates the incoming and the outgoing *operators* $\hat{\boldsymbol{a}}$ and $\hat{\boldsymbol{b}}$ in analogy with Eq. (10.5). The field operators satisfy

$$\{\hat{\psi}_\alpha(\boldsymbol{r}', t), \hat{\psi}^\dagger_\alpha(\boldsymbol{r}'', t)\} = \delta(\boldsymbol{r}' - \boldsymbol{r}''), \tag{10.18a}$$

[8] The time reversal is applied on the system which consists of electrons, scatterer and leads. It leaves the external magnetic field invariant ($\hat{\mathcal{J}}\boldsymbol{A}\hat{\mathcal{J}} = \boldsymbol{A}$) since it does not act on the sources of the field.

$$\{\hat{\psi}_\alpha(\boldsymbol{r}',t),\hat{\psi}_\alpha(\boldsymbol{r}'',t)\}=\{\hat{\psi}^\dagger_\alpha(\boldsymbol{r}',t),\hat{\psi}^\dagger_\alpha(\boldsymbol{r}'',t)\}=0. \tag{10.18b}$$

The current operator in lead α in the Heisenberg picture is given by

$$\hat{I}_\alpha(z,t)=2_s\frac{-ie}{2m}\int dxdy\ \left[\hat{\psi}^\dagger_\alpha(\boldsymbol{r},t)\left(\partial_z\hat{\psi}_\alpha(\boldsymbol{r},t)\right)-\left(\partial_z\hat{\psi}^\dagger_\alpha(\boldsymbol{r},t)\right)\hat{\psi}_\alpha(\boldsymbol{r},t)\right], \tag{10.19}$$

where the prefactor 2_s accounts for the spin degeneracy. Substituting the field operators for the left lead from Eq. (10.16a), we obtain

$$\hat{I}_L(t)=\frac{e}{\pi}\int\frac{d\mathcal{E}d\mathcal{E}'}{2\pi}\,e^{i(\mathcal{E}-\mathcal{E}')t}\sum_n\left(\hat{a}^\dagger_{L\mathcal{E}n}\hat{a}_{L\mathcal{E}'n}-\hat{b}^\dagger_{L\mathcal{E}n}\hat{b}_{L\mathcal{E}'n}\right). \tag{10.20}$$

Here we used that the transport is governed by electrons in the vicinity of the Fermi surface and neglected the energy dependence of momentum in the energy window given by temperature and applied bias.

The observable current is obtained by averaging $\hat{I}_L(t)$ over the appropriate many-body electron state in the left lead. However, in the presence of bias, the leads are out of equilibrium and the electron state in the leads is not known a priori. Since the leads are ballistic and the scattering in the middle region is elastic, there are no inelastic processes available to provide equilibration in the junction. On the other hand, the terminals which act as electron reservoirs are macroscopic and inelastic processes are present. The terminals support many transport modes which carry infinitesimal currents per mode. The current perturbs the state of the electrons in terminals only weakly, and the electrons are in thermal equilibrium. Because the contacts are reflectionless, the *incoming states* in the leads can be populated only by electrons emerging from the nearby terminals. This means that the electrons in the *incoming states* are in equilibrium with the corresponding terminals, *regardless of the applied bias*. The outgoing states are populated by electrons emerging from both terminals and are characterized by some nonequilibrium distribution functions. Therefore, the proper way to average $\hat{I}_L(t)$ is first to express it entirely in terms of a-operators of incoming states with the help of the scattering matrix, and then average with respect to the equilibrium state using

$$\langle\hat{a}^\dagger_{\alpha\mathcal{E}'n'}\hat{a}_{\alpha\mathcal{E}''n''}\rangle=\delta_{n'n''}2\pi\delta(\mathcal{E}'-\mathcal{E}'')\ f_\alpha(\mathcal{E}'). \tag{10.21}$$

Here $f_\alpha(\mathcal{E})=\{\exp[(\mathcal{E}-\mu_\alpha)/T_e]+1\}^{-1}$ is the Fermi distribution with μ_α being the chemical potential of the lead α and T_e the temperature. For a discussion of other subtle points of the scattering formalism we refer to [15].

After averaging of Eq. (10.20) and using the unitarity of the scattering matrix we obtain

$$I_L=\frac{e}{\pi}\int d\mathcal{E}\ \mathrm{Tr}(\boldsymbol{t}^\dagger\boldsymbol{t})\ [f_L(\mathcal{E})-f_R(\mathcal{E})]. \tag{10.22}$$

Here $\boldsymbol{t}$ and $\boldsymbol{t}^\dagger$ are energy-dependent. Introducing the probability $\mathcal{T}_n(\mathcal{E})=(\boldsymbol{t}^\dagger\boldsymbol{t})_{nn}=\sum_m|t_{mn}(\mathcal{E})|^2$ that the incoming state $\phi^+_{L\mathcal{E}n}$ is transmitted into any outgoing state $\phi^+_{R\mathcal{E}m}$, we find

$$I_L=\frac{e}{\pi}\int d\mathcal{E}\ \sum_n\mathcal{T}_n(\mathcal{E})\ [f_L(\mathcal{E})-f_R(\mathcal{E})]. \tag{10.23}$$

From Eq. (10.10a) follows $\mathcal{T}_n(\mathcal{E})+\mathcal{R}_n(\mathcal{E})=1$ and $\mathcal{T}_n,\mathcal{R}_n\le 1$, where $\mathcal{R}_n(\mathcal{E})=(\boldsymbol{r}^\dagger\boldsymbol{r})_{nn}$ is the reflection probability for the incoming state $\phi^+_{L\mathcal{E}n}$. Another useful representation of I_L is in terms of the eigenvalues $T_n(\mathcal{E})$ of the matrix $\boldsymbol{t}^\dagger\boldsymbol{t}$, which

are also real numbers between 0 and 1 [not to be confused with $\mathcal{T}_n(\mathcal{E})$]. The average current in terms of $T_n(\mathcal{E})$ reads

$$I_L = \frac{e}{\pi} \int d\mathcal{E} \; \sum_n T_n(\mathcal{E}) \; [f_L(\mathcal{E}) - f_R(\mathcal{E})]. \tag{10.24}$$

Equations (10.23) and (10.24) give the average current through the phase coherent conductor in terms of its microscopic scattering properties characterized by $\mathcal{T}_n(\mathcal{E})$ or $T_n(\mathcal{E})$. These transmissions contain complicated interference effects within the scatterer which are very sensitive on the energies of the incoming electrons. For a large number of scattering channels, they change as a function of energy on the scale $\Delta\mathcal{E}$ which is much smaller than the transport energy scale set by applied voltage and temperature. Therefore, the transmissions in Eqs. (10.23) and (10.24) can be replaced by their coarse-grained values, $\langle T_n \rangle \equiv \langle T_n(\mathcal{E}) \rangle_{\Delta\mathcal{E}}$, which vary smoothly with energy. At low temperatures and bias voltages ($T_e, |eV| \ll \mu_R$, with $\mu_L = \mu_R + eV$), we can neglect the energy dependence of the averaged eigenvalues $\langle T_n \rangle$. In this case Eq. (10.24) reduces to $I_L = GV$, where

$$G = \frac{e^2}{\pi} \sum_n \langle T_n \rangle. \tag{10.25}$$

Equation (10.25) is the multichannel Landauer formula for conductance.

The separation of energy scales present in Eq. (10.24) persists in other transport properties as well, as long as the number of channels is sufficiently large. The coarse-grained powers of transmission eigenvalues $\langle T_n^k(\mathcal{E}) \rangle_{\Delta\mathcal{E}}$ are important because they determine not only the average current but the noise and the full charge transfer statistics as well. These quantities can be efficiently calculated using the circuit theory of mesoscopic transport, which we present in Chapter IV.[9)]

In the following we consider a completely open junction without scattering, having N transport channels with $T_n = 1$. From Eq. (10.25) we find that the resistance of such a junction is finite and given by $G_C^{-1} = \pi/e^2 N \approx 13\mathrm{k}\Omega/N$, which certainly is not negligible. This resistance originates from the contacts between terminals and leads. In our model we have assumed reflectionless contacts, which means that the electrons in the outgoing states in the leads enter the terminals without backscattering. However, this is not true for the electrons emerging from the terminals into the leads. These electrons have to be redistributed from the many current-carrying modes in the terminals to just a few such modes in the leads on the length scale of the contact constriction. This gives rise to significant backscattering at the contacts, characterized by the contact resistance G_C^{-1}. Therefore, the total resistance of the junction is the sum of the contact resistance and resistance due to the scatterer, $G^{-1} = G_C^{-1} + G_S^{-1}$, where the latter vanishes for the completely open junction [15].

An important result of Eq. (10.25) is the prediction of conductance quantization in mesoscopic conductors. The number of transversal modes in a hard-wall junction of width W can be estimated as $N = 2W/\lambda_F$. Increasing the width of the contact, more and more transversal modes contribute to the transport and the conductance increases in steps of e^2/π (for $T_n = 1$). The effect has been observed experimentally

[9)] The averages of transmission eigenvalues $\langle T_n^k \rangle$ can be obtained also by using random matrix theory [46]. In this case the averaging is performed by taking the scattering matrix as random, while preserving the corresponding symmetry properties [Eqs. (10.9) and (10.15)]. However, the procedure is less straightforward than the circuit theory and becomes involved when several junctions are combined to form a network.

in a 2DEG layer formed at the interface of GaAs/AlGaAs heterostructure with $\lambda_F = 42$nm [17, 18, 122]. The contact is defined electrostatically by depleting the 2DEG below the split-gate on top of the heterostructure. Up to 16 conductance steps have been observed by changing the width of the contact from $W = 0$ to $W_{\max} = 360$nm at temperature 0.6K. The effect is not visible in metallic contacts due to the small Fermi wavelength $\lambda_F = 3 - 10$Å.

§ **10.5. Current noise power.** By using the scattering approach it is possible to address not only the average current through the junction, but also current correlations. First we give some general definitions and then focus on the particular 2-terminal scattering problem.

For a 2-terminal junction, the current correlation function is defined by

$$S_I(t', t'') = \frac{1}{2}\left\langle \{\Delta\hat{I}(t'), \Delta\hat{I}(t'')\}\right\rangle, \tag{10.26}$$

where $\Delta\hat{I}(t) = \hat{I}(t) - \langle\hat{I}\rangle$, and the average is taken over the incoming states in equilibrium with the reservoirs, as discussed in § 10.4. Taking the Fourier transform of Eq. (10.26) we obtain

$$S_I(\Omega', \Omega'') = \frac{1}{2}\left\langle \{\Delta\hat{I}(\Omega'), \Delta\hat{I}(\Omega'')\}\right\rangle, \tag{10.27}$$

with the convention $S_I(\Omega', \Omega'') = \int dt'dt''\ S_I(t', t'')\ e^{i\Omega' t'} e^{i\Omega'' t''}$. The zero-frequency component (the so called current noise power) is of a particular interest because it is proportional to the fluctuation of the number of charges N transmitted through the junction within the measurement time

$$S_I(\Omega' = \Omega'' = 0) = e^2\Big\langle (N - \langle N\rangle)^2\Big\rangle. \tag{10.28}$$

Here N is a classical stochastic variable and the averaging is over the probability distribution $\mathcal{P}(N)$.

For a static bias, S_I depends only on the time difference, $S_I(t', t'') = S_I(t' - t'')$, which results in $S_I(\Omega', \Omega'') = 2\pi\delta(\Omega' + \Omega'')S_I(\Omega')$ and

$$S_I(t' - t'') = \frac{1}{2}\left\langle \{\Delta\hat{I}(t'), \Delta\hat{I}(t'')\}\right\rangle = \int_{-\infty}^{\infty} \frac{d\Omega}{2\pi}\ S_I(\Omega)\ e^{-i\Omega(t'-t'')}. \tag{10.29}$$

The quantity $S_I(\Omega)$ is the spectral weight of current fluctuations at any instant of time

$$\left\langle [\Delta\hat{I}(t)]^2\right\rangle = \int_{-\infty}^{\infty} \frac{d\Omega}{2\pi}\ S_I(\Omega), \tag{10.30}$$

with the left-hand side being independent of t. Similarly as before, the zero-frequency component is related to the fluctuation of the number of transmitted charges by

$$S_I(\Omega = 0) = \frac{e^2}{t_0}\Big\langle (N - \langle N\rangle)^2\Big\rangle. \tag{10.31}$$

Here t_0 is the preset measurement time which is much larger than the characteristic time scale on which the current fluctuations are correlated.

In the following we consider a coherent 2-terminal scatterer and a static applied bias voltage ($\mu_L = \mu_R + eV$). From Eqs. (10.20) and (10.26) we obtain the following

result for $S_I(\Omega = 0)$ [26, 34]

$$S_I = \frac{e^2}{\pi} \int d\mathcal{E} \ \left(\mathrm{Tr}(\boldsymbol{t}^\dagger \boldsymbol{t}) \ [f_L(1-f_L) + f_R(1-f_R)] + \mathrm{Tr}[\boldsymbol{t}^\dagger \boldsymbol{t}(\mathbf{1} - \boldsymbol{t}^\dagger \boldsymbol{t})] \ (f_L - f_R)^2 \right). \tag{10.32}$$

Here we used the unitarity of the $\boldsymbol{S}$-matrix and Wick's theorem for the average of products of a-operators. We note that all matrix elements $(\boldsymbol{t}^\dagger \boldsymbol{t})_{nm}$ take part in the current noise power, in contrast to just the diagonal ones which contribute to the average current [Eq. (10.23)]. In other words, current fluctuations depend on the transmission amplitudes t_{nm} while the current itself depends just on the transmission probabilities $|t_{nm}|$. After coarse-graining in energy, the current noise power reads

$$S_I = \frac{e^2}{\pi} \int d\mathcal{E} \sum_n \{ \langle T_n \rangle \ [f_L(1-f_L) + f_R(1-f_R)] + \langle T_n(1-T_n) \rangle \ (f_L - f_R)^2 \}, \tag{10.33}$$

where we denote $\langle T_n^k \rangle = \langle T_n^k(\mathcal{E}) \rangle_{\Delta\mathcal{E}}$ for brevity. For low temperatures and applied voltages we can neglect the energy dependence of $\langle T_n^k \rangle$ and perform the integration. The current noise power reduces to

$$S_I = \frac{e^2}{\pi} \sum_n \langle T_n \rangle \ 2T_e + \frac{e^2}{\pi} \sum_n \langle T_n(1-T_n) \rangle \ \left[eV \coth\left(\frac{eV}{2T_e} \right) - 2T_e \right]. \tag{10.34}$$

In the equilibrium state, for no bias applied, the number of transmitted charges fluctuates only due to the thermal fluctuations of occupation numbers (the so called thermal, equilibrium, or Johnson-Nyquist noise [11, 12]). In this case S_I is given by

$$S_I^{\mathrm{eq}} = 2T_e G, \tag{10.35}$$

which is a manifestation of the fluctuation-dissipation theorem [1, 14, 123] (see § 25 in the Appendix). In the limit of large applied bias $|eV| \gg T_e$, thermal fluctuations are negligible and the noise originates from the stochastic nature of charge transmission through the scatterer (the so called shot noise)

$$S_I^{\mathrm{shot}} = \frac{e^2}{\pi} \sum_n \langle T_n(1-T_n) \rangle \ |eV|. \tag{10.36}$$

The magnitude of the shot noise power is usually characterized by the Fano factor

$$F = \frac{S_I^{\mathrm{shot}}}{|eI|}, \tag{10.37}$$

where $|eI|$ is the Schottky formula [2] for the noise power of rare uncorrelated transfer events described by the Poisson distribution $\mathcal{P}(N) = \langle N \rangle^N e^{-\langle N \rangle}/N!$. For the system which we consider, the Fano factor is given by

$$F = \frac{\sum_n \langle T_n(1-T_n) \rangle}{\sum_n \langle T_n \rangle}. \tag{10.38}$$

The nonequilibrium shot noise power carries information which is not contained in the conductance, as discussed in Chapter I. Here we focus on just two aspects. If the measured shot noise power coincides with the Schottky value ($F = 1$), then the variance of the transmitted charge is equal to its mean, $\langle (N - \langle N \rangle)^2 \rangle = \langle N \rangle$, which is an indication of rare uncorrelated electron transfers (Poisson process). For the scattering problem which we consider, this happens for low transmission probabilities $\langle T_n \rangle \ll 1$ in *all* eigenchannels. However, to confirm that the process is indeed Poissoninan, it is necessary to check that the higher-order cumulants are all

equal to the mean. In § 13.2 we will obtain this result using the circuit theory of charge transport. Experimentally, this has been done for the variance and the third cumulant in a highly resistive tunnel junction [104].

The shot noise power provides more information about transmission eigenvalues. From Eq. (10.36) we see that the shot noise contains the averaged sum of squares $\langle T_n^2 \rangle$, while the conductance is proportional to $\langle T_n \rangle$. This motivates the following definition of the distribution of transmission eigenvalues

$$\rho(T, \mathcal{E}) = \sum_n \langle \delta[T - T_n(\mathcal{E})] \rangle_{\Delta\mathcal{E}}, \tag{10.39}$$

which satisfies

$$\int_0^1 dT\ T^k \rho(T) = \sum_n \langle T_n^k \rangle, \tag{10.40}$$

for $k = 1, 2, \ldots$. We emphasize that the averaging in Eq. (10.39) smears the delta-like singularities, resulting in a continuous T-dependence of $\rho(T)$ (see also § 10.6). For example, the transmission distributions for a diffusive wire [46], an open chaotic cavity [64–66], and disordered interface [70] are given by

$$\rho_d(T) = \frac{\tilde{G}}{2T\sqrt{1-T}}, \tag{10.41}$$

$$\rho_c(T) = \frac{2\tilde{G}}{\pi\sqrt{T(1-T)}}, \tag{10.42}$$

$$\rho_i(T) = \frac{\tilde{G}}{\pi T^{3/2}\sqrt{1-T}}, \tag{10.43}$$

with Fano factors $F_d = 1/3$, $F_c = 1/4$, and $F_i = 1/2$, respectively. Here the distributions are normalized to dimensionless conductance $\tilde{G} = \int_0^1 dT\ T\rho(T)$. In § 13.4 we will obtain these results easily within the circuit-theory formalism.

The transmission distribution and the noise are shown on Fig. 9 (a,b) for different junctions. Surprisingly, the distributions are bimodal instead of bell-shaped, with a large density of open and closed channels and a suppressed density of channels of intermediate transparency. The fact that the main part of the electronic states is localized in metals with dimensions exceeding the mean free path, and the conduction is due to a relatively small number of open channels, has been shown first by Dorokhov [47,48]. The contribution of channels with different transparencies to the current is shown in Fig. 9 (c). We see that the transport in diffusive wires and chaotic cavities is dominated by open channels. For a disordered interface, the low-transparency and high-transparency channels participate in transport equally. This is because of the increased number of closed channels which compensates for their low transparency. The situation concerning noise is quite different, as shown in Fig. 9 (d). Here the channels of intermediate transparencies give the dominant contribution in the case of an open cavity, while for the diffusive wire and the disordered interface the noise is predominantly due to the large number of scattering events in closed channels. Further information on the distribution of transmission eigenvalues $\rho(T)$ can be obtained, at least in principle, from the higher-order current correlators which contain higher-order averages $m_k = \sum_n \langle T_n^k \rangle$. For a diffusive wire, chaotic cavity, and disordered interface, the moments m_k (in units of $\tilde{G}$) are given

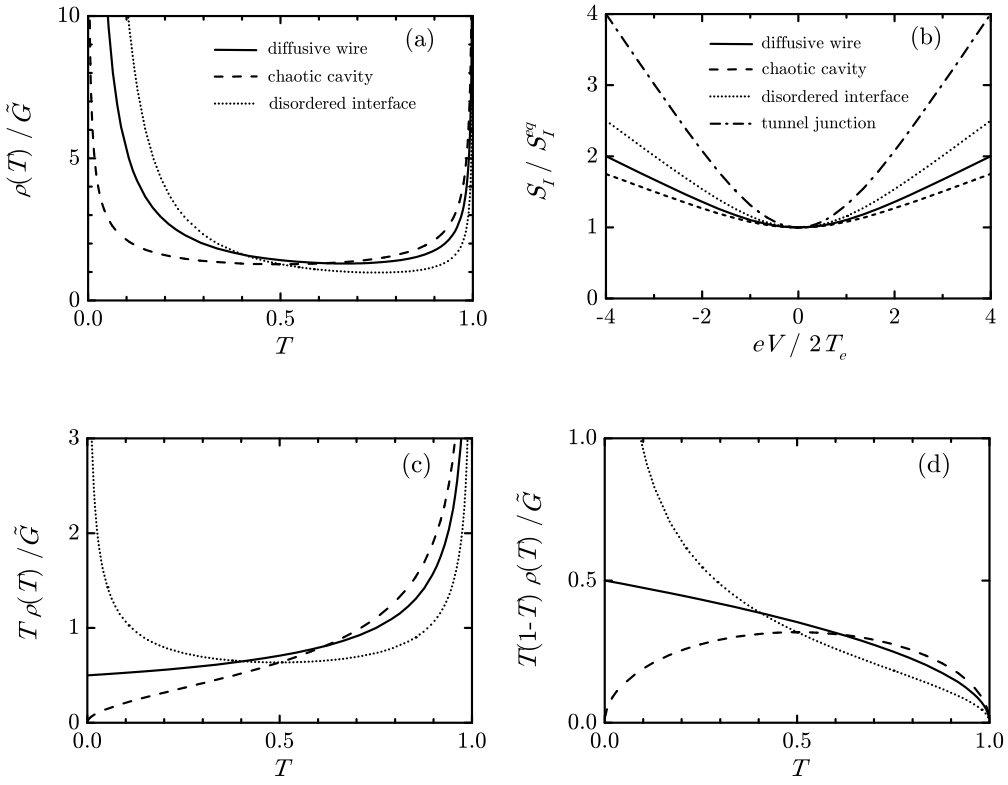

Fig. 9: *The distribution of transmission eigenvalues (a) and current noise power (b) are shown for different junctions: diffusive wire (solid curve), symmetric chaotic cavity (dashed curve), strongly disordered interface (dotted curve), and tunnel junction [$T_n \ll 1$, dash-dotted curve in panel (b)]. The transmission distribution is normalized to the dimensionless conductance $\tilde{G} = \int_0^1 dT\, T\rho(T)$ and the current noise power to the thermal value $S_I^{\rm eq} = 2T_eG$. The transmission distributions are bimodal, with increased densities of closed and open transport channels and suppressed densities of the intermediate ones. The contributions of various transmission channels to the current $I = (e^2V/\pi)\int dT\, T\rho(T)$ and shot noise power $S_I^{shot} = (|e^3V|/\pi)\int dT\, T(1-T)\rho(T)$ are shown in panels (c) and (d), respectively.*

by $m_k^{(d)} = 2^{k-1}(k-1)!/(2k-1)!!$, $m_k^{(c)} = (k\, m_k^{(d)})^{-1}$, and $m_k^{(i)} = [(2k-1)\, m_k^{(d)}]^{-1}$, respectively, where $k = 1, 2, \ldots$. From the experimental point of view, the higher-order current correlators are increasingly more difficult to measure.

Equation (10.38) for the Fano factor is valid in the limit of many transport channels in which case the averaging of transmission probabilities takes place. For a short ballistic contact with a few open channels the averaging is not effective. The Fano factor in this case is given by $F = T(1-T)/(N+T)$, where N is the number of fully open channels and T is the transmission of the channel which is partially open. The conductance of such a junction is given by $\tilde{G} = N + T$ (in units of e^2/π) and the Fano factor becomes $F = (\tilde{G} - \lfloor\tilde{G}\rfloor)(\lfloor\tilde{G}\rfloor + 1 - \tilde{G})/\tilde{G}$ where the integer part $\lfloor\tilde{G}\rfloor = N$ denotes the number of open channels. The Fano factor as a function of conductance is shown in Fig. 10. In the pinch-off region, as the point contact is closed, the Fano factor approaches the classical Schottky value $F = 1$. At the conductance plateaus, the contact is open and the shot noise vanishes ($F = 0$).

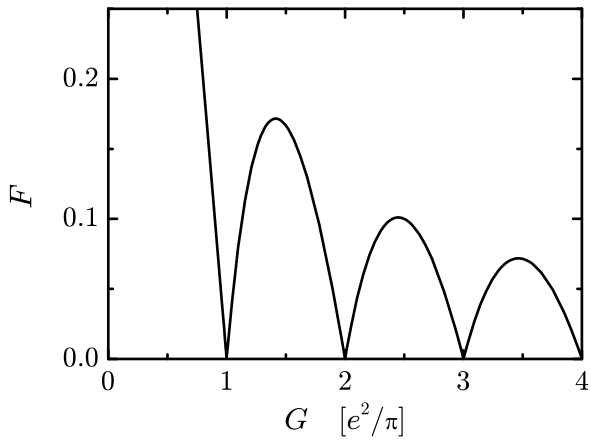

Fig. 10: *Fano factor F as a function of conductance G (in units of e^2/π) for a short ballistic contact with a few open channels. In this case no averaging of transmission eigenvalues takes place. The shot noise vanishes at the conductance plateaus when the contact is completely open. At the transitions between the plateaus, the last transport channel is partially open and the shot noise is non-zero.*

In the simplest model which we consider here, only one channel can be partially open while all the others are either completely open or completely closed. The noise suppression at the conductance plateaus is very sensitive on the presence of partially open channels. For example, if two channels with $T_1 = 0.9$ and $T_2 = 0.1$ are present at the conductance plateau, the noise is suppressed by 80% only. The Fano factor in ballistic quantum point contacts has been measured as a function of the conductance in [40–42]. In experiments, the heat dissipated at the contact raises the effective temperature of the electronic subsystem and results in a thermal noise contribution which is proportional to the current and can be mistaken for shot noise (§ 3). After correcting for the heating effects, the results of Ref. [41] are in good agreement with the simple model presented here. In the more recent experiment [42], the Fano factor has been measured for an ac driven quantum point contact with a zero net dc current. The noise in this case originates from the stochastic transport of electrons and holes generated by an ac voltage. After correcting for the heating effects, the results are in perfect agreement with the Fano factor shown in Fig. 10.

§ **10.6. Universality of transport properties.** In this paragraph we will analyze the effect of energy averaging in Eq. (10.39). This averaging appears because of the difference between the energy scale relevant for transport (which is set by the temperature and applied voltage) and the one on which transmission eigenvalues $T_n(\mathcal{E})$ change. The latter is much smaller because the transmissions fluctuate as a function of energy due to interference effects within the scatterer. Therefore, energy averaging will lead to phase averaging. We will analyze this effect using a double-barrier toy model with a single transport channel. Already this simple system will provide interesting insights. We will see how phase averaging restores Ohm's law of adding resistances in series. It also leads to a transmission probability which is a stochastic variable with a continuous distribution, even for a single channel scattering at barriers. In the tunnel limit, the double-barrier junction behaves like a strongly disordered interface [70] with random scattering potential which is localized on a length scale comparable to the Fermi wavelength. Finally, in the limit of a

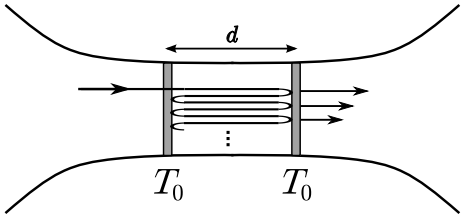

Fig. 11: **Schematic representation of a double-barrier junction.** *The total transmission amplitude is composed of processes with different numbers of reflections between the barriers. The transmission through the system is perfect for electrons with resonant energies corresponding to a phase of $2\pi n$ acquired in one scattering cycle.*

large number of scattering channels, phase self-averaging takes place. The averaged transmission distribution becomes universal, i.e., independent of microscopic details of the junction [113].

Let us consider a system of two identical junctions in series positioned at distance d, as shown in Fig. 11. For simplicity we assume energy-independent transmission amplitudes and consider longitudinal electron propagation with only one transversal quantization mode. The total transmission coefficient through the structure is given by

$$\tilde{T}(\mathcal{E}) = \frac{T_0^2}{1 + R_0^2 - 2R_0 \cos[\phi(\mathcal{E})]}, \tag{10.44}$$

where $T_0 = 1 - R_0$ is the transmission coefficient of a single junction, $\mathcal{E} = p^2/2m$ is the energy of the incoming electron, and $\phi(\mathcal{E}) = 2pd$ is the phase acquired during one scattering cycle between the barriers. At resonant energies corresponding to $\phi = 2\pi n$ (with integer n) the transmission through the structure is perfect with $\tilde{T} = 1$.

Now we analyze what happens if we have a beam of incoming electrons with energies equally distributed in the interval $\Delta\mathcal{E}$ around $\mathcal{E}$. Monoenergetic electrons are transmitted with probability $\tilde{T}(\mathcal{E}')$, with the total transmission for the beam being the average $\langle \tilde{T}(\mathcal{E}) \rangle_{\Delta\mathcal{E}} = (\Delta\mathcal{E})^{-1} \int_{\mathcal{E}-\Delta\mathcal{E}/2}^{\mathcal{E}+\Delta\mathcal{E}/2} \tilde{T}(\mathcal{E}') d\mathcal{E}'$. Because of the linear relation between energy and momentum in the vicinity of the Fermi surface, we can replace energy-averaging $\langle \tilde{T}(\mathcal{E}) \rangle_{\Delta\mathcal{E}}$ by phase-averaging $\langle \tilde{T}(\phi) \rangle_{\Delta\phi}$ over the interval $\Delta\phi = 2\pi(\mathcal{E}_F \lambda_F/d)^{-1} \Delta\mathcal{E}$. For a sufficiently large interval $\Delta\mathcal{E} \gg \mathcal{E}_F \lambda_F/d$ (but still much smaller than the applied voltage and temperature), the average can be taken over one period

$$\langle \tilde{T} \rangle = \int_0^{2\pi} \frac{d\phi}{2\pi} \, \tilde{T}(\phi) = \frac{T_0}{2 - T_0}. \tag{10.45}$$

Equation (10.45) represents Ohm's law of adding resistances in series. We emphasize that the resistances *of the scatterers* are the ones which add up, i.e., we have to correct for the contact resistance of one propagation mode present in our system (cf. page 40). Indeed, from Eq. (10.45) we obtain $\langle \tilde{T} \rangle^{-1} - R_C = (T_0^{-1} - R_C) + (T_0^{-1} - R_C)$, with $R_C = 1$ being the contact resistance in units of π/e^2. In the tunnel limit ($T_0 \ll 1$) the contact resistance is negligible and we have simply $\langle \tilde{T} \rangle^{-1} = T_0^{-1} + T_0^{-1}$.

Therefore, the averaging of interference effects over the energies of incoming electrons recovers Ohm's law.[10)]

To obtain the average values of higher-order powers $\langle \tilde{T}^k \rangle$, it is convenient first to calculate the distribution function

$$\rho(T) = \langle \delta[T - \tilde{T}(\phi)] \rangle_{\Delta\phi} = \int_0^{2\pi} \frac{d\phi}{2\pi}\, \delta[T - \tilde{T}(\phi)]. \tag{10.46}$$

For a given $\rho(T)$, the averages $\langle \tilde{T}^k \rangle$ can be obtained by integration

$$\langle \tilde{T}^k \rangle = \int_0^1 dT\, T^k\, \rho(T). \tag{10.47}$$

The function $\rho(T)$ has a direct physical interpretation. Let us consider ϕ as a classical stochastic variable, equally distributed over the interval $(0, 2\pi)$. In this case $\tilde{T}(\phi)$ is also a stochastic variable, with probability distribution $\rho(T)$ given by Eq. (10.46) [cf. Eq. (5.2)]. This corresponds to the following picture: Instead of taking the energy-phase relation $\phi = \phi(\mathcal{E})$ as deterministic and performing the averaging of transport properties over phases acquired by the incoming electrons of different energies, we can treat the phase as a stochastic variable. In the latter case each electron is transmitted with probability $\tilde{T}$, which is a stochastic variable distributed according to $\rho(T)$. This analysis shows that the very origin of phase averaging is often irrelevant: it may occur due to energy uncertainties in the incoming electron beam, or because of intrinsic imperfections or fluctuations within the device.

Performing the integration in Eq. (10.46) we obtain [52, 71]

$$\rho(T) = \frac{\langle \tilde{T} \rangle}{\pi T \sqrt{\left(T - \langle \tilde{T} \rangle^2\right)\left(1 - T\right)}} \tag{10.48}$$

for $T > \langle \tilde{T} \rangle^2$ and $\rho(T) = 0$ otherwise, where $\langle \tilde{T} \rangle$ is the dimensionless conductance given by Eq. (10.45).[11)] We see that phase averaging smears the delta-like singularities in Eq. (10.46), giving a continuous T-dependence of $\rho(T)$. Another important feature of $\rho(T)$ is the bimodality: the transport channels are predominantly either open or closed, with diverging densities. The distribution $\rho(T)$ is shown in Fig. 12 in comparison with the statistics of $\tilde{T}(\phi)$ obtained from 10^5 realizations of the random phase ϕ. In the tunnel limit $T_0 \ll 1$, the transmission distribution $\rho(T)$ of a double-barrier system reduces to the one of a strongly disordered interface given by Eq. (10.43).[12)] In § 13.4 we will obtain the same result by using the circuit-theory approach.

The phase averaging of the conductance as a function of temperature and applied voltage has been studied experimentally in [122]. The quantum point contact is defined by a split-gate on high mobility GaAs/AlGaAs heterostructure with the Fermi energy $\mathcal{E}_F \approx 12\text{meV}$ corresponding to the wavelength $\lambda_F \approx 40\text{nm}$. The

[10)] For different junctions with transmission probabilities T_1 and T_2 we have $\tilde{T}(\phi) = T_1T_2/[1 + R_1R_2 - 2\sqrt{R_1R_2}\cos(\phi)]$. After averaging we obtain $\langle \tilde{T} \rangle = T_1T_2/(T_1 + T_2 - T_1T_2)$ and Ohm's law again holds, $\langle \tilde{T} \rangle^{-1} - 1 = (T_1^{-1} - 1) + (T_2^{-1} - 1)$.

[11)] If the junctions are different, then $\rho(T) = T_1T_2/[\pi T\sqrt{4T_1T_2T - (T\Delta + T_1T_2)^2}]$ for $T_- < T < T_+$, and $\rho(T) = 0$ otherwise. The cutoffs at low and high transmissions are given by $T_\pm = T_1T_2/(1 \mp \sqrt{1 - \Delta})^2$ with $\Delta = T_1 + T_2 - T_1T_2$.

[12)] The low-transmission cutoff at $T = \langle \tilde{T} \rangle^2$ is important for the normalization $\int_0^1 dT\rho(T) = 1$. However, it gives a negligible contribution in the averages $\langle \tilde{T}^k \rangle$ ($k \geq 1$) and can be ignored.

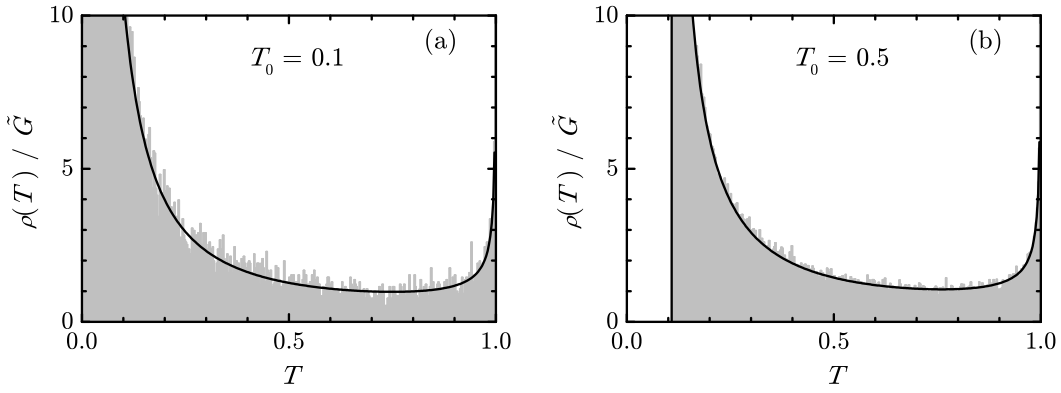

Fig. 12: *The distributions of transmission eigenvalues for a double-barrier junction shown in Fig. 11. The barrier transparencies are* $T_0 = 0.1$ *[panel (a)] and* $T_0 = 0.5$ *[panel (b)]. The distribution is normalized to the dimensionless conductance* $\tilde{G} = T_0/(2 - T_0)$*. The histograms show the statistics of* $\tilde{T}(\phi)$ *for* 10^5 *realizations of the random phase* ϕ*. For low barrier transparency the distribution coincides with the one of a strongly disordered interface, while for more transparent barriers it shifts towards open channels with a low-transmission cutoff at* $T = \tilde{G}^2$*.*

lithographic width of the contact is $W = 250$nm and is much smaller than the elastic mean free path ($l_e = 9\mu$m at $T_e = 4.2$K). At subkelvin temperatures ($T_e = 0.6$K) the authors observe up to 16 conductance steps as the point contact is widened. In the transition regions between the quantized plateaus conductance oscillations are visible, which are attributed to resonant transmission in the highest occupied channel. These oscillations are most pronounced on the transition between the first and the second conductance plateau. The length of the second channel $d \approx 140$nm is estimated from the number of resonances, in agreement with the expected size of the depleted region around the gates (about 200nm). As the transport energy scale increases above 0.5meV (which corresponds to $4T_e$ for temperature-dominated transport and to eV for a bias-dominated one), the resonances in the conductance disappear due to phase averaging in Eq. (10.24). If the temperature is increased even more, $4T_e > 1.5$meV, the thermal energy becomes comparable to the channel spacing and the conductance quantization is also destroyed. The previous analysis has been made for a junction with just a few transport channels. The measured energy scale of 0.5meV for the onset of the phase averaging in this case is much smaller than the estimate $\mathcal{E}_F\lambda_F/d \approx 3.5$meV from our double-barrier model, which is needed to justify the coarse-graining of transmission probabilities $T_n^k \to \langle T_n^k \rangle$ in Eqs. (10.25) and (10.33). Thus, for a contact with a small number of channels, the exact expressions given by Eqs. (10.24) and (10.32) have to be used.

In multichannel junctions there is yet another source of phase averaging. The transmission distribution has to be summed over independent eigenchannels, each having in principle a different phase offset. Therefore, the summation over many transverse channels results in phase self-averaging, $\sum_n T_n^k \to \sum_n \langle T_n^k \rangle$. An important consequence is that the transmission distribution $\rho(T)$ becomes universal, i.e., independent on microscopic details such as shape of the conductor or the spatial dependence of the resistivity. For example, the transmission distribution for a disordered bulk conductor in the diffusive (metallic) regime with $l \ll L \ll Nl$ is given

by $\rho_d(T) = \tilde{G}/(2T\sqrt{1-T})$ [46], where L is the length of a wire, l is the mean free path, $N \gg 1$ is the number of propagating modes, and $\tilde{G}$ is the dimensionless conductance. This distribution leads to the universal $F = 1/3$ suppression of the shot noise power with respect to the classical Poissonian value, regardless of microscopic details (§ 3). Another signature of universality is the existence of universal conductance fluctuations [24, 25], where the conductance changes from sample to sample by a value of the order of e^2/π, again regardless of the shape and resistivity distribution. Recent experiments show that the universal diffusive limit is reached also in lead contacts of width much smaller than the mean free path, supporting just a few transport modes [124]. In this case the band structure of the lead results in an effect similar to averaging and the universality is restored even in the absence of many channels or disorder. Chaotic cavities also exhibit universal transport properties. For sufficiently small contact openings, the electron dwell time in the cavity is larger than the time needed for a localized wave packet to spread over the cavity. In this case the electron momentum in the cavity is isotropized, i.e., the information about the initial direction of propagation is lost. The transmission distribution through the cavity is given by $\rho_c(T) = 2\tilde{G}/[\pi\sqrt{T(1-T)}]$ [64–66], with universal shot noise power suppression of $F = 1/4$ [68, 69]. In general, the universality can be broken by extended defects such as tunnel barriers, grain boundaries, or interfaces [43] at which the voltage changes abruptly, or by the presence of ballistic regions in which the transport is not diffusive. In the case of the cavity, the universality can be broken also by relatively large openings which enable direct transmission from one lead to another. In this case transport depends on the geometry of the system, like the position and size of the contacts [67].

§ 11. Green's functions

In this paragraph we introduce the formalism of Green's functions in the form which is used in solid-state physics. The formalism comes in different variants, depending on the system under consideration. Interacting many-body systems in thermal equilibrium can be described by zero-temperature or finite-temperature (imaginary time, Matsubara) Green's functions. Systems out of equilibrium can be described by nonequilibrium (Keldysh) Green's functions. A complete introduction to the formalism, including all different techniques, is beyond the scope of this Thesis and we refer the reader to the more specialized books [125–132] and articles [133–136] on the subject. In the following we focus on the nonequilibrium Keldysh technique.[13)]

§ 11.1. Definition of the Green's functions. The Green's function technique, being a perturbative method, has a wide range of applications in various branches of physics. In contrast to the ordinary theory of perturbations, which is in practice usually limited just to a few low orders, in the Green's functions formalism it is possible to take into account certain processes in *all* orders. This is usually done by construction of the appropriate diagrammatic technique, in which certain diagrams recursively appear as subdiagrams of larger ones. In this case, an exact summation of the entire class of diagrams is possible. The remaining diagrams, which cannot be summed in this way, are calculated to some finite order. Various classes of diagrams often have a direct physical interpretation. Therefore,

[13)] For a comprehensive and less formal introduction to nonequilibrium Green's functions see, e.g., Ref. [15].

the diagrammatic technique has a twofold importance: On one hand it points out the different physical processes relevant for the problem under consideration, and, on the other, it takes into account some of the processes exactly while providing a controlled and systematic way of including the rest approximately. The price to be paid is that although the general layout of the theory is common, the corresponding diagrammatic rules are different for each class of systems (i.e., Hamiltonians) and have to be constructed separately. In the following we give the general definitions of the Green's functions and in § 27 we provide more specific formulas used in the BCS theory of superconductivity.

Let us consider a macroscopic system of interacting particles in an external field described by the Hamiltonian

$$\hat{\mathcal{H}}(t) = \hat{H} + \hat{H}'(t). \tag{11.1}$$

Here $\hat{H} = \hat{H}_0 + \hat{H}_{\rm int}$, where $\hat{H}_0$ is the Hamiltonian of noninteracting particles, $\hat{H}_{\rm int}$ is a time-independent interaction, and $\hat{H}'(t)$ is an external time-dependent perturbation. We work in the grand canonical ensemble in which $\hat{H}_0$ includes the term $-\mu\hat{N}$, with μ being the chemical potential and $\hat{N}$ the particle number operator. We assume that there is no external perturbation at times $t < t_0$ [$\hat{H}'(t < t_0) = 0$] and the system is in equilibrium with the thermostat at temperature T_e. The equilibrium state is described by the statistical operator

$$\hat{\rho}_H = \frac{1}{Z}\, e^{-\beta\hat{H}}, \tag{11.2}$$

where $Z = {\rm Tr}(e^{-\beta\hat{H}})$ and $\beta = 1/T_e$. At $t = t_0$ the external perturbation is switched on and the system evolves according to the full Hamiltonian $\hat{\mathcal{H}}(t)$.

The goal of nonequilibrium statistical mechanics is the calculation of expectation values of observables at times $t > t_0$:

$$\langle \hat{A}_{\mathcal{H}}(t) \rangle_H \equiv {\rm Tr}\left(\hat{\rho}_H \hat{A}_{\mathcal{H}}(t) \right). \tag{11.3}$$

Here $\hat{A}_{\mathcal{H}}(t) = \hat{U}^\dagger(t,t_0)\hat{A}\hat{U}(t,t_0)$ is the Heisenberg picture of an observable $\hat{A}$ and the average is taken with respect to the interacting equilibrium state $\hat{\rho}_H$. The evolution operator $\hat{U}$ is given by the Schrödinger equation

$$i\frac{\partial \hat{U}(t,t_0)}{\partial t} = \hat{\mathcal{H}}(t)\hat{U}(t,t_0), \qquad \hat{U}(t_0,t_0) = 1. \tag{11.4}$$

A formal solution of Eq. (11.4) is given by

$$\hat{U}(t,t_0) = T e^{-i\int_{t_0}^{t} \hat{\mathcal{H}}(t')dt'}, \tag{11.5}$$

where T denotes time ordering.[14)] In the absence of a time-dependent perturbation, the Hamiltonian does not depend on time explicitly and Eq. (11.5) reduces to $\hat{U}(t,t_0) = e^{-i(t-t_0)\hat{H}}$.

From Eq. (11.3) it is apparent where the main difficulty in the many-body theory of interacting systems lies: The trace in Eq. (11.3) can be calculated by using Wick's theorem only for noninteracting particles with $\hat{\mathcal{H}} = \hat{H}_0$. For the interacting system Wick's theorem fails, and the trace cannot be calculated by simple means. The problem can be avoided by using the interaction picture for observables (instead

[14)] The inverse operator is given by $\hat{U}^\dagger(t,t_0) \equiv [\hat{U}(t,t_0)]^\dagger = \tilde{T} e^{i\int_{t_0}^{t} \hat{\mathcal{H}}(t)dt}$ where $\tilde{T}$ denotes anti-time ordering.

of the Heisenberg picture) in which they evolve according to the noninteracting Hamiltonian $\hat{H}_0$. In addition, it is necessary to express the average $\langle \cdots \rangle_H$ over the interacting state in terms of the average $\langle \cdots \rangle_{H_0}$ over the noninteracting one. In the following we define the Green's functions which are auxiliary objects used to efficiently implement the above procedure.

§ **11.2. Real-time Green's functions.** The time-ordered Green's function $G_{\alpha\beta}(x', x'')$ for a system of particles described by Eq. (11.1) is defined by[15)]

$$G_{\alpha\beta}(x', x'') = -i \left\langle T\hat{\psi}_{\alpha\mathcal{H}}(x')\hat{\psi}^\dagger_{\beta\mathcal{H}}(x'') \right\rangle_H = \begin{cases} -i\langle \hat{\psi}_{\alpha\mathcal{H}}(x')\hat{\psi}^\dagger_{\beta\mathcal{H}}(x'')\rangle_H, & t' > t'' \\ \pm i\langle \hat{\psi}^\dagger_{\beta\mathcal{H}}(x'')\hat{\psi}_{\alpha\mathcal{H}}(x')\rangle_H, & t'' > t' \end{cases}. \tag{11.6}$$

Here $\psi_{\mathcal{H}}$ are the field operators in the Heisenberg picture, α and β are the spin indices, $x \equiv (t, \boldsymbol{r})$ is the short notation for the space and time arguments, and the upper (lower) sign refers to fermions (bosons). When performing the time ordering in Eq. (11.6), the quantum statistics of the system should be taken into account: the transposition of $\hat{\psi}$ and $\hat{\psi}^\dagger$ changes the sign for fermions and leaves the sign unchanged for bosons. The time-ordered Green's function is often denoted as $G^{--}_{\alpha\beta}(x', x'')$.

Besides the time-ordered Green's function G^{--}, several other Green's functions are used in the nonequilibrium theory: the anti-time-ordered (G^{++}), the lesser (G^{-+}), the greater (G^{+-}), the retarded (G^R), the advanced (G^A), and the Keldysh (G^K) Green's functions. Below we list all definitions, with the spin indices included in $x = (t, \boldsymbol{r}, \alpha)$:

$$G^{--}(x', x'') = -i \left\langle T\hat{\psi}_{\mathcal{H}}(x')\hat{\psi}^\dagger_{\mathcal{H}}(x'') \right\rangle_H, \tag{11.7a}$$

$$G^{++}(x', x'') = -i \left\langle \tilde{T}\hat{\psi}_{\mathcal{H}}(x')\hat{\psi}^\dagger_{\mathcal{H}}(x'') \right\rangle_H, \tag{11.7b}$$

$$G^{-+}(x', x'') \equiv G^<(x', x'') = \pm i \left\langle \hat{\psi}^\dagger_{\mathcal{H}}(x'')\hat{\psi}_{\mathcal{H}}(x') \right\rangle_H, \tag{11.7c}$$

$$G^{+-}(x', x'') \equiv G^>(x', x'') = -i \left\langle \hat{\psi}_{\mathcal{H}}(x')\hat{\psi}^\dagger_{\mathcal{H}}(x'') \right\rangle_H, \tag{11.7d}$$

and

$$G^R(x', x'') = -i\,\theta(t' - t'') \left\langle [\hat{\psi}_{\mathcal{H}}(x'), \hat{\psi}^\dagger_{\mathcal{H}}(x'')]_\pm \right\rangle_H, \tag{11.8a}$$

$$G^A(x', x'') = i\,\theta(t'' - t') \left\langle [\hat{\psi}_{\mathcal{H}}(x'), \hat{\psi}^\dagger_{\mathcal{H}}(x'')]_\pm \right\rangle_H, \tag{11.8b}$$

$$G^K(x', x'') = -i \left\langle [\hat{\psi}_{\mathcal{H}}(x'), \hat{\psi}^\dagger_{\mathcal{H}}(x'')]_\mp \right\rangle_H. \tag{11.8c}$$

In the previous formulas $\tilde{T}$ is the anti-time ordering, θ is the step function, the upper (lower) sign corresponds to fermions (bosons) and $[\ ,\ ]_\pm$ denotes the (anti) commutator. The Green's functions defined by Eqs. (11.7) and (11.8) satisfy the following relations:

$$G^{-+}_{\alpha'\alpha''}(t, \boldsymbol{r}'; t, \boldsymbol{r}'') - G^{+-}_{\alpha'\alpha''}(t, \boldsymbol{r}'; t, \boldsymbol{r}'') = i\delta_{\alpha'\alpha''}\delta(\boldsymbol{r}' - \boldsymbol{r}''), \tag{11.9a}$$

$$G^{--}(x', x'') = -[G^{++}(x'', x')]^*, \tag{11.9b}$$

[15)] We follow the convention which is usually used in the literature [126–132]. The definition given in Ref. [125] uses a different sign convention.

$$G^{-+}(x',x'') = -[G^{-+}(x'',x')]^*, \tag{11.9c}$$
$$G^{+-}(x',x'') = -[G^{+-}(x'',x')]^*, \tag{11.9d}$$

and

$$G^A(x',x'') = [G^R(x'',x')]^*, \tag{11.10a}$$
$$G^K = G^{--} + G^{++} = G^{-+} + G^{+-}, \tag{11.10b}$$
$$G^R = G^{--} - G^{-+} = G^{+-} - G^{++}, \tag{11.10c}$$
$$G^A = G^{--} - G^{+-} = G^{-+} - G^{++}. \tag{11.10d}$$

The definitions and properties listed above are valid both for fermions and bosons. In the following we focus only on fermions, having in mind the application of the theory to electron transport in mesoscopic devices.

The equilibrium zero-temperature theory is formulated in terms of the time-ordered Green's function G^{--} only. In the nonequilibrium theory, the four different Green's functions $G^{\pm\pm}$ appear originally. However, because of the linear relation $G^{--} + G^{++} = G^{-+} + G^{+-}$, only three of them are linearly independent. Therefore, without loss of generality, we can choose to work with $G^{R,A,K}$. Furthermore, because of the symmetry relation between G^R and G^A given by Eq. (11.10a), the complete theory can be formulated, in principle, in terms of just two Green's functions, say G^A and G^K. However, in practice, one usually uses either the full set $G^{\pm\pm}$ or the reduced one $G^{R,A,K}$, because the equations can be cast in a compact matrix form. At the end of a calculation, it is easy to switch between various Green's functions using the properties given by Eqs. (11.9) and (11.10). In § 11.4 we introduce the equilibrium zero-temperature theory and in § 11.6 we generalize it to the nonequilibrium case.

For the stationary and spatially homogeneous system, the Green's functions depend only on the difference of arguments $t = t' - t''$ and $\boldsymbol{r} = \boldsymbol{r}' - \boldsymbol{r}''$ and can be Fourier transformed with respect to t and $\boldsymbol{r}$ (see § 29 in Appendix). The transformed functions satisfy:[16)]

$$G^{--}(\mathcal{E},\boldsymbol{p}) = -[G^{++}(\mathcal{E},\boldsymbol{p})]^*, \tag{11.11a}$$
$$G^A(\mathcal{E},\boldsymbol{p}) = [G^R(\mathcal{E},\boldsymbol{p})]^*, \tag{11.11b}$$
$$\mathrm{Re}[G^{+-}(\mathcal{E},\boldsymbol{p})] = \mathrm{Re}[G^{-+}(\mathcal{E},\boldsymbol{p})] = 0. \tag{11.11c}$$

The poles of the Green's function $G^{--}(\mathcal{E},\boldsymbol{p}) \equiv G(\mathcal{E},\boldsymbol{p})$ determine the spectrum $\mathcal{E}(\boldsymbol{p})$ of quasiparticle excitations of the system by $[G(\mathcal{E}-\mu,\boldsymbol{p})]^{-1} = 0$.

For the stationary (not necessary homogeneous) system, the spectral function $A_\alpha(\mathcal{E},\boldsymbol{r})$ is defined by[17)]

$$A_\alpha(\mathcal{E},\boldsymbol{r}) = -2\ \mathrm{Im}[G^R_{\alpha\alpha}(\mathcal{E};\boldsymbol{r},\boldsymbol{r})]. \tag{11.12}$$

In equilibrium, the spectral function reads: $A_\alpha(\mathcal{E},\boldsymbol{r}) = -iG^{-+}_{\alpha\alpha}(\mathcal{E};\boldsymbol{r},\boldsymbol{r})/f(\mathcal{E}) = iG^{+-}_{\alpha\alpha}(\mathcal{E};\boldsymbol{r},\boldsymbol{r})/[1-f(\mathcal{E})]$, where $f(\mathcal{E}) = (e^{\beta\mathcal{E}}+1)^{-1}$ is the Fermi distribution. The spectral function is real and positive, $A_\alpha(\mathcal{E},\boldsymbol{r}) \geq 0$, and satisfies

$$N_\alpha(\boldsymbol{r}) = \left\langle \hat{\psi}^\dagger_{\alpha\mathcal{H}}(t,\boldsymbol{r})\hat{\psi}_{\alpha\mathcal{H}}(t,\boldsymbol{r})\right\rangle_H = \int_{-\infty}^{\infty}\frac{d\mathcal{E}}{2\pi}\,A_\alpha(\mathcal{E},\boldsymbol{r})f(\mathcal{E}), \tag{11.13}$$

---

16) For simplicity we assume spin-independent scattering.

17) We define the spectral function with respect to the coordinate single-particle basis $\{|\boldsymbol{r}\rangle\}$. For a different choice of the basis, the definition and subsequent formulas are analogous.

with $N_\alpha(\boldsymbol{r})$ being the particle density. From Eq. (11.13) we conclude that the quantity $\mathcal{V}_\alpha(\mathcal{E},\boldsymbol{r}) = (2\pi)^{-1}A_\alpha(\mathcal{E},\boldsymbol{r})$ is the local density of states (i.e., the number of states per unit energy and volume in vicinity of $\boldsymbol{r}$), with each state of energy $\mathcal{E}$ being occupied with probability $f(\mathcal{E})$. The global density of states (the number of states per unit energy) is given by

$$\mathcal{V}_\alpha(\mathcal{E}) = \frac{1}{2\pi}\int d\boldsymbol{r}\; A_\alpha(\mathcal{E},\boldsymbol{r}). \tag{11.14}$$

The Green's functions for the noninteracting Fermi gas in equilibrium are given by

$$G^{(0)--}(\mathcal{E},\boldsymbol{p}) = \text{p.v.}\,\frac{1}{\mathcal{E}-\xi_{\boldsymbol{p}}} + i[2f(\boldsymbol{p})-1]\;\pi\delta(\mathcal{E}-\xi_{\boldsymbol{p}}), \tag{11.15a}$$

$$G^{(0)-+}(\mathcal{E},\boldsymbol{p}) = if(\boldsymbol{p})\;2\pi\delta(\mathcal{E}-\xi_{\boldsymbol{p}}), \tag{11.15b}$$

$$G^{(0)+-}(\mathcal{E},\boldsymbol{p}) = -i[1-f(\boldsymbol{p})]\;2\pi\delta(\mathcal{E}-\xi_{\boldsymbol{p}}), \tag{11.15c}$$

$$G^{(0)++}(\mathcal{E},\boldsymbol{p}) = -\,\text{p.v.}\,\frac{1}{\mathcal{E}-\xi_{\boldsymbol{p}}} + i[2f(\boldsymbol{p})-1]\;\pi\delta(\mathcal{E}-\xi_{\boldsymbol{p}}), \tag{11.15d}$$

and

$$G^{(0)R}(\mathcal{E},\boldsymbol{p}) = \frac{1}{\mathcal{E}-\xi_{\boldsymbol{p}}+i0}, \tag{11.16a}$$

$$G^{(0)A}(\mathcal{E},\boldsymbol{p}) = \frac{1}{\mathcal{E}-\xi_{\boldsymbol{p}}-i0}, \tag{11.16b}$$

$$G^{(0)K}(\mathcal{E},\boldsymbol{p}) = i[2f(\boldsymbol{p})-1]\;2\pi\delta(\mathcal{E}-\xi_{\boldsymbol{p}}). \tag{11.16c}$$

Here $f(\boldsymbol{p}) = (e^{\beta\xi_{\boldsymbol{p}}}+1)^{-1}$, $\xi_{\boldsymbol{p}} = \boldsymbol{p}^2/2m-\mu$, the principal value is denoted by p.v., and the spin factors $\delta_{\alpha\beta}$ are omitted for brevity. The infinitesimal imaginary parts in denominators appear due to the shifts in energy $\mathcal{E}\to\mathcal{E}\pm i0$ needed to ensure the convergence of the Fourier transformations of $G^R(t'-t'')$ $[G^A(t'-t'')]$. From Eq. (11.16a) and using $(\mathcal{E}-\xi_{\boldsymbol{p}}+i0)^{-1} = \text{p.v.}(\mathcal{E}-\xi_{\boldsymbol{p}})^{-1} - i\pi\delta(\mathcal{E}-\xi_{\boldsymbol{p}})$ we recover the usual result for the density of states of a noninteracting homogeneous system $\mathcal{V}^{(0)}_\alpha(\mathcal{E},\boldsymbol{r}) = (2\pi)^{-3}\int d\boldsymbol{p}\;\delta(\mathcal{E}-\xi_{\boldsymbol{p}})$, independent of α and $\boldsymbol{r}$. In the interacting case, the lifetime of single-particle states of energy $\xi_{\boldsymbol{p}}$ is finite. In the vicinity of the Fermi surface, the effect can be taken into account by adding a small imaginary term to the energy $\xi_{\boldsymbol{p}}\to\xi_{\boldsymbol{p}}-i\tau_{\boldsymbol{p}}^{-1}$ (with $\tau_{\boldsymbol{p}}$ being the lifetime, $\tau_{\boldsymbol{p}}^{-1}\ll|\xi_{\boldsymbol{p}}|$). From Eqs. (11.12) and (11.16a) we obtain that an interaction results in a broadening of the spectral function which assumes the form of a Lorentzian $A_\alpha(\mathcal{E},\boldsymbol{p}) = 2\pi V\;(\pi\tau_{\boldsymbol{p}})^{-1}[(\mathcal{E}-\xi_{\boldsymbol{p}})^2+\tau_{\boldsymbol{p}}^{-2}]^{-1}$, where V is the volume.

§ **11.3. One-particle averages.** In this paragraph we obtain the expression for averages of one-particle observables in terms of the Green's functions. Let $\hat{F} = \sum_a \hat{f}^{(a)}$ be a one-particle operator in the Schrödinger picture, where $\hat{f}^{(a)}$ act on the individual particles labelled by a. The second-quantized form of $\hat{F}$ in the Heisenberg picture is given by

$$\hat{F}_{\mathcal{H}}(t) = \sum_{\alpha\beta}\int d\boldsymbol{r}\;\hat{\psi}^\dagger_{\alpha\mathcal{H}}(t,\boldsymbol{r})\hat{f}^{(1)}_{\alpha\beta}(\boldsymbol{r})\hat{\psi}_{\beta\mathcal{H}}(t,\boldsymbol{r}). \tag{11.17}$$

Here $\hat{f}^{(1)}_{\alpha\beta}(\boldsymbol{r})$ is the operator for an individual particle in coordinate representation (Schrödinger picture) which acts on $\boldsymbol{r}$ in $\hat{\psi}_{\beta\mathcal{H}}(t,\boldsymbol{r})$. The average $F(t) = \langle\hat{F}_{\mathcal{H}}(t)\rangle_H$ is

given by

$$F(t) = -i \sum_{\alpha\beta} \int d\boldsymbol{r} \left[\hat{f}^{(1)}_{\alpha\beta}(\boldsymbol{r}) G_{\beta\alpha}(t, \boldsymbol{r}; t+0, \boldsymbol{r}') \right]_{\boldsymbol{r}'=\boldsymbol{r}} . \tag{11.18}$$

Here $\hat{f}^{(1)}_{\alpha\beta}(\boldsymbol{r})$ acts only on $\boldsymbol{r}$ in $G(t, \boldsymbol{r}; t+0, \boldsymbol{r}')$ and the limit $\boldsymbol{r}' = \boldsymbol{r}$ is taken after the action of $\hat{f}$. For example, the particle-number density and momentum density operators in the Schrödinger picture are given by

$$\hat{N}(\boldsymbol{r}) = \sum_{\alpha} \hat{\psi}^{\dagger}_{\alpha}(\boldsymbol{r}) \hat{\psi}_{\alpha}(\boldsymbol{r}) \tag{11.19}$$

and

$$\hat{\boldsymbol{P}}(\boldsymbol{r}) = -\frac{i}{2} \sum_{\alpha} \left[\hat{\psi}^{\dagger}_{\alpha}(\boldsymbol{r}) \left(\nabla \hat{\psi}_{\alpha}(\boldsymbol{r}) \right) - \left(\nabla \hat{\psi}^{\dagger}_{\alpha}(\boldsymbol{r}) \right) \hat{\psi}_{\alpha}(\boldsymbol{r}) \right] . \tag{11.20}$$

The corresponding averages can be expressed in terms of the time-ordered Green's function by

$$N(t, \boldsymbol{r}) = -i \sum_{\alpha} G_{\alpha\alpha}(t, \boldsymbol{r}; t+0, \boldsymbol{r}) \tag{11.21}$$

and

$$\boldsymbol{P}(t, \boldsymbol{r}) = -\frac{1}{2} \left[(\nabla' - \nabla'') \sum_{\alpha} G_{\alpha\alpha}(t, \boldsymbol{r}'; t+0, \boldsymbol{r}'') \right]_{\boldsymbol{r}'=\boldsymbol{r}''=\boldsymbol{r}} . \tag{11.22}$$

In the stationary state (when the Hamiltonian does not depend on time explicitly) the Green's functions depend only on the time difference $t = t' - t''$, and N and $\boldsymbol{P}$ become time-independent. Equations (11.20) and (11.22) are valid in the absence of an external electromagnetic field. If a field with the vector potential $\boldsymbol{A}(t, \boldsymbol{r})$ is present, the ∇ operators should be replaced by $\nabla \mp i(e/c)\boldsymbol{A}$ when acting on $\hat{\psi}$ ($\hat{\psi}^{\dagger}$).

§ **11.4. Diagrammatic technique at zero temperature.** The analysis in the previous paragraph shows the importance of the Green's functions: If the Green's function is known, then the averages of *arbitrary* one-particle operators are given by Eq. (11.18). Therefore, the main goal of many-body theory is to provide a method for obtaining Green's functions.

In the following we illustrate the method in the simplest case of a system of interacting particles at zero temperature without an external time-dependent perturbation [$\hat{\mathcal{H}} = \hat{H}_0 + \hat{H}_{\rm int}$, $\hat{H}'(t) = 0$]. Let us assume that the system was initially noninteracting and in a nondegenerate ground state $|\phi_0\rangle$. The interaction is adiabatically switched on at $t = -\infty$ and adiabatically switched off at $t = \infty$. Since an adiabatic evolution does not introduce transitions to states of different energy, the final state is the same as the initial ground state, up to a phase factor: $|\phi\rangle = e^{i\varphi}|\phi_0\rangle$. The zero-temperature Green's function is given by

$$G(x', x'') = -i \left\langle T \hat{\psi}_{\mathcal{H}}(x') \hat{\psi}^{\dagger}_{\mathcal{H}}(x'') \right\rangle_0 , \tag{11.23}$$

where we have suppressed spin indices and $\langle \cdots \rangle_0 = \langle \phi_0 | \cdots | \phi_0 \rangle$ denotes averaging over the initial ground state of the noninteracting system. It is convenient to change to the interaction picture, in which ψ-operators evolve with respect to the noninteracting Hamiltonian $\hat{H}_0$. The operators $\psi_{\mathcal{H}}$ in the Heisenberg picture are related to the operators ψ_{H_0} in the interaction picture by

$$\hat{\psi}_{\mathcal{H}}(t, \boldsymbol{r}) = \hat{S}^{\dagger}(t, -\infty)\ \hat{\psi}_{H_0}(t, \boldsymbol{r})\ \hat{S}(t, -\infty), \tag{11.24a}$$

$$\hat{\psi}^{\dagger}_{\mathcal{H}}(t, \boldsymbol{r}) = \hat{S}^{\dagger}(t, -\infty)\ \hat{\psi}^{\dagger}_{H_0}(t, \boldsymbol{r})\ \hat{S}(t, -\infty). \tag{11.24b}$$

Here $\hat{S}$ denotes the evolution operator in the interaction picture which is given by

$$\hat{S}(t,t_0) = Te^{-i\int_{t_0}^{t} dt' \hat{H}^{\rm int}_{H_0}(t')}, \tag{11.25}$$

with

$$\hat{H}^{\rm int}_{H_0}(t) = \hat{U}^{\dagger}_{H_0}(t,-\infty)\ \hat{H}_{\rm int}\ \hat{U}_{H_0}(t,-\infty) \tag{11.26}$$

and $\hat{U}_{H_0}(t,t_0) = e^{-i\hat{H}_0(t-t_0)}$. For a system with single- and two-particle interactions $U^{(1)}(\boldsymbol{r})$ and $U^{(2)}(\boldsymbol{r}_1-\boldsymbol{r}_2)$ (which describe, for example, interactions with a static inhomogeneous external field and interparticle interactions, respectively), equation (11.26) reads

$$\begin{aligned}\hat{H}^{\rm int}_{H_0}(t) = &\int d\boldsymbol{r}\ \hat{\psi}^{\dagger}_{H_0}(t,\boldsymbol{r})\ U^{(1)}(\boldsymbol{r})\ \hat{\psi}_{H_0}(t,\boldsymbol{r}) \\ &+\frac{1}{2}\int d\boldsymbol{r}d\boldsymbol{r}'\ \hat{\psi}^{\dagger}_{H_0}(t,\boldsymbol{r})\hat{\psi}^{\dagger}_{H_0}(t,\boldsymbol{r}')\ U^{(2)}(\boldsymbol{r}-\boldsymbol{r}')\ \hat{\psi}_{H_0}(t,\boldsymbol{r}')\hat{\psi}_{H_0}(t,\boldsymbol{r}).\end{aligned} \tag{11.27}$$

Equations (11.25) and (11.27) express the evolution operator $\hat{S}$ in terms of the noninteracting field operators ψ_{H_0}.

Substituting Eqs. (11.24) into Eq. (11.23) we find

$$G(x',x'') = -i\left\langle \hat{S}^{\dagger}\ T\big[\hat{\psi}_{H_0}(x')\hat{\psi}^{\dagger}_{H_0}(x'')\ \hat{S}\big]\right\rangle_0. \tag{11.28}$$

Here $\hat{S}\equiv\hat{S}(\infty,-\infty)$ and we used the following properties of the evolution operator

$$\hat{S}(t_3,t_1) = \hat{S}(t_3,t_2)\hat{S}(t_2,t_1), \tag{11.29a}$$

$$\hat{S}^{\dagger}(t_3,t_1) = \hat{S}^{\dagger}(t_2,t_1)\hat{S}^{\dagger}(t_3,t_2). \tag{11.29b}$$

The Green's function can be further simplified using that the whole evolution changes the ground state only by a phase factor: $|\phi\rangle = \hat{S}(\infty,-\infty)|\phi_0\rangle = e^{i\varphi}|\phi_0\rangle$. Finally, we obtain

$$G(x',x'') = \frac{-i\left\langle T\big[\hat{\psi}_{H_0}(x')\hat{\psi}^{\dagger}_{H_0}(x'')\ \hat{S}\big]\right\rangle_0}{\langle\hat{S}\rangle_0}. \tag{11.30}$$

For the noninteractig system $\hat{S}=1$ and the Green's function reduces to

$$G^{(0)}(x',x'') = -i\left\langle T\hat{\psi}_{H_0}(x')\hat{\psi}^{\dagger}_{H_0}(x'')\right\rangle_0. \tag{11.31}$$

Equation (11.30) is the starting point of a diagrammatic method to calculate the Green's function G. An important property of Eq. (11.30) is that $G(x',x'')$ is expressed entirely in terms of field operators of a *noninteracting system* and the averaging is also performed with respect to a *noninteracting* ground state. Therefore, it is possible to expand the evolution operator $\hat{S}$ in powers of the interaction potential and apply Wick's theorem for the averages of products of ψ_{H_0}-operators. For example, expanding the numerator of iG given by Eq. (11.30) we obtain

$$\begin{aligned}&\left\langle T\big[\hat{\psi}_{H_0}(x')\hat{\psi}^{\dagger}_{H_0}(x'')\ \hat{S}\big]\right\rangle_0 = \\ &\qquad\sum_{n=0}^{\infty}\frac{(-i)^n}{n!}\int dt_1\cdots dt_n\ \left\langle T\hat{\psi}_{H_0}(x')\hat{\psi}^{\dagger}_{H_0}(x'')\hat{H}^{\rm int}_{H_0}(t_1)\cdots\hat{H}^{\rm int}_{H_0}(t_n)\right\rangle_0.\end{aligned} \tag{11.32}$$

After substituting $\hat{H}^{\rm int}_{H_0}$ from Eq. (11.27) and applying the Wick's theorem, we end up with an expression which contains just the following types of averages:

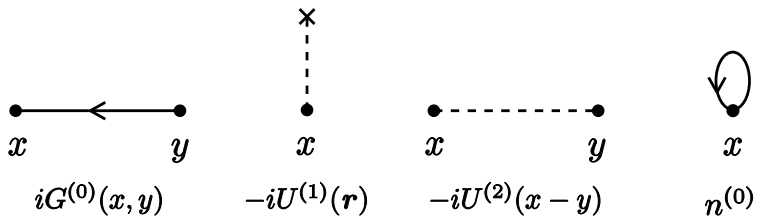

Fig. 13: **Basic diagram elements.** *The solid line represents the noninteracting Green's function $iG^{(0)}(x,y)$. The end points (so-called vertices) are associated with the arguments x and y. The order of arguments is indicated by the arrow which points in the direction of time propagation. The dashed line with a single vertex x represents the interaction with an external field and corresponds to $-iU^{(1)}(\boldsymbol{r})$. The dashed line with two vertices x and y represents a two-particle interaction term $-iU^{(2)}(x-y) \equiv -i\delta(t_x - t_y)U^{(2)}(\boldsymbol{r}_x - \boldsymbol{r}_y)$. [In this case there is no need to specify the order of arguments because $U^{(2)}(x-y) = U^{(2)}(y-x)$.] The simple solid-line loop stands for the noninteracting particle density $n^{(0)}$.*

$\langle T\hat{\psi}_{H_0}(x)\hat{\psi}^\dagger_{H_0}(y)\rangle_0 = iG^{(0)}(x,y)$, $\langle T\hat{\psi}^\dagger_{H_0}(y)\hat{\psi}_{H_0}(x)\rangle_0 = -iG^{(0)}(x,y)$, and $\langle\hat{\psi}^\dagger_{H_0}(x) \times \hat{\psi}_{H_0}(x)\rangle_0 = n^{(0)} \equiv N^{(0)}/V = (2m\mu)^{3/2}/(3\pi^2)$. Therefore, the exact Green's function G is expressed in terms of the Green's functions of a noninteracting system $G^{(0)}$ and the noninteracting particle density $n^{(0)}$.

The summation in Eq. (11.32) can be performed systematically by using a diagrammatic representation of different terms. The basic diagram elements are shown in Fig. 13. By expansion of Eq. (11.32), it is easy to see that each diagram consists of two outer $G^{(0)}$-lines with vertices x' and x'', and a number of inner vertices $x_1, x_2, \ldots$ in which two $G^{(0)}$-lines and one interaction line meet. A few low-order diagrams are shown in Fig. 14. They correspond to the following terms on the right hand side of Eq. (11.32):

$$\text{(a):}\quad i\int dx\; U^{(1)}(\boldsymbol{r})\; G^{(0)}(x',x)G^{(0)}(x,x''), \tag{11.33a}$$

$$\text{(b):}\quad -\int dx_1dx_2\; U^{(2)}(x_1-x_2)\; G^{(0)}(x',x_1)G^{(0)}(x_1,x_2)G^{(0)}(x_2,x''), \tag{11.33b}$$

$$\text{(c):}\quad in^{(0)}\int dx_1dx_2\; U^{(2)}(x_1-x_2)\; G^{(0)}(x',x_1)G^{(0)}(x_1,x''), \tag{11.33c}$$

$$\text{(d):}\quad G^{(0)}(x',x'')\int dx_1dx_2\; U^{(2)}(x_1-x_2)\; G^{(0)}(x_2,x_1)G^{(0)}(x_1,x_2). \tag{11.33d}$$

The diagrams shown in Fig. 14 (a) – (c) are connected, while the one shown in (d) is disconnected. The disconnected diagram contains a closed loop unattached to the connected part with the outer vertices x' and x''. Higher-order disconnected diagrams may contain one or more disconnected parts. These parts give multiplicative contributions to the diagram.

The important property of a diagrammatic technique is that the contribution of all disconnected parts, *in all orders of perturbation theory*, exactly cancels the denominator $\langle\hat{S}\rangle_0$ in Eq. (11.30) [126]. Therefore, to calculate G it is sufficient to consider only connected diagrams. Furthermore, all diagrams of the same form, which differ in a permutation of labels of internal vertices, give the same contribution and cancel the factor $1/n!$ on the right hand side of Eq. (11.32). Thus, only topologically nonequivalent diagrams should be taken into account. We summarize

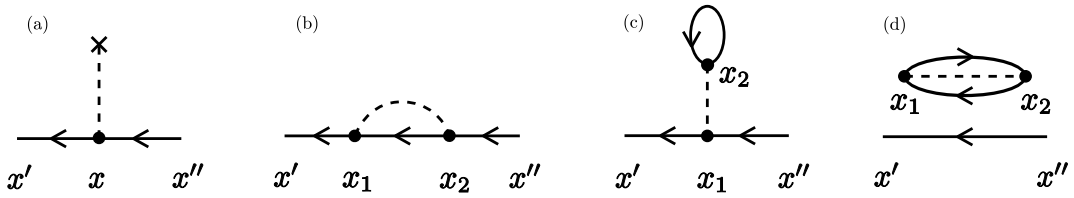

Fig. 14: *Several first-order diagrams which illustrate the usage of the basic diagram elements shown in Fig. 13. The outer $G^{(0)}$-lines contain outer vertices x' and x''. In the inner vertices, two $G^{(0)}$-lines and one interaction line meet. The corresponding analytical expressions are given by Eq.* (11.33). *The diagrams (a) – (c) are connected while (d) is disconnected. Note that the disconnected parts give a multiplicative contributions to the diagram, Eq.* (11.33*d*).

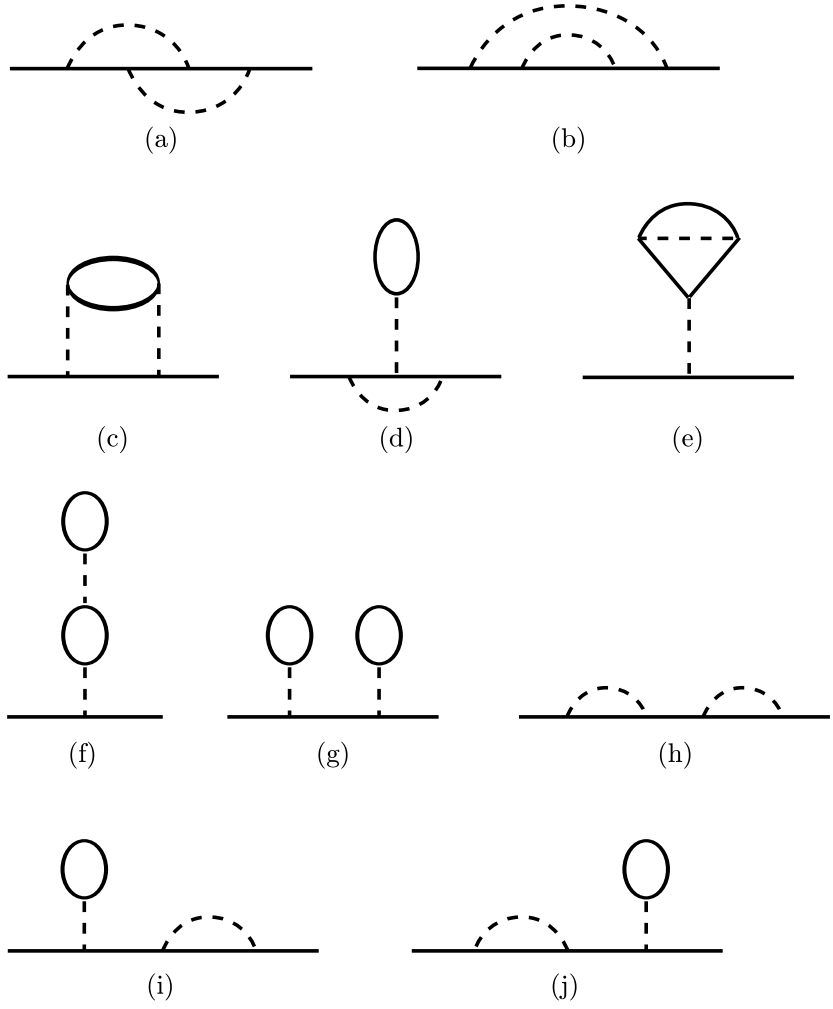

Fig. 15: *The second-order diagrams for the case of two-particle interactions. The labels of vertices are suppressed for simplicity. The diagrams shown in panels (a) – (f) are irreducible because they cannot be split into 2 subdiagrams connected with a single solid line. The diagrams (g) – (j) are reducible.*

this by writing symbolically

$$G(x', x'') = -i \left\langle T\left[\hat{\psi}_{H_0}(x')\hat{\psi}^{\dagger}_{H_0}(x'')\ \hat{S}\right]\right\rangle_{0\ \mathrm{con}}, \tag{11.34}$$

where "con" denotes that the perturbation expansion is done in terms of connected and topologically nonequivalent diagrams only.

We now formulate the set of rules which are used to calculate the correction $iG^{(n)}(x', x'')$ of order n [127]:

(1) Form all connected, topologically nonequivalent diagrams with external points x' and x'' and n dashed lines, where in each vertex one dashed and two solid lines meet.
(2) Associate the diagram elements with the corresponding Green's functions and interaction potentials as shown in Fig. 13.
(3) Integrate over all internal vertex coordinates x ($dx = dtd\boldsymbol{r}$), and sum over all internal spin variables.
(4) Multiply the result with $(-1)^L$, where L denotes the number of closed solid-line loops with more than one vertex.

As an illustration, we show in Fig. 15 all 10 diagrams of second-order for the case of a two-particle interaction. The first-order diagrams are shown in Fig. 14 (b) and (c).

§ **11.5. Self-energy.** The most important property of a diagrammatic technique, which makes it advantageous over the ordinary perturbation theory, is the possibility of a partial summation of diagrams in blocks. According to the general rules discussed in the previous paragraph, the coefficient which multiplies a diagram does not depend on its order.[18] Therefore, the subdiagrams have analytical representations which are independent of the properties of the composite (total) diagram, and can be calculated separately. Furthermore, it is possible to sum up several subdiagrams and form new diagrammatic blocks which can be used to build more complicated ones.[19] One of these blocks is the self-energy.

In order to define the self-energy let us divide all diagrams for G into two groups: the reducible diagrams which can be split into 2 subdiagrams connected with a single solid line, and the rest which are the irreducible ones. Among the second-order diagrams shown in Fig. 15, the diagrams (a) – (f) are irreducible, while (g) – (j) are reducible. The contribution δG of all irreducible diagrams can be written in the following form

$$\delta[iG(x', x'')] = \int dx_1 dx_2 \; iG^{(0)}(x', x_1) \; [-i\Sigma(x_1, x_2)] \; iG^{(0)}(x_2, x''). \tag{11.35}$$

Here we explicitly denote the outer $G^{(0)}$-lines, while the self-energy term $-i\Sigma$ stands for the sum of all inner irreducible parts.

It is convenient to associate the exact Green's function and the self-energy with a diagram elements as shown in Fig. 16 (a,b). Since all irreducible diagrams are contained in the self-energy, the exact Green's function consists of self-energy parts connected with $G^{(0)}$-lines [Fig. 16 (c)]. Therefore, the exact Green's function is given

---

[18] This is because the factor $1/n!$ on the right hand side of Eq. (11.32) is cancelled by $n!$ equal contributions of different pairings of ψ-operators. This is taken into account by considering only topologically nonequivalent diagrams.

[19] Here we note that in the finite-temperature Green's functions technique, the thermodynamic potential $\Omega_{\rm td}$ can also be represented in terms of connected topologically nonequivalent diagrams. In contrast to the diagrams for G which are open (with two outer vertices), the diagrams for $\Omega_{\rm td}$ are closed (with no outer vertices). In this case the analytical representations do depend on the order of the diagrams, which makes the block-summations inconvenient [126].

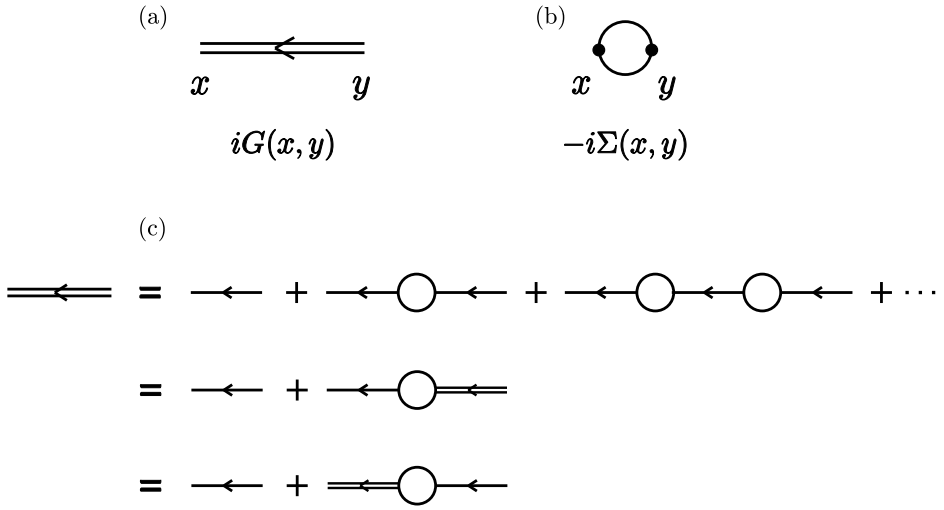

Fig. 16: *The exact Green's function [panel (a)] and the self-energy [panel (b)] are associated with the double solid line and the circle, respectively. The diagrammatic expansion of the exact Green's function in terms of the self-energy is shown in panel (c).*

by the following left and right Dyson equations:

$$G(x', x'') = G^{(0)}(x', x'') + \int dx_1 dx_2 \; G^{(0)}(x', x_1)\Sigma(x_1, x_2)G(x_2, x'') \qquad (11.36a)$$

$$= G^{(0)}(x', x'') + \int dx_1 dx_2 \; G(x', x_1)\Sigma(x_1, x_2)G^{(0)}(x_2, x''). \qquad (11.36b)$$

Equations (11.36) express the exact Green's function G in terms of the self-energy Σ which contains just irreducible diagrams. The exact summation of Σ is not possible in general since this would represent an exact solution of the interacting problem. Various approximation schemes are used instead, depending on the system under consideration [125, 129, 130].

§ **11.6. Nonequilibrium (Keldysh) Green's functions.** In the previous paragraphs we have introduced the diagrammatic technique for the calculation of the Green's function G in equilibrium at zero temperature. The starting point was Eq. (11.30) in which G was expressed in terms of the field operators and the initial state of a *noninteracting system*. In this paragraph we outline the Keldysh Green's functions technique which is applicable both at finite temperatures and out of equilibrium [128, 130, 133].

First we generalize the notion of evolution by assuming that the time arguments lie on the ordered Keldysh contour C depicted in Fig. 17. The contour C consists

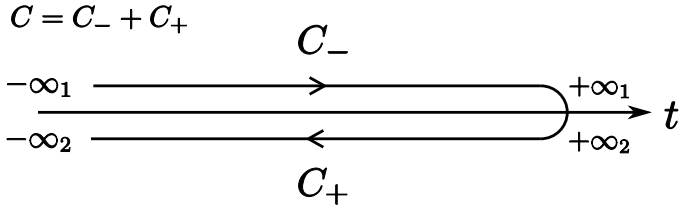

Fig. 17: **Definition of the Keldysh contour.***The contour consists of the forward propagation branch C_- and the backward propagation branch C_+ which are connected at $t = +\infty$.*

of the forward branch C_- and the backward branch C_+ which are connected at $t = +\infty$. The generalized evolution operator along the contour is defined by

$$\hat{U}_{\mathcal{H}}(t', t'') = T_c \, e^{-i \int_{ct''}^{t'} \hat{\mathcal{H}}(t) dt}. \tag{11.37}$$

Here $t', t'' \in C$ and the time-ordering T_c and the integration $\int_c dt$ are performed along the contour. The time-ordering T_c coincides with T ($\tilde{T}$) on the C_- (C_+) branch. For example, if the initial time $t'' \in C_-$ and the final time $t' \in C_+$ we have

$$\begin{aligned} \hat{U}_{\mathcal{H}}(t', t'') &= \left(\tilde{T} e^{-i \int_{+\infty_2}^{t'} \hat{\mathcal{H}}(t) dt}\right) \left(T e^{-i \int_{t''}^{+\infty_1} \hat{\mathcal{H}}(t) dt}\right) \\ &= \left(\tilde{T} e^{i \int_{t'}^{+\infty} \hat{\mathcal{H}}(t) dt}\right) \left(T e^{-i \int_{t''}^{+\infty} \hat{\mathcal{H}}(t) dt}\right). \end{aligned} \tag{11.38}$$

The Hamiltonian $\hat{\mathcal{H}}(t)$ is taken to be the same on both branches. The evolution of the field operators along the contour is defined by $\hat{\psi}_{\mathcal{H}}(x) = \hat{U}^{\dagger}_{\mathcal{H}}(t, -\infty_1) \, \hat{\psi}(\boldsymbol{r}) \, \hat{U}_{\mathcal{H}}(t, -\infty_1)$ and $\hat{\psi}^{\dagger}_{\mathcal{H}}(x) = \hat{U}^{\dagger}_{\mathcal{H}}(t, -\infty_1) \, \hat{\psi}^{\dagger}(\boldsymbol{r}) \, \hat{U}_{\mathcal{H}}(t, -\infty_1)$ where $t \in C$. From Eq. (11.37) we obtain $\hat{U}_{\mathcal{H}}(t', -\infty_1) = T \exp[-i \int_{-\infty}^{t'} \hat{\mathcal{H}}(t) dt]$, i.e., the contour-ordered evolution from the initial time $t'' = -\infty_1$ to $t' \in C$ coincides with the usual evolution from $-\infty$ to t', regardless the branch of t'. Therefore, the field operators $\psi_{\mathcal{H}}(x)$ also coincide with the usual ones, regardless the branch. This is because the forward evolution from t' to ∞ on C_- is cancelled by the backward evolution from ∞ to t' on C_+.[20)]

A quantity which possesses a simple diagrammatic expansion is the contour-ordered Green's function defined by

$$G_c(x', x'') = -i \left\langle T_c \hat{\psi}_{\mathcal{H}}(x') \hat{\psi}^{\dagger}_{\mathcal{H}}(x'') \right\rangle_H = \begin{cases} -i \langle \hat{\psi}_{\mathcal{H}}(x') \hat{\psi}^{\dagger}_{\mathcal{H}}(x'') \rangle_H, & t' >_c t'' \\ i \langle \hat{\psi}^{\dagger}_{\mathcal{H}}(x'') \hat{\psi}_{\mathcal{H}}(x') \rangle_H, & t'' >_c t' \end{cases}, \tag{11.39}$$

where $t', t'' \in C$. Rewriting $\psi_{\mathcal{H}}$ in the interaction picture with respect to $\hat{H}$, we obtain

$$G_c(x', x'') = -i \left\langle T_c \big[\hat{\psi}_H(x') \hat{\psi}^{\dagger}_H(x'') \hat{S}_{H'_H} \big] \right\rangle_H. \tag{11.40}$$

Here $\hat{S}_{H'_H} \equiv \hat{S}_{H'_H}(-\infty_2, -\infty_1)$ is the contour-ordered evolution operator in the interaction picture, defined in analogy with Eq. (11.37). Next we express the averaging $\langle \cdots \rangle_H$ over the interacting state in terms of the averaging $\langle \cdots \rangle_{H_0}$ over the non-interacting one. To do this, we consider the decomposition $\hat{H} = \hat{H}_0 + \hat{H}_{\rm int}$ and use the definition of the evolution operator $\hat{S}_{H^{\rm int}_{H_0}}$ in the interaction picture with respect to H_0: $\hat{U}_H(t, t_0) = \hat{U}_{H_0}(t, t_0) \hat{S}_{H^{\rm int}_{H_0}}(t, t_0)$. Since $\hat{H}$ and $\hat{H}_0$ do not depend on time we have $e^{-i\hat{H}(t-t_0)} = e^{-i\hat{H}_0(t-t_0)} \hat{S}_{H^{\rm int}_{H_0}}(t, t_0)$. Putting $t = t_0 - i\beta$ we find $e^{-\beta \hat{H}} = e^{-\beta \hat{H}_0} \hat{S}^{(i)}$, where we denote $\hat{S}^{(i)} \equiv \hat{S}_{H^{\rm int}_{H_0}}(t_0 - i\beta, t_0)$ and assume ordering along the imaginary time axis as depicted in Fig. 18 (a). The contour-ordered Green's function becomes

$$G_c(x', x'') = \frac{-i \left\langle \hat{S}^{(i)} T_c \big[\hat{\psi}_H(x') \hat{\psi}^{\dagger}_H(x'') \hat{S}_{H'_H} \big] \right\rangle_{H_0}}{\left\langle \hat{S}^{(i)} \right\rangle_{H_0}}. \tag{11.41}$$

[20)] In § 13.1 we present an extension of the Keldysh technique in which the Hamiltonian $\hat{\mathcal{H}}(t)$ is different at C_- and C_+ branches. In this case the contour-ordered evolution $\hat{U}_{\mathcal{H}}(t, -\infty_1)$ and operators $\psi_{\mathcal{H}}(x)$ also differ at different branches of t.

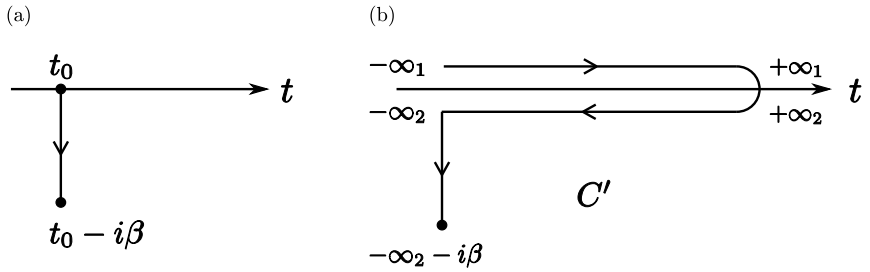

Fig. 18: *Panel (a): The ordering on the imaginary time axis which is used to express the average* $\langle \cdots \rangle_H$ *in terms of* $\langle \cdots \rangle_{H_0}$. *Panel (b): The complete contour* C' *which is used in the Keldysh technique. The time dependent part of Hamiltonian* $H'(t)$ *is defined to vanish on the imaginary branch of* C'.

Finally, it is necessary to express the ψ_H operators in terms of ψ_{H_0}. For $t' >_c t''$ we obtain

$$T_c\big[\hat{\psi}_H(x')\hat{\psi}^\dagger_H(x'')\hat{S}_{H'_H}\big] = \hat{S}_{H'_H}(-\infty_2, t')\hat{S}^\dagger_{H^{\rm int}_{H_0}}(t', -\infty_1)\hat{\psi}_{H_0}(t')\hat{S}_{H^{\rm int}_{H_0}}(t', -\infty_1)$$
$$\times \hat{S}_{H'_H}(t', t'')\hat{S}^\dagger_{H^{\rm int}_{H_0}}(t'', -\infty_1)\hat{\psi}^\dagger_{H_0}(t'')\hat{S}_{H^{\rm int}_{H_0}}(t'', -\infty_1)\hat{S}_{H'_H}(t'', -\infty_1). \quad (11.42)$$

The product of operators $\hat{S}_{H^{\rm int}_{H_0}}$ and $\hat{S}_{H'_H}$ can be transformed in the following way. Let us consider the two ways of decomposing the total Hamiltonian, $\hat{\mathcal{H}}(t) = \hat{H} + \hat{H}'(t)$ and $\hat{\mathcal{H}}(t) = \hat{H}_0 + \hat{V}(t)$, where $\hat{H} = \hat{H}_0 + \hat{H}_{\rm int}$ and $\hat{V}(t) = \hat{H}_{\rm int} + \hat{H}'(t)$. The Heisenberg evolution $\hat{U}_{\mathcal{H}}$ which corresponds to the first decomposition is given by $\hat{U}_{\mathcal{H}} = \hat{U}_H\hat{S}_{H'_H} = \hat{U}_{H_0}\hat{S}_{H^{\rm int}_{H_0}}\hat{S}_{H'_H}$, while the one which corresponds to the second is $\hat{U}_{\mathcal{H}} = \hat{U}_{H_0}\hat{S}_{V_{H_0}}$. Therefore, we find $\hat{S}_{H^{\rm int}_{H_0}}\hat{S}_{H'_H} = \hat{S}_{V_{H_0}}$. Substituting into Eq. (11.42) and using that $\hat{S}_{H'_H}(t', t'') = \hat{S}_{H'_H}(t', -\infty_1)\hat{S}^\dagger_{H'_H}(t'', -\infty_1)$ and $\hat{S}_{H'_H}(-\infty_2, t') = \hat{S}^\dagger_{H'_H}(t', -\infty_1)$ we obtain

$$T_c\big[\hat{\psi}_H(x')\hat{\psi}^\dagger_H(x'')\hat{S}_{H'_H}\big] = \hat{S}_{V_{H_0}}(-\infty_2, t')\hat{\psi}_{H_0}(t')\hat{S}_{V_{H_0}}(t', t'')\hat{\psi}^\dagger_{H_0}(t'')\hat{S}_{V_{H_0}}(t'', -\infty_1). \quad (11.43)$$

If we define $\hat{H}'(t) \equiv 0$ on the imaginary part of the contour depicted in Fig. 18 (a), we can write in a compact form

$$\hat{S}^{(i)}T_c\big[\hat{\psi}_H(x')\hat{\psi}^\dagger_H(x'')\hat{S}_{H'_H}\big] = T_{c'}\big[\hat{\psi}_{H_0}(x')\hat{\psi}^\dagger_{H_0}(x'')\hat{S}_{V_{H_0}}\big]. \quad (11.44)$$

Here $\hat{S}_{V_{H_0}} \equiv \hat{S}_{V_{H_0}}(-\infty_2 - i\beta, -\infty_1)$ and the ordering $T_{c'}$ is performed along the contour C' depicted in Fig. 18 (b). A similar analysis shows that the result holds also for $t'' >_c t'$. The operator $\hat{S}^{(i)}$ can be written as $\hat{S}^{(i)} = T_{c'}\hat{S}_{V_{H_0}}$ and the contour-ordered Green's function reduces to

$$G_c(x', x'') = \frac{-i\left\langle T_{c'}\big[\hat{\psi}_{H_0}(x')\hat{\psi}^\dagger_{H_0}(x'')\hat{S}_{V_{H_0}}\big]\right\rangle_{H_0}}{\left\langle T_{c'}\hat{S}_{V_{H_0}}\right\rangle_{H_0}}. \quad (11.45)$$

Equation (11.45) is the starting point of the Keldysh diagrammatic technique. It expresses G_c in terms of the noninteracting field operators averaged over the initial equilibrium state of a noninteracting system. The diagrammatic technique is obtained by expanding $\hat{S}_{V_{H_0}}$ and applying the statistical Wick theorem. The result is obtained readily by noting that Eq. (11.45) has the same structure as Eq. (11.30) which has been discussed in the zero-temperature case. Therefore, the

diagrams in the Keldysh technique are exactly the same as in the zero-temperature case. In particular, the denominator of Eq. (11.45) cancels the contribution of all disconnected diagrams in all orders, which allows to restrict the consideration just to connected and topologically nonequivalent ones:

$$G_c(x',x'') = -i\left\langle T_{c'}\left[\hat{\psi}_{H_0}(x')\hat{\psi}^\dagger_{H_0}(x'')\hat{S}_{V_{H_0}}\right]\right\rangle_{H_0\ \mathrm{con}}. \tag{11.46}$$

The only modification in the Keldysh technique is the different analytical representation of diagrams which takes into account that the time arguments can be on different branches.

The contour-ordered Green's function G_c reduces to $G^{\pm\pm}$ given by Eq. (11.7), depending on the branch of time arguments:[21)]

$$t' \in C_i,\ t'' \in C_j \quad \Rightarrow \quad G_c(x',x'') = G^{ij}(x',x''), \tag{11.47}$$

where $i,j \in \{-,+\}$. The last equation establishes a mapping between the contour-ordered and the matrix Keldysh Green's function $\breve{G}$ defined by

$$G_c(x',x'') \quad \to \quad \breve{G}(x',x'') \equiv \begin{pmatrix} G^{--}(x',x'') & G^{-+}(x',x'') \\ G^{+-}(x',x'') & G^{++}(x',x'') \end{pmatrix}. \tag{11.48}$$

The rules which are used to calculate correction $iG^{(n)ij}(x',x'')$ of order n are similar as in the zero-temperature case, with the following modifications [128]. In the Keldysh technique, vertices acquire an additional branch index $k = \{-,+\}$. A solid line with vertices $(xk;yl)$ is associated with $iG^{(0)kl}(x,y)$. A dashed line with the single vertex (xk) is associated with the single-particle interaction potential $\mathrm{sgn}(k)\, iU^{(1)}(x)$. A dashed line with two vertices is labelled with equal branch indices, $(xk;yk)$, and corresponds to the two-particle interaction potential $\mathrm{sgn}(k)\, iU^{(2)}(x-y)$. A solid line loop with the vertex (xk) corresponds to $n^{(0)}$, irrespective of the branch index. The correction $iG^{(n)ij}(x',x'')$ is calculated by summing up all connected and topologically nonequivalent diagrams of nth order with outer vertices $(x'i;x''j)$ and all possible branch labellings of inner vertices.[22)]

§ **11.7. Dyson equations.** The self-energy in the Keldysh technique is introduced in analogy with the zero-temperature case, with G and Σ replaced by Keldysh matrices $\breve{G}$ and $\breve{\Sigma}$. The matrix components of $\breve{\Sigma}$ are denoted as

$$\breve{\Sigma} \equiv \begin{pmatrix} \Sigma^{--} & \Sigma^{-+} \\ \Sigma^{+-} & \Sigma^{++} \end{pmatrix} \tag{11.49}$$

and satisfy $\Sigma^{--} + \Sigma^{-+} + \Sigma^{+-} + \Sigma^{++} = 0$ [128]. The exact Keldysh Green's function is given by Dyson equations

$$\breve{G}(x',x'') = \breve{G}^{(0)}(x',x'') + \int dx_1 dx_2\ \breve{G}^{(0)}(x',x_1)\breve{\Sigma}(x_1,x_2)\breve{G}(x_2,x'') \tag{11.50a}$$

$$= \breve{G}^{(0)}(x',x'') + \int dx_1 dx_2\ \breve{G}(x',x_1)\breve{\Sigma}(x_1,x_2)\breve{G}^{(0)}(x_2,x''). \tag{11.50b}$$

---

21) The imaginary part of the contour C' takes into account correlations in the initial state introduced by $\hat{H}_{\mathrm{int}}$ before the external perturbation $\hat{H}'(t)$ is turned on. If the initial correlations are negligible [e.g., if the system is in the equilibrium state $\hat{\rho}_{H_0}$ before switching on $\hat{H}'(t)$], then the imaginary part of the contour C' can be neglected [133].

22) In an alternative formulation [133], the diagrammatic technique is performed in terms of the Keldysh matrices rather than matrix components. In this case the diagram elements and vertices acquire matrix structure which takes account of the branch labelling.

By applying $\hat{G}^{-1}_{0x} \equiv i\partial_t - \hat{h}_0(x)$ on Eq. (11.50) we obtain the left and right Dyson equations in integro-differential form:

$$\hat{G}^{-1}_{0x'}\,\breve{G}(x',x'') = \breve{\tau}_3\delta(x'-x'') + \int dx\ \breve{\tau}_3\breve{\Sigma}(x',x)\breve{G}(x,x''), \tag{11.51a}$$

$$\hat{G}^{-1*}_{0x''}\,\breve{G}(x',x'') = \breve{\tau}_3\delta(x'-x'') + \int dx\ \breve{G}(x',x)\breve{\Sigma}(x,x'')\breve{\tau}_3. \tag{11.51b}$$

Here $\hat{h}_0(x) = -\nabla^2/2m - \mu$ and we used that $\hat{G}^{-1}_{0x'}\,\breve{G}^{(0)}(x',x'') = \hat{G}^{-1*}_{0x''}\,\breve{G}^{(0)}(x',x'') = \breve{\tau}_3\delta(x'-x'')$.

Equations (11.50) and (11.51) contain a redundancy which is associated with the linear dependence of the matrix components. Without loss of generality we can choose the linearly independent components $G^{R,A,K}$ given by Eq. (11.10), and introduce a new matrix representation by

$$\check{G} \equiv \check{L}\check{\tau}_3\breve{G}\check{L}^\dagger = \begin{pmatrix} G^R & G^K \\ 0 & G^A \end{pmatrix}, \qquad \check{\Sigma} \equiv \check{L}\breve{\Sigma}\check{\tau}_3\check{L}^\dagger = \begin{pmatrix} \Sigma^R & \Sigma^K \\ 0 & \Sigma^A \end{pmatrix}. \tag{11.52}$$

Here $\check{L} = (\check{1} - i\check{\tau}_2)/\sqrt{2}$ and

$$\Sigma^K = \Sigma^{--} + \Sigma^{++} = -(\Sigma^{+-} + \Sigma^{-+}), \tag{11.53a}$$

$$\Sigma^R = \Sigma^{--} + \Sigma^{-+} = -(\Sigma^{++} + \Sigma^{+-}), \tag{11.53b}$$

$$\Sigma^A = \Sigma^{--} + \Sigma^{+-} = -(\Sigma^{++} + \Sigma^{-+}). \tag{11.53c}$$

In the new representation, the Dyson equations (11.50) and (11.51) become

$$\check{G}(x',x'') = \check{G}^{(0)}(x',x'') + \int dx_1dx_2\ \check{G}^{(0)}(x',x_1)\check{\Sigma}(x_1,x_2)\check{G}(x_2,x'') \tag{11.54a}$$

$$= \check{G}^{(0)}(x',x'') + \int dx_1dx_2\ \check{G}(x',x_1)\check{\Sigma}(x_1,x_2)\check{G}^{(0)}(x_2,x'') \tag{11.54b}$$

and

$$\hat{G}^{-1}_{0x'}\,\check{G}(x',x'') = \check{1}\delta(x'-x'') + \int dx\ \check{\Sigma}(x',x)\check{G}(x,x''), \tag{11.55a}$$

$$\hat{G}^{-1*}_{0x''}\,\check{G}(x',x'') = \check{1}\delta(x'-x'') + \int dx\ \check{G}(x',x)\check{\Sigma}(x,x''). \tag{11.55b}$$

The four Dyson equations (11.54) and (11.55) are equivalent. Each of them constitutes a complete set of equations for the components $\check{G}^{R,A,K}$. Furthermore, because of the symmetry relation between G^R and G^A given by Eq. (11.10a), the whole theory can be formulated in terms of G^A and G^K only. However, the two coupled equations for G^A and G^K are difficult to solve because of the complicated integral (or integro-differential) structure and the presence of the self-energy term. The equations simplify considerably in the quasiclassical approximation which neglects the fast oscillations of Green's functions with respect to the relative coordinate $\boldsymbol{r}' - \boldsymbol{r}''$ (on the scale of Fermi wavelength λ_F) and keeps the slow change with respect to the center of mass coordinate $\boldsymbol{r} = (\boldsymbol{r}' + \boldsymbol{r}'')/2$. The quasiclassical theory is elaborated in detail in Ref. [125]. The self-energy is usually calculated approximately, depending on the interaction in question. For example, the averaging over nonmagnetic impurities with potential $u(\boldsymbol{r})$ is described by

$$\check{\Sigma}_{\mathcal{E}'\mathcal{E}''}(\boldsymbol{p},\boldsymbol{p}-\boldsymbol{k}) = n_{\rm imp}\int \frac{d\boldsymbol{p}_1}{(2\pi)^3}\,|u(\boldsymbol{p}-\boldsymbol{p}_1)|^2\,\check{G}_{\mathcal{E}'\mathcal{E}''}(\boldsymbol{p}_1,\boldsymbol{p}_1-\boldsymbol{k}) \tag{11.56}$$

in the self-consistent Born approximation, where $n_{\rm imp}$ is the impurity concentration. The expression for $\check{\Sigma}$ can be further simplified by taking into account that transport properties are governed by the electrons in the vicinity of the Fermi surface, $|\boldsymbol{p}|, |\boldsymbol{p}_1| \approx p_F$. In this case $|u(\boldsymbol{p}-\boldsymbol{p}_1)| = |u(\theta)|$ where $\theta = \angle(\boldsymbol{p}, \boldsymbol{p}_1)$. For isotropic scattering $|u(\theta)| = |u| = \text{const}$ and we obtain

$$\check{\Sigma}_{\mathcal{E}'\mathcal{E}''}(\boldsymbol{p}, \boldsymbol{p}-\boldsymbol{k}) = \frac{1}{2\pi\mathcal{V}(0)\tau_{\rm imp}} \int \frac{d\boldsymbol{p}_1}{(2\pi)^3}\, \check{G}_{\mathcal{E}'\mathcal{E}''}(\boldsymbol{p}_1, \boldsymbol{p}_1-\boldsymbol{k}). \tag{11.57}$$

The characteristic time for impurity scattering $\tau_{\rm imp}$ is given by $\tau_{\rm imp}^{-1} = 2\pi\mathcal{V}(0)n_{\rm imp}|u|^2$, where $\mathcal{V}(0) = mp_F/2\pi^2$ is the density of states per spin per volume at the Fermi level.[23)] We note that $\check{\Sigma}$ for isotropic scattering does not depend on direction of the incoming momentum $\boldsymbol{p}$.

§ **11.8. Averages in the Keldysh technique. Distribution function.** To complete the introduction to the nonequilibrium Keldysh technique, we have to specify the relationship between the Green's functions $G^{R,A,K}$ and observable quantities. As already discussed in § 11.3, the one-particle averages can be obtained from Eq. (11.18) using the time-ordered Green's function $G_{\beta\alpha}(t, \boldsymbol{r}; t+0, \boldsymbol{r}')$. This way of expressing one-particle averages is particularly useful in the equilibrium zero-temperature technique in which only the time-ordered Green's function appears. In the nonequilibrium technique it is more convenient to use the lesser Green's function which is continuous at equal time arguments and reduces to the time-ordered one, $G^{-+}_{\beta\alpha}(t, \boldsymbol{r}; t, \boldsymbol{r}') = G_{\beta\alpha}(t, \boldsymbol{r}; t+0, \boldsymbol{r}')$. The lesser Green's function G^{-+} can be expressed in terms of $G^{R,A,K}$ using Eqs. (11.10):

$$G^{-+} = \frac{1}{2}\big(G^K + G^A - G^R\big). \tag{11.58}$$

Equations (11.18) and (11.58) give the prescription of how to calculate one-particle averages in terms of $G^{R,A,K}$.

In the following we consider the occupation numbers of single-particle states for the many-body system out of equilibrium. Let $\{|f\rangle|\alpha\rangle\}$ be the uncorrelated single-particle basis with α being the spin index and f the set of discrete orbital quantum numbers. The occupation numbers of orbital states are given by $n_f(t) = \sum_\alpha \langle \hat{a}^\dagger_{f\alpha\mathcal{H}}(t)\hat{a}_{f\alpha\mathcal{H}}(t)\rangle_H$, with the sum taken over both spin orientations. The total number of particles is given by $N = \sum_f n_f$. Transforming Eq. (11.21) to the f-basis, we find

$$n_f(t) = \int d\boldsymbol{r}' d\boldsymbol{r}''\, \varphi^*_f(\boldsymbol{r}')\varphi_f(\boldsymbol{r}'') \sum_\alpha [-iG^{-+}_{\alpha\alpha}(t, \boldsymbol{r}'; t, \boldsymbol{r}'')], \tag{11.59}$$

where $\varphi_f(\boldsymbol{r}) \equiv \langle \boldsymbol{r}|f\rangle$. Substituting G^{-+} from Eq. (11.58) and using that $G^A - G^R = G^{-+} - G^{+-}$ and the relation (11.9*a*) between the lesser and the greater Green's functions at equal times we obtain

$$n_f(t) = \frac{1 - h_f(t)}{2}, \tag{11.60}$$

[23)] The mean free path and diffusion constant are defined by $l = v_F\tau_{\rm imp}$ and $D = v_F l/3$. The normal-state Drude conductivity is given by $\sigma_n = ne^2\tau_{\rm imp}/m = 2\mathcal{V}(0)e^2D$ where $n = p_F^3/3\pi^2$ is the electron density. The self-consistent Born approximation is the lowest order approximation in $u/\mathcal{E}_F, 1/(p_F l) \ll 1$.

where

$$h_f(t) = \int d\boldsymbol{r}' d\boldsymbol{r}''\ \varphi_f^*(\boldsymbol{r}')\varphi_f(\boldsymbol{r}'') \sum_\alpha \left[iG^K_{\alpha\alpha}(t,\boldsymbol{r}';t,\boldsymbol{r}'')\right]. \tag{11.61}$$

Therefore, the average occupations of the single-particle states out of equilibrium are completely determined by the Keldysh component G^K.

Often it is convenient to choose the momentum single-particle eigenbasis $\{|\boldsymbol{p}\rangle\}$. In this case it is useful to define the generalized particle distribution function $n(t,\boldsymbol{r},\boldsymbol{p})$ as the Fourier transform of $-iG^{-+}$ with respect to the relative coordinate (the so called mixed coordinate-momentum or Wigner representation):

$$n(t,\boldsymbol{r},\boldsymbol{p}) = \int d\boldsymbol{r}'\ e^{-i\boldsymbol{p}\boldsymbol{r}'} \sum_\alpha \left[-iG^{-+}_{\alpha\alpha}\left(t,\boldsymbol{r}+\frac{\boldsymbol{r}'}{2};t,\boldsymbol{r}-\frac{\boldsymbol{r}'}{2}\right)\right]. \tag{11.62}$$

From Eq. (11.21) we find that the particle number density $N(t,\boldsymbol{r})$ and the average occupation numbers $N(t,\boldsymbol{p})$ are given by

$$N(t,\boldsymbol{r}) = \int \frac{d\boldsymbol{p}}{(2\pi)^3}\ n(t,\boldsymbol{r},\boldsymbol{p}), \qquad N(t,\boldsymbol{p}) = \int d\boldsymbol{r}\ n(t,\boldsymbol{r},\boldsymbol{p}), \tag{11.63a,b}$$

with the normalization to the total number of particles given by

$$N = \int d\boldsymbol{r}\ N(t,\boldsymbol{r}) = \int \frac{d\boldsymbol{p}}{(2\pi)^3}\ N(t,\boldsymbol{p}). \tag{11.64}$$

For the noninteracting gas in equilibrium, the lesser Green's function is given by Eq. (11.15b) and the generalized distribution $n(t,\boldsymbol{r},\boldsymbol{p})$ reduces to the Fermi function $f(\boldsymbol{p})$, independent on t and $\boldsymbol{r}$. We emphasize that, in general, $n(t,\boldsymbol{r},\boldsymbol{p})$ is not positive definite and therefore cannot be interpreted as the joint coordinate-momentum distribution function. (Such an interpretation is forbidden by the quantum mechanical uncertainty relations.) Only the integrated quantities $N(t,\boldsymbol{r})$ and $N(t,\boldsymbol{p})$ given by Eq. (11.63) represent the true coordinate and momentum distributions, respectively. Similarly as before, the generalized distribution $n(t,\boldsymbol{r},\boldsymbol{p})$ is completely determined by the Keldysh component G^K by

$$n(t,\boldsymbol{r},\boldsymbol{p}) = \frac{1-h(t,\boldsymbol{r},\boldsymbol{p})}{2}, \tag{11.65}$$

where

$$h(t,\boldsymbol{r},\boldsymbol{p}) = \int d\boldsymbol{r}'\ e^{-i\boldsymbol{p}\boldsymbol{r}'} \sum_\alpha \left[iG^K_{\alpha\alpha}\left(t,\boldsymbol{r}+\frac{\boldsymbol{r}'}{2};t,\boldsymbol{r}-\frac{\boldsymbol{r}'}{2}\right)\right]. \tag{11.66}$$

In general, the presence of time-dependent terms in the Hamiltonian also affects the density of states. The effect is important in bulk semiconductors in strong ac fields and is known as dynamical Franz-Keldysh effect [137, 138]. In the presence of a time-dependent drive, the Green's functions depend on two time arguments t' and t'' and the spectral function and the density of states given by Eqs. (11.12) and (11.14) have to be generalized such that the Fourier transform is performed with respect to the relative time $t = t' - t''$, while keeping the dependence on the center-of-mass time coordinate $T = (t' + t'')/2$. The generalized density of states $\mathcal{V}(\mathcal{E},T)$ develops drive-dependent features both in time and energy, which is seen experimentally by the modified absorption spectra in a semiconductor near the optical absorption edge [139]. An efficient truncation method for the calculation of Green's functions in time-dependent fields has been developed by Brandes [140].

CHAPTER IV

Circuit theory and full counting statistics

In Chapter II, the cumulant generating function has been introduced as an efficient way to characterize a set of random variables and obtain the joint probability distribution. Furthermore, the decomposition of a total cumulant generating function into a sum of simpler ones reveals the independent constitutive processes, thus leading to a novel physical understanding. While this concept is general and independent on the particular stochastic system under consideration, the very technique to obtain the cumulant generating function depends on microscopic properties of the system and is system specific. In § 6 – § 9 we gave examples in which it was possible to identify the cumulant generating functions directly.

In this Chapter we present the theory which enables the calculation of statistics of charge transfer in mesoscopic conductors: the formalism of full counting statistics. The field has been pioneered more than a decade ago by Levitov and Lesovik [141] for the case of dc biased multiterminal junctions and generalized to the case of ac bias by Ivanov and Levitov [142] and Levitov, Lee, and Lesovik [143]. Nowadays the research in the field of full counting statistics is very active and several theoretical approaches exist. The reason for this increased interest is that the full counting statistics provides the most detailed information on the charge transfer, which becomes accessible due to advancements of nanofabrication technology and experimental techniques. The semiclassical cascade approach to higher-order current correlators based on the Boltzmann-Langevin equations has been developed by Nagaev *et al.* [144, 145]. The stochastic path integral theory of full counting statistics was introduced by Pilgram *et al.* [146, 147]. In this chapter we present the quantum-mechanical theory of full counting statistics based on extension of the Keldysh-Green's function technique [91, 92, 148, 149]. The theory has been formulated in a discretized form of the circuit theory [66, 150] which provides the efficient method of calculation with the least computational effort. A generalization for multiterminal circuits has been put forward by Nazarov and Bagrets [151]. The theory has been reviewed by Belzig [152] and Nazarov [113].

This chapter is organized as follows. In § 12 we make the connection between the Keldysh-Green's function technique in mesoscopic transport and the scattering formalism. The central result is given by Eqs. (12.1) and (12.3) which express the current through a generic conductor in terms of its scattering properties and the Keldysh-Green's functions of the leads. These important relations are the starting point for the discrete version of the theory which is a quantum counterpart of the traditional circuit theory. The solution strategy is also discussed in § 12. In § 13 we present the extension of the formalism which enables the calculation of the higher-order current correlators and charge transfer statistics. The method is described in more detail for two-terminal junctions in § 13.2 and generalized to multiterminal circuits in § 13.3. In the case of two-terminal junctions, the method reduces to a set of coupled scalar equations: the scalar circuit theory (§ 13.4). It provides an efficient

technique to calculate the transmission distribution of the composite junction if the scattering properties of the constitutive elements are known. An illustration of the full circuit theory is given in § 13.5 in which the current cross correlations are studied in a 3-terminal beam splitter geometry. Further examples can be found in the review articles [113, 152] and the references therein.

§ 12. Circuit theory

The Green's function formalism described in § 11 is a powerful method of calculation of thermodynamic and transport properties of many-body systems. Starting from the microscopic Hamiltonian, the theory provides a system of Dyson equations for the exact Green's functions. If the Green's functions are known, the averages of one-particle observables can be obtained easily. However, the system of Dyson equations is very difficult to solve. This is because of the complicated integral (or integro-differential) structure of these equations and the presence of a self-energy term which is not known analytically. The self-energy is usually calculated approximately within a certain accuracy and the equations are further simplified using the quasiclassical approximation [125]. This results in a set of partial differential equations which have to be solved numerically with appropriate boundary conditions [134]. Although much simpler than the full theory, the quasiclassical approach also becomes involved when applied to complicated mesoscopic structures which can contain many different junctions and more than two terminals.

The circuit theory of mesoscopic transport developed by Nazarov [150] is a convenient theoretical framework which captures the main results of the full theory and is easily applicable to mesoscopic structures of arbitrary complex geometry. The starting point of the circuit theory is the expression for the current through the coherent mesoscopic conductor sandwiched between two terminals. The current is expressed in terms of a matrix current which is defined by

$$\check{I}_2 = \sum_n \frac{2_s T_n[\check{G}_1, \check{G}_2]}{4 + T_n(\{\check{G}_1, \check{G}_2\} - 2)}. \tag{12.1}$$

Here $\check{I}_2$ flows from the terminal 1 into the terminal 2 and the summation is performed over the set of transmission eigenvalues $\{T_n\}$ of the conductor with the factor 2_s taking into account spin degeneracy. The terminals are macroscopic and provide good isotropization of the quasiparticle distribution function. They are described by the quasiclassical Keldysh-Green's functions $\check{G}_{1,2}(\mathcal{E}', \mathcal{E}'')$ which do not depend on coordinates and satisfy the following normalization condition:

$$\check{G}_i^2 = \check{1}. \tag{12.2}$$

The normalization implies that $\check{G}_{1,2}$ commute with $\{\check{G}_1, \check{G}_2\}$, which justifies the notation used in Eq. (12.1). In the presence of a time-dependent drive acting on a terminal, the corresponding Green's function depends on both energy arguments and the products of Green's functions in Eqs. (12.1) and (12.2) have to be interpreted in terms of a convolution over internal indices, e.g., $(\check{G}_1\check{G}_2)(\mathcal{E}', \mathcal{E}'') = (2\pi)^{-1} \int d\mathcal{E}_1 \check{G}_1(\mathcal{E}', \mathcal{E}_1)\check{G}_2(\mathcal{E}_1, \mathcal{E}'')$. In this case the energy (or time) coordinates represent additional matrix indices. In the stationary state, the Green's functions $\check{G}_i$ and the matrix currents $\check{I}_i$ are diagonal in energy, $\check{G}_i(\mathcal{E}', \mathcal{E}'') = 2\pi\delta(\mathcal{E}' - \mathcal{E}'')\check{G}_i(\mathcal{E}')$ (and similar for $\check{I}_i$). Explicit formulas for the Green's functions $\check{G}_i$ of terminals in the normal and superconducting states are given in § 27 in Appendix.

The average current which flows into terminal 2 is given by

$$I_2 = \frac{e}{t_0}\,\frac{1}{4}\,\mathrm{Tr}_{\mathcal{E}}\left(\check{\tau}_K \check{I}_2\right). \tag{12.3a}$$

Here t_0 is the measurement time and $\check{\tau}_K = \check{\tau}_1 \otimes \bar{\tau}_3$ is the matrix in the Keldysh($\check{}$) $\otimes$ Nambu($\bar{}$) space. The trace operation in Eq. (12.3a) is taken both in Keldysh-Nambu and energy indices. Equation (12.3a) is given for the case in which the superconducting terminal is present. If the junction is in the normal state, then it is sufficient to consider the electron component only because the particles and holes decouple and give equal contributions. In this case the Nambu matrix structure can be ignored and the expression for the average current becomes

$$I_2 = \frac{e}{t_0}\,\frac{1}{2}\,\mathrm{Tr}_{\mathcal{E}}(\check{\tau}_K \check{I}_2), \tag{12.3b}$$

where $\check{\tau}_K = \check{\tau}_1$ in Keldysh($\check{}$) space.

As an example, we calculate the average currents for a junction sandwiched between two terminals. Each terminal can be in the normal or in the superconducting state. First we consider normal terminals, with the terminal 1 biased by the voltage $eV > 0$ with respect to the terminal 2. The Green's functions $\check{G}_{1,2}$ in the normal state are given by Eq. (27.4). From Eqs. (12.1) and (12.3a) we obtain

$$I_2 = \frac{e}{\pi}\sum_n T_n \int d\mathcal{E}[n_1(\mathcal{E}) - n_2(\mathcal{E})] = \left(\frac{e^2}{\pi}\sum_n T_n\right)V, \tag{12.4}$$

which coincides with Eq. (10.24) obtained within scattering approach.

For the case of superconducting terminal 2, the Green's function $\check{G}_2$ reduces to $\check{G}_2 = \check{1}\bar{\tau}_2$ at subgap voltages and temperatures ($|eV|, T_e \ll |\Delta|$) and we find

$$I_2 = \left(\frac{e^2}{\pi}\sum_n 2R_n\right)V. \tag{12.5}$$

Here $R_n = T_n^2/(2-T_n)^2$ is the coefficient of Andreev reflection [82] in nth transport channel. The additional factor of two which appears in Eq. (12.5) signifies that the charge is transferred in pairs in each channel. Equation (12.5) has been obtained previously using the scattering approach and the explicit coupling between the electron and hole states [83, 153]. The conductance of a completely open junction (with $T_n = 1$) in the presence of a superconducting terminal is doubled with respect to its normal-state value, $G_{NS} = 2G_N$. Interestingly, the conductance of a diffusive wire stays the same, $G_{NS} = G_N$, because of $\int dT\; 2R(T)\rho_d(T) = \int dT\; T\rho_d(T)$ with the distribution of transmission eigenvalues $\rho_d(T)$ given by Eq. (10.41). The derivation of $G_{NS} = G_N$ presented here assumes that the junction is in the metallic diffusive regime and coherent. However, the result holds also for the incoherent diffusive junction [83].

In the following we consider two superconducting terminals with the pair potentials $\Delta_{1,2} = |\Delta|e^{i\phi_{1,2}}$ and no bias applied. The corresponding Green's functions are given by Eqs. (27.5) and (27.7). In this case some extra care has to be taken regarding the infinitesimal shifts of the poles of the Green's functions. From Eq. (12.1) we obtain

$$\mathrm{Tr}\left(\check{\tau}_K \check{I}_2\right) = \sum_n \frac{2\pi\sin(\phi)h(\mathcal{E})|\Delta|T_n}{\sqrt{1 - T_n\sin^2(\phi/2)}}\left(\frac{1}{\pi}\frac{\delta}{\delta^2 + a_-^2} - \frac{1}{\pi}\frac{\delta}{\delta^2 + a_+^2}\right). \tag{12.6}$$

Here the trace is performed in the Keldysh-Nambu space only, $\phi = \phi_2 - \phi_1$ is the phase difference between the superconductors, $h(\mathcal{E}) = \tanh(\mathcal{E}/2T_e)$, and $a_\pm = \mathcal{E} \pm |\Delta|\sqrt{1 - T_n \sin^2(\phi/2)}$. The terms in brackets reduce to the Dirac delta functions, $\pi^{-1}\delta/(\delta^2 + a_\pm^2) \to \delta(a_\pm)$ for $\delta \to 0+$. Performing the integration over energy we obtain

$$I_2(\phi) = \frac{e|\Delta|}{2} \sum_n \frac{T_n \sin(\phi)}{\sqrt{1 - T_n \sin^2(\phi/2)}} \tanh\left(\frac{|\Delta|\sqrt{1 - T_n \sin^2(\phi/2)}}{2T_e} \right). \qquad (12.7)$$

Equation (12.7) is the generalization of the Josephson current-phase relation for the case of a short junction[24)] with arbitrary distribution of transmission eigenvalues [154]. In the tunnel limit ($T_n \ll 1$) Eq. (12.7) reduces to the well-known result for the temperature dependence of Josephson current [155] $I_2(\phi) = I_c^{(0)} \sin(\phi) \tanh(|\Delta|/2T_e)$, first obtained by Ambegaokar and Baratoff [156]. Here $I_c^{(0)} = G_N \pi |\Delta|/2e$ and G_N is the normal-state conductance. For completely open junction ($T_n = 1$) we obtain $I_2(\phi) = 2I_c^{(0)} \sin(\phi/2) \tanh[|\Delta| \cos(\phi/2)/2T_e]$, in agreement with Ref. [157]. For a diffusive junction, the summation over transport channels has to be replaced by integration over transmission distribution $\rho_d(T)$ given by Eq. (10.41). At zero temperature we obtain $I_2(\phi) = 2I_c^{(0)} \cos(\phi/2)\, \mathrm{atanh}[\sin(\phi/2)]$, in agreement with Ref. [158].

The examples given above illustrate the importance of Eqs. (12.1) and (12.3): they summarize the knowledge on coherent mesoscopic conductors in a general and very compact way. The conductances in the normal and superconducting states, as well as different forms of the Josephson current-phase relations are all obtained from the same formula, supplied with the corresponding Green's functions at the terminals as boundary conditions. The matrix inversion in Eq. (12.1) automatically takes into account proper coupling between the electron and hole states, which otherwise has to be performed explicitly within the scattering approach.

The method allows generalization to the more complicated networks of mesoscopic junctions. The central concept in this generalization is the notion of *node* as a part of a junction in which the quasiparticle distribution is isotropic, i.e., independent on the direction of propagation. The nodes are described by the quasiclassical Keldysh-Green's functions which depend only on energy and satisfy the normalization condition $\check{G}^2 = \check{1}$. In this respect the nodes are similar to terminals, except for the distribution functions which are the nonequilibrium ones. Different nodes are coupled through *connectors*, each being characterized by the set of transmission eigenvalues. After specifying the nodes and connectors, the full theory reduces to the finite number of discrete elements. For the given Green's functions of terminals, the Green's functions of internal nodes are determined from the matrix current conservations and the normalization conditions [150]. After the Green's functions of nodes are obtained, the average currents are computed using Eq. (12.3).

The solution strategy for the 'quantum circuits' very much resembles the use of Kirchhoff laws for the classical electrical circuits. In the classical case, internal nodes are characterized by voltages to be determined from the current conservations. In the quantum case, the role of voltages is taken by the matrix Green's functions (which are subject to the normalization constraint) and the scalar currents are replaced by

[24)] The length of the junction should be much smaller than the coherence length, $L \ll \xi$. The coherence length in the clean limit ($l \gg 2\pi\xi_0$) is given by $\xi_0(T_e) = \hbar v_F/\pi\Delta(T_e)$ and in the dirty limit ($l \ll 2\pi\xi_0$) by $\xi(T_e) = \sqrt{\xi_0(0) l}(1 - T_e/T_c)^{-1/2}$. Here l is the mean free path and $T_c = \Delta_0/1.76$ is the critical temperature.

the matrix currents. The important difference is that the matrix currents depend on the Green's functions in a complicated nonlinear way, which involves matrix inversion [Eq. (12.1)]. In practice, the set of circuit-theory matrix equations can be solved numerically using the method of iterations [113, 150]. For example, the matrix current conservation at the node $\check{G}_c$ is given by $[\check{M}, \check{G}_c] = 0$ with

$$\check{M} = \sum_i \sum_n \frac{T_n^{(i)} \check{G}_i}{4 + T_n^{(i)}(\{\check{G}_i, \check{G}_c\} - 2)}. \tag{12.8}$$

Here the summation is performed over all nodes and terminals $\check{G}_i$ connected to the node $\check{G}_c$. Starting from the initial guess for $\{\check{G}_i\}$ and $\check{G}_c$, we first find the transformation $\check{P}^{-1} \dots \check{P}$ which brings $\check{M}$ into diagonal form: $\check{M}' = \check{P}^{-1}\check{M}\check{P}$. The matrix $\check{P}$ contains the eigenvectors of $\check{M}$ as its columns. The updated matrix $\check{G}_c$ is given by $\check{G}_c^{\rm new} = \check{P}\,\mathrm{sgn}[\mathrm{Re}(\check{M}')]\check{P}^{-1}$. The matrix $\check{G}_c^{\rm new}$ commutes with $\check{M}$ and satisfies the normalization condition $(\check{G}_c^{\rm new})^2 = \check{1}$. The procedure is then repeated for all internal nodes and iterated until the predefined accuracy is reached. The integration over energy in Eq. (12.3) requires repeated computation for many slightly different values of energy. This integration can be significantly speeded up by using the results for the previous energy slice as the initial guess for the next one.

In the following we discuss the assumptions which justify the discretization of the system into the set of nodes and connectors. The disretization is heuristic, similarly as in the classical electric circuits. The parts of a device in which the voltage is nearly constant can be regarded as nodes. The constrictions, interfaces, and disordered regions over which the voltage drops are significant are connectors. However, the quantum nature of mesoscopic junctions brings more stringent conditions on the nodes and connectors, which are not present in the classical case. Equation (12.1) for the matrix current through the connector assumes that the connector is coherent. Therefore, the connectors should be short enough, such that all transport energy scales (given by the applied voltage, temperature, and the pair potential) are much smaller than the Thouless energy: $|eV|, T_e, |\Delta| \ll E_{\rm Th} = \hbar D/L^2$. Concerning nodes, the essential requirement is that the quasiparticle distribution function is isotropic. An example of the node is the chaotic cavity with openings small enough such that the particle dwell time $\tau_{\rm dwell}$ is much larger than the time $\tau_{\rm e}$ needed for the wave packet to spread over the cavity. In this way the information on the initial direction of propagation is lost and the quasiparticle distribution is isotropized. The time $\tau_{\rm e}$ is given by the inverse Thouless energy, $\tau_{\rm e}^{-1} \simeq E_{\rm Th} = (\hbar v_F/L^2)\min(l, L)$ where l is the mean free path and L is the linear dimension of a cavity. The particle dwell time is given by $\tau_{\rm dwell}^{-1} \simeq G\delta/e^2$ where G is the total conductance of all cavity contacts and $\delta \ll E_{\rm Th}$ is the mean level spacing in the cavity [46]. Here, G and δ take into account both spin orientations. The average level spacing is defined by $\delta = (V\mathcal{V}_0)^{-1}$ [$\delta = (A\mathcal{V}_0)^{-1}$] in the case of a 3D (2D) cavity, where $\mathcal{V}_0 = m^2 v_F/\pi^2\hbar^3$ ($\mathcal{V}_0 = m/\pi\hbar^2$) is the density of states per unit volume (area) at the Fermi energy. For $\tau_{\rm dwell} \gg \tau_{\rm e}$ good isotropization is achieved irrespective microscopic details such as the shape of a cavity or whether the motion in the cavity is ballistic or diffusive. Therefore, the diffusive parts of the junction can be regarded as nodes, provided they are sandwiched between connectors of not too large conductance, $G\hbar/e^2 \ll E_{\rm Th}/\delta$ ($E_{\rm Th}/\delta \gg 1$). This condition does not require G to be smaller than the conductance quantum. For the sufficiently large ratio $E_{\rm Th}/\delta$, the circuit theory (which requires many transport channels) is applicable even for the completely open contacts.

§ 13. Full counting statistics

§ 13.1. Extended Keldysh technique. The cumulant generating function of the statistics of transferred charge in a general quantum system has been obtained by Nazarov and Kindermann [159], see also [103, 143]. In some situations, which include conductors in the normal state and normal-superconductor junctions, the cumulant generating function $\mathcal{S}(\chi)$ is given by

$$e^{\mathcal{S}(\chi)} = \left\langle \left(\tilde{T} e^{i \int_0^{t_0} dt\, [\hat{H} + (\chi/2e)\hat{I}]} \right) \left(T e^{-i \int_0^{t_0} dt\, [\hat{H} - (\chi/2e)\hat{I}]} \right) \right\rangle_{H_0} . \tag{13.1}$$

Here $\hat{H} = \hat{H}_0 + \hat{H}_{\rm int}$ is the Hamiltonian of the electronic subsystem in the Schrödinger picture where $\hat{H}_0$ is the noninteracting part (which includes the term $-\mu\hat{N}$) and $\hat{H}_{\rm int}$ is the interaction which takes into account scattering at impurities, interaction with external fields, and interparticle interactions. The system can be driven by time-dependent external fields in which case $\hat{H} = \hat{H}(t)$. The current operator in the Schrödinger picture is denoted by $\hat{I}$ and χ is the counting field. The time integration is performed over the measurement time t_0 which is the largest time scale in the problem, much larger than the characteristic time of the system dynamics. The proof that $\mathcal{S}(\chi)$ given by Eq. (13.1) represents the cumulant generating function of the number of charges transferred within measurement time is beyond the scope of this Thesis. The detailed derivation and analysis can be found in [159] and [103]. In this paragraph we present an extension of the Keldysh-Green's function technique which provides a method to calculate the $\mathcal{S}(\chi)$ and can be cast in the form of the circuit theory [152]. For simplicity we consider a junction in the normal state. The derivation for a normal-superconductor junction is analogous.

First, let us denote $\hat{\mathcal{H}}_\chi = \hat{H} + \hat{H}'_\chi$ where $\hat{H}'_\chi = -(\chi/2e)\hat{I}$. The cumulant generating function $\mathcal{S}(\chi)$ can be expressed in terms of the evolution operator $\hat{U}_{\mathcal{H}_\chi}(t_0, 0)$ as $e^{\mathcal{S}(\chi)} = \left\langle (\hat{U}_{\mathcal{H}_{-\chi}})^\dagger \hat{U}_{\mathcal{H}_\chi} \right\rangle_{H_0}$. In the interaction picture $\hat{U}_{\mathcal{H}_\chi} = \hat{U}_H \hat{S}_{H'^\chi_H}$ and we obtain $e^{\mathcal{S}(\chi)} = \left\langle \left(\hat{S}_{H'^{-\chi}_H} \right)^\dagger \hat{S}_{H'^\chi_H} \right\rangle_{H_0}$, i.e.,

$$e^{\mathcal{S}(\chi)} = \left\langle \left(\tilde{T} e^{i \int_0^{t_0} dt\, (\chi/2e) \hat{I}_H(t)} \right) \left(T e^{-i \int_0^{t_0} dt\, (-\chi/2e) \hat{I}_H(t)} \right) \right\rangle_{H_0} . \tag{13.2}$$

Now, let us formally define the operator $\hat{H}'_c(t)$ which is different at two branches of the Keldysh contour,

$$\hat{H}'_c(t) = \begin{cases} -\frac{\chi}{2e}\hat{I}, & t \in C_-, \\ +\frac{\chi}{2e}\hat{I}, & t \in C_+. \end{cases} \tag{13.3}$$

Using the contour-ordered evolution operator $\hat{S}_{H'^c_H} = T_c e^{-i \int_c dt\, \hat{H}'^c_H(t)}$ we find

$$e^{\mathcal{S}(\chi)} = \left\langle \hat{S}_{H'^c_H} \right\rangle_{H_0} . \tag{13.4}$$

In order to formulate the diagrammatic technique for the calculation of $\mathcal{S}(\chi)$ it is convenient to define the contour-ordered Green's function with respect to $\hat{S}_{H'^c_H}$:

$$G_c(x', x''; \chi) = \frac{-i \left\langle T_c \left[\hat{\psi}_H(x') \hat{\psi}^\dagger_H(x'') \hat{S}_{H'^c_H} \right] \right\rangle_{H_0}}{\left\langle \hat{S}_{H'^c_H} \right\rangle_{H_0}} \tag{13.5a}$$

$$= \frac{-i\left\langle T_c\big[\hat\psi_{H_0}(x')\hat\psi^\dagger_{H_0}(x'')\hat S_{V^c_{H_0}}\big]\right\rangle_{H_0}}{\left\langle \hat S_{V^c_{H_0}}\right\rangle_{H_0}}. \qquad (13.5b)$$

Here G_c depends on the counting field χ as a parameter. In the last step we have defined

$$\hat V_c(t) = \hat H_{\rm int} + \hat H'_c(t) \qquad (13.6)$$

and disregarded the initial correlations which correspond to imaginary part of the Keldysh contour[21] (cf. § 11.6). Equation (13.5b) is the starting point of the extended Keldysh technique. It has the identical structure as Eq. (11.45) of the usual Keldysh technique but now with different Hamiltonians at the forward and backward branches of the contour. Therefore, the diagrams in the extended technique remain the same as in the standard one, including cancellation of disconnected diagrams and the denominator of Eq. (13.5b),

$$G_c(x',x'';\chi) = -i\left\langle T_c\big[\hat\psi_{H_0}(x')\hat\psi^\dagger_{H_0}(x'')\hat S_{V^c_{H_0}}\big]\right\rangle_{H_0\ \rm con}. \qquad (13.7)$$

The analytical representation of diagrams changes in the sense that different values of $\hat V_c(t)$ have to be taken into account depending on the branch of t.

As before, it is convenient to define the matrix function G^{ij},

$$G_c(x',x'';\chi) \to \breve G(x',x'';\chi) = \begin{pmatrix} G^{--} & G^{-+} \\ G^{+-} & G^{++}\end{pmatrix}, \qquad (13.8)$$

where $G^{ij}(x',x'';\chi) = G_c(x',x'';\chi)$ for $t'\in C_i$ and $t''\in C_j$. Here we emphasize that the simple relations between the matrix components given by Eqs. (11.9) *no longer hold* in the extended technique. In particular $G^{--}+G^{++} \neq G^{-+}+G^{+-}$, i.e., all components G^{ij} have to be taken into account. Thus, the formulas for averages in the extended Keldysh technique cannot be inferred from the ones in the standard technique. The meaningful formulas for averages in the extended technique have to be re-derived using the definition given by Eq. (13.5).

From Eqs. (13.2) and (13.5a) follows that

$$\frac{\partial\mathcal{S}(\chi)}{\partial(i\chi)} = \frac{-i}{2e}\int dt \int_S d\boldsymbol{S}\cdot\hat{\boldsymbol{j}}(\boldsymbol{r}) \times\big[G^{--}(t,\boldsymbol{r}';t+0,\boldsymbol{r}'';\chi)+G^{++}(t,\boldsymbol{r}';t-0,\boldsymbol{r}'';\chi)\big], \qquad (13.9)$$

where $\hat{\boldsymbol{j}}(\boldsymbol{r}) = 2_s[-(ie/2m)(\nabla'-\nabla'')-(e^2/mc)\boldsymbol{A}]_{\boldsymbol{r}'=\boldsymbol{r}''=\boldsymbol{r}}$ is the current density operator. Let us define the extended matrix current $\breve I(t',t'';\chi)$ and the extended current $I(\chi)$ by

$$\breve I(t',t'';\chi) = \frac{-i}{e}\int_S d\boldsymbol{S}\cdot\hat{\boldsymbol{j}}(\boldsymbol{r})\,\breve G(x',x'';\chi), \qquad I(\chi) = \frac{e}{t_0}\,\frac{1}{2}\,{\rm Tr}\,\breve I, \qquad (13.10a,b)$$

where the trace operation is taken both in the matrix and in the time (or energy) indices. In the $\breve G$-matrix representation defined by $\breve G = \breve L\breve\tau_3\breve G\breve L^\dagger$ with $\breve L = (\breve 1 - i\breve\tau_2)/\sqrt{2}$ we have

$$\check I(t',t'';\chi) = \frac{-i}{e}\int_S d\boldsymbol{S}\cdot\hat{\boldsymbol{j}}(\boldsymbol{r})\,\check G(x',x'';\chi), \qquad I(\chi) = \frac{e}{t_0}\,\frac{1}{2}\,{\rm Tr}\left(\check\tau_1\check I\right). \qquad (13.11a,b)$$

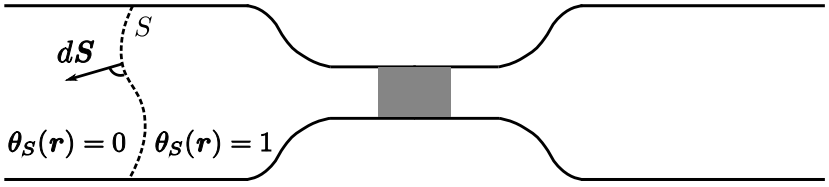

Fig. 19: *The charges transferred through the cross section S are counted. The generalized step function $\theta_S(\boldsymbol{r})$ is defined such that $\theta_S(\boldsymbol{r}) = 0$ [$\theta_S(\boldsymbol{r}) = 1$] at positions left (right) from S. Function $\theta_S(\boldsymbol{r})$ is continuous and changes from 0 to 1 in the vicinity of S on the length scale larger than the Fermi wavelength but much smaller than the mean free path.*

The expression for the cumulant generating function reduces to

$$\frac{\partial \mathcal{S}(\chi)}{\partial(i\chi)} = \frac{t_0}{e} I(\chi) = \frac{1}{2}\,\mathrm{Tr}\left(\check{\tau}_1 \check{I}\right). \tag{13.12}$$

Equation (13.12) gives the physical meaning to the formally introduced extended Keldysh-Green's functions: the statistics of the charge transferred through the cross section S over the long time interval is expressed in terms of the components of $\check{G}(x', x''; \chi)$. In the case in which there is no charge accumulation in the parts of the system the current is conserved and the result does not depend on the choice of the cross section.

In the following we discuss how to efficiently calculate the extended Keldysh Green's function $\check{G}(x', x''; \chi)$ when the current is conserved. First, let us notice that Eqs. (13.10) and (13.11) have exactly the same form as in the standard Keldysh technique which is obtained for $\chi = 0$. This suggests that the standard circuit theory for the average current developed in § 12 can be used also in the extended case without modification. However, we have to check that the extended Green's functions $\check{G}(\chi)$ in the terminals satisfy the normalization condition $[\check{G}(\chi)]^2 = \check{1}$. To do so we first obtain the Dyson equation in the extended technique. The single-particle operator $\hat{h}'_c(t, \boldsymbol{r})$ whose second-quantized form is given by Eq. (13.3) is

$$\hat{h}'_c(t, \boldsymbol{r}) = \frac{\chi_c(t)}{e}\,[-\nabla\theta_S(\boldsymbol{r})] \cdot \hat{\boldsymbol{j}}(\boldsymbol{r}). \tag{13.13}$$

Here

$$\chi_c(t) = \begin{cases} -\frac{\chi}{2}, & t \in C_-, \\ +\frac{\chi}{2}, & t \in C_+, \end{cases} \tag{13.14}$$

and $\theta_S(\boldsymbol{r})$ is a generalized step function introduced as shown in Fig. 19. The generalized step function $\theta_S(\boldsymbol{r})$ is continuous over the cross section S and takes the value $\theta_S = 0$ ($\theta_S = 1$) at the left (right) side of S. The length scale at which $\theta_S(\boldsymbol{r})$ changes continuously from 0 to 1 in the vicinity of S is assumed to be larger than the Fermi wavelength but much smaller than the mean free path (it is convenient to choose the cross section in the terminal). Therefore $\int d\boldsymbol{r}\,[-\nabla\theta_S(\boldsymbol{r})]\cdot = \int_S d\boldsymbol{S}\cdot$ and we obtain

$$\hat{H}'_c(t) = \int d\boldsymbol{r}\;\hat{\psi}^\dagger(\boldsymbol{r})\hat{h}'_c(t, \boldsymbol{r})\hat{\psi}(\boldsymbol{r}). \tag{13.15}$$

The Dyson equations in the extended technique can be obtained from the standard ones given by Eqs. (11.51a) and (11.55a) with the substitution

$$\hat{h}_0(\boldsymbol{r}) \to \hat{h}_0(\boldsymbol{r}) + \check{\tau}_3\,\frac{\chi}{2e}[\nabla\theta_S(\boldsymbol{r})] \cdot \hat{\boldsymbol{j}}(\boldsymbol{r}) \tag{13.16}$$

in the $\check{G}(\chi)$ representation, and

$$\hat{h}_0(\boldsymbol{r}) \to \hat{h}_0(\boldsymbol{r}) + \check{\tau}_1 \frac{\chi}{2e}[\nabla\theta_S(\boldsymbol{r})] \cdot \hat{\boldsymbol{j}}(\boldsymbol{r}) \tag{13.17}$$

in the $\check{G}(\chi)$ representation. In Eqs. (11.51b) and (11.55b) these operators are acting on the Green's functions from the right. Here we emphasize again that all components of $\check{G}(\chi)$ and $\check{\Sigma}(\chi)$ are nonzero in general. The term $\hat{h}'_c$ contains a δ-like singularity $\nabla\theta_S(\boldsymbol{r})$ which can be incorporated into the Green's function by matching the solutions across S. The Green's functions in the terminals are quasiclassical $\check{G} = \check{G}_{t',t''}(\boldsymbol{p}_F, \boldsymbol{r}; \chi)$ and we can use the stationary Eilenberger or the nonstationary Eliashberg equation [125] to match the solutions. In both cases it is sufficient to keep only the singular term and the term with the spatial derivative in the vicinity of S [152]

$$-i\boldsymbol{v}_F \cdot \nabla \check{G}_{t',t''}(\boldsymbol{p}_F, \boldsymbol{r}; \chi) + \left[\frac{\chi}{2}[\nabla\theta_S(\boldsymbol{r})] \cdot \boldsymbol{v}_F \check{\tau}_1, \check{G}_{t',t''}(\boldsymbol{p}_F, \boldsymbol{r}; \chi)\right] = 0. \tag{13.18}$$

The solution in the vicinity of S is given by

$$\check{G}_{t',t''}(\boldsymbol{p}_F, \boldsymbol{r}; \chi) = e^{-i\chi\theta_S(\boldsymbol{r})\check{\tau}_1/2}\, \check{G}_{t',t''}(\boldsymbol{p}_F, \boldsymbol{r}; \chi = 0)\, e^{i\chi\theta_S(\boldsymbol{r})\check{\tau}_1/2}. \tag{13.19}$$

At the distances several mean free paths away from the interface, the diffusive approximation is valid and the quasiclassical Green's function is independent on the position. Finally, we obtain

$$\check{G}(t', t''; \chi) = e^{-i\chi\check{\tau}_1/2}\, \check{G}(t', t''; \chi = 0)\, e^{i\chi\check{\tau}_1/2}. \tag{13.20}$$

Equation (13.20) expresses the extended quasiclassical Keldysh-Green's function $\check{G}(\chi)$ at the right hand side of S towards the junction in terms of the standard Keldysh-Green's function $\check{G}(\chi = 0)$ at the left hand side of S towards the terminal. Since the standard quasiclassical functions satisfy $[\check{G}(\chi = 0)]^2 = \check{1}$, the same is true for the extended ones,

$$[\check{G}(\chi)]^2 = \check{1}, \tag{13.21}$$

where we assume the convolution over time (or energy) indices. Therefore, the circuit theory of § 12 is directly applicable in the extended technique with the Green's functions of the terminals modified according to Eq. (13.20).

§ **13.2. Two-terminal junctions.** In this paragraph we specify the cumulant generating function for the two-terminal junction in the normal state, characterized by transmission eigenchannels $\{T_n\}$. We choose to count charges which enter the left terminal. The extended Green's function of the left terminal is given by

$$\check{G}_1(\chi) = e^{-i\chi\check{\tau}_1/2}\, \check{G}_1(\chi = 0)\, e^{i\chi\check{\tau}_1/2}. \tag{13.22}$$

The Green's function of the right terminal coincides with the standard one, $\check{G}_2 = \check{G}_2(\chi_2 = 0)$. The extended matrix current which enters the left terminal is given by Eq. (12.1):

$$\check{I}_1(\chi) = -\sum_n \frac{2_s T_n[\check{G}_1(\chi), \check{G}_2(0)]}{4 + T_n(\{\check{G}_1(\chi), \check{G}_2(0)\} - 2)}. \tag{13.23}$$

The cumulant generating function of the transferred charge is given by

$$\frac{\partial \mathcal{S}(\chi)}{\partial(i\chi)} = \frac{1}{2}\,\mathrm{Tr}\left[\check{\tau}_1 \check{I}_1(\chi)\right]. \tag{13.24}$$

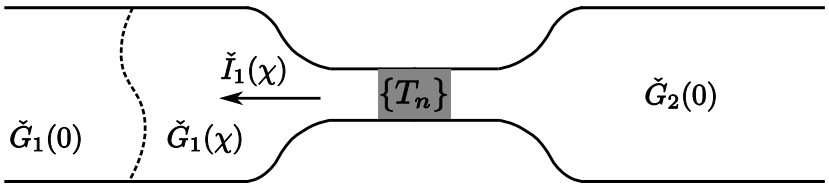

Fig. 20: *The schematic representation of the extended circuit theory for the two terminal junction. The charges which enter the left terminal are counted. The extended matrix current $\check{I}_1(\chi)$ is given by the extended Green's function $\check{G}_1(\chi)$ of the left terminal and the standard Green's function $\check{G}_2(0)$ of the right terminal.*

Using that $\check{G}_1(\chi)$ and $\check{G}_2(0)$ commute with $\{\check{G}_1(\chi), \check{G}_2(0)\}$ and the invariance of the trace under cyclic permutations, it is straightforward to verify

$$\frac{\partial \mathcal{S}(\chi)}{\partial(i\chi)} = \sum_n \mathrm{Tr}\left(\frac{T_n \partial_{i\chi}\{\check{G}_1(\chi), \check{G}_2(0)\}}{4 + T_n(\{\check{G}_1(\chi), \check{G}_2(0)\} - 2)}\right). \tag{13.25}$$

This equation can be integrated under the trace, and we obtain

$$\mathcal{S}(\chi) = \sum_n \mathrm{Tr}\ln\left[\check{1} + \frac{T_n}{2}\left(\frac{\{\check{G}_1(\chi), \check{G}_2(0)\}}{2} - \check{1}\right)\right]. \tag{13.26}$$

The $\mathcal{S}(\chi)$ given by Eq. (13.26) is normalized, $\mathcal{S}(\chi = 0) = 0$, because the standard Keldysh-Green's functions of normal terminals satisfy $\{\check{G}_1(0), \check{G}_2(0)\} = 2$ (see § 27). The trace operation is taken both in the Keldysh and in time (or energy) indices. The convolution over the internal time (or energy) indices is assumed.

In the case of a normal-superconductor junction the Green's functions $\check{G}_{1,2}$ are 4×4 matrices in the Keldysh($\check{}$)-Nambu($\bar{}$) space (§ 27). The extended Green's function $\check{G}_1(\chi)$ is given by

$$\check{G}_1(\chi) = e^{-i\chi\check{\tau}_K/2}\, \check{G}_1(\chi = 0)\, e^{i\chi\check{\tau}_K/2} \tag{13.27}$$

where $\check{\tau}_K = \check{\tau}_1 \otimes \bar{\tau}_3$. The extended matrix current $\check{I}_1(\chi)$ is again given by Eq. (13.23). The extended current is defined by Eq. (12.3*a*) with the factor of $1/2$ with respect to the normal-state case, which corrects for the doubled matrix size. Therefore, the cumulant generating function for the normal-superconductor junction is given by

$$\mathcal{S}(\chi) = \frac{1}{2}\sum_n \mathrm{Tr}\ln\left[\check{1} + \frac{T_n}{2}\left(\frac{\{\check{G}_1(\chi), \check{G}_2(0)\}}{2} - \check{1}\right)\right], \tag{13.28}$$

with the trace taken in Keldysh, Nambu, and time (or energy) indices. The χ-independent normalization constant is omitted for brevity.

Equivalence with the Levitov determinant formula. The cumulant generating function of the charge transferred in the multiterminal junctions is given by the determinant formula

$$\mathcal{S}(\{\chi\}) = \ln\det\left[1 + \boldsymbol{n}\left(\boldsymbol{S}^\dagger \boldsymbol{\Lambda}^\dagger_{\{\chi\}} \boldsymbol{S} \boldsymbol{\Lambda}_{\{\chi\}} - 1\right)\right] \tag{13.29a}$$

$$= \mathrm{Tr}\ln\left[1 + \boldsymbol{n}\left(\boldsymbol{S}^\dagger \boldsymbol{\Lambda}^\dagger_{\{\chi\}} \boldsymbol{S} \boldsymbol{\Lambda}_{\{\chi\}} - 1\right)\right]. \tag{13.29b}$$

This equation has been first obtained by Levitov and Lesovik [141] (see also [143] and [160]). A more elementary derivation has been given by Klich [161]. Some mathematical aspects of the determinant regularization which is needed in the presence of a time dependent drive have been discussed in [162].

In Eq. (13.29), the set of counting fields $\{\chi\}$ is assigned to different terminals. Here $\boldsymbol{n}$ represents the matrix of occupation numbers of the terminals which is diagonal in the terminal indices and scalar in transport channels, $\boldsymbol{S}$ is the scattering matrix of the multiterminal junction, and $\boldsymbol{\Lambda}_{\{\chi\}}$ is the transformation which incorporates the counting fields. The determinant (or trace) is taken with respect to terminal, channel, energy, and spin indices. For the two-terminal junction we have

$$\boldsymbol{n} = \begin{pmatrix} n_1 & 0 \\ 0 & n_2 \end{pmatrix}, \qquad \boldsymbol{S} = \begin{pmatrix} \boldsymbol{r} & \boldsymbol{t}' \\ \boldsymbol{t} & \boldsymbol{r}' \end{pmatrix}, \qquad \boldsymbol{\Lambda}_\chi = \begin{pmatrix} e^{-i\chi} & 0 \\ 0 & 1 \end{pmatrix}. \tag{13.30}$$

Here $n_{1,2}$ are the occupation numbers of the left and right leads which are scalars in channel and spin indices. The counting field χ is assigned to the left lead. It is scalar in channel and spin indices, which corresponds to the charge counting irrespective the channel or spin. In the case of dc voltage bias $n_{1,2}$ are diagonal in energy with $n_i(\mathcal{E}', \mathcal{E}'') = [e^{\beta(\mathcal{E}'-\mu_i)} + 1]^{-1}\, 2\pi\delta(\mathcal{E}' - \mathcal{E}'')$. In the presence of time-dependent drive the occupation numbers $n_i(\mathcal{E}', \mathcal{E}'')$ are not diagonal in energy and do not commute. The voltage drive $V(t)$ can be incorporated via the gauge transformation in time representation $n \to UnU^\dagger$ with $U(t', t'') = e^{-i\int_0^{t'} eV(t)dt}\delta(t' - t'')$, where we assume the convolution over internal time indices (see § 27). It is convenient to perform the polar decomposition of the scattering matrix [46]

$$\boldsymbol{S} = \begin{pmatrix} \boldsymbol{U} & 0 \\ 0 & \boldsymbol{V} \end{pmatrix} \boldsymbol{S}' \begin{pmatrix} \boldsymbol{U}' & 0 \\ 0 & \boldsymbol{V}' \end{pmatrix}, \qquad \boldsymbol{S}' = \begin{pmatrix} -\sqrt{\boldsymbol{R}} & \sqrt{\boldsymbol{T}} \\ \sqrt{\boldsymbol{T}} & \sqrt{\boldsymbol{R}} \end{pmatrix}. \tag{13.31}$$

Here $\boldsymbol{U}$, $\boldsymbol{V}$, $\boldsymbol{U}'$, and $\boldsymbol{V}'$ are unitary matrices in transport channels and $\boldsymbol{T} = \mathrm{diag}(T_1, T_2, \ldots)$ and $\boldsymbol{R} = \boldsymbol{1} - \boldsymbol{T}$ are diagonal matrices of transmission and reflection eigenchannels. Equation (13.29a) for the two-terminal junction reduces to

$$\begin{aligned} \mathcal{S}(\chi) &= 2_s \ln\det\left[1 + \boldsymbol{n}\left(\boldsymbol{S}'\boldsymbol{\Lambda}^\dagger\boldsymbol{S}'\boldsymbol{\Lambda} - 1\right)\right] \\ &= 2_s \ln\det\begin{pmatrix} 1 + n_1(e^{-i\chi} - 1)\,\boldsymbol{T} & -n_1(e^{i\chi} - 1)\sqrt{\boldsymbol{TR}} \\ n_2(e^{-i\chi} - 1)\sqrt{\boldsymbol{TR}} & 1 + n_2(e^{i\chi} - 1)\,\boldsymbol{T} \end{pmatrix}, \end{aligned} \tag{13.32}$$

where 2_s takes into account the spin degree of freedom. Since the operators in the first (the second) row commute, the determinant can be calculated by blocks. Using Eq. (28.1) we obtain

$$\mathcal{S}(\chi) = 2_s \sum_p \mathrm{Tr}_\mathcal{E} \ln\left[1 + (1 - n_1)n_2T_p(e^{i\chi} - 1) + n_1(1 - n_2)T_p(e^{-i\chi} - 1)\right] \tag{13.33a}$$

$$= 2_s \sum_p \mathrm{Tr}_\mathcal{E} \ln\left[1 + n_2(1 - n_1)T_p(e^{i\chi} - 1) + (1 - n_2)n_1T_p(e^{-i\chi} - 1)\right]. \tag{13.33b}$$

Here we also used the matrix identity $\ln\det(\boldsymbol{M}) = \mathrm{Tr}\ln(\boldsymbol{M})$.

Equations (13.33) are valid for a dc bias applied and energy-dependent transmission probabilities. In this case the occupation numbers $n_{1,2}$ are diagonal in energy and commute with each other and with $T_p(\mathcal{E})$. The trace over energy reduces simply to the integration and we obtain

$$\begin{aligned} \mathcal{S}(\chi) = \frac{t_0}{\pi}\sum_p \int d\mathcal{E}\ \ln\big(1 + [1 - n_1(\mathcal{E})]n_2(\mathcal{E})T_p(e^{i\chi} - 1) \\ + n_1(\mathcal{E})[1 - n_2(\mathcal{E})]T_p(e^{-i\chi} - 1)\big). \end{aligned} \tag{13.34}$$

Here we used $n_i(\mathcal{E},\mathcal{E}) = n_i(\mathcal{E})\ 2\pi\delta(\mathcal{E}=0)$, where $\delta(\mathcal{E}=0) = t_0/(2\pi)$ with t_0 being the measurement time. The form of $\mathcal{S}(\chi)$ shows that the electron transfers at different energies are independent. The probability for the electron transfer from the right to the left lead at energy $\mathcal{E}$ is proportional to the probability $n_2(\mathcal{E})$ that the state in the right lead is occupied, the probability $1-n_1(\mathcal{E})$ that the state in the left lead is empty, and the probability $T_p(\mathcal{E})$ of transfer across the scatterer. A similar analysis holds for the electron transfer from left to right. The average current and the current noise power are given by $I = (e/t_0)\partial_{i\chi}\mathcal{S}|_{\chi=0}$ and $S_I = (e^2/t_0)\partial^2_{i\chi}\mathcal{S}|_{\chi=0}$, in agreement with Eqs. (10.24) and (10.33).

Equations (13.33) are also valid for the time-dependent voltage applied and energy-independent transmission probabilities. In this case $n_{1,2}(\mathcal{E}',\mathcal{E}'')$ do not commute with each other. However, the order of n_1 and n_2 can be exchanged, as shown by Eqs. (13.33*a*) and (13.33*b*). The logarithm has to be calculated with the matrix structure of $n_{1,2}$ in energy indices taken into account. This is because time-dependent drive mixes the electron states with different energies. The statistics of charge transfer in the presence of time-dependent drive is discussed in detail in Chapter VII.

In the following we calculate $\mathcal{S}(\chi)$ using the circuit-theory expression given by Eq. (13.26). As before, it is convenient to rewrite the equation in terms of $\ln\det(\cdots)$, then take the determinant by blocks using Eq. (28.1), and restore $\mathrm{Tr}\ln(\cdots)$ at the end. The result is

$$\mathcal{S}(\chi) = \sum_p \mathrm{Tr}_{\mathcal{E}} \ln\left[1 + (1-n_1)n_2T_p(e^{i\chi}-1) + n_1(1-n_2)T_p(e^{-i\chi}-1)\right] + \sum_p \mathrm{Tr}_{\mathcal{E}} \ln\left[1 + n_2(1-n_1)T_p(e^{i\chi}-1) + (1-n_2)n_1T_p(e^{-i\chi}-1)\right]. \quad (13.35)$$

Since both terms give the same contribution, the result coincides with the Levitov formula given by Eq. (13.33).

§ **13.3. Multiterminal circuits.** In order to apply the Levitov determinant formula given by Eq. (13.29) it is necessary to know the scattering matrix of the multiterminal junction. Obtaining the scattering matrix of a complex mesoscopic structure is a nontrivial task. In practice, the junction often consists of the scattering regions (connectors) and the isotropization regions (nodes). In this case it is more convenient to use the circuit theory to combine connectors and nodes together to form the junction. The cumulant generating function in a multiterminal circuit is given by the sum of the contributions of all connected pairs of nodes [163]

$$\mathcal{S}(\vec{\chi}) = \sum_{(ij)} \mathcal{S}_{ij}(\vec{\chi}), \quad (13.36)$$

where each connection is counted only once. Here $\vec{\chi} = (\chi_1,\ldots,\chi_N)$ is the set of the counting fields of terminals. The indices i and j label terminals (with $i,j = 1,\ldots,N$) and all internal nodes (with $i,j = N+1,\ldots$). The $\mathcal{S}_{ij}(\vec{\chi})$ of the connected pair of nodes is given by

$$\mathcal{S}_{ij}(\vec{\chi}) = \frac{1}{(2)}\sum_n \mathrm{Tr}\ln\left[\check{1} + \frac{T_n^{(ij)}}{2}\left(\frac{\{\check{G}_i(\vec{\chi}),\check{G}_j(\vec{\chi})\}}{2} - \check{1}\right)\right] \quad (13.37)$$

with the transmission eigenvalues $T_n^{(ij)}$ being independent on the direction of the charge propagation, $T_n^{(ij)} = T_n^{(ji)}$ [114]. The prefactor 1/2 is used in the case in which a superconducting terminal is present.

The solution strategy is the following. First, the Green's functions of terminals are known. They are given by the gauge-like transformations of the standard quasiclassical Green's functions $\check{G}_i(\chi_i) = e^{-i\chi_i\check{\tau}_K/2}\ \check{G}_i(0)\ e^{i\chi_i\check{\tau}_K/2}$, $i = 1, \ldots, N$. We emphasize that the Green's functions of terminals depend on the corresponding counting field only. The Green's functions of internal nodes $\check{G}_i(\vec{\chi})$ $(i = N+1, \ldots)$ depend on all counting fields. They are obtained from the set of matrix current conservation equations

$$\sum_{j\in i} \check{I}_{ij}(\vec{\chi}) = 0, \qquad \check{I}_{ij}(\vec{\chi}) = \sum_n \frac{2_s T_n^{(ij)}[\check{G}_i(\vec{\chi}), \check{G}_j(\vec{\chi})]}{4 + T_n^{(ij)}(\{\check{G}_i(\vec{\chi}), \check{G}_j(\vec{\chi})\} - 2)} \tag{13.38}$$

and the normalization conditions $[\check{G}_i(\vec{\chi})]^2 = \check{1}$. Here the summation goes over all terminals and internal nodes connected to the internal node i. The system of equations can be solved by iteration, as discussed in § 12. Once the Green's functions of internal nodes are known, the cumulant generating function $\mathcal{S}(\vec{\chi})$ is given by Eq. (13.36).

Proof of the summation formula. The charge transferred in the terminal j is given by the state $\check{G}_j$ of the terminal and the state $\check{G}_{c_j}$ of the adjacent internal node c_j coupled to it. Therefore, to prove Eq. (13.36) we have to verify that $\mathcal{S}(\vec{\chi})$ satisfies[25)]

$$\frac{\partial\mathcal{S}(\vec{\chi})}{\partial(i\chi_j)} = \frac{1}{2}\,\mathrm{Tr}\left(\check{\tau}_1\check{I}_{c_j j}(\vec{\chi})\right), \tag{13.39}$$

for all terminals $j = 1, \ldots, N$. First we give a proof for the circuit which consists of a single internal node c coupled to several terminals, and then extend it to the arbitrary circuit. The following mathematical property is useful: If $\check{G}(\vec{\chi})^2 = \check{1}$ and $[\check{A}, \check{G}(\vec{\chi})] = 0$, then

$$\mathrm{Tr}\{\check{A}, \partial_{i\chi_j}\check{G}(\vec{\chi})\} = 0. \tag{13.40}$$

This property follows after taking the derivative of $\check{G}(\vec{\chi})^2 = \check{1}$, multiplying both sides by $\check{A}\check{G}(\vec{\chi})$ and taking the trace.

From Eq. (13.36) we obtain

$$\frac{\partial\mathcal{S}(\vec{\chi})}{\partial(i\chi_j)} = \sum_k\sum_n \mathrm{Tr}\left(\frac{T_n^{(k)}(\{\partial_{i\chi_j}\check{G}_k, \check{G}_c\} + \{\check{G}_k, \partial_{i\chi_j}\check{G}_c\})}{4 + T_n^{(k)}(\{\check{G}_k, \check{G}_c\} - 2)}\right), \tag{13.41}$$

where k labels terminals and n labels transport channels. The second term in Eq. (13.41), with $\{\check{G}_k, \partial_{i\chi_j}\check{G}_c\}$, can be written as $\mathrm{Tr}\{\check{A}, \partial_{i\chi_j}\check{G}_c\}$ where

$$\check{A} = \sum_k\sum_n \frac{T_n^{(k)}\check{G}_k}{4 + T_n^{(k)}(\{\check{G}_k, \check{G}_c\} - 2)}. \tag{13.42}$$

The matrix $\check{A}$ commutes with $\check{G}_c$ due to matrix current conservation $\sum_k \check{I}_k = 0 = [\check{A}, \check{G}_c]$. This implies $\mathrm{Tr}\{\check{A}, \partial_{i\chi_j}\check{G}_c\} = 0$ [Eq. (13.40)], and the term vanishes from Eq. (13.41). Concerning the first term in Eq. (13.41), we notice that $\partial_{i\chi_j}\check{G}_k = \delta_{jk}[\check{\tau}_1, \check{G}_j]/2$ because the Green's function $\check{G}_k$ in the terminal depends on the counting

[25)] We consider the circuit in the normal state. The proof for the superconducting circuit is analogous.

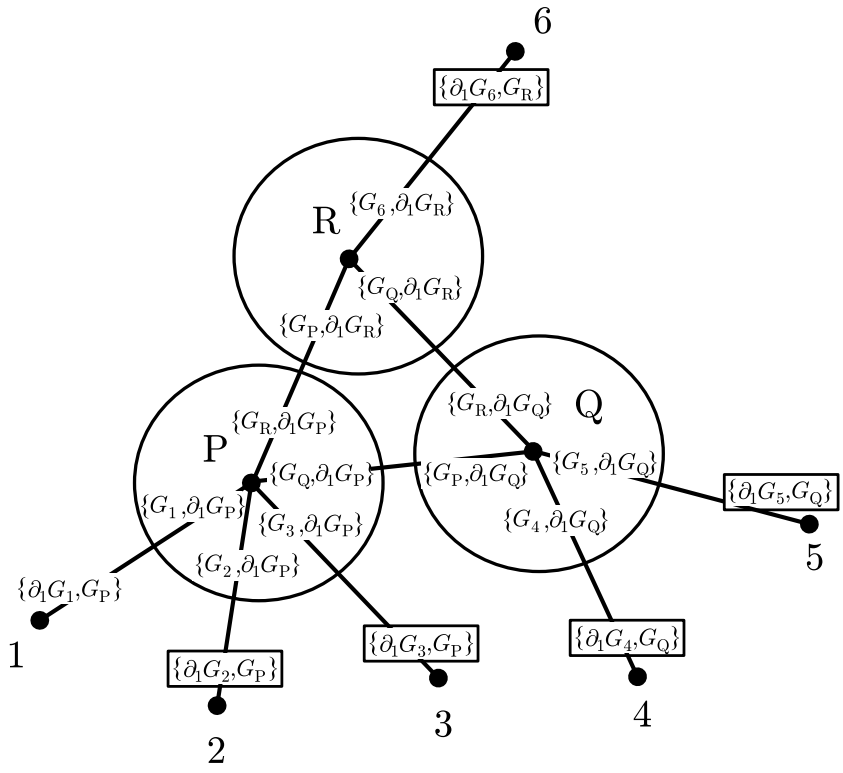

Fig. 21: *The proof of the summation formula given by Eq.* (13.36). *The statistics of the charge transferred into terminal* 1 *depends on the state* $\check{G}_1$ *of the terminal and the state* $\check{G}_P$ *of the node coupled to it. The terms enclosed in circles vanish due to matrix current conservation. The terms enclosed in rectangles are zero because the corresponding Green's functions do not depend on* χ_1.

field χ_k only. Using the invariance of the trace upon cyclic permutations, Eq. (13.41) reduces to Eq. (13.39).

Extension to the arbitrary circuit. In the case of multiterminal circuit with several internal nodes, the sum over k in Eq. (13.41) has to be replaced by the sum over all connected pairs of nodes. Let us consider $\partial\mathcal{S}(\vec{\chi})/\partial(i\chi_1)$. Figure 21 shows numerators of Eq. (13.41) for one particular circuit. Terms enclosed in circles around internal nodes give zero after summation in Eq. (13.41) because of the matrix current conservation. Terms enclosed in rectangles at terminals $k = 2, 3, \ldots$ are zero because the Green's functions of terminals do not depend on χ_1. The only non-zero term in Eq. (13.41) is the one with $\{\partial_{i\chi_1}\check{G}_1, \check{G}_P\}$ at the terminal $j = 1$, which reduces to Eq. (13.39).

§ **13.4. Distribution of transmission eigenvalues.** The circuit-theory equations simplify considerably in the case of a two-terminal junction in the normal state [66, 113]. First, let us consider a junction with two connectors with transmission eigenvalues $\{T_n^{(1)}\}$ and $\{T_n^{(2)}\}$ in series. The Green's functions of the terminals are $\check{G}_1$ and $\check{G}_2$ and the Green's function of the central node is $\check{G}_c$. In general, $\check{G}_c$ can be written as a linear combination $\check{G}_c = c + \vec{g}_c \cdot \vec{\tau}$ where $\vec{\tau} = (\check{\tau}_1, \check{\tau}_2, \check{\tau}_3)$. From $\check{G}_c^2 = c^2 + \vec{g}_c^2 + 2c\vec{g}_c \cdot \vec{\tau} = \check{1}$ we obtain that $c = 0$ and $\vec{g}_c^2 = 1$. The vector $\vec{g}_c$ can be expanded as $\vec{g}_c = \alpha\vec{g}_1 + \beta\vec{g}_2 + \vec{g}'$, where $\vec{g}_{1,2}$ are given by $\check{G}_{1,2} = \vec{g}_{1,2} \cdot \vec{\tau}$ and $\vec{g}'$ is perpendicular to $\vec{g}_{1,2}$. From the matrix current conservation we obtain $\vec{g}' = 0$. Therefore, $\check{G}_c$ can be expressed as a linear combination of the Green's functions of

terminals, $\check{G}_c = \alpha\check{G}_1 + \beta\check{G}_2$. Because $\check{G}_i^2 = \check{1}$, the products of the Green's functions $\check{G}_i\check{G}_j$ $(i,j = 1,2,c)$ commute with each other and can be treated as scalars, effectively. From $\check{G}_1\check{G}_2 = (\check{G}_1\check{G}_c)(\check{G}_c\check{G}_2)$ we see that it is convenient to introduce a 'voltage drop' across the connector by $\check{\phi}_{12} = -i\ln(\check{G}_1\check{G}_2)$. The voltage drops commute with each other and are additive, $\check{\phi}_{12} = \check{\phi}_{1c} + \check{\phi}_{c2}$. A similar discussion holds for the case of several junctions in series.

The matrix current and the cumulant generating function of a connector can be expressed in terms of the scalar functions $I(\phi)$ and $\mathcal{S}(\phi)$:

$$\check{I} = iI[\phi = -i\ln(\check{G}_1\check{G}_2)], \qquad \mathcal{S} = \operatorname{Tr}\mathcal{S}[\phi = -i\ln(\check{G}_1\check{G}_2)], \tag{13.43}$$

where

$$I(\phi) = \sum_n \frac{T_n\sin(\phi)}{1 - T_n\sin^2(\phi/2)}, \qquad \mathcal{S}(\phi) = \sum_n \ln[1 - T_n\sin^2(\phi/2)]. \tag{13.44}$$

For the tunnel junction ($T_n \ll 1$), ballistic point contact ($T_n = 1$), and diffusive wire [113]:

$$I_{\text{tun}}(\phi) = \frac{G}{G_Q}\sin(\phi), \qquad \mathcal{S}_{\text{tun}}(\phi) = -\frac{G}{G_Q}\sin^2(\phi/2), \tag{13.45a}$$

$$I_{\text{qpc}}(\phi) = \frac{G}{G_Q}2\tan(\phi/2), \qquad \mathcal{S}_{\text{qpc}}(\phi) = \frac{G}{G_Q}2\ln[\cos(\phi/2)], \tag{13.45b}$$

$$I_{\text{diff}}(\phi) = \frac{G}{G_Q}\,\phi, \qquad \mathcal{S}_{\text{diff}}(\phi) = -\frac{G}{G_Q}\,\phi^2/4, \tag{13.45c}$$

where G is the conductance and $G_Q = e^2/\pi$. Equations (13.44) can be rewritten in terms of the distribution of transmission eigenvalues [c.f. Eq. (10.39)]:

$$I(\phi) = \int_0^1 dT\rho(T)\frac{T\sin(\phi)}{1 - T\sin^2(\phi/2)}, \qquad \mathcal{S}(\phi) = \int_0^1 dT\rho(T)\ln[1 - T\sin^2(\phi/2)], \tag{13.46}$$

with $\rho(T)$ being normalized to the total conductance, $\int dTT\rho(T) = G/G_Q$. If the current $I(\phi)$ is known, the distribution $\rho(T)$ can be obtained from the inverse transformation. Let us put $\phi = i\theta + \pi$:

$$I(i\theta + \pi) = \int_0^1 dT\rho(T)\frac{-i\sinh(\theta)}{T^{-1} - \cosh^2(\theta/2)}. \tag{13.47}$$

Choosing $\cosh^2(\theta/2) = T'^{-1} + i0$ and using that $(x \pm i0)^{-1} = (\text{p.v. } x^{-1}) \mp i\pi\delta(x)$ we obtain

$$\rho(T) = \frac{1}{2\pi}\frac{1}{T\sqrt{1-T}}\operatorname{Re} I\left[\phi = \pi - 0 + 2i\operatorname{arccosh}\left(\frac{1}{\sqrt{T}}\right)\right]. \tag{13.48}$$

The solution strategy for the two-terminal junctions is the following. For the given voltage drop ϕ across the junction, the voltages $\phi_i = \phi_i(\phi)$ of internal nodes are determined from the current conservation. The current $I(\phi)$ is then calculated between a pair of neighboring nodes. The transmission distribution $\rho(T)$ for the composite junction is obtained from Eq. (13.48). The statistics of charge transfer is given by Eq. (13.33), with the summation over transport channels replaced by integration over $\rho(T)$. Alternatively, the statistics of charge transfer can be obtained from $\mathcal{S}(\chi_1,\chi_2) = \operatorname{Tr}\mathcal{S}\{\phi = -i\ln[\check{G}_1(\chi_1)\check{G}_2(\chi_2)]\}$ with $\mathcal{S}(\phi)$ given by integration of current, $\mathcal{S}(\phi) = -\int d\phi\, I(\phi)/2$, or by summation of the contributions of the adjacent

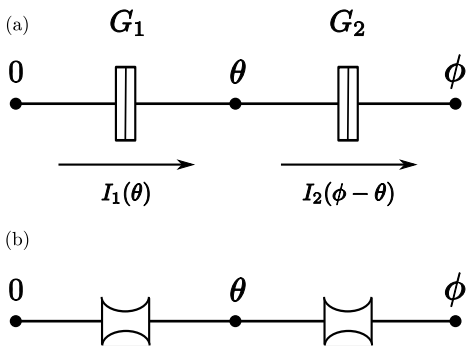

Fig. 22: *The circuit-theory representation of two tunnel junctions (a) and two ballistic contacts (b) in series. The 'voltage' $\theta = \theta(\phi)$ of internal node is obtained from the current conservation $I_1(\theta) = I_2(\phi - \theta)$. The transmission distribution of the composite junction is obtained from $I(\phi) = I_1[\theta(\phi)]$ using Eq.* (13.48).

pairs of nodes $\mathcal{S}(\phi) = \sum_i \mathcal{S}_i[\phi_{i+1}(\phi) - \phi_i(\phi)]$. This approach can be advantageous because it avoids the integration over the transmission distribution $\rho(T)$.

To illustrate the method, we obtain the distribution $\rho(T)$ for the cases of two tunnel junctions and two ballistic contacts in series, as shown in Fig. 22 [66, 113]. The conductances of the junctions are G_1 and G_2. From the current conservation $I(\phi) = I_1(\theta) = I_2(\phi - \theta)$ we obtain

$$I(\phi) = \frac{G_1 G_2 \sin(\phi)}{G_Q \sqrt{G_1^2 + G_2^2 + 2G_1 G_2 \cos(\phi)}} \tag{13.49}$$

for the double tunnel junction. From Eq. (13.48) we find

$$\rho_{2\mathrm{tun}}(T) = \frac{G/G_Q}{\pi\sqrt{T^3(T_0 - T)}} \tag{13.50}$$

for $T < T_0 = 4G_1G_2/(G_1+G_2)^2$, and $\rho_{2\mathrm{tun}}(T) = 0$ otherwise, with $G = G_1G_2/(G_1 + G_2)$. The Fano factor for the double tunnel junction is given by $F_{2\mathrm{tun}} = (G_1^2 + G_2^2)/(G_1 + G_2)^2$. The distribution $\rho_{2\mathrm{tun}}(T)$ is shown in Fig. 23 (a) for different values of the junction asymmetry G_1/G_2. For asymmetric junction $G_1 \neq G_2$, a gap in the transmission distribution exists at high transmission probabilities. For the symmetric case $G_1 = G_2$, the resonances open highly transmissive channels. The same distribution has been obtained previously in § 10.6 using the simple ballistic double-barrier model of low transparency and averaging over the phase shifts.

For the double point contact we have

$$I(\phi) = \frac{G_1 + G_2}{G_Q} \cot(\phi/2) \left(\sqrt{1 + \frac{4G_1G_2}{(G_1+G_2)^2} \tan^2(\phi/2)} - 1 \right). \tag{13.51}$$

The distribution of the transmission eigenvalues for the composite junction is given by [66]

$$\rho_{2\mathrm{qpc}}(T) = \frac{G_1 + G_2}{G_Q} \frac{1}{2\pi T} \sqrt{\frac{T - T_0}{1 - T}} \tag{13.52}$$

for $T > T_0 = (G_1 - G_2)^2/(G_1 + G_2)^2$, and $\rho_{2\mathrm{qpc}}(T) = 0$ otherwise. This distribution results in the Fano factor $F_{2\mathrm{qpc}} = G_1G_2/(G_1 + G_2)^2$. The distribution $\rho_{2\mathrm{qpc}}(T)$ is shown in Fig. 23 (b) for different values of the junction asymmetry G_1/G_2. The node coupled to the terminals by ballistic contacts represents a circuit-theory model

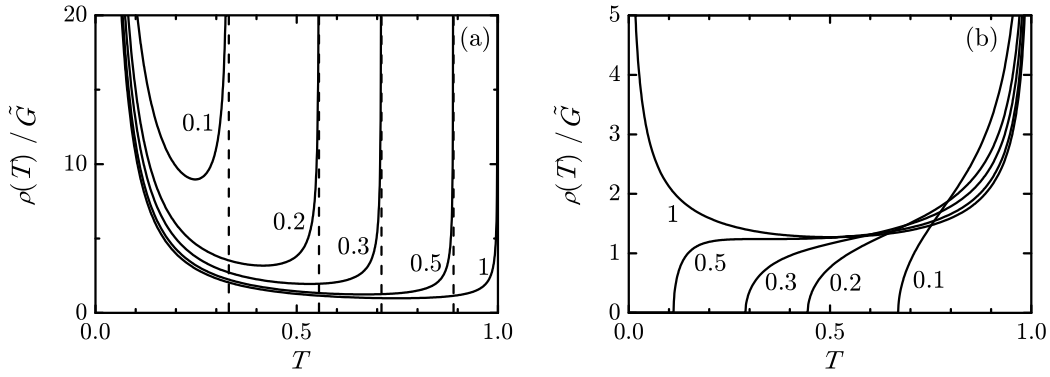

Fig. 23: *The distributions of transmission eigenvalues for two tunnel junctions (a) and two ballistic contacts (b) in series. Numbers indicate the ratio G_1/G_2. Transmission distributions are normalized to the same value of the total conductance, $\int dT\, T\rho(T) \equiv G/G_Q = \tilde{G}$.*

of a chaotic cavity. The diffusive scattering in the cavity or the chaotic scattering at the boundaries provide the isotropization of the electronic motion. Indeed, the same result can be obtained using the random matrix theory [46] with the scattering matrix being a member of the Dyson circular ensemble.

We conclude this paragraph by a remark on diffusive connectors. Because of the linear $I - \phi$ relation, the concatenation of the diffusive connectors does not change the shape of the overall transmission distribution: the combined junction is again diffusive. Furthermore, the diffusive limit is universal in the sense that it is reached for the large number of junctions in series (for the fixed total conductance), independent on the individual properties of the junctions. This is because the voltage drops across the junctions are small and the $I - \phi$ relations can be linearized. The representation of a diffusive wire as an array of tunnel junctions can be beneficial computationally in the problems which require dephasing [91] or heating effects distributed within the junction to be taken into account.

§ **13.5. Current cross correlations.** Current cross correlations in different terminals of a multiterminal circuit in normal state are negative at any temperature [34]. However, in the presence of a superconducting terminal, the current cross correlations in normal terminals can be of either sign. The current in a normal terminal is the sum of electron and hole contributions. The current cross correlation between normal terminals α and β is given by $\langle \Delta\hat{I}_\alpha \Delta\hat{I}_\beta \rangle = \sum_{\mu,\nu} \langle \Delta\hat{I}^\mu_\alpha \Delta\hat{I}^\nu_\beta \rangle$ where $\mu, \nu = \mathrm{e}, \mathrm{h}$ label electron and hole currents. As shown by Anantram and Datta [164], the electron-electron and the hole-hole cross correlation term $\langle \Delta\hat{I}^{\mathrm{e}}_\alpha \Delta\hat{I}^{\mathrm{e}}_\beta \rangle + \langle \Delta\hat{I}^{\mathrm{h}}_\alpha \Delta\hat{I}^{\mathrm{h}}_\beta \rangle$ is negative, while the mixed electron-hole term $\langle \Delta\hat{I}^{\mathrm{e}}_\alpha \Delta\hat{I}^{\mathrm{h}}_\beta \rangle + \langle \Delta\hat{I}^{\mathrm{h}}_\alpha \Delta\hat{I}^{\mathrm{e}}_\beta \rangle$ is positive ($\alpha \neq \beta$). The overall sign of the current cross correlation depends on the relative strength of the two terms and can be of either sign depending on the interplay between normal and Andreev reflection probability at the superconductor and the proximity effect induced within the junction [26]. In the normal state junction, the mixed electron-hole term vanishes and the cross correlations at different terminals are negative.

In the following we study a chaotic cavity coupled to a superconductor and the two normal terminals. The normal terminals (drains) are biased by the voltage

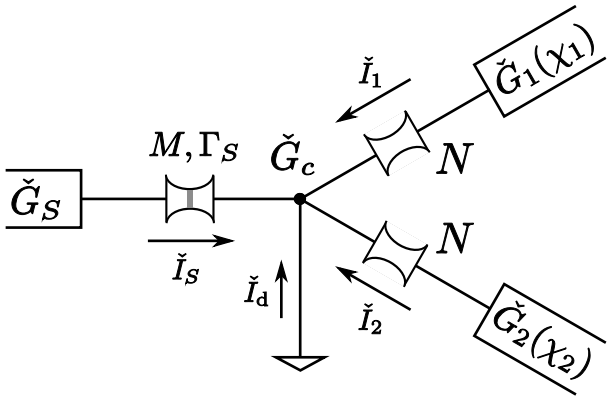

Fig. 24: *The circuit theory representation of a cavity coupled to the superconductor and two normal terminals. The coupling to the superconductor is via quantum point contact with M channels of transparency Γ_S and to the normal terminals via ballistic point contacts with N channels. The Green's function of a cavity has to be obtained from the matrix current conservation and the normalization condition. The matrix current $\check{I}_\mathrm{d}$ models the suppression of the proximity effect in the cavity and carries no charge current.*

V with respect to the superconductor (source). We are interested in the current cross correlations in the drain leads. This system has been studied by Samuelsson and Büttiker [165, 166] as a function of the normal backscattering at the cavity-superconductor interface in the limits of fully developed and fully suppressed proximity effect in the cavity. The charge transfer statistics has been obtained by Börlin *et al.* [167] for the tunnel couplings of the cavity to the leads in the presence of the proximity effect. The charge transfer statistics in the absence of the proximity effect in the cavity has been obtained by Belzig and Samuelsson [168]. The noise and charge transfer statistics in a two terminal double junction have been studied by Bignon *et al.* [169] and Samuelsson [93] as a function of the quasiparticle dwell time in the cavity, giving rise to the partially suppressed proximity effect.

In this paragraph we study current cross correlations in a 3-terminal setup taking into account finite quasiparticle dwell time. Alternatively, the suppression of the proximity effect can be varied by applying a small magnetic field. The circuit theory representation of the system is depicted in Fig. 24. The cavity is coupled to the superconductor via quantum point contact with M channels of transparency Γ_S and to the normal terminals via ballistic contacts with N channels. The normal terminals are biased by voltage V with respect to the superconductor. In the limit of low temperatures and bias voltages smaller than the superconducting gap, $T_e \ll |eV| \ll |\Delta|$, the Green's functions of the superconductor and the normal terminals are given by

$$\check{G}_S = \check{1} \otimes \bar{\tau}_2, \qquad \check{G}_i = e^{-i\chi_i \check{\tau}_K/2} \begin{pmatrix} \bar{\tau}_3 & -2 \\ 0 & -\bar{\tau}_3 \end{pmatrix} e^{i\chi_i \check{\tau}_K/2}. \tag{13.53}$$

Here $\check{G}_{1,2}$ are given for the energy interval $|\mathcal{E}| < |eV|$ relevant for transport and $\check{\tau}_K = \check{\tau}_1 \otimes \bar{\tau}_3$. The matrix currents which flow from the terminals into the cavity are given by

$$\check{I}_S = \frac{2M\Gamma_S[\check{G}_S, \check{G}_c]}{4 + \Gamma_S(\{\check{G}_S, \check{G}_c\} - 2)}, \tag{13.54a}$$

$$\check{I}_i = \frac{2N[\check{G}_i, \check{G}_c]}{2 + \{\check{G}_i, \check{G}_c\}}, \tag{13.54b}$$

$$\check{I}_\mathrm{d} = -i\frac{\mathcal{E}}{E_\mathrm{d}}(2N + M\Gamma_S)[\check{1} \otimes \bar{\tau}_3, \check{G}_c]. \tag{13.54c}$$

Here $\check{I}_\mathrm{d}$ is the so called coherence leakage current [150]. It takes into account breaking of the electron-hole correlations in the cavity, i.e., the suppression of the proximity effect due to the fact that the electron and hole at the same energy $\mathcal{E}$ from the Fermi level have a slightly different wave vectors. The parameter E_d is equal to the inverse quasiparticle dwell time in the cavity (§ 12). For $E_\mathrm{d} \gg |eV|$ ($E_\mathrm{d} \ll |eV|$) the proximity effect is fully developed (suppressed). The Green's function of the cavity $\check{G}_c = \check{G}_c(\mathcal{E}; \chi_1, \chi_2)$ is obtained from the matrix current conservation $\check{I}_S + \check{I}_1 + \check{I}_2 + \check{I}_d \equiv [\check{M}, \check{G}_c] = 0$ and the normalization condition $\check{G}_c^2 = \check{1}$ using the method of iterations described in § 12. Here

$$\begin{aligned}\check{M} \equiv & \frac{2M\Gamma_S\check{G}_S}{4 + \Gamma_S(\{\check{G}_S, \check{G}_c\} - 2)} + \frac{2N\check{G}_1}{2 + \{\check{G}_1, \check{G}_c\}} \\ & + \frac{2N\check{G}_2}{2 + \{\check{G}_2, \check{G}_c\}} - i\frac{\mathcal{E}}{E_\mathrm{d}}(2N + M\Gamma_S)\ \check{1} \otimes \bar{\tau}_3.\end{aligned} \tag{13.55}$$

The convergence of the method can be improved by adding a term proportional to the Green's function of the cavity, $\check{M} \to \check{M} + \lambda\check{G}_c$, which does not change the fixed point. After the $\check{G}_c(\mathcal{E}; \chi_1, \chi_2)$ is obtained, the matrix currents can be calculated using Eqs. (13.54). The current cross correlation in the normal terminals is given by

$$\begin{aligned}S_{12} &= \frac{e^2}{t_0}\frac{\partial^2\mathcal{S}(\chi_1, \chi_2)}{\partial(i\chi_1)\partial(i\chi_2)}\bigg|_{\chi_{1,2}=0} \\ &= \left(\frac{\partial}{\partial(i\chi_2)}\frac{e^2}{8\pi}\int_{-|eV|}^{|eV|} d\mathcal{E}\ \mathrm{Tr}\left(\check{\tau}_K\check{I}_1(\mathcal{E}; \chi_1 = 0; \chi_2)\right)\right)_{\chi_2=0}\end{aligned} \tag{13.56}$$

where the trace is taken in the Keldysh-Nambu space. An analogous formula in terms of $\check{I}_2$ is obtained by taking the derivative over χ_2 first.

The current cross correlation S_{12} is shown in Fig. 25 for negligible normal backscattering between the cavity and the superconductor ($\Gamma_S = 1$). The suppression of the proximity effect in the cavity is controlled by varying the inverse quasiparticle dwell time E_d. The limits of developed (top curve) and fully suppressed proximity effect (bottom curve) coincide with analytical results of Samuelsson and Büttiker [165, 166]:

$$\frac{S_{12}}{S_0} = \frac{(1+\gamma)^2}{2\gamma^2}\left(\frac{1}{1+\gamma} - \frac{2\gamma}{f} - \frac{f^2 - 16\gamma^3}{f^{5/2}}\right) \tag{13.57a}$$

for $E_\mathrm{d}/|eV| \gg 1$, and

$$\frac{S_{12}}{S_0} = -\frac{\gamma^2(1+\gamma)}{(2+\gamma)^4} \tag{13.57b}$$

for $E_\mathrm{d}/|eV| \ll 1$. Here $f(\gamma) = 1 + 6\gamma + \gamma^2$, $\gamma = 2N/M$, and $S_0 = G_Q N|eV|$. In the presence of the proximity effect, the current cross correlation S_{12} is positive (negative) for $\gamma \lesssim 0.5$ ($\gamma \gtrsim 0.5$). In the former case the positive electron-hole cross correlation term gives the dominant contribution while in the latter case the negative electron-electron and hole-hole cross correlation term is the dominant one [165]. In

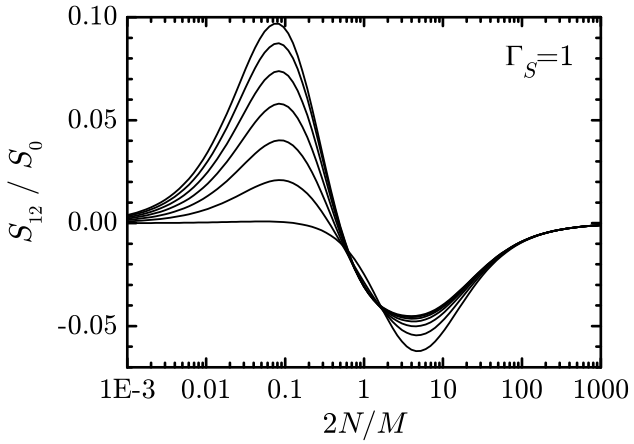

Fig. 25: *The current cross correlation S_{12} in units of $S_0 = G_Q N|eV|$ in the limit of negligible normal backscattering at the cavity-superconductor contact, $\Gamma_S = 1$. Different curves show the crossover from the developed proximity effect (top) to the fully suppressed one (bottom) as the parameter E_d is decreased: $E_\mathrm{d}/|eV| = 3$, 2.5, 2, 1.5, 1, 0.5, 0.01.*

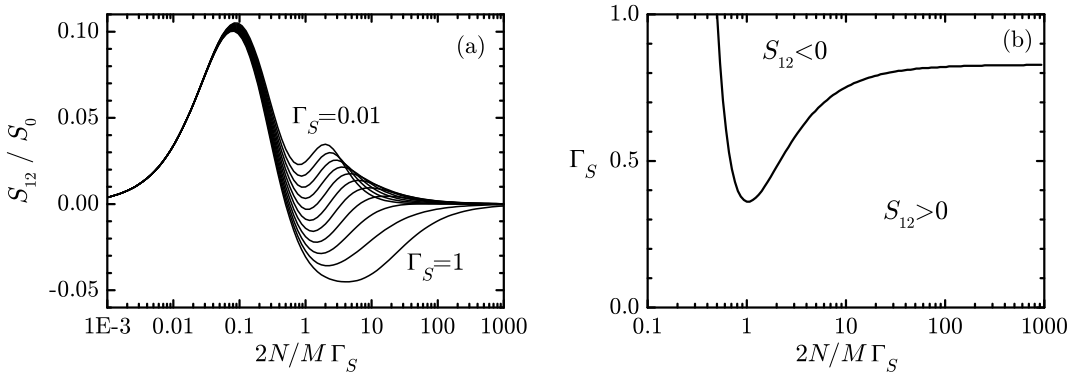

Fig. 26: *Current cross correlations S_{12} are shown as a function of the normal backscattering Γ_S at the cavity-superconductor interface for fully developed proximity effect ($E_\mathrm{d} \gg |eV|$). The curves in panel (a) correspond to $\Gamma_S = 0.01$, 0.1, 0.2, …, 0.9, 1, from top to bottom. The crossover from $S_{12} < 0$ to $S_{12} > 0$ as a function of Γ_S is shown in panel (b) with the solid line denoting $S_{12} = 0$. In the limit $2N/M\Gamma_S \gg 1$ the results do not depend on the proximity effect and $S_{12}/S_0 = (M/2N)R_A(1 - 2R_A)$ with $R_A = \Gamma_S^2/(2 - \Gamma_S)^2$. The crossover from $S_{12} < 0$ to $S_{12} > 0$ is at $R_A = 1/2$, i.e., $\Gamma_S \approx 0.83$.*

the absence of the proximity effect, the cross correlations S_{12} are always negative for $\Gamma_S = 1$, independent of γ.

The effect of the normal backscattering Γ_S at the cavity-superconductor interface is shown in Fig. 26 (a) for the case of developed proximity effect. As the normal backscattering increases, the current cross correlations S_{12} become positive. Figure 26 (b) shows the crossover from $S_{12} < 0$ to $S_{12} > 0$ as a function of Γ_S. The normal backscattering at the superconductor shifts S_{12} towards the positive values also in the absence of the proximity effect [166]. In the limit of the dominant coupling to the normal terminals $2N/M\Gamma_S \gg 1$, the charges transferred across the

junction exhibit only one Andreev reflection at the cavity-superconductor interface. The transfer from the cavity to the normal leads is practically reflectionless. In this case the results do not depend on the proximity effect. The charge transfer statistics can be obtained from the simple counting, as in § 8. The electrons are transferred from the superconductor to the cavity *in pairs* with probability $R_A = \Gamma_S^2/(2-\Gamma_S)^2$ in each transport channel. The electrons are then independently partitioned into the normal terminals with probability 1/4 to end up in the same branch and 1/2 to end up in different branches. Therefore, the cumulant generating function is given by $\mathcal{S}(\chi_1,\chi_2) = (eVt_0/\pi)M\ln[1-R_A+(R_A/4)(e^{2i\chi_1}+e^{2i\chi_2})+(R_A/2)e^{i(\chi_1+\chi_2)}]$ where eVt_0/π is the number of attempts and M is the number of channels. The current cross correlation is given by $S_{12} = (e^2/t_0)\partial^2_{i\chi_1,i\chi_2}\mathcal{S}|_{\chi=0} = (G_Q M|eV|/2)R_A(1-2R_A)$, with $S_{12} < 0$ for $R_A > 1/2$.

In conclusion, we have analyzed current cross correlations in a 3-terminal beam splitter geometry using circuit theory of charge transport. The advantage of the approach is in straightforward application of the method and direct numerical implementation of the circuit-theory rules. Also, the calculation can be easily extended to access the higher-order current correlations at finite temperatures and the probability distribution of transferred charge.

CHAPTER V

Counting statistics of Andreev scattering in a cavity

§ 14. Introduction

In this Chapter we study the full counting statistics of coherent charge transport in a chaotic cavity using the circuit theory of mesoscopic transport. We show that the system of matrix equations for the Green's function of the cavity can be solved, effectively, as a system of scalar equations independently of the type of leads and without resorting to the matrix components or parametrizations. As an application we find the Green's function for an open asymmetric cavity between arbitrary leads. For the special case of a cavity between the superconductor and normal metal, we find the cumulant generating function and the first three cumulants and discuss the interplay between superconducting proximity effect and scattering properties of the junction. The results are compared with those for a normal-state junction [170] and for different couplings of a cavity to the leads. Current correlations in a structure with high-quality contacts between a cavity and superconductor have been studied experimentally by Choi *et al.* [89] recently.

§ 15. Model

The system we consider is a chaotic cavity coupled to two terminals by mesoscopic junctions characterized by the transmission eigenvalues $\{T_n^{(1)}\}$ and $\{T_n^{(2)}\}$, respectively. Charging of the cavity is negligible if the cavity is large enough and the conductances of the junctions $g_{1,2}$ are much larger than the conductance quantum $G_Q = e^2/\pi$. We assume an isotropic quasiparticle distribution function inside the cavity due to chaotic scattering. The decoherence effects as well as the energy dependence of transmission eigenvalues can be neglected if the total dwell time in the cavity is small with respect to time scales set by the inverse temperature and bias voltage. We apply the circuit theory of mesoscopic transport with the specific parts of the system represented by the corresponding discrete circuit elements, as shown in Fig. 27. The terminals are characterized by known quasiclassical matrix Green's functions $\check{G}_{1,2}$ which depend on the quasiparticle energy, temperature, chemical potential, and counting field and satisfy the normalization condition $\check{G}_1^2 = \check{G}_2^2 = \check{1}$. The Green's functions of terminals are not necessarily the ones of bulk electrodes – for example, they can be nodes that are part of a larger circuit. In the following we will refer to these nodes as terminals. The formulation below is independent of the matrix structure, provided the 'terminal' Green's functions obey the normalization conditions. The chaotic cavity is represented as an internal node associated with an unknown Green's function $\check{G}_c$, which will be obtained from the matrix current conservation and the normalization condition $\check{G}_c^2 = \check{1}$. Left and right junctions ($i = 1, 2$), depicted as connectors, carry matrix currents (see § 12)

$$\check{I}_i = -\sum_n \frac{2_s T_n^{(i)} [\check{G}_i, \check{G}_c]}{4 + T_n^{(i)} (\{\check{G}_i, \check{G}_c\} - 2)}, \tag{15.1}$$

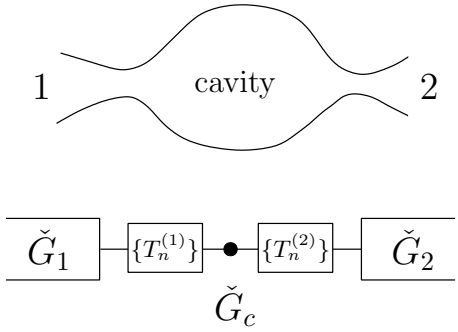

Fig. 27: *A chaotic cavity coupled to the leads by two junctions with transmission eigenvalues* $\{T_n^{(1)}\}$ *and* $\{T_n^{(2)}\}$ *(top). The discrete circuit-theory representation of the system is shown in the lower part. The leads and cavity are characterized by the corresponding matrix Green's functions. The junctions, depicted as connectors, carry conserved matrix currents.*

which flow from the cavity into the leads. The current conservation $\check{I}_1 + \check{I}_2 = 0$ for the Green's function $\check{G}_c$ of the cavity reduces to

$$\left[\check{p}_1\check{G}_1 + \check{p}_2\check{G}_2, \check{G}_c\right] = 0, \tag{15.2}$$

with

$$\check{p}_i = \sum_n \frac{T_n^{(i)}}{4 + T_n^{(i)}(\{\check{G}_i, \check{G}_c\} - 2)}. \tag{15.3}$$

Here we have used the commutation of $\check{p}_{1(2)}$ with $\check{G}_{1(2)}$ and $\check{G}_c$, which is a consequence of the normalization $\check{G}_i^2 = \check{G}_c^2 = \check{1}$, and the matrix property

$$\check{A}^2 = \check{1} \quad \Rightarrow \quad [\check{A}, \{\check{A}, \check{B}\}] = 0. \tag{15.4}$$

We can solve Eq. (15.2) assuming that $\check{p}_1$ and $\check{p}_2$ depend only on the anticommutator of the Green's functions of the terminals, $\check{p}_i = \check{p}_i(\{\check{G}_1, \check{G}_2\})$, and commute with $\check{G}_1$, $\check{G}_2$, and $\check{G}_c$ in accordance with Eq. (15.4). As a result, the Green's function of the cavity can be expressed in terms of Green's functions of the terminals in the form

$$\check{G}_c = \frac{\check{p}_1}{\check{c}}\check{G}_1 + \frac{\check{p}_2}{\check{c}}\check{G}_2, \tag{15.5}$$

where the matrix $\check{c} = \check{c}(\{\check{G}_1, \check{G}_2\})$ accounts for the normalization of $\check{G}_c$. From Eq. (15.5) and by using the normalization conditions $\check{G}_c^2 = \check{G}_1^2 = \check{G}_2^2 = \check{1}$ we obtain the system of equations

$$\check{c}^2 = \check{p}_1^2 + \check{p}_2^2 + \check{p}_1\check{p}_2\check{\mathcal{G}}\,, \tag{15.6}$$

$$\check{c}\,\check{\mathcal{G}}_1 = 2\check{p}_1 + \check{p}_2\check{\mathcal{G}}\,, \tag{15.7}$$

$$\check{c}\,\check{\mathcal{G}}_2 = 2\check{p}_2 + \check{p}_1\check{\mathcal{G}}\,, \tag{15.8}$$

where $\check{\mathcal{G}}_i = \{\check{G}_i, \check{G}_c\}$ and $\check{\mathcal{G}} = \{\check{G}_1, \check{G}_2\}$. This system can be treated, effectively, as a system of scalar equations because all matrices that appear in Eqs. (15.6)–(15.8) depend only on $\check{\mathcal{G}}$ and commute with each other.

The cumulant generating function $\mathcal{S}(\chi)$ of charge transfer can be obtained as a sum of the actions of the connected pairs of nodes (§ 13.3)

$$\mathcal{S}(\chi) = \frac{t_0}{4\pi}\sum_{i=1,2}\sum_n \int d\mathcal{E}\ \mathrm{Tr}\ln\left[\check{1} + \frac{T_n^{(i)}}{2}\left(\frac{\check{\mathcal{G}}_i}{2} - \check{1}\right)\right], \tag{15.9}$$

where the total measurement time t_0 is much larger than the characteristic time scale on which the current fluctuations are correlated. The χ-independent term in the cumulant generating function [given by the normalization requirement $\mathcal{S}(\chi=0)=0$] is omitted for brevity throughout this Chapter. Also, we recall that because of current conservation, it is sufficient to introduce a counting field χ at one lead only, while the full counting field dependence can be obtained by setting $\chi=\chi_1-\chi_2$.

The cumulant generating function $\mathcal{S}$ depends only on the anticommutator $\check{\mathcal{G}}(\chi)$ and is invariant to the exchange of the leads $\check{G}_1 \leftrightarrow \check{G}_2$ or, equivalently, to exchange of the junctions $\{T_n^{(1)}\} \leftrightarrow \{T_n^{(2)}\}$ [see Eqs. (15.2) and (15.3)]. Therefore, the same invariance persists [152,169,170] in all coherent (or low bias) transport properties of two-terminal double junctions – such as current (conductance), noise (Fano factor), and higher cumulants – independently of the type of leads or specific properties of the junctions. This invariance does not hold in the presence of dephasing [93, 169] which can be modelled by an additional lead that carries the coherence leakage current [26, 28, 46, 150].

In the following we consider an analytically tractable case of a chaotic cavity coupled to the terminals by two quantum point contacts with N_1 and N_2 open channels, respectively. The transmission eigenvalues of the contacts are $T_n^{(i)}=1$ for $n=1,\ldots,N_i$ and $T_n^{(i)}=0$ otherwise. From Eq. (15.3) and Eqs. (15.6)–(15.8) we find

$$\check{c}=\frac{N_1+N_2}{2}\left(1+\sqrt{1-\frac{4N_1N_2}{(N_1+N_2)^2}\frac{\check{\mathcal{G}}-2}{\check{\mathcal{G}}+2}}\right)^{-1} \tag{15.10}$$

and

$$\frac{\check{p}_{1,2}}{\check{c}}=\frac{1}{2}\left(\pm\frac{N_1-N_2}{N_1+N_2}+\sqrt{1-\frac{4N_1N_2}{(N_1+N_2)^2}\frac{\check{\mathcal{G}}-2}{\check{\mathcal{G}}+2}}\right). \tag{15.11}$$

The Green's function of the cavity and cumulant generating function are given by Eqs. (15.5) and (15.9), respectively. A formally similar result has been obtained recently by Bulashenko [170] using 2×2 Green's functions in Keldysh space which can be expanded over the Pauli matrices. Physically, this implies that the whole circuit is in the normal state, although it is permitted that the terminals are nodes of a larger (normal-state) mesoscopic network. In our approach we do not rely on this expansion and make no assumptions on the particular matrix structure, except for the usual normalization condition. Therefore, Eqs. (15.10) and (15.11) are valid for *any type of terminals*. For example, one terminal can be superconducting, with the Green's function having Keldysh-Nambu matrix structure, or the chaotic cavity can be a part of the larger multiterminal network which consists of different heterojunctions. Additional degrees of freedom – for instance, spin – can be included as well. We emphasize, again, that our solution only resorts to the normalization condition of the terminals. In the case in which the cavity is part of a larger network, Green's functions $\check{G}_{1,2}$ have to be determined by circuit rules. The result for $\check{G}_c$ is valid in this case as well, which can simplify the numerical solution of larger circuits.

It is interesting to check that an alternative approach can give the same result. Coherent connectors in the circuit theory are described by a cumulant generating function of the form

$$\mathcal{S}(\chi)=\frac{t_0}{4\pi}\int d\mathcal{E}\int_0^1 d\mathcal{T}\,\rho(\mathcal{T})\ \mathrm{Tr}\ln\left[\check{1}+\frac{\mathcal{T}}{2}\left(\frac{\check{\mathcal{G}}(\chi)}{2}-\check{1}\right)\right], \tag{15.12}$$

where $\rho(\mathcal{T})$ is the distribution of transmission eigenvalues $\{T_n\}$ for the composite junction. Using the distribution of transmission eigenvalues for an open chaotic cavity [46, 66]

$$\rho_c(\mathcal{T}) = \frac{N_1+N_2}{2\pi}\,\frac{1}{\mathcal{T}}\sqrt{\frac{\mathcal{T}-\mathcal{T}_0}{1-\mathcal{T}}}, \tag{15.13}$$

for $\mathcal{T}_0 < \mathcal{T} < 1$ and $\rho_c(\mathcal{T}) = 0$ otherwise, with $\mathcal{T}_0 = (N_1-N_2)^2/(N_1+N_2)^2$, we obtain $S(\chi)$ as given by Eqs. (15.9)–(15.11). This demonstrates the consistency of the circuit-theory approach with the random matrix theory of scattering matrices.

§ 16. Superconductor – cavity – normal metal junction

In the following we calculate the statistics of charge transport through a chaotic cavity sandwiched between a superconductor and a normal-metal. We present a detailed analysis of the first three cumulants – current, current noise power, and the third cumulant of the current – for an open chaotic cavity at temperatures and bias voltages well below the superconducting gap Δ, when Andreev scattering is the dominant process of the charge transfer. At low energies and temperatures the 4×4 matrix Green's function of the superconductor is $\check{G}_S \equiv \check{G}_1 = \check{1}\bar{\tau}_2$ in the Keldysh($\check{}$)$\otimes$Nambu($\bar{}$) space. The Green's function $\check{G}_N = \check{G}_N(\mathcal{E},\chi) \equiv \check{G}_2$ of the normal terminal incorporates the counting field according to

$$\check{G}_N = e^{-i\chi\check{\tau}_K/2}\,\check{G}_N^0\,e^{i\chi\check{\tau}_K/2}, \tag{16.1}$$

where $\check{\tau}_K = \check{\tau}_1\bar{\tau}_3$ and $\check{\tau}_i$ and $\bar{\tau}_i$ are Pauli matrices. The bare Green's function of the normal-metal lead is given by

$$\check{G}_N^0 = \begin{pmatrix} \bar{\tau}_3 & 2\bar{K} \\ 0 & -\bar{\tau}_3 \end{pmatrix}, \quad \bar{K} = \begin{pmatrix} 1-2f_N^+ & 0 \\ 0 & 1-2f_N^- \end{pmatrix}, \tag{16.2}$$

where $f_N^\pm = \{\exp[(\pm\mathcal{E}+eV)/k_BT_e]+1\}^{-1}$ accounts for the voltage bias of the normal-metal lead, with the energy $\mathcal{E}$ measured in respect to the chemical potential of the superconductor. From Eqs. (15.9)–(15.11), we find the following expression for the cumulant generating function:

$$\mathcal{S}(\chi) = \frac{t_0}{2\pi}\int d\mathcal{E}\sum_{j=1,2} N_j \ln\left(r_j + \sqrt{r_j^2 - 64N_j^4(1+a)}\right), \tag{16.3}$$

where

$$r_{1(2)} = a(N_1-N_2)^2 + (3N_{1(2)}+N_{2(1)})^2 + \sqrt{(1+a)[a(N_1-N_2)^4 + (N_1^2+N_2^2+6N_1N_2)^2]}\,. \tag{16.4}$$

Here, $a = (e^{2i\chi}-1)\tilde{f}_N^+\tilde{f}_N^- + (e^{-2i\chi}-1)f_N^+f_N^-$ and $\tilde{f}_N^\pm = 1-f_N^\pm$, with a being related to the double-degenerate eigenvalues of $\check{\mathcal{G}} = \{\check{G}_S,\check{G}_N\}$ given by $\lambda_{1,2} = \pm 2i\sqrt{a}$. From Eq. (16.3) we obtain the average current, the current noise power, and the third cumulant according to $I = (e/t_0)\partial_{i\chi}\mathcal{S}|_{\chi=0}$, $S_I = (e^2/t_0)\partial_{i\chi}^2\mathcal{S}|_{\chi=0}$, and $C_I = (e^3/t_0)\partial_{i\chi}^3\mathcal{S}|_{\chi=0}$, respectively. They are given by

$$I = \frac{G_S}{2e}\int d\mathcal{E}\;(\tilde{f}_N^+\tilde{f}_N^- - f_N^+f_N^-), \tag{16.5}$$

$$S_I = G_S\int d\mathcal{E}\;[(\tilde{f}_N^+\tilde{f}_N^- + f_N^+f_N^-) - \gamma_1(\tilde{f}_N^+\tilde{f}_N^- - f_N^+f_N^-)^2], \tag{16.6}$$

and

$$C_I = 2eG_S \int d\mathcal{E}\ (\tilde{f}_N^+ \tilde{f}_N^- - f_N^+ f_N^-) \times [1 - 3\gamma_1(\tilde{f}_N^+ \tilde{f}_N^- + f_N^+ f_N^-) + 2\gamma_2(\tilde{f}_N^+ \tilde{f}_N^- - f_N^+ f_N^-)^2], \quad (16.7)$$

with the total conductance of S-cavity-N junction,

$$G_S = \frac{2e^2}{h}(N_1 + N_2)\left(1 - \frac{N_1 + N_2}{q}\right), \quad (16.8)$$

and the low-temperature Fano factor [28]

$$F_S = \frac{16N_1^2 N_2^2 (N_1 + N_2)}{q^4[q - (N_1 + N_2)]}. \quad (16.9)$$

Here $q = \sqrt{(N_1 + N_2)^2 + 4N_1N_2}$, $\gamma_1 = 1 - F_S/2$, and $\gamma_2 = 1 - F_S[1 - 2N_1N_2(2N_1 + N_2)(N_1 + 2N_2)/q^4]$. After the energy integration in Eq. (16.5), the usual relation $I = G_S V$ is obtained, while the integration in Eqs. (16.6) and (16.7) yields

$$\frac{S_I}{2G_S T_e} = 1 + (F_S/2)\ [v \coth(v) - 1] \quad (16.10)$$

$$= \begin{cases} 1 + (F_S/6)\ v^2, & |v| \ll 1, \\ 1 - F_S/2 + (F_S/2)\ |v|, & |v| \gg 1, \end{cases} \quad (16.11)$$

and

$$\frac{C_I}{eG_S T_e} = 12(\gamma_1 - \gamma_2)\left[\coth(v) + v\left(\frac{1 - \gamma_2}{3(\gamma_1 - \gamma_2)} - \coth^2(v)\right)\right] \quad (16.12)$$

$$= \begin{cases} 2F_S\ v, & |v| \ll 1, \\ \pm 12(\gamma_1 - \gamma_2) + 4(1 - 3\gamma_1 + 2\gamma_2)\ v, & \pm v \gg 1, \end{cases} \quad (16.13)$$

respectively, with $v = eV/T_e$.

The cumulant generating function, Eq. (16.3), takes into account the superconductor proximity effect in the quasiclassical approximation as well as interchannel mixing inside the cavity in the presence of quantum point contacts. In comparison with the normal-state junction (see [170]), Eqs. (16.5)–(16.7) contain products of electron and hole distribution functions due to the Andreev process, which is the mechanism of the charge transport. For example, the term $f_N^+ f_N^- = f_N^+(1 - \tilde{f}_N^-)$ can be interpreted as the probability for an electron emerging from the lead N to be reflected back as a hole, where f_N^+ and $\tilde{f}_N^-$ are the electron- and hole-state occupation numbers. The energy-independent prefactors G_S, γ_1, and γ_2 are also modified by the electron-hole correlations introduced by the superconductor. This change of transport properties due to superconductor proximity effect can be revealed by considering a general S/N junction with transmission distribution $\rho(\mathcal{T})$, at low temperatures and bias voltages ($T_e, |eV| \ll \Delta$). In this case Eq. (15.12) reduces to

$$\mathcal{S}(\chi) = \frac{t_0}{4\pi} \int d\mathcal{E} \int_0^1 dR_A\ \rho_A(R_A) \ln[1 + R_A\ a(\chi)], \quad (16.14)$$

where $\lambda_{1,2} = \pm 2i\sqrt{a}$ are double-degenerate eigenvalues of $\check{\mathcal{G}}$. Equation (16.14) is a multichannel generalization of the single-channel result for an S/N contact obtained by Muzykantskii and Khmelnitskii [171]. In the fully coherent regime, which we consider here, the distribution of Andreev reflection eigenvalues $\rho_A(R_A)$ is simply

related to the distribution of transmissions $\rho(\mathcal{T})$ of the corresponding normal-state junction: $\rho_A(R_A) = 2\rho(\mathcal{T})d\mathcal{T}/dR_A$. The probability of the Andreev reflection is given by $R_A = \mathcal{T}^2/(2-\mathcal{T})^2$ and appears in Eq. (16.14) due to electron-hole symmetry at energies well below the superconducting gap and the inverse dwell time in the cavity. Normal scattering processes are suppressed, and $\mathcal{S}(\chi)$ depends on the counting field through $e^{\pm 2i\chi}$, which accounts for the effective charge of $2e$ that is transferred across the structure in each elementary event of Andreev scattering. In the case of strong electron-hole dephasing within the structure, electrons and holes decouple and the system can be mapped onto an effective normal-state junction [166,168,169] for which the cumulant generating function is given by Eq. (15.12) with the corresponding modification of transmission distribution $\rho(\mathcal{T})$ and boundary conditions $\check{\mathcal{G}}$. In the crossover regime, transport through the structure is not simply related to the normal-state transmission properties and can be described by an effective energy-dependent distribution ρ_A [92] which takes into account the effects of dephasing (coherence leakage currents) at characteristic energies of the order of Thouless energy.

Expanding Eq. (16.14) in the χ field and taking the derivatives, we obtain the current, current noise power, and the third cumulant in the coherent regime as given by Eqs. (16.5)–(16.7), with conductance

$$\tilde{G}_S = 2\int_0^1 d\mathcal{T}\rho(\mathcal{T})\ R_A, \tag{16.15}$$

$\gamma_1 = 2\tilde{G}_S^{-1}\int_0^1 d\mathcal{T}\rho(\mathcal{T})R_A^2$, and $\gamma_2 = 2\tilde{G}_S^{-1}\int_0^1 d\mathcal{T}\rho(\mathcal{T})R_A^3$, where $\tilde{G}_S = G_S/G_Q$. In particular, the Fano factor and the slope of the third cumulant at high bias are given by

$$F_S = \frac{4}{\tilde{G}_S}\int_0^1 d\mathcal{T}\rho(\mathcal{T})\ R_A(1-R_A) \tag{16.16}$$

and

$$\frac{\partial C_I}{\partial(e^2 I)} = \frac{8}{\tilde{G}_S}\int_0^1 d\mathcal{T}\rho(\mathcal{T})\ R_A(1-R_A)(1-2R_A), \tag{16.17}$$

respectively. These expressions are similar to the normal-state ones except for the effective charge doubling and the presence of the Andreev reflection probability R_A instead of normal transmission $\mathcal{T}$, in agreement with previous results obtained within the scattering approach [84]. Using the transmission distribution $\rho_c(\mathcal{T})$ given by Eq. (15.13), we recover the results for an open asymmetric cavity, which were obtained from the circuit theory without the explicit knowledge of $\rho(\mathcal{T})$ for the composite junction.

The total conductance G_S [normalized to the normal-state value $G_N = g_1 g_2/(g_1+g_2)$] and the Fano factor F_S of the S-cavity-N junction are shown in Fig. 28 as functions of the junction asymmetry and for different couplings between the cavity and terminals. For the symmetric quantum-point-contact coupling $g_1/g_2 = 1$, the conductance ratio has the minimal value $G_S/G_N = 2(2-\sqrt{2}) \approx 1.17$, while the Fano factor is maximal, $F_S = (\sqrt{2}+1)/4 \approx 0.60$. In the highly asymmetric limit, $G_S/G_N = 2$ and $F_S = 8g_{min}/g_{max} \approx 0$ (Fig. 28, solid curves). The vanishing of the shot noise in this case is due to the perfect transparency of the dominant (the one which is weakly coupled) quantum point contact. For the case of two tunnel junctions [93, 152] instead of quantum point contacts, the trend is opposite: for the symmetric coupling, $G_S/G_N = 1/\sqrt{2} \approx 0.71$ is maximal and $F_S = 3/4$ is minimal,

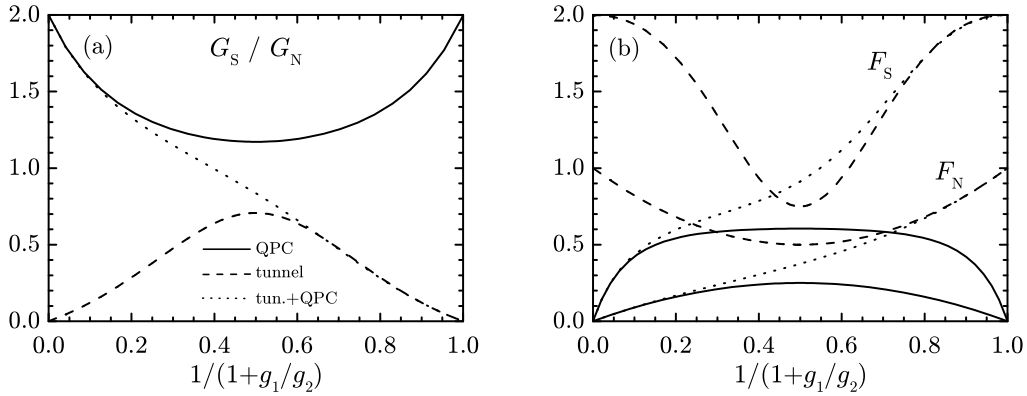

Fig. 28: *Conductance G_S [panel (a)] and the Fano factor F_S [panel (b)] of the S-cavity-N junction as a function of the junction asymmetry $1/(1 + g_1/g_2)$. Results for three different couplings of a cavity to the leads are shown for comparison: coupling by quantum point contacts (solid curves), tunnel junctions (dashed curves), and coupling by tunnel junction from the S side and quantum point contact from the N side (dotted curves). The conductance is normalized to the normal-state value $G_N = g_1 g_2/(g_1 + g_2)$, with $g_i = G_Q N_i$ for quantum point contacts and $g_i = G_Q \sum_n T_n^{(i)}$ for tunnel junctions. The Fano factors F_N for the corresponding normal-state junctions are shown in panel (b) for comparison.*

and for the highly asymmetric coupling, $G_S/G_N = g_{min}/g_{max} \approx 0$ and $F_S = 2$ (see Fig. 28, dashed curves). We point out that these different trends can be used to probe the quality of the contacts. The dotted curves in Fig. 28 show numerical results for the conductance and the Fano factor of a cavity coupled to a superconductor by a tunnel junction and to a normal lead by quantum point contact. We find that the transport properties of the system are not affected by the type of coupling to the superconductor when the quantum point contact on the normal side dominates. This limit is reached at the conductance ratio $g_1/g_2 \gtrsim 5$ of the tunnel- and quantum-point-contact coupling of the cavity to the leads. Therefore, the junction that corresponds to the model of an open chaotic cavity can be realized either with two good quality quantum point contacts from the both sides or it can be an asymmetric junction with only the normal-side quantum point contact of a high quality. The latter is easier to fabricate, and the required asymmetry can be achieved by increasing the contact area of the cavity to the superconductor. Experimentally, the conductance and current noise power have been measured recently by Choi *et al.* [89] in a setup which is very similar to the system we have analyzed. As the estimates from Ref. [89] show, it is possible to fabricate a high-quality contact between cavity and superconductor. The measured values of the Fano factors $F_S = 0.58 \pm 0.10$ and $F_N = 0.25 \pm 0.04$ across the junction in the superconducting- and normal-state regimes, respectively, are in agreement with the model of a symmetric open chaotic cavity [compare with the solid curves in Fig. 28 (b)]. However, the measured conductance ratio $G_S/G_N \approx 0.90$ is in discrepancy with the conductance ratio $G_S/G_N = 1.17$ predicted by this simple model. The difference may originate from the inelastic quasiparticle scattering at the disordered superconductor interface, nonuniversal correction due to relatively large openings of the cavity [67] or dephasing of quasiparticles due to an additional lead which is left floating in the experiment.

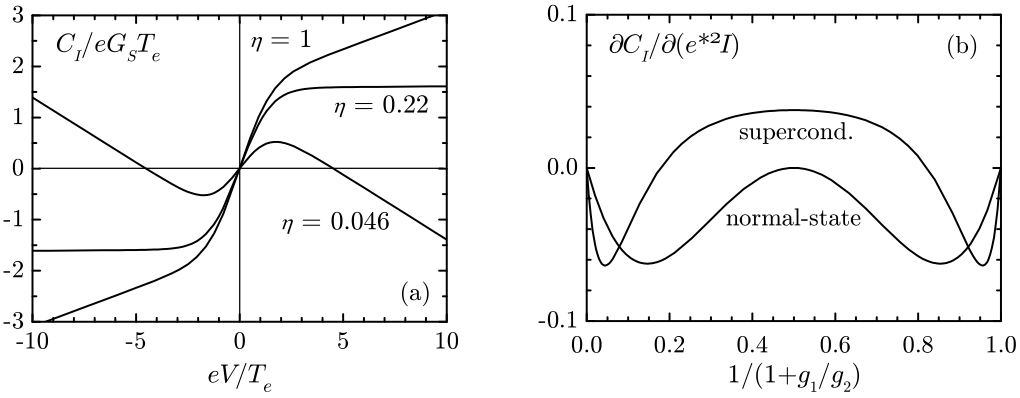

Fig. 29: *The third cumulant as a function of bias-to-temperature ratio [panel (a)], shown for three characteristic junction asymmetries: C_I has the maximal positive slope at high biases for symmetric coupling $\eta = g_{min}/g_{max} = 1$, saturates at high biases for $\eta \approx 0.22$, and has maximal negative slope for $\eta \approx 0.046$. The high-bias slope of the third cumulant is shown in panel (b) as a function of the junction asymmetry, with the normal-state value given for comparison. Effective charge is $e^* = 2e$ and $e^* = e$ for the superconducting and normal-state junction, respectively.*

At high temperatures $T_e \gg |eV|$, current noise power is thermally dominated and linear in conductance and temperature [see Eq. (16.11)], as expected from the fluctuation-dissipation theorem. Thus, to extract the Fano factor from the current noise power measurement, it is necessary to be in the low-temperature, shot noise regime $T_e \ll |eV|$. Experimentally, this requires high bias voltages at which nonlinear $I-V$ characteristics occur, especially in a strongly interacting electron systems, with a difficulty how to distinguish the shot noise contribution from the contribution of thermal noise modified by nonlinear conductance.

Finally, we point out the difference between the superconducting and normal-state asymptotic behavior of the third cumulant at high biases. For an asymmetric open cavity coupled to normal-metal leads, the slope of the voltage-dependent third cumulant is negative, reaching zero for the symmetric cavity [170]. When one lead is superconducting, this slope is negative for highly asymmetric couplings and positive for symmetric couplings [Fig. 29 (b)], with the crossover at $\eta = g_{min}/g_{max} = \sqrt{3+2\sqrt{2}} - \sqrt{2+2\sqrt{2}} \approx 0.22$. Thus, in the normal-state regime the third cumulant changes sign at high enough biases, while in the superconducting case this happens only if the junction is sufficiently asymmetric. This difference originates from the interchannel mixing inside the cavity in the presence of the superconducting proximity effect [152] and can be attributed to the skewness [170] of the Andreev reflection probability distribution function $\rho_A(R_A) = 2\rho_c(\mathcal{T})d\mathcal{T}/dR_A$ [compare with Eqs. (16.15)–(16.17)]. For the normal-state symmetric cavity, the transmission distribution is symmetric – i.e., $\rho_c(\mathcal{T}) = \rho_c(1-\mathcal{T})$ (Fig. 30) – leading to the saturation of the third cumulant at high bias. If the junction is asymmetric, then the gap at low transmissions opens at $0 < \mathcal{T} < \mathcal{T}_0$, shifting the weight of the distribution towards the open channels, $\rho_c(\mathcal{T}) < \rho_c(1-\mathcal{T})$ for $0 < \mathcal{T} < 1/2$, and the high-bias slope of the third cumulant becomes negative. When one lead is superconducting, the weight of distribution $\rho_A(R_A)$ for the symmetric cavity is at low values of the Andreev reflection probabilities, $\rho_A(R_A) > \rho_A(1-R_A)$ for $0 < R_A < 1/2$ (Fig. 30), leading

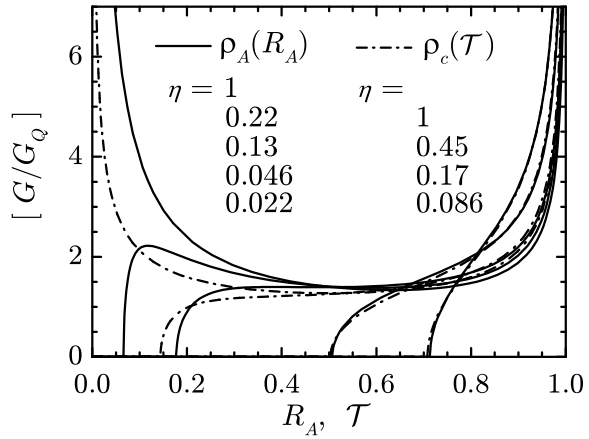

Fig. 30: *Distribution of the Andreev reflection probabilities* $\rho_A(R_A) = 2\rho_c(\mathcal{T})d\mathcal{T}/dR_A$ *(solid curves) and the distribution of transmission eigenvalues* $\rho_c(\mathcal{T})$ *(dash-dotted curves) for an open chaotic cavity, shown for different asymmetries of the junction* $\eta = g_{min}/g_{max}$ *(from top to bottom).*

to the positive high-bias slope of the third cumulant. Only for large asymmetries of the junction does the gap that opens at low R_A prevail and the distribution ρ_A shifts towards the open Andreev channels and the third cumulant becomes negative (Fig. 29). It is interesting to note that the maximally negative slopes of the third cumulant in the normal and in the Andreev case are approximately equal (if the latter are corrected for the effective charge). From Fig. 30 it is seen that indeed the eigenvalue distributions are very similar for these values, with the effect of a superconductor being the change of a junction asymmetry. We believe it would be interesting to confirm these predictions experimentally. They provide much more detailed information on the transmission eigenvalue and Andreev reflection eigenvalue distributions, which go beyond the information obtained from conductance and noise measurements.

§ 17. Summary

In this Chapter, we have studied the charge transport statistics in coherent two-terminal double junctions within the circuit theory of mesoscopic transport. We have shown that the system of circuit-theory matrix equations for the Green's function of the central cavity can be solved, effectively, as a system of scalar equations independently on the type of the leads. For an asymmetric cavity coupled to the leads by quantum point contacts, the Green's function is expressed in a closed analytical form in terms of the matrix Green's functions of the leads. The full counting statistics and the first three cumulants are obtained for a special case of an open cavity between a superconductor and a normal metal, at temperatures and bias voltages below the superconducting gap.

The same results can be obtained by applying the circuit theory while considering the whole structure as a single connector, with the cumulant generating function integrated over the distribution of transmission eigenvalues of the composite junction. This approach manifestly reveals how the subgap transport in S/N structures is affected both by the effective charge doubling due to the Andreev process and by

modification of the transmission properties due to electron-hole correlations introduced by the superconductor.

For an open cavity, the Fano factor is enhanced with respect to the corresponding normal-state junction, in agreement with the experimental results by Choi *et al.* [89] where the high-quality contacts between a cavity and superconductor have been made. In comparison to the tunnel coupling, the conductance and Fano factor exhibit opposite trends as a function of the junction asymmetry, which can be used to experimentally probe the quality of the contacts. The third cumulant is strongly affected by the presence of a superconductor. In contrast to the normal-state case, in which the third cumulant changes the sign at high enough biases, in the case in which one lead is superconducting this happens only if the junction is sufficiently asymmetric. This difference originates from the skewness [170] of the Andreev reflection distribution function, which is in favor of closed Andreev channels for a moderate asymmetries of the junction.

CHAPTER VI

Transport in arrays of chaotic cavities

§ 18. Introduction

Higher-order correlators of current fluctuations in mesoscopic conductors have been studied extensively over the last decade both theoretically [26–28,34,46,172,173] and experimentally [60, 68, 69, 85, 86, 88, 89, 99, 100, 104, 174–176]. The reason is that they contain, in general, additional information to the usual differential conductance such as higher moments of the transmission eigenvalue distribution, the value of the effective charge involved in transport processes, the size of internal energy scales of the system or the correlations intrinsic to the many-body state of entangled systems [30, 32, 177]. While the conductance is proportional to the average transmission probability of the structure at low temperatures, the current noise power S_I depends on the second moment of transmission eigenvalue distribution which is characterized by the Fano factor $F = S_I/|eI| = [\sum_n T_n(1 - T_n)]/\sum_n T_n$. Here e is the electron charge, I is the average current through the sample, and T_n are the transmission eigenvalues. Recent experiments on noise confirmed the theoretical predictions [28, 46] on the universal distributions of transmission eigenvalues in a metallic diffusive wire [60, 174] and in an open chaotic cavity [68, 69] with Fano factors $F = 1/3$ and $F = 1/4$, respectively. The crossover from a single cavity to the diffusive wire limit as the number of internal junctions increases was studied experimentally by Oberholzer *et al.* [68, 69] and Song *et al.* [175] recently.

Particle-hole correlations introduced by a superconducting terminal also modify the noise. The low temperature noise of the subgap transport is doubled for tunnel junctions [88] and in diffusive normal wires in contact with a superconductor [85, 86, 99]. The noise in an open cavity is found to be more than two times larger in the superconducting state [89] than in the corresponding normal state junction, in agreement with theoretical predictions [28].

The third correlator contains the first three moments of transmission eigenvalue distribution and is related to the asymmetry of the distribution [170]. In contrast to the current noise which is thermally dominated at temperatures larger than the bias voltage according to the fluctuation-dissipation theorem, the third correlator is in this regime proportional to the current, without the need to correct for the thermal noise. However, higher-order correlators are increasingly more difficult to measure because of the statistical fluctuations [178] and the influence of environment [32,100]. Recent measurements of the third-order correlations of voltage fluctuations across the nonsuperconducting tunnel junctions by Bomze *et al.* [104] confirmed the Poisson statistics of electron transfer at negligible coupling of the system to environment.

The statistical theory of transport, full counting statistics [141, 143, 179, 180], provides the most detailed description of charge transfer in mesoscopic conductors. The semiclassical cascade approach to higher-order cumulants based on the Boltzmann-Langevin equations has been developed by Nagaev *et al.* [144, 145]. The stochastic path integral theory of full counting statistics was introduced by Pilgram

et al. [146,147]. The quantum-mechanical theory of full counting statistics based on the extended Keldysh-Green's function technique [91,92,148,149] in the discretized form of the circuit theory [66,150] was put forward for multiterminal circuits by Nazarov and Bagrets [151]. In this Chapter we use the circuit theory [113,152] to study the elastic quasiparticle transport in arrays of chaotic cavities focusing on the crossover from a single cavity to the universal limit of a diffusive wire [43,45] as the number of inner contacts increases. We find the analytical expressions for the distribution of transmission eigenvalues, the cumulant generating function and the first three cumulants both in the normal and in the superconducting state, generalizing the previous results on noise [68,69] in such a system to all higher-order correlations. The similar finite-size effects on the noise and the third correlator have been studied numerically by Roche and Douçot [181] within an exclusion model. Ballistic to diffusive crossover in metallic conductors with obstacles as a function of increasing disorder has been studied by Macêdo [182,183] within the scaling theory of transport combined with the circuit theory. The effects of Coulomb interaction on the current and noise in chaotic cavities and diffusive wires have been studied by Golubev *et al.* [184–186]. The noise in series of junctions has been measured by Oberholzer *et al.* [68,69] and Song *et al.* [175] recently.

§ 19. Transport in arrays of cavities

The system we consider consists of chaotic cavities in series between N identical junctions characterized by N_{ch} transverse channels with transmission eigenvalues $\{T_n\}$. We can neglect the energy dependence of the transmission eigenvalues of the system if the electron dwell time is small with respect to time scales set by the inverse temperature and applied voltage. Also we neglect the charging effects assuming that the conductances of the junctions are much larger than the conductance quantum $G_Q = e^2/\pi$. The quasiparticle distribution function is isotropic between junctions due to chaotic scattering in the cavities. We apply the circuit theory of mesoscopic transport and represent the specific parts of the system by the corresponding discrete circuit elements, as shown in Fig. 31. The Greens functions of the leads are denoted as $\check{G}_0(0) \equiv \check{G}_L(0)$ and $\check{G}_N(\chi) \equiv \check{G}_R(\chi)$, while the Greens functions of the internal nodes are $\check{G}_i(\chi)$, $i = 1, \ldots, N-1$. The counting field χ can be incorporated through the boundary condition [152] at the right lead according to

$$\check{G}_N(\chi) = e^{-i\chi\check{\tau}_K/2}\, \check{G}_N(0)\, e^{i\chi\check{\tau}_K/2}. \tag{19.1}$$

Here $\check{G}_{0,N}(0)$ are the bare Greens functions of the Fermi leads in the Keldysh($\check{}$) $\otimes$ Nambu($\bar{}$) space, $\check{\tau}_i$ and $\bar{\tau}_i$ are the Pauli matrices and $\check{\tau}_K = \check{\tau}_1\bar{\tau}_3$. The connection between adjacent nodes is described in general by a matrix current [150]

$$\check{I}_{i,i+1} = -\sum_{n=1}^{N_{ch}} \frac{2_s T_n[\check{G}_{i+1}, \check{G}_i]}{4 + T_n(\{\check{G}_{i+1}, \check{G}_i\} - 2)}, \tag{19.2}$$

which flows from the node i to the node $i+1$. The set of circuit-theory equations for the Greens functions of the internal nodes consists of matrix current conservations $\check{I}_{i,i+1} = \text{const}$ and normalization conditions $\check{G}_i^2 = 1$. As shown in Ref. [187], we can seek for the solution in the form $\check{G}_i = \check{F}_{iL}(\{\check{G}_0, \check{G}_N\})\, \check{G}_0 + \check{F}_{iR}(\{\check{G}_0, \check{G}_N\})\, \check{G}_N$, where the functions $\check{F}_{iL,R}$ depend only on the anticommutator $\{\check{G}_0, \check{G}_N\}$ and therefore commute with all $\check{G}_j$. As a consequence, the anticommutators $\{\check{G}_i, \check{G}_j\}$ depend only on $\{\check{G}_0, \check{G}_N\}$ and commute with all $\check{G}_k$. We emphasize that the above consideration

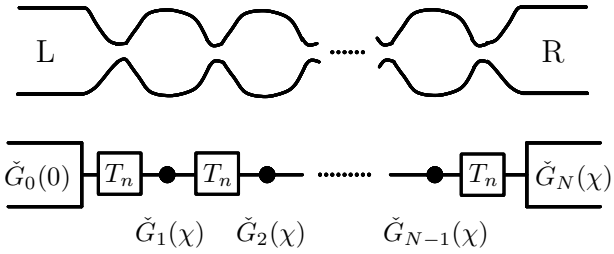

Fig. 31: *An array of chaotic cavities in series between the Fermi leads (top) and the discrete circuit-theory representation of the system (bottom). The leads and the cavities are associated with the corresponding matrix Greens functions $\check{G}_i$. The junctions are characterized by a set of transmission eigenvalues $\{T_n\}$. The matrix current is conserved throughout the circuit.*

is independent of the particular matrix structure of the Greens functions and relies only on the quasiclassical normalization conditions $\check{G}_i^2 = 1$. Because the junctions are identical, the matrix current conservation reduces to [187]

$$\check{G}_i = \frac{\check{G}_{i-1} + \check{G}_{i+1}}{\sqrt{\{\check{G}_{i-1}, \check{G}_{i+1}\} + 2}}. \tag{19.3}$$

Taking the anticommutator of Eq. (19.3) with $\check{G}_i$ and $\check{G}_{i+1}$, respectively, we find that $\{\check{G}_{i-1}, \check{G}_i\} = \{\check{G}_i, \check{G}_{i+1}\} \equiv \check{\mathcal{G}}'$, for all i. Our aim is to find $\check{\mathcal{G}}'$ in terms of $\check{\mathcal{G}} \equiv \{\check{G}_0, \check{G}_N\}$. Now we take the anticommutator of Eq. (19.3) with $\check{G}_0$ and obtain the following difference equation

$$\check{\gamma}_{i+1} - \check{\mathcal{G}}'\check{\gamma}_i + \check{\gamma}_{i-1} = 0, \tag{19.4}$$

where $\check{\gamma}_i = \{\check{G}_0, \check{G}_i\}$. After solving Eq. (19.4) with the boundary conditions $\check{\gamma}_0 = 2$ and $\check{\gamma}_N = \check{\mathcal{G}}$, and using that $\check{\gamma}_1 = \check{\mathcal{G}}'$, we find

$$\check{\mathcal{G}}' = [(\check{\mathcal{G}} + \sqrt{\check{\mathcal{G}}^2 - 4})/2]^{1/N} + [(\check{\mathcal{G}} - \sqrt{\check{\mathcal{G}}^2 - 4})/2]^{1/N}. \tag{19.5}$$

The cumulant generating function $\mathcal{S}(\chi)$ of charge transfer through the structure can be obtained as a sum of the actions of the connected pairs of nodes (§ 13.3). For identical junctions in series $\mathcal{S}(\chi)$ reduces to the contribution of a single junction multiplied by N:

$$\mathcal{S}(\chi) = \frac{t_0}{4\pi} \int d\mathcal{E}\ \mathrm{Tr}[\tilde{\mathcal{S}}(\chi)], \tag{19.6}$$

with

$$\tilde{\mathcal{S}}(\chi) = N \sum_{n=1}^{N_{ch}} \ln \left[\check{1} + \frac{T_n}{2} \left(\frac{\check{\mathcal{G}}'}{2} - \check{1} \right) \right]. \tag{19.7}$$

Here t_0 is the total measurement time which is much larger than the characteristic time scale on which the current fluctuations are correlated. For a large number of junctions, $N \gg 1$, the cumulant generating function given by Eq. (19.6) approaches the universal limit of a diffusive wire [66, 180]

$$\mathcal{S}(\chi) = \frac{t_0 \tilde{g}}{16\pi} \int d\mathcal{E}\ \mathrm{Tr} \left[\mathrm{arccosh}^2 \left(\frac{\check{\mathcal{G}}}{2} \right) \right], \tag{19.8}$$

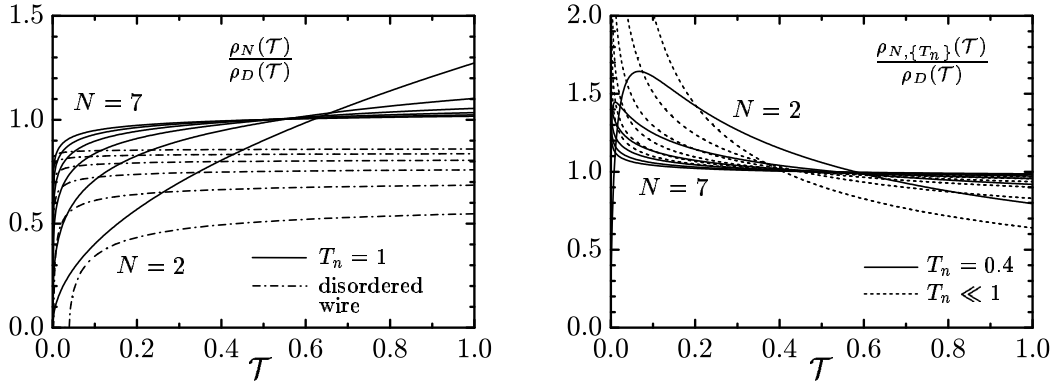

Fig. 32: *Distribution of transmission eigenvalues for N open contacts in series (left panel) and for contacts of lower transparency $T_n = 0.4$ and $T_n \ll 1$ (right panel), normalized to the transmission distribution of a diffusive wire $\rho_D(\mathcal{T})$. The ballistic to diffusive crossover in a metallic disordered wire is shown for comparison (left panel, dash-dotted curves) as a function of increasing disorder $L/l = N - 1$.*

which does not depend on the specific scattering properties $\{T_n\}$ of a single junction, the shape of the conductor or the impurity distribution [43, 45, 113]. Here $\tilde{g} = (\sum_n T_n)/N$ is the total conductance of a wire in units of G_Q.

The distribution of transmission eigenvalues of a composite junction $\rho_{N,\{T_n\}}(\mathcal{T})$ is directly related to the cumulant generating function by [66]

$$\rho_{N,\{T_n\}}(\mathcal{T}) = \frac{1}{\pi \mathcal{T}^2}\ \mathrm{Im}\left(\frac{\partial \tilde{\mathcal{S}}(\zeta)}{\partial \zeta}\Big|_{\zeta=-1/\mathcal{T}-i\,0}\right), \tag{19.9}$$

where $\zeta = (\check{\mathcal{G}} - 2)/4$. From Eqs. (19.5), (19.7) and (19.9) we find

$$\rho_{N,\{T_n\}}(\mathcal{T}) = \rho_D(\mathcal{T})\ \frac{\sin(\pi/N)}{\pi/N} \times \left\langle \frac{4T_n[(b^{1/N} + b^{-1/N})(2 - T_n) + 2T_n \cos(\pi/N)]}{[(b^{1/N} + b^{-1/N})(2 - T_n) + 2T_n \cos(\pi/N)]^2 - 4(1 - T_n)(b^{1/N} - b^{-1/N})^2} \right\rangle . \tag{19.10}$$

Here $\rho_D(\mathcal{T}) = (\tilde{g}/2)(1/\mathcal{T}\sqrt{1-\mathcal{T}})$ is the transmission distribution of a diffusive wire, $b = (1+\sqrt{1-\mathcal{T}})^2/\mathcal{T}$, and $\langle \cdots \rangle = (\sum_n \cdots)/(\sum_n T_n)$ denotes the averaging over the transmission eigenvalues of a single junction. For N open contacts in series ($T_n = 1$) Eq. (19.10) reduces to

$$\rho_N(\mathcal{T}) = \rho_D(\mathcal{T})\ \frac{\sin(\pi/N)}{\pi/N} \times \frac{4\mathcal{T}^{1/N}}{(1+\sqrt{1-\mathcal{T}})^{2/N} + (1-\sqrt{1-\mathcal{T}})^{2/N} + 2\mathcal{T}^{1/N}\cos(\pi/N)}. \tag{19.11}$$

The crossover from a single cavity to the diffusive regime as the number of junctions N increases is shown in Fig. 32 for open contacts (left panel) and for contacts of lower transparency $T_n = 0.4$ and $T_n \ll 1$ (right panel). The transmission distribution of a metallic disordered wire of the length L and the mean free path l is shown for comparison (dash-dotted curves in Fig. 32; cf. Ref. [46]).

The transmission eigenvalue distributions given by Eqs. (19.10) and (19.11) can be probed experimentally by measuring higher-order correlators of current fluctuations across the junction at low temperatures. The first three moments of charge transport statistics are related to the average current, the current noise power and the third correlator according to $I = (e/t_0)\partial_{i\chi}\mathcal{S}|_{\chi=0}$, $S_I = (e^2/t_0)\partial^2_{i\chi}\mathcal{S}|_{\chi=0}$, and $C_I = (e^3/t_0)\partial^3_{i\chi}\mathcal{S}|_{\chi=0}$, respectively. In the linear regime, which we consider here, the current is proportional to the bias voltage with conductance given by $\tilde{g} = (\sum_n T_n)/N = \int_0^1 d\mathcal{T}\rho_{N,\{T_n\}}(\mathcal{T})\ \mathcal{T}$ in units of G_Q. At temperatures much lower than the bias voltage, the current noise power and the third correlator are linear in the current, with the slopes given by the Fano factor

$$F = \frac{\partial S_I}{\partial(eI)} = \frac{1}{\tilde{g}}\int_0^1 d\mathcal{T}\rho_{N,\{T_n\}}(\mathcal{T})\ \mathcal{T}(1-\mathcal{T}) \tag{19.12}$$

and the "skewness"

$$C = \frac{\partial C_I}{\partial(e^2I)} = \frac{1}{\tilde{g}}\int_0^1 d\mathcal{T}\rho_{N,\{T_n\}}(\mathcal{T})\ \mathcal{T}(1-\mathcal{T})(1-2\mathcal{T}), \tag{19.13}$$

respectively. For the normal-state junction the two parameters are given by

$$F = \frac{1}{3}\left(1 + \frac{2-3\langle T_n^2\rangle}{N^2}\right) \tag{19.14}$$

and

$$C = \frac{1}{15}\left(1 + \frac{5(2-3\langle T_n^2\rangle)}{N^2} + \frac{4-30\langle T_n^2(1-T_n)\rangle}{N^4}\right). \tag{19.15}$$

The Fano factor given by Eq. (19.14) coincides with the result previously obtained within Boltzmann-Langevin approach which takes into account both cavity noise and partition noise at the contacts and was confirmed experimentally for up to three open contacts in series [68,69]. The sign of C is related to the asymmetry of transmission distribution [170], being negative (positive) when the weight of the distribution is shifted towards open (closed) transmission channels. Equation (19.15) shows that closed channels prevail in the composite junction for $N > 2$ even for completely open inner contacts, in agreement with Eq. (19.11).

Now we focus on the junction sandwiched between a normal-metal and a superconductor in the coherent regime in which we can neglect the particle-hole dephasing ($E_{\rm Th} \gg |eV|, T_e, \Delta$ where $E_{\rm Th}$ is the inverse dwell time). At temperatures and bias voltages smaller than the superconducting gap Δ, the transport properties can be obtained by integrating the Andreev reflection probability $R_A = \mathcal{T}^2/(2-\mathcal{T})^2$ over the transmission distribution [28, 187] and correcting for the effective charge $e^* = 2e$. The conductance, the Fano factor and the skewness are given by $\tilde{g}_S = \int_0^1 d\mathcal{T}\ \rho_{N,\{T_n\}}(\mathcal{T})\ R_A$ (in units of $2G_Q$),

$$F_S = \frac{\partial S_I}{\partial(e^*I)} = \frac{1}{\tilde{g}_S}\int_0^1 d\mathcal{T}\rho_{N,\{T_n\}}(\mathcal{T})\ R_A(1-R_A), \tag{19.16}$$

and

$$C_S = \frac{\partial C_I}{\partial(e^{*2}I)} = \frac{1}{\tilde{g}_S}\int_0^1 d\mathcal{T}\rho_{N,\{T_n\}}(\mathcal{T})\ R_A(1-R_A)(1-2R_A), \tag{19.17}$$

respectively. For N open contacts in series we find

$$\tilde{g}_S = \frac{N_{ch}}{2N}\frac{1}{\cos^2(\pi/4N)}, \qquad F_S = \frac{1}{3}\Big[1 - \frac{1}{4N^2}\Big(\frac{3}{\cos^2(\pi/4N)} - 2\Big)\Big], \tag{19.18}$$

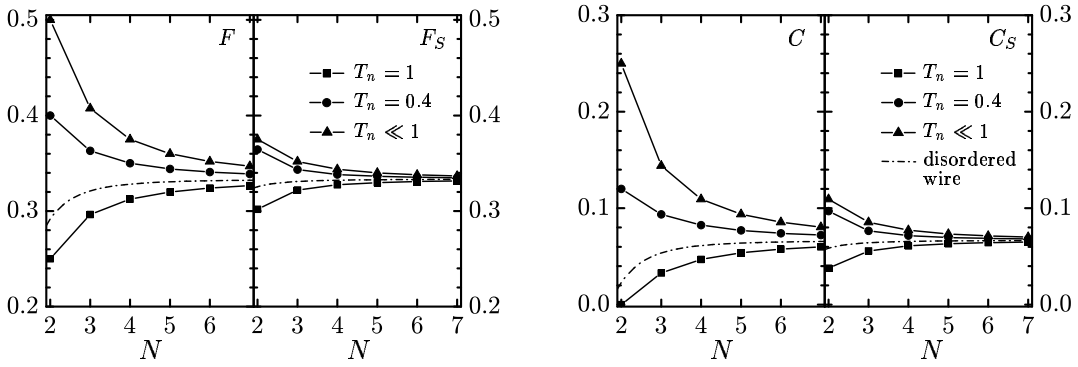

Fig. 33: *The Fano factor F (left panel) and the skewness C (right panel) as a function of the number of contacts in series N, shown for different contact transparencies. The corresponding distributions of transmission eigenvalues of the composite junctions are shown in Fig. 33. The Fano factors F_S and the skewnesses C_S (normalized by $e^* = 2e$) of the superconducting junctions are given for comparison. Ballistic to diffusive crossover in a disordered wire ($L/l = N - 1$) is shown by dash-dotted curves.*

and

$$C_S = \frac{1}{15}\Big[1 - \frac{5}{4N^2}\Big(\frac{3}{\cos^2(\pi/4N)} - 2\Big) + \frac{1}{8N^4}\Big(2 + 15\frac{\sin^2(\pi/4N)}{\cos^4(\pi/4N)}\Big)\Big]. \qquad (19.19)$$

The skewness C_S given by eq. (19.19) is positive for $N > 1$ which indicates that the asymmetry of the Andreev reflection distribution $\rho_{NA}(R_A) = \rho_N(\mathcal{T})d\mathcal{T}/dR_A$ is in favor of closed Andreev channels [187]. For the more general case of N contacts characterized by transmission eigenvalues $\{T_n\}$ we obtain $\tilde{g}_S = (\sum_n \alpha_n)/N$ and $F_S = 1 - (\sum_n \alpha_n\beta_n)/(\sum_n \alpha_n)$, where

$$\alpha_n = \frac{R_n^A + \sqrt{R_n^A}\cos(\pi/2N)}{[1 + \sqrt{R_n^A}\cos(\pi/2N)]^2}, \qquad (19.20)$$

$$\beta_n = \frac{2}{3} - \frac{1}{6N^2}\left(1 - 6\alpha_n + \frac{3\sqrt{R_n^A}}{\sqrt{R_n^A} + \cos(\pi/2N)}\right), \qquad (19.21)$$

and $R_n^A = T_n^2/(2 - T_n)^2$. Fano factors and skewnesses for the normal-state and superconducting junctions are shown in Fig. 33 as a function of the number of contacts in series and for different contact transparencies. It is interesting to note that in the coherent superconducting regime, which we consider here, the higher-order correlators satisfy the approximate scaling relations $F_S(N) \approx F(2N)$ and $C_S(N) \approx C(2N)$ which are exact for incoherent Andreev transport [168]. For large N this results in the full reentrance of transport properties of a diffusive wire in contact with a superconductor [91, 92] as a function of the particle-hole coherence.

§ 20. Summary

In this Chapter, we have studied the transport properties of several chaotic cavities in series using the circuit theory of mesoscopic transport. We obtained the analytical expression for the distribution of transmission eigenvalues of the composite junction as a function of the number of contacts and the scattering properties of a single contact. This distribution generalizes the previous results on noise in such a system [68, 69] to all higher-order cumulants. As an example we found the first three cumulants of the charge transfer statistics both for the normal-state junction and in

the case when one lead is superconducting. The sign of the third cumulant at high bias can be used to probe the asymmetry of the transmission eigenvalue distribution: it is negative (positive) when the weight of the distribution is more on open (closed) transport channels. As the number of contacts increases, all transport properties approach the universal limit of a diffusive wire [43, 45]. While the crossover from a few cavities to the diffusive-wire limit has already been studied through the noise in the normal state [68, 69, 175], experimental investigations of either higher-order correlators or cavities in contact with a superconductor are still to come.

CHAPTER VII

Elementary transport processes in a voltage-driven junction

§ 21. Introduction

The most detailed description of the charge transfer in coherent conductors is a statistical one. At constant bias, the full counting statistics (FCS) of electron transfer [141] can be directly interpreted in terms of elementary events independent at different energies. The FCS approach is readily generalized to the case of a time-dependent voltage bias [142, 143]. The current fluctuations in coherent systems driven by a periodic voltage strongly depend on the shape of the driving [94], which frequently is not apparent in the average current [95]. The noise power, for instance, exhibits at low temperatures a piecewise linear dependence on the dc voltage with kinks corresponding to integer multiples of the ac drive frequency and slopes which depend on the shape and the amplitude of the ac component. This dependence has been observed experimentally in normal coherent conductors [42, 98] and diffusive normal metal–superconductor junctions [99].

The question which we address in this Chapter is: What are the elementary processes of charge transfer driven by a general time-dependent voltage? The time dependence mixes the electron states at different energies [95] which makes this question both interesting and non-trivial. The first step in this research has been made in [188] for a special choice of the time-dependent voltage. The authors have considered a superposition of overlapping Lorentzian pulses of the same sign ("solitons"), with each pulse carrying a single charge quantum. The resulting charge transfer is unidirectional with a binomial distribution of transmitted charges. The number of attempts per unit time for quasiparticles to traverse the junction is given by the dc component of the voltage, independent of the overlap between the pulses and their duration [160]. It has been shown that such superposition minimizes the noise reducing it to that of a corresponding dc bias. A microscopic picture behind the soliton pulses has been revealed only recently [189]. In contrast to a general voltage pulse which can in principle create a random number of electron-hole pairs with random directions, a soliton pulse at zero temperature always creates a single electron-hole pair with quasiparticles moving in opposite directions. One of the quasiparticles (say, electron) comes to the contact and takes part in the transport while the hole goes away. This results in the charge transfer statistics which is of a single-particle type. Therefore, soliton pulses can be used to create minimal excitation states with "pure" electrons excited from the filled Fermi sea and no holes left below. The existence of such states can be probed by noise measurements [96, 189–191].

The simplest multi-particle charge transfer statistics is obtained for the soliton-antisoliton voltage pulses of opposite signs and without dc offset [160]. The charge transfer in this case is bidirectional with zero mean and vanishing higher-order odd cumulants. The width of distribution and higher-order even cumulants strongly depend on the relative position of the pulses and their duration. Thus, the statistics of

charge transfer cannot be interpreted in terms of independent elementary excitations associated with individual pulses.

In [97] we have identified the independent elementary processes for an arbitrary time-dependent driving applied to a generic conductor. The details of calculation and the physical interpretation are presented in the following. Recently, the constraints on the charge transfer statistics have been obtained for instant *time dependent* scattering at zero temperature [192].

§ 22. Full counting statistics and elementary processes

The system we consider is the coherent mesoscopic junction sandwiched between two terminals with a time-dependent voltage applied. We neglect charging effects and assume instantaneous scattering at the contact with quasiparticle dwell times much smaller than the characteristic time scale of the voltage variations. Since a generic conductor at low energies can be represented as a collection of independent transport channels, it is enough to specify elementary events for a single channel of transmission T. The cumulant generating function for a multichannel junction is obtained by summation over channels, $\mathcal{S}(\chi) = \sum_{\{T\}} \mathcal{S}(\chi, T)$. The approach we use is the nonequilibrium Keldysh-Green's function technique, extended to access the full counting statistics, as described in § 13. The Green's functions of the left (1) and right (2) leads are given by

$$\check{G}_1 = e^{-i\chi\check{\tau}_1/2} \begin{pmatrix} 1 & 2\tilde{h} \\ 0 & -1 \end{pmatrix} e^{i\chi\check{\tau}_1/2}, \qquad \check{G}_2 = \begin{pmatrix} 1 & 2h \\ 0 & -1 \end{pmatrix}, \tag{22.1}$$

where $\check{\tau}_1 = \left(\begin{smallmatrix} 0 & 1 \\ 1 & 0 \end{smallmatrix}\right)$ is a matrix in Keldysh($\check{}$) space. Hereafter we use a compact operator notation in which the time (or energy) indices are suppressed and the products are interpreted in terms of convolution over internal indices, e.g., $(\check{G}_1\check{G}_2)(t', t'') = \int dt_1 \check{G}_1(t', t_1)\check{G}_2(t_1, t'')$ (and similar in the energy representation). The equilibrium Green's function $\check{G}_2(t' - t'')$ depends only on time difference. In the energy representation $\check{G}_2(\mathcal{E}', \mathcal{E}'')$ is diagonal in energy indices with $h(\mathcal{E}', \mathcal{E}'') = \tanh(\mathcal{E}'/2T_e)\, 2\pi\delta(\mathcal{E}' - \mathcal{E}'')$. Here the quasiparticle energy $\mathcal{E}$ is measured with respect to the chemical potential in the absence of the bias and T_e is the temperature. The Green's function $\check{G}_1(t', t'')$ depends on two time (or energy) arguments. It takes into account the effect of applied voltage $V(t)$ across the junction through the gauge transformation $\tilde{h} = UhU^\dagger$ which makes $\check{G}_1$ nondiagonal in energy representation. The unitary operator U is given by $U(t', t'') = f(t')\delta(t' - t'')$ in the time representation, where $f(t') = \exp[-i\int_0^{t'} eV(t)dt]$. The cumulant generating function $\mathcal{S}(\chi)$ of the charge transfer through the junction is given by Eq. (13.26):

$$\mathcal{S}(\chi) = \mathrm{Tr}\ln\left[\check{1} + \frac{T}{2}\left(\frac{\{\check{G}_1, \check{G}_2\}}{2} - \check{1}\right)\right]. \tag{22.2}$$

Here the trace and products of Green's functions include both summation in Keldysh indices and integration over time (energy). For a dc voltage bias, $\check{G}_1$ and $\check{G}_2$ are diagonal in energy indices and $\mathcal{S}(\chi)$ is readily interpreted in terms of elementary events independent at different energies [152]. To deduce the elementary events in the presence of time-dependent voltage drive it is necessary to diagonalize $\{\check{G}_1, \check{G}_2\}_{\mathcal{E}'\mathcal{E}''}$. The diagonalization procedure is described in the following.

For the anticommutator of the Green's functions we find $\{\check{G}_1, \check{G}_2\}/2 - \check{1} = -2\sin(\chi/2)(\check{\mathcal{A}} + \check{\mathcal{B}})$, with

$$\check{\mathcal{A}} = \begin{pmatrix} 1 & b \\ 0 & 0 \end{pmatrix} \otimes A \quad \text{and} \quad \check{\mathcal{B}} = \begin{pmatrix} 0 & -b \\ 0 & 1 \end{pmatrix} \otimes B. \tag{22.3}$$

Here $A = (1 - h\tilde{h})\sin(\chi/2) + i(h - \tilde{h})\cos(\chi/2)$, $B = (1 - \tilde{h}h)\sin(\chi/2) + i(h - \tilde{h})\cos(\chi/2)$, $b = -i\cot(\chi/2)$, and $\otimes$ is the tensor product. Since $\check{\mathcal{A}}\check{\mathcal{B}} = \check{\mathcal{B}}\check{\mathcal{A}} = 0$, the operators $\check{\mathcal{A}}$ and $\check{\mathcal{B}}$ commute and satisfy for integer n:

$$(\check{\mathcal{A}} + \check{\mathcal{B}})^n = \begin{pmatrix} 1 & b \\ 0 & 0 \end{pmatrix} \otimes A^n + \begin{pmatrix} 0 & -b \\ 0 & 1 \end{pmatrix} \otimes B^n. \tag{22.4}$$

Therefore, $\mathcal{S}(\chi)$ given by Eq. (22.2) reduces to[26)]

$$\mathcal{S} = \mathrm{Tr}\ln\left[1 - T\sin\left(\frac{\chi}{2}\right)A\right] + \mathrm{Tr}\ln\left[1 - T\sin\left(\frac{\chi}{2}\right)B\right]. \tag{22.5}$$

A further simplification of $\mathcal{S}(\chi)$ is possible in the zero temperature limit, in which the hermitian h-operators are involutive: $h^2 = \tilde{h}^2 = 1$. The operators $h\tilde{h}$ and $\tilde{h}h$ are mutually inverse and commute with each other. Because $h\tilde{h}$ is unitary, it has the eigenvalues of the form $e^{i\alpha_k}$ with real α_k, and possesses an orthonormal eigenbasis $\{\mathbf{v}_{\alpha_k}\}$. The *typical* eigenvalues of $h\tilde{h}$ (or $\tilde{h}h$) appear in pairs $e^{\pm i\alpha}$ with the corresponding eigenvectors $\mathbf{v}_\alpha$ and $\mathbf{v}_{-\alpha} = h\mathbf{v}_\alpha$. In the basis $(\mathbf{v}_\alpha, \mathbf{v}_{-\alpha})$ operators $h\tilde{h}$ and $\tilde{h}h$ are diagonal and given by $h\tilde{h} = \mathrm{diag}(e^{i\alpha}, e^{-i\alpha})$ and $\tilde{h}h = \mathrm{diag}(e^{-i\alpha}, e^{i\alpha})$. The eigensubspaces $\mathrm{span}(\mathbf{v}_\alpha, \mathbf{v}_{-\alpha})$ of the anticommutator $\{h, \tilde{h}\}$ are invariant with respect to h, $\tilde{h}$, and A because of $[h, \{h, \tilde{h}\}] = [\tilde{h}, \{h, \tilde{h}\}] = 0$. The operators h and $\tilde{h}$ are anti-diagonal in the basis $(\mathbf{v}_\alpha, \mathbf{v}_{-\alpha})$, with matrix components $h_{12} = 1$, $h_{21} = 1$, $\tilde{h}_{12} = e^{-i\alpha}$, and $\tilde{h}_{21} = e^{i\alpha}$. The operator A can be diagonalized in invariant subspaces, with typical eigenvalues given by

$$\Lambda = 2\sin(\alpha/2)\left(\sin(\alpha/2)\sin(\chi/2) \pm i\sqrt{1 - \sin^2(\alpha/2)\sin^2(\chi/2)}\right). \tag{22.6}$$

Similarly, we obtain the same eigenvalues of the operator B. From Eqs. (22.5) and (22.6) we obtain the contribution $\mathcal{S}_1$ to the generating function,

$$\mathcal{S}_1(\chi) = 2\sum_k \ln\left[1 + TR\sin^2\left(\frac{\alpha_k}{2}\right)\left(e^{i\chi} + e^{-i\chi} - 2\right)\right] \tag{22.7}$$

(with $R = 1 - T$) which is associated with the paired eigenvalues $e^{\pm i\alpha_k}$.

There are, however, some *special* eigenvectors of $h\tilde{h}$ which do not appear in pairs. The pair property discussed above was based on the assumption that $\mathbf{v}_\alpha$ and $h\mathbf{v}_\alpha = \mathbf{v}_{-\alpha}$ are linearly independent vectors. In the special case, these vectors are the same apart from a coefficient. Therefore, the special eigenvectors of $h\tilde{h}$ are the eigenvectors of both h and $\tilde{h}$ with eigenvalues ± 1. This means that the special eigenvectors posses *chirality*, with positive (negative) chirality defined by $h\mathbf{v} = \mathbf{v}$ and $\tilde{h}\mathbf{v} = -\mathbf{v}$ ($h\mathbf{v} = -\mathbf{v}$ and $\tilde{h}\mathbf{v} = \mathbf{v}$). From Eq. (22.5) we obtain the contribution $\mathcal{S}_2$ given by

$$\mathcal{S}_2(\chi) = 2\sum_l \ln[1 + T(e^{-i\kappa_l\chi} - 1)] \tag{22.8}$$

[26)] Equation (22.5) is equivalent to Eq. (13.35) with $n = (1 - h)/2$.

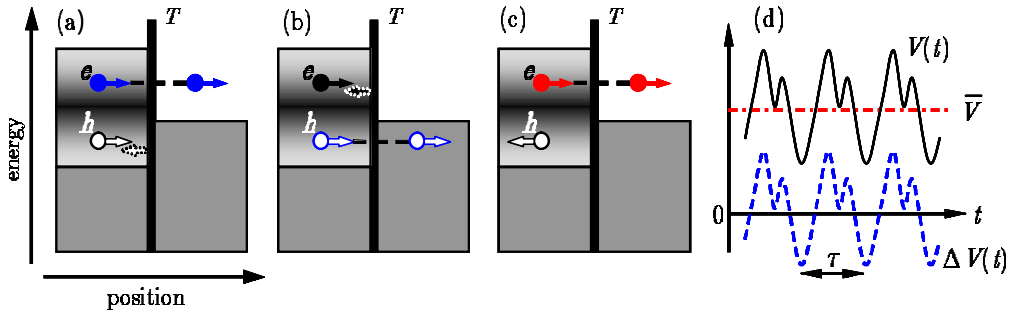

Fig. 34: *Schematic representation of elementary events: bidirectional (a, b) and unidirectional (c). Shifts of the effective chemical potential in the left lead due to time-dependent voltage drive are indicated by shading. For periodic drive, the dc voltage component [panel (d), dash-dotted line] describes unidirectional charge transfer, while the ac component (dashed curve) describes bidirectional events affecting the noise and higher-order even cumulants.*

which is associated with the special eigenvectors. Here l labels the special eigenvectors and κ_l is the chirality.

The total cumulant generating function of the charge transfer for arbitrary voltage drive is given by $\mathcal{S}(\chi) = \mathcal{S}_1(\chi) + \mathcal{S}_2(\chi)$. The elementary transfer events can be inferred from the form of $\mathcal{S}$, as it has been done in [193, 194]. The answer is surprisingly simple. There are two kinds of such events: The *bidirectional* events which are described by $\mathcal{S}_1$ and the *unidirectional* events which are described by $\mathcal{S}_2$. These events are discussed in detail in § 7. In the course of a *bidirectional* event k an electron-hole pair is created with probability $\sin^2(\alpha_k/2)$, with α_k being determined by the details of the time-dependent voltage. The electron and hole move in the *same* direction reaching the scatterer. The charge transfer occurs if the electron is transmitted and the hole is reflected, or vice versa [Fig. 34(a,b)]. The probabilities of both outcomes, TR (R being reflection coefficient), are the same. Therefore, the bidirectional events do not contribute to the average current and odd cumulants of the charge transferred although they do contribute to the noise and higher-order even cumulants. A specific example of a bidirectional event for a soliton-antisoliton pulse was given in [160].

The *unidirectional* events are the same as for a constant bias or a soliton pulse. They are characterized by chirality $\kappa_l = \pm 1$ which gives the direction of the charge transfer. An electron-hole pair is always created in the course of the event, with electron and hole moving in opposite directions [Fig. 34(c)]. Either electron ($\kappa_l = 1$) or hole ($\kappa_l = -1$) passes the contact with probability T, thus contributing to the current.

The cumulant-generating function given by Eqs. (22.7) and (22.8), together with the interpretation, is the main result of this Chapter. It holds at zero temperature only: since the elementary events are the electron-hole pairs created by the applied voltage, the presence of thermally excited pairs will smear the picture. Equations (22.7) and (22.8) contain the complete χ-field dependence in explicit form which allows for the calculation of higher-order cumulants and charge transfer statistics for arbitrary time-dependent voltage. The probability that N charges are transmitted within the time of measurement is given by $\mathcal{P}(N) = (2\pi)^{-1} \int_{-\pi}^{\pi} d\chi \exp[\mathcal{S}(\chi) - iN\chi]$ [cf. Eq. (4.15)]. Higher-order derivatives of $\mathcal{S}$ with respect to χ are proportional to

the cumulants of transmitted charge, or equivalently, to higher-order current correlators at zero frequency. The details of the driving are contained in the set of parameters $\{\alpha_k\}$ and separated from the χ-field dependence. This opens an interesting possibility to excite the specific elementary processes and design the charge transfer statistics by appropriate time dependence of the applied voltage, with possible applications in production and detection of the many-body entangled states [177,194,195].

§ 23. Periodic voltage drive

In the following we focus on a periodic voltage drive $V(t+\tau) = V(t)$ with the period $\tau = 2\pi/\omega$. In this case the probabilities of bidirectional events $p_k = \sin^2(\alpha_k/2)$, given by the eigenvalues $e^{\pm i\alpha_k}$ of $h\tilde{h}$, can be easily obtained by matrix diagonalization.

The operator $\tilde{h}$ couples only energies which differ by an integer multiple of ω, which allows to map the problem into the energy interval $0 < \mathcal{E} < \omega$ while retaining the discrete matrix structure in steps of ω. Therefore, the trace operation in Eq. (22.2) becomes an integral over $\mathcal{E}$ and the trace in discrete matrix indices. The operator $h\tilde{h}$ in the energy representation is given by

$$(h\tilde{h})_{nm}(\mathcal{E}) = \mathrm{sgn}(\mathcal{E}+n\omega) \sum_{k=-\infty}^{\infty} \tilde{f}_{n+k}\tilde{f}^*_{m+k}\, \mathrm{sgn}(\mathcal{E}-k\omega-e\bar{V}), \tag{23.1}$$

with

$$\tilde{f}_n = \frac{1}{\tau}\int_0^\tau dt\; e^{-i\int_0^t dt'\, e\Delta V(t')} e^{in\omega t}. \tag{23.2}$$

Here $\bar{V} = (1/\tau)\int V(t)dt$ is the dc voltage offset and $\Delta V(t) = V(t) - \bar{V}$ is the ac voltage component. The coefficients $\tilde{f}_n$ satisfy

$$\sum_{k=-\infty}^{\infty} \tilde{f}_{n+k}\tilde{f}^*_{m+k} = \delta_{nm} \qquad \text{and} \qquad \sum_{n=-\infty}^{\infty} n|\tilde{f}_n|^2 = 0. \tag{23.3}$$

To evaluate $\mathcal{S}(\chi)$ for a given periodic voltage drive $V(t)$ it is necessary to diagonalize $(h\tilde{h})_{nm}(\mathcal{E})$. First we analyze the contribution of typical eigenvalues $e^{\pm i\alpha}$. The matrix $(h\tilde{h})_{nm}(\mathcal{E})$ is piecewise constant for $\mathcal{E} \in (0,\omega_1)$ and $\mathcal{E} \in (\omega_1,\omega)$, where $\omega_1 = e\bar{V} - N\omega$ and $N = \lfloor e\bar{V}/\omega \rfloor$ is the largest integer less than or equal $e\bar{V}/\omega$. The eigenvalues $e^{\pm i\alpha_{kL(R)}}$ of $(h\tilde{h})_{nm}$ are calculated for $\mathcal{E} \in (0,\omega_1)$ $[\mathcal{E} \in (\omega_1,\omega)]$ using finite-dimensional matrices, with the cutoff in indices n and m being much larger than the characteristic scale on which $|\tilde{f}_n|$ vanish. Further increase of the size of matrix just brings more eigenvalues with $\alpha_k = 0$ which do not contribute to $\mathcal{S}(\chi)$, and does not change the rest with $\alpha_k \neq 0$. This is a signature that all important Fourier components of the drive are taken into account. The eigenvalues $e^{\pm i\alpha_{kL(R)}}$ give rise to two terms, $\mathcal{S}_1 = \mathcal{S}_{1L} + \mathcal{S}_{1R}$, with

$$\mathcal{S}_{1L,R}(\chi) = M_{L,R}\sum_k \ln\left[1 + TR\sin^2\left(\frac{\alpha_{kL,R}}{2}\right)(e^{i\chi}+e^{-i\chi}-2)\right]. \tag{23.4}$$

Here $M_L = t_0\omega_1/\pi$, $M_R = t_0(\omega-\omega_1)/\pi$, and t_0 is the total measurement time which is much larger than τ and the characteristic time scale on which the current fluctuations are correlated.

The special eigenvectors all have the same chirality which is given by the sign of the dc offset $\bar{V}$. For $e\bar{V} > 0$, there are $N_1 = N+1$ special eigenvectors for $\mathcal{E} \in (0,\omega_1)$

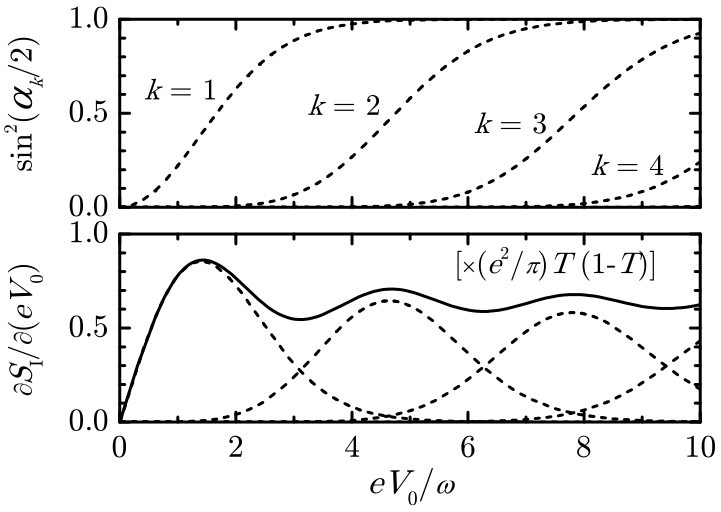

Fig. 35: *The probabilities of elementary events for harmonic drive* $V(t) = V_0\cos(\omega t)$ *are shown in the upper panel. With increasing amplitude* V_0 *more and more eigenvalues* α_k *come into play and contribute to transport. The derivative of the noise power with respect to* V_0 *(solid line) decomposed into contributions (dashed line) of elementary events is shown in the lower panel.*

and $N_2 = N$ for $\mathcal{E} \in (\omega_1, \omega)$. Because $e\bar{V} = N_1\omega_1 + N_2(\omega - \omega_1)$, the effect of the special eigenvectors is the same as of the dc bias

$$\mathcal{S}_2(\chi) = \frac{t_0 e\bar{V}}{\pi}\ln[1 + T(e^{-i\chi} - 1)]. \tag{23.5}$$

Comparing Eqs. (22.8) and (23.5) we see that unidirectional events for periodic drive are uncountable. The summation in Eq. (22.8) stands both for the energy integration in the interval ω and the trace in the discrete matrix indices. In the limit of a single pulse $\omega \to 0$ unidirectional events remain uncountable for a generic voltage, while being countable, e.g., for soliton pulses carrying integer number of charge quanta [160].

Equations (23.4) and (23.5) determine the charge transfer statistics at zero temperature for an arbitrary periodic voltage applied. The generating function consists of a binomial part ($\mathcal{S}_2$) which depends on the dc offset $\bar{V}$ only, and a contribution of the ac voltage component ($\mathcal{S}_1$) [Fig. 34(d)]. The latter is the sum of two terms which depend on the number of unidirectional attempts per period $e\bar{V}/\omega$. The simplest statistics is obtained for an integer number of attempts for which $\mathcal{S}_{1L}$ vanishes [142]. The parameters $\{\tilde{f}_n\}$ for the optimal Lorentzian pulses

$$V_L(t) = \frac{2\tau_L}{e}\sum_{k=-\infty}^{\infty}\frac{1}{(t-k\tau)^2+\tau_L^2} = \frac{2\pi}{e\tau}\frac{\sinh(2\pi\tau_L/\tau)}{\cosh(2\pi\tau_L/\tau)-\cos(2\pi t/\tau)} \tag{23.6}$$

of width $\tau_L > 0$ are given by

$$\tilde{f}_{-1} = -e^{-2\pi\tau_L/\tau}, \qquad \tilde{f}_n = \begin{cases} e^{-2\pi n\tau_L/\tau} - e^{-2\pi(n+2)\tau_L/\tau}, & n \geq 0 \\ 0, & n < -1 \end{cases} \tag{23.7}$$

(see § 23.2). In this case $\mathcal{S}_{1L} = \mathcal{S}_{1R} = 0$ and the statistics is *exactly* binomial with one electron-hole excitation per period, in agreement with Refs. [160, 189].

We conclude this paragraph by noting that the elementary events at zero temperature can be probed by noise measurements. For example, in the case of an ac drive with $\bar{V} = 0$, only bidirectional events of R-type remain [$\mathcal{S}(\chi) = \mathcal{S}_{1R}(\chi)$]. The current noise power is given by[27)]

$$S_I = \frac{2e^2\omega}{\pi} T(1-T) \sum_k \sin^2\left(\frac{\alpha_k}{2}\right). \tag{23.8}$$

Both the number of events and their probabilities increase with increasing the driving amplitude V_0, which results in the characteristic oscillatory change of the slope of S_I. The decomposition of $\partial S_I/\partial V_0$ into contributions of elementary events for harmonic drive $V(t) = V_0 \cos(\omega t)$ is shown in Fig. 35.

The interpretation of the shot noise in terms of electron-hole pair excitations has been discussed in Ref. [96] in the regime of low-amplitude driving $eV_0 \ll \omega$. In this case only one electron-hole pair is excited per period with probability $p_1 \equiv \sin^2(\alpha_1/2) \approx [J_1(eV_0/\omega)]^2$. Remarkably, Fig. 35 shows that the single electron-hole pair is excited not only for small amplitudes but also for amplitudes comparable or even larger than the drive frequency, up to $eV_0 \lesssim 2\omega$. This extended range of validity can be covered by taking into account the higher-order terms in the expression for probability: $p_1 \approx \sum_{n=1}^{\infty} n[J_n(eV_0/\omega)]^2$. The first 3 terms approximate the exact p_1 shown in Fig. 35 to accuracy better than 0.3% for $eV_0 \lesssim 2\omega$.

§ **23.1. Cumulants at finite temperatures.** The full counting statistics and the corresponding elementary transport processes obtained in the previous paragraph are valid description in the low temperature limit only, in which electron-hole pairs are created by the applied voltage and no thermally excited pairs exist. Formally, the diagonalization of the anticommutator $\{\check{G}_1, \check{G}_2\}_{\mathcal{E}'\mathcal{E}''}$ in energy indices, which is needed to deduce the elementary processes, is based on the involution property of h-operators, $h^2 = \tilde{h}^2 = 1$. This property no longer holds at finite temperatures which are comparable to the applied voltage. Nevertheless, the method we use enables the efficient and systematic analytic calculation of the higher-order cumulants at finite temperatures. The cumulants can be obtained directly from Eq. (22.5) by expansion in the counting field to the certain order before taking the trace. The trace of a *finite number of terms* can be taken in the original basis in which $\check{G}_1$ and $\check{G}_2$ are defined. In the following we illustrate the approach by calculation of the average current $I = (e/t_0)\partial_{i\chi}\mathcal{S}|_{\chi=0}$, the current noise power $S_I = (e^2/t_0)\partial^2_{i\chi}\mathcal{S}|_{\chi=0}$ and the third cumulant $C_I = (e^3/t_0)\partial^3_{i\chi}\mathcal{S}|_{\chi=0}$ at finite temperatures. From Eq. (22.5) we obtain

$$\partial_{i\chi}\mathcal{S}|_{\chi=0} = T\,\mathrm{Tr}_{\mathcal{E}}(\tilde{h} - h), \tag{23.9a}$$

$$\partial^2_{i\chi}\mathcal{S}|_{\chi=0} = T\,\mathrm{Tr}_{\mathcal{E}}(1 - h\tilde{h}) - (T^2/2)\,\mathrm{Tr}_{\mathcal{E}}[(h-\tilde{h})^2], \tag{23.9b}$$

$$\begin{aligned}\partial^3_{i\chi}\mathcal{S}|_{\chi=0} =& (T^3/2)\,\mathrm{Tr}_{\mathcal{E}}(\tilde{h}^3 - h^3) + (3/2)T^2(1-T)\,\mathrm{Tr}_{\mathcal{E}}[h\tilde{h}(\tilde{h}-h)] \\ &+ T[1-(3T/2)]\,\mathrm{Tr}_{\mathcal{E}}(\tilde{h}-h).\end{aligned} \tag{23.9c}$$

In energy representation, the operators h and $\tilde{h}$ are given by

$$h(\mathcal{E}', \mathcal{E}'') = h(\mathcal{E}')\, 2\pi\delta(\mathcal{E}' - \mathcal{E}'') = \sum_{k,m} \tilde{f}_k \tilde{f}^*_{k+m} h(\mathcal{E}')\, 2\pi\delta(\mathcal{E}'' - \mathcal{E}' - m\omega), \tag{23.10a}$$

[27)] Throughout this Thesis we use the definition for the current correlation function given by Eq. (10.26). In [97] the current correlation function is defined with an additional prefactor of 2.

$$\tilde{h}(\mathcal{E}',\mathcal{E}'') = \sum_{k,m} \tilde{f}_k \tilde{f}^*_{k+m} h(\mathcal{E}' - k\omega - e\bar{V})\, 2\pi\delta(\mathcal{E}'' - \mathcal{E}' - m\omega). \qquad (23.10b)$$

Here $h(\mathcal{E}) = \tanh(\mathcal{E}/2T_e)$ and we used the properties of $\{\tilde{f}_n\}$ given by Eq. (23.3). After integration over energy in Eqs. (23.9) we obtain the average current $I = (e^2/\pi)\big(\sum_p T_p\big)\bar{V}$. The current noise power and the third cumulant are given by

$$S_I = \frac{e^2}{\pi} \sum_p \left[T_p^2 2T_e + T_p(1-T_p) \sum_{n=-\infty}^{\infty} |\tilde{f}_n|^2 (e\bar{V} + n\omega) \coth\left(\frac{e\bar{V}+n\omega}{2T_e}\right)\right] \qquad (23.11)$$

and

$$C_I = \frac{e^3}{\pi}\Bigg\{ e\bar{V} \sum_p T_p(1-T_p^2) + 3\sum_p T_p^2(1-T_p) \times \sum_{n=-\infty}^{\infty} |\tilde{f}_n|^2 \left[2T_e \coth\left(\frac{e\bar{V}+n\omega}{2T_e}\right) - (e\bar{V}+n\omega)\coth^2\left(\frac{e\bar{V}+n\omega}{2T_e}\right)\right]\Bigg\}. \qquad (23.12)$$

Here we restored the summation over transport channels T_p for clarity.

The average current is linear in dc voltage offset, which is consistent with the initial assumption of energy-independent transmission eigenvalues and instant scattering at the contact. The result for the current noise power, Eq. (23.11), describes the photon-assisted noise for arbitrary periodic voltage drive. The coefficients $\tilde{f}_n$ for harmonic drive $V(t) = \bar{V} + V_0\cos(\omega t)$ are given by the Bessel functions, $\tilde{f}_n = J_n(eV_0/\omega)$, and Eq. (23.11) reduces to the previous results obtained by Lesovik and Levitov [94] and Pedersen and Büttiker [95] (see also [26]). The accurate noise measurements at finite temperatures in the presence of the harmonic driving are performed in [42]. The results are in excellent agreement with Eq. (23.11).

In the following we discuss the low- and high-temperature limits of S_I and C_I. At high temperatures $T_e \gg |e\bar{V}|, n_0\omega$, with $n_0\omega$ being the characteristic energy scale on which $|\tilde{f}_{n_0}|$ vanish, the current noise power reduces to the thermal equilibrium value $S_I = 2T_eG$, which is just a manifestation of the fluctuation-dissipation theorem. The third cumulant is in this regime proportional to the average current, $C_I = e^2FI$, where $F = [\sum_p T_p(1-T_p)]/(\sum_p T_p)$ is the Fano factor. At high temperatures S_I and C_I carry no information on the details of the time-dependent voltage drive.

At low temperatures $T_e \ll |e\bar{V}|, n_0\omega$, the current noise power reduces to

$$S_I = \frac{e^2}{\pi} \sum_p T_p(1-T_p) \sum_{n=-\infty}^{\infty} |\tilde{f}_n|^2 (e\bar{V}+n\omega)\,\mathrm{sgn}(e\bar{V}+n\omega). \qquad (23.13)$$

In this case S_I is a piecewise linear function of the dc voltage offset $\bar{V}$ with kinks corresponding to integer multiples of the driving frequency $e\bar{V}/\omega = N$ and slopes which depend on the shape and the amplitude of the ac voltage component. The derivative $\partial S_I/\partial\bar{V}$ consists of a series of steps given by

$$\left(\Delta\frac{\partial S_I}{\partial\bar{V}}\right)_{e\bar{V}=N\omega} = \left.\frac{\partial S_I}{\partial\bar{V}}\right|_{N+0} - \left.\frac{\partial S_I}{\partial\bar{V}}\right|_{N-0} = \frac{2e^3}{\pi}\left(\sum_p T_p(1-T_p)\right)|\tilde{f}_{-N}|^2. \qquad (23.14)$$

All steps add up to $(2e^3/\pi)\sum_p T_p(1-T_p)$ because of $\sum_n |\tilde{f}_n|^2 = 1$. The steps in $\partial S_I/\partial\bar{V}$ were measured for harmonic drive in normal [98] and normal-superconductor [99] junctions. In the superconducting state they appear at integer values of $2e\bar{V}/\omega$,

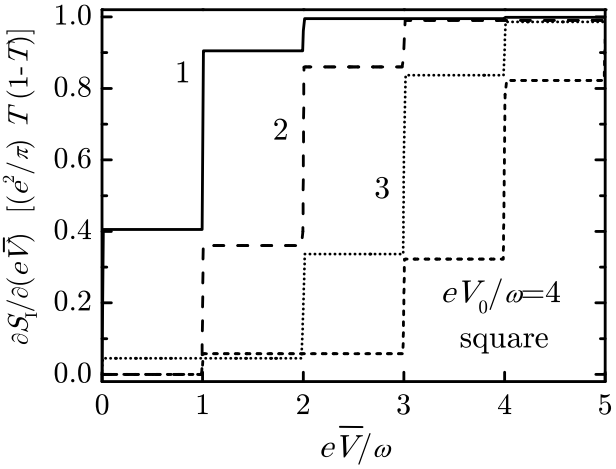

Fig. 36: *The slope $\partial S_I/\partial(e\bar{V})$ of the current noise power S_I as a function of the dc voltage offset $\bar{V}$ is shown for the square-shaped voltage drive of amplitude V_0. In general, the slope changes at integer values of $e\bar{V}/\omega$ according to Eq.* (23.14). *However, for the square-shaped drive with integer amplitude $eV_0/\omega = N$, the slope remains unchanged at $e\bar{V}/\omega = N + 2k$, $k \neq 0$.*

which can be interpreted as a signature of the elementary charge transport processes in units of $e^* = 2e$. The effective charge is doubled in the superconducting state due to the Andreev process. We point out that for a general voltage drive, certain steps at integer values of $e^*\bar{V}/\omega = N$ may vanish if the corresponding coefficient $\tilde{f}_{-N} = 0$. For example, for a square-shaped drive with integer amplitude $e^*V_0/\omega = N$, the steps at $e^*\bar{V}/\omega = N + 2k$ ($k \neq 0$) vanish. This is illustrated in Fig. 36 for a normal-state junction. Since $S_I(\bar{V})$ is an even function of $\bar{V}$, only the positive part with $e\bar{V} > 0$ is shown.

At low temperatures, the third cumulant reduces to $C_I = e^2F_3I$, where $F_3 = [\sum_p T_p(1-T_p)(1-2T_p)]/(\sum_p T_p)$. Unlike the current noise power, the third cumulant at low temperatures does not depend on the ac component of the voltage drive. This is because the bidirectional processes, which are created by the ac voltage component, do not contribute to odd-order cumulants at low temperatures [Eq. (23.4)].

We conclude this paragraph by comparison of two formulas for the current noise power at zero temperature. For simplicity we take $\bar{V} = 0$ and consider a single transport channel. Equation (23.13) for the current noise power reduces to

$$S_I = \frac{2e^2\omega}{\pi} T(1-T) \sum_{n=1}^{\infty} n|\tilde{f}_n|^2. \tag{23.15}$$

Here we used Eq. (23.3) to restrict the summation to the positive n only. On the other hand, the current noise power is also given by Eq. (23.8). Regardless the similar form, the physical content of these two equations is very different. Both equations give the same result for S_I as a consequence of the invariance of trace. However, Eq. (23.8) has been obtained by taking the trace in Eq. (22.2) in the basis in which $\{\check{G}_1, \check{G}_2\}$ is diagonal. Therefore, the cumulant generating function is decomposed into contributions of elementary and statistically independent processes. The terms which appear in Eq. (23.8) are the contributions of these processes to the noise. Equation (23.15) has been obtained by taking the trace in a basis in which $\{\check{G}_1, \check{G}_2\}$

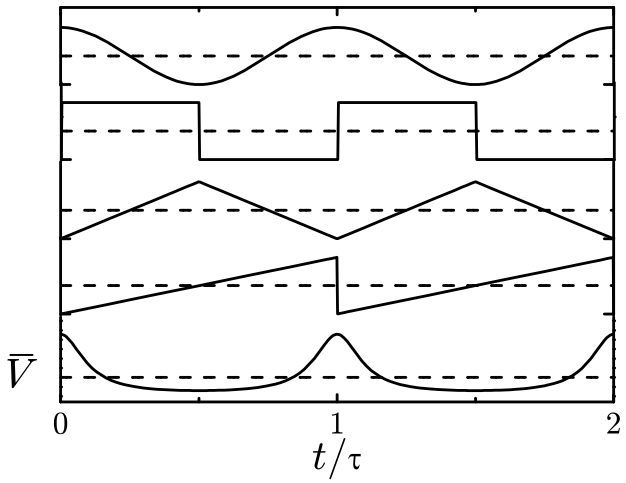

Fig. 37: *Different periodic bias voltages: cosine, square, triangle, sawtooth, and Lorentzian pulses (top to bottom). The bias voltages are characterized by the dc offset voltage $\bar{V}$, the amplitude V_0 of the ac component, and the period $\tau = 2\pi/\omega$.*

is not diagonal. Although the end result for S_I is the same, the individual terms which appear in Eq. (23.15) have no direct physical interpretation.

In the limit of small-amplitude voltage drive, $eV_0 \ll \omega$, only one electron-hole pair is excited per period with probability $p_1 \equiv \sin^2(\alpha_1/2)$. Comparing Eqs. (23.8) and (23.15) we obtain that in this case $p_1 = \sum_{n=1}^{\infty} n|\tilde{f}_n|^2$. In fact, as shown in Fig. 35 for harmonic drive, the assumption of small amplitudes can be relaxed to the amplitudes comparable or even larger than the drive frequency. The accuracy of this approximation depends on the shape of time-dependent voltage drive (cf. Fig. 35 and Fig. 41).

§ **23.2. Comparison of different time-dependent voltages.** In the following we compare the elementary events and the noise generated by different time-dependent bias voltages. The bias voltage $V(t) = \bar{V} + \Delta V(t)$ consists of the dc voltage component $\bar{V}$ and the periodic ac component $\Delta V(t) = \Delta V(t+\tau)$ with the period $\tau = 2\pi/\omega$ and zero mean value. We focus on standard voltage signals such as cosine, square, triangle, and sawtooth, as depicted in Fig. 37. We also present results for Lorentzian voltage pulses which provide the simplest charge transfer statistics for certain amplitudes. The ac voltage component is characterized by the parameters $\tilde{f}_n$ given by Eq. (23.2). In the following we obtain these parameters for the driving voltages of interest.

The cosine voltage drive of amplitude V_0 is given by

$$\Delta V(t) = V_0 \cos(\omega t). \tag{23.16}$$

The coefficients $\tilde{f}_n$ can be calculated using the Jacobi-Anger expansion [105]

$$e^{iz\sin(\theta)} = \sum_{n=-\infty}^{\infty} J_n(z)\, e^{in\theta}, \tag{23.17}$$

where J_n are the Bessel functions of the first kind. The coefficients $\tilde{f}_n$ are given by

$$\tilde{f}_n = J_n\left(\frac{eV_0}{\omega}\right). \tag{23.18}$$

The square voltage drive is given by

$$\Delta V(t) = \begin{cases} V_0, & 0 < t < \tau/2, \\ -V_0, & \tau/2 < t < \tau. \end{cases} \tag{23.19}$$

For noninteger values of eV_0/ω, the coefficients $\tilde{f}_n$ are given by

$$\tilde{f}_n = \frac{2}{\pi}\,\frac{eV_0}{\omega}\,\frac{\sin\left[\frac{\pi}{2}\left(n-\frac{eV_0}{\omega}\right)\right]}{n^2-\left(\frac{eV_0}{\omega}\right)^2}\,e^{i\frac{\pi}{2}\left(n-\frac{eV_0}{\omega}\right)}. \tag{23.20}$$

For integer values of eV_0/ω, the coefficients $\tilde{f}_n$ are obtained by taking the limit of the above formula.

The sawtooth voltage drive is given by

$$\Delta V(t) = 2V_0 t/\tau - V_0 \tag{23.21}$$

for $0 < t < \tau$. In this case

$$\begin{aligned}\tilde{f}_n = \frac{1}{2\sqrt{2}}\frac{e^{-i\pi/4}}{\sqrt{eV_0/\omega}}\,e^{i\frac{\pi}{2}\frac{[(eV_0/\omega)+n]^2}{eV_0/\omega}}\,\Bigg[&\operatorname{erf}\left(\sqrt{\frac{\pi}{2}}\,e^{i\pi/4}\,\frac{(eV_0/\omega)-n}{\sqrt{eV_0/\omega}}\right)\\ &+\operatorname{erf}\left(\sqrt{\frac{\pi}{2}}\,e^{i\pi/4}\,\frac{(eV_0/\omega)+n}{\sqrt{eV_0/\omega}}\right)\Bigg].\end{aligned} \tag{23.22}$$

Here $\operatorname{erf}(z) = (2/\sqrt{\pi})\int_0^z dt\ \exp(-t^2)$ is the error function.

The triangle voltage drive is characterized by

$$\Delta V(t) = \begin{cases} 4V_0 t/\tau - V_0, & 0 < t < \tau/2, \\ -4V_0 t/\tau + 3V_0, & \tau/2 < t < \tau. \end{cases} \tag{23.23}$$

In this case

$$\begin{aligned}\tilde{f}_n =& \frac{ie^{i\pi/4}}{4\sqrt{eV_0/\omega}}\,e^{i\frac{\pi}{4}\frac{[(eV_0/\omega)+n]^2}{eV_0/\omega}}\\ &\times\left[\operatorname{erf}\left(\frac{\sqrt{\pi}}{2}\,e^{i5\pi/4}\,\frac{(eV_0/\omega)+n}{\sqrt{eV_0/\omega}}\right)+\operatorname{erf}\left(\frac{\sqrt{\pi}}{2}\,e^{i5\pi/4}\,\frac{(eV_0/\omega)-n}{\sqrt{eV_0/\omega}}\right)\right]\\ &-\frac{ie^{-i\pi/4}}{4\sqrt{eV_0/\omega}}\,e^{-i\frac{\pi}{4}\frac{(eV_0/\omega)^2-6(eV_0 n/\omega)+n^2}{eV_0/\omega}}\\ &\times\left[\operatorname{erf}\left(\frac{\sqrt{\pi}}{2}\,e^{i3\pi/4}\,\frac{(eV_0/\omega)+n}{\sqrt{eV_0/\omega}}\right)+\operatorname{erf}\left(\frac{\sqrt{\pi}}{2}\,e^{i3\pi/4}\,\frac{(eV_0/\omega)-n}{\sqrt{eV_0/\omega}}\right)\right].\end{aligned} \tag{23.24}$$

The voltage drive which consists of Lorentzian voltage pulses of width τ_L is given by

$$\begin{aligned}\Delta V(t) &= -V_0 + \frac{V_0}{\pi}\sum_{k=-\infty}^{\infty}\frac{\tau\tau_L}{(t-k\tau)^2+\tau_L^2}\\ &= -V_0 + \frac{V_0\sinh(2\pi\tau_L/\tau)}{\cosh(2\pi\tau_L/\tau)-\cos(2\pi t/\tau)}.\end{aligned} \tag{23.25}$$

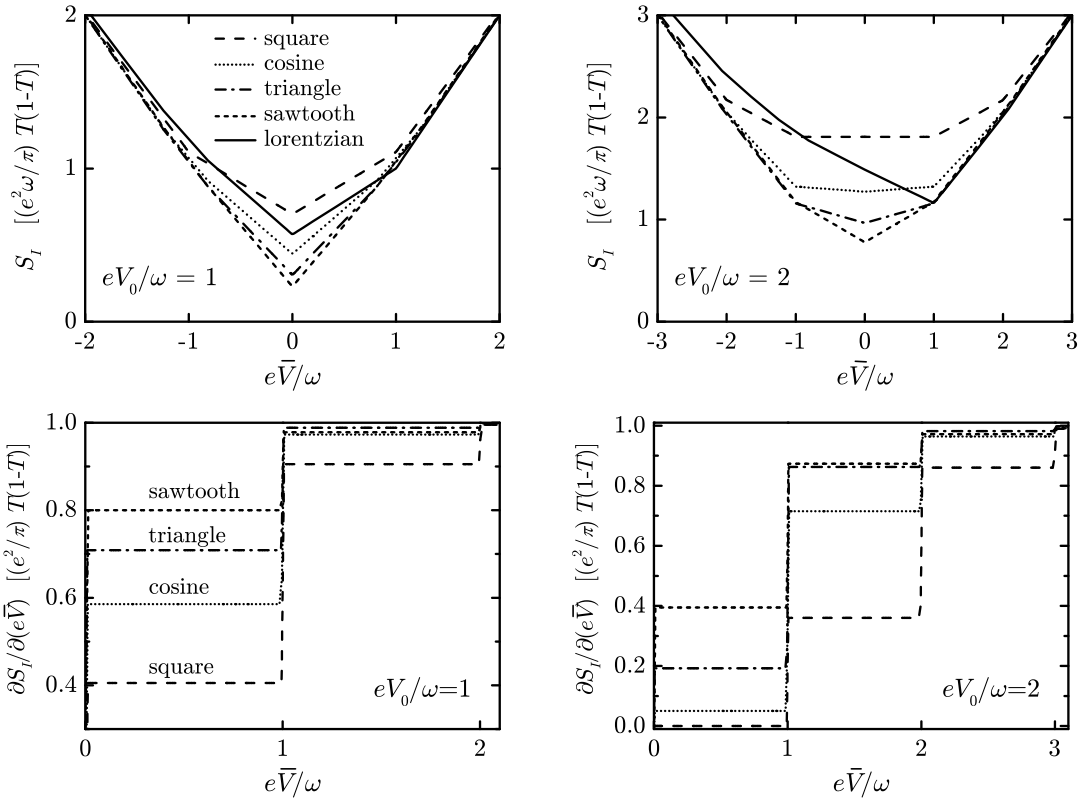

Fig. 38: *The current noise power S_I as a function of the dc offset voltage $\bar{V}$ at constant ac amplitude V_0 is shown for different time-dependent driving voltages (top row). The width of Lorentzian pulses is $\tau_L = 0.1\tau$. The slopes $\partial S_I/\partial\bar{V}$ are shown in the bottom row.*

The total voltage $V(t) = \bar{V} + \Delta V(t)$ varies between $V_{\min} = \bar{V} + V_0[\tanh(\pi\tau_L/\tau) - 1]$ and $V_{\max} = \bar{V} + V_0[\mathrm{cotanh}(\pi\tau_L/\tau) - 1]$. The coefficients $\tilde{f}_n$ are given by

$$\tilde{f}_n = e^{-i\pi eV_0/\omega} \int_{-1/2}^{1/2} dx \, \frac{\{\sin[\pi(x+iy)]\}^{eV_0/\omega}}{\{\sin[\pi(x-iy)]\}^{eV_0/\omega}} \, e^{i2\pi\left(\frac{eV_0}{\omega}+n\right)x}, \tag{23.26}$$

where $y = \tau_L/\tau$. For integer values $eV_0/\omega = N > 0$ we obtain the simplified expressions:

$$\tilde{f}_n = (-1)^N 2\pi i \operatorname*{Res}_{x=iy} \left(\frac{\{\sin[\pi(x+iy)]\}^N}{\{\sin[\pi(x-iy)]\}^N} \, e^{i2\pi(n+N)x} \right) \tag{23.27}$$

for $n > -N$, $\tilde{f}_n = 0$ for $n < -N$, and $\tilde{f}_{n=-N} = (-1)^N e^{-2\pi Ny}$. In particular, the coefficients $\tilde{f}_n$ for $eV_0/\omega = 1$ are given by Eq. (23.7). For $eV_0/\omega = 2$ we obtain $\tilde{f}_n = e^{-2\pi ny}(1 - e^{-4\pi y})[n + 1 - (n+3)e^{-4\pi y}]$ for $n > -2$, $\tilde{f}_{-2} = e^{-4\pi y}$, and $\tilde{f}_n = 0$ otherwise.

The current noise power S_I at low temperatures is given by Eq. (23.13). The S_I is a piecewise linear function of the offset voltage $\bar{V}$, with kinks at integer values of $e\bar{V}/\omega$. At zero offset voltage, the current noise power $S_I(\bar{V} = 0)$ is non-zero and is given by Eq. (23.15). The dependence $S_I(\bar{V})$ at constant amplitude V_0 and for different time-dependent bias voltages is shown in Fig. 38 (top). The slopes $\partial S_I/\partial\bar{V}$ are shown in Fig. 38 (bottom). For all bias voltages considered here (except for Lorentzian pulses) the coefficients $\tilde{f}_n$ satisfy $|\tilde{f}_n| = |\tilde{f}_{-n}|$ which results in S_I being

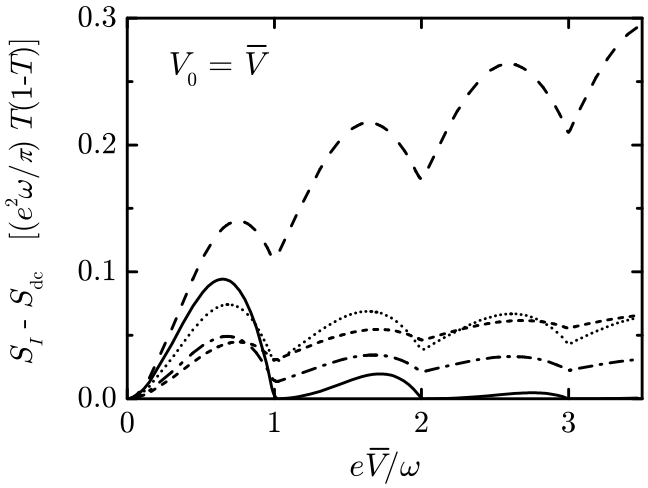

Fig. 39: *The excess noise $S_I - S_{\rm dc}$ with respect to the dc noise level $S_{\rm dc} = (e^2/\pi)T(1-T)e\bar{V}$ is shown for different time-dependent bias voltages: square (dashed), cosine (dotted), triangle (dash-dotted), sawtooth (short-dashed), and Lorentzian pulses (solid line).*

an even function of the offset voltage $\bar{V}$. It is interesting to note that $\tilde{f}_0 = 0$ for a square-shaped voltage drive of amplitude $eV_0/\omega = 2k$, where k is an integer. In this case the noise does not depend on $\bar{V}$ for $|e\bar{V}/\omega| < 1$ and the step in $\partial S_I/\partial\bar{V}$ vanishes at $\bar{V} = 0$. This effect is within the reach of the present experimental technology. In [98] the steps at $e\bar{V}/\omega = 0, \pm 1$ have been observed for the cosine drive with amplitudes ranging between $eV_0/\omega = 1$ and $eV_0/\omega = 2$. The steps have been observed also in the diffusive wire in contact with a superconductor [99] at offset voltages $e^*\bar{V}/\omega = 0, \pm 1$ for the cosine drive with amplitudes ranging between $e^*V_0/\omega = 1$ and $e^*V_0/\omega = 2$. Here $e^* = 2e$ accounts for the doubled effective charge involved in the Andreev process.

The Lorentzian voltage drive is characteristic because it provides the simplest one-particle charge transfer statistics given by Eq. (23.5). This is achieved for impulses carrying an integer number of charge quanta $eV_0/\omega = N$ and at offset voltages $\bar{V} \geq V_0$. The noise is reduced to the minimal noise level of the effective dc bias $S_{\rm dc} = (e^2/\pi)T(1-T)e\bar{V}$. A formal reason for this is the vanishing of the coefficients $\tilde{f}_n = 0$ for $n < -N$ [cf. Eqs. (23.13) and (23.14)]. A possibility to observe the noise minimization is to consider voltage drive with $V_0 = \bar{V}$. The excess noise $S_I - S_{\rm dc}$ is shown in Fig. 39 for different time-dependent bias voltages. In the case of Lorentzian pulses, the noise is minimal and equal to $S_{\rm dc}$ at integer values of $eV_0/\omega = e\bar{V}/\omega$ [160, 188].

The excess noise $S_I - S_{\rm dc}$ is due to bidirectional transport events which are described by Eq. (23.4). There are two types of bidirectional events labelled by L and R with different numbers of attempts given by $M_L = t_0\omega_1/\pi$ and $M_R = t_0(\omega - \omega_1)/\pi$. Here $\omega_1 = e\bar{V} - \lfloor e\bar{V}/\omega \rfloor\omega$ and $\lfloor e\bar{V}/\omega \rfloor$ is the largest integer less than or equal $e\bar{V}/\omega$. The elementary events occur with probabilities $p_{kL(R)} \equiv \sin^2(\alpha_{kL(R)}/2)$ which are obtained by diagonalization of $(h\tilde{h})_{nm}(\mathcal{E})$ for $\mathcal{E} \in (0, \omega_1)$ $[\mathcal{E} \in (\omega_1, \omega)]$ as discussed

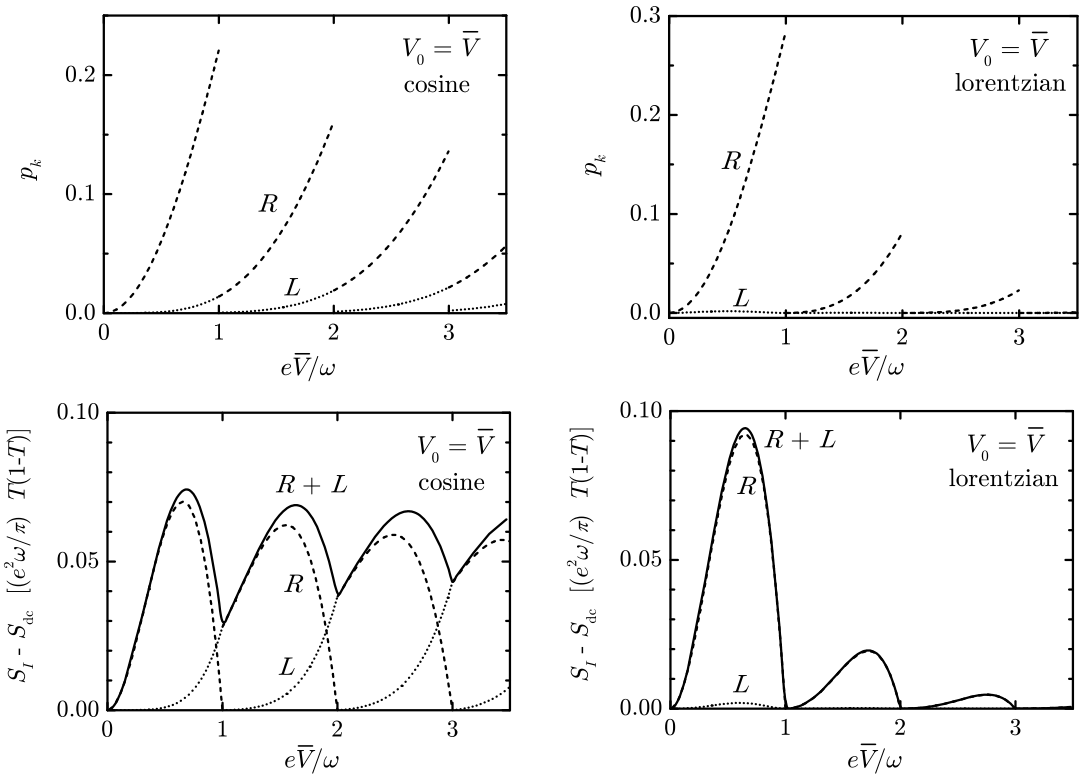

Fig. 40: *The probabilities p_{kL} (dotted lines) and p_{kR} (dashed lines) of elementary events are shown for the cosine time-dependent voltage bias and Lorentzian voltage pulses (top). For the cosine drive, one elementary event of the L-type and one of the R-type can be created per period ($k = 1$). For the Lorentzian pulses, only one R-type event can be created. The decomposition of the excess noise into contributions of elementary events is shown below.*

in § 23. The excess noise is given by $S_I - S_{\rm dc} = (e^2/t_0)\partial^2_{i\chi}\mathcal{S}_2|_{\chi=0}$:

$$S_I - S_{\rm dc} = \frac{2e^2}{\pi} T(1-T) \left(\omega_1 \sum_k p_{kL} + (\omega - \omega_1) \sum_k p_{kR} \right). \tag{23.28}$$

The probabilities $p_{kL(R)}$ for the cosine voltage bias and the Lorentzian voltage pulses as a function of voltage $\bar{V} = V_0$ are shown in Fig. 40 (top). The decomposition of the excess noise into contributions of elementary events is shown in Fig. 40 (bottom). For the cosine voltage drive with $\bar{V} = V_0$, the two bidirectional events (one of L-type and another of R-type) are excited per period with significant probability. The L-type events transform continuously into R-type ones at integer values of $e\bar{V}/\omega$, while the R-type events disappear. The step-like evolution of the probabilities of R-type events as a function of voltage does not introduce discontinuities in the current noise because the corresponding number of attempts vanishes. Instead, the interplay between L and R events results in kinks and the local minima at integer values of $e\bar{V}/\omega$, as shown in Fig. 40 (bottom). The L-type (R-type) events give the dominant contributions as $e\bar{V}/\omega$ approaches the integer values from the left (right) because of the number of attempts which is proportional to ω_1 ($\omega - \omega_1$). In the case of the Lorentzian voltage drive with $\bar{V} = V_0$, only one bidirectional R-type event can be excited. At integer values $e\bar{V}/\omega = eV_0/\omega = N$ the excess noise vanishes.

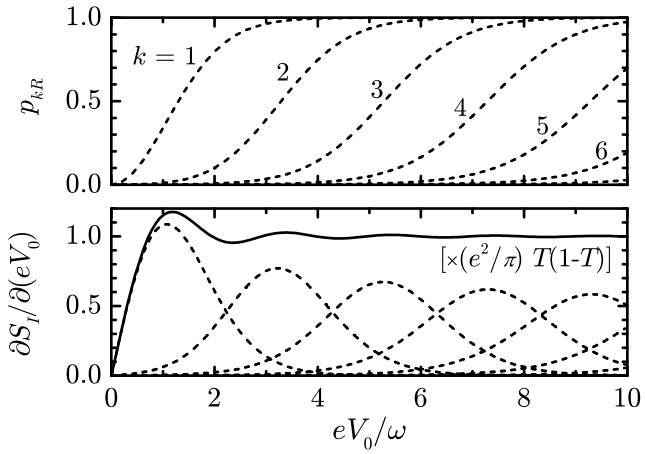

Fig. 41: *The probabilities of elementary events for a square-shaped ac voltage drive of amplitude V_0 are shown in the upper panel. The derivative of the noise power with respect to V_0 (solid line) decomposed into contributions (dashed lines) of elementary events is shown in the lower panel.*

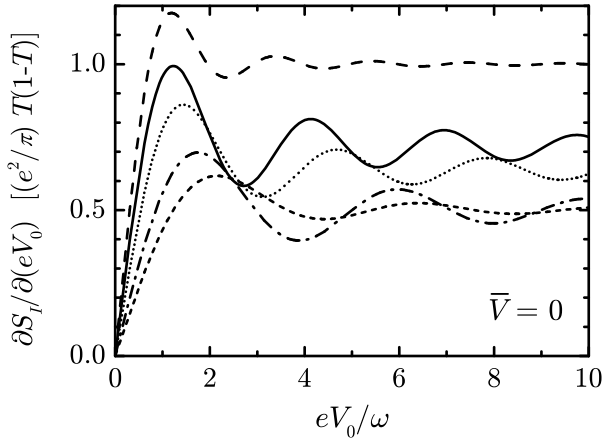

Fig. 42: *The slope of the current noise power $\partial S_I/\partial(eV_0)$ as a function of the amplitude V_0 for different ac driving voltages ($\bar{V} = 0$): square (dashed), cosine (dotted), triangle (dash-dotted), sawtooth (short-dashed), and Lorentzian pulses (solid line). The oscillations are due to elementary events which are created as the voltage amplitude is increased.*

In the following we consider a voltage drive with $\bar{V} = 0$ which creates bidirectional events only. A bidirectional event represents an electron-hole excitation in which both particles are injected towards the scatterer. These events contribute to the noise and even-order cumulants at low temperatures. The average current and odd-order cumulants vanish. The cumulant generating function reduces to $\mathcal{S}_{1R}(\chi)$ which is given by Eq. (23.4). The elementary events can be seen in the slope of the current noise power $\partial S_I/\partial V_0$ which exhibits oscillatory behavior as a function of the amplitude V_0 due to new events entering the transport. The probabilities p_k of elementary events and the decomposition of $\partial S_I/\partial V_0$ into contributions of elementary events for the cosine voltage drive are shown in Fig. 35. The probabilities p_k and the slope $\partial S_I/\partial V_0$ for the square voltage drive are shown in Fig. 41. A comparison

of different time-dependent voltages is shown in Fig. 42.

Bidirectional events with the unit probability $p_k = 1$ represent electron-hole pairs which are created and injected towards the scatterer in *each* voltage cycle. In this case the electron and the hole transfers are statistically independent:

$$\mathcal{S}_k(\chi) = \frac{t_0\omega}{\pi}\ln[1 + TR(e^{i\chi} + e^{-i\chi} - 2)] = \frac{t_0\omega}{\pi}\ln[1 + T(e^{i\chi} - 1)] + \frac{t_0\omega}{\pi}\ln[1 + T(e^{-i\chi} - 1)]. \tag{23.29}$$

Bidirectional events which are created with the probability $0 < p_k < 1$ are described by the cumulant generating function $\mathcal{S}_k(\chi) = (t_0\omega/\pi)\ln[1 + TRp_k(e^{i\chi} + e^{-i\chi} - 2)]$ which cannot be interpreted in terms of independent electron and hole transfers.

The noninteracting theory which we use is applicable for the frequency ω of the applied voltage much smaller than the time scales set by the inverse dwell time $\tau_{\rm d}^{-1}$ and the inverse RC time τ_{RC}^{-1} of the contact. In a typical experimental situation[28] $\tau_{RC} \ll \tau_{\rm d}$. Therefore, the applicability of the noninteracting theory is expected to be limited by the dwell time, $\omega \ll \tau_{\rm d}^{-1}$. However, as shown in [191], the photon-assisted noise $S_I(\omega)$ in the leading order $(eV_0/\omega)^2 \ll 1$ does not depend on the dwell time. Therefore, in a weakly-driven normal junction the noninteracting theory is applicable in a larger frequency range $\omega \ll \tau_{RC}^{-1}$.

The effect of a finite dwell time on the photon assisted noise has been studied in [196] for arbitrary strength of the voltage drive. At the constant amplitude $eV_0/\omega \gtrsim 1$, a maximum in $\partial S_I/\partial\omega$ develops at the frequency $\omega \sim \tau_{\rm d}^{-1}$. The frequency dependence of the noise on the scale of the inverse dwell time can be understood as follows. When an electron enters the cavity, after a very short time $\sim \tau_{RC}$, the charge rearranges to keep the cavity neutral. The distribution function $n(\mathcal{E};t) = \int d\tau\; n(t+\tau/2, t-\tau/2)\; e^{i\mathcal{E}\tau}$ relaxes on a much longer time scale given by $\tau_{\rm d}$. The photon-assisted noise $S_I(\omega)$ probes the electronic distribution function and depends on the frequency ω on the same scale.

At the finite value of $\omega\tau_{\rm d}$, the differential noise $\partial S_I/\partial V_0$ as a function of V_0 is increased with respect to the case $\omega\tau_{\rm d} \ll 1$ which is shown in Fig. 42. The increase is of the order of 20% for $\omega\tau_{\rm d} \simeq 1$. The positions of the maxima and the minima are only slightly shifted. This is consistent with the experiments of Schoelkopf *et al.* [98] and Kozhevnikov *et al.* [99] which can be described by the noninteracting theory even though the frequency of the ac signal applied is comparable or larger than the inverse dwell time.

§ **23.3. Multiterminal charge transfer statistics.** In the previous paragraphs we have discussed the charge transfer statistic and the elementary transport processes in a voltage-driven 2-terminal junction. In the following we study a multiterminal beam splitter geometry depicted in Fig. 43. The source terminal is biased with a time-dependent periodic voltage $V(t)$ and through a mesoscopic conductor attached to several outgoing terminals. The conductor is characterized by a set of transmission eigenvalues $\{T_n\}$. The outgoing leads are characterized by conductances g_i. We are interested in the limit in which the outgoing leads play a role of a detector and only weakly perturb the charge transfer across the conductor. This

[28] For example, for a cavity of a linear dimension L with the mean level spacing δ and the charging energy $E_C = e^2/C_\Sigma$, the ratio $\tau_{RC}/\tau_{\rm d} \approx \delta/E_C \sim (\lambda_F/L)^{d-1} \ll 1$. Here the charging energy is estimated as $E_C \sim e^2/L$. The parameter $d = 2$ for a cavity formed in a 2DEG and $d = 3$ for a metallic grain.

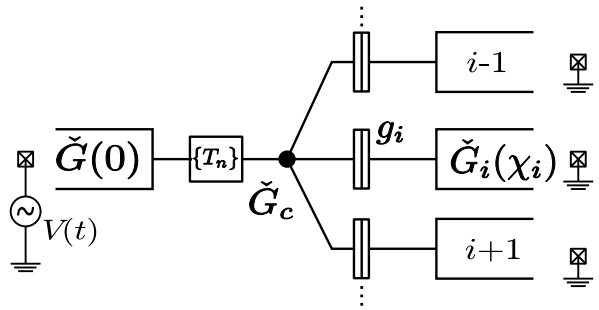

Fig. 43: **Schematic representation of a multiterminal beam splitter.** *The source terminal is biased with a time-dependent voltage $V(t)$ with respect to the outgoing terminals. The total conductance $g = \sum_i g_i$ of the outgoing leads is assumed to be much larger than the conductance $(e^2/\pi)\sum_n T_n$ of the source contact.*

is achieved when the conductance $g \equiv \sum_i g_i$ to the outgoing leads is much larger than the conductance $(e^2/\pi)\sum_n T_n$ of a conductor. In this case the particles which traverse the conductor enter the outgoing terminals with negligible backreflection into the source terminal. A similar setup with spin-selective outgoing contacts has been used in [194] to reveal singlet electron states.

The cumulant generating function is calculated similarly as in § 22 for the 2-terminal case. In contrast to § 22, here we assign the counting fields χ_i to the outgoing terminals. The Green's function $\check{G}(0)$ of the source terminal and the Green's functions $\check{G}_i(\chi_i)$ of the outgoing ones are given by

$$\check{G}(0) = \begin{pmatrix} 1 & 2\tilde{h} \\ 0 & -1 \end{pmatrix}, \qquad \check{G}_i(\chi_i) = e^{-i\chi_i\check{\tau}_1/2} \begin{pmatrix} 1 & 2h \\ 0 & -1 \end{pmatrix} e^{i\chi_i\check{\tau}_1/2}. \tag{23.30}$$

Here $\tilde{h}$ and h are the matrices in time (or energy) indices defined in § 22. The Green's function $\check{G}_c$ of the internal node has to be obtained from matrix current conservation and normalization condition $\check{G}_c^2 = \check{1}$. In the limit $g \gg (e^2/\pi)\sum_n T_n$, the node C is strongly coupled to the outgoing terminals and the $\check{G}_c$ can be obtained in the lowest order with the terminal $\check{G}$ unattached. For simplicity we assume that the node C is coupled to the outgoing terminals via tunnel junctions. In this case matrix current conservation reduces to

$$\left[\sum_i g_i \check{G}_i(\chi_i), \check{G}_c\right] = 0. \tag{23.31}$$

In the following we work in the low-temperature limit in which $h^2 = \tilde{h}^2 = 1$. It is convenient to seek for the solution in the form $\check{G}_c = \vec{p}_c \cdot \check{\vec{\tau}}$ where $\check{\vec{\tau}} = (\check{\tau}_1, \check{\tau}_2, \check{\tau}_3)$. From Eqs. (23.30) and (23.31) we obtain

$$\vec{p}_c = (h, ihc - s, ihs + c) \tag{23.32}$$

where $c = \sum_i \tilde{g}_i \cos(\chi_i)$, $s = \sum_i \tilde{g}_i \sin(\chi_i)$, and $\tilde{g}_i = g_i/g$.

The cumulant generating function of the charge transferred is given by

$$\mathcal{S}(\{\chi\}) = \sum_n \mathrm{Tr}\ln\left[\check{1} + \frac{T_n}{2}\left(\frac{\{\check{G}(0), \check{G}_c(\{\chi\})\}}{2} - \check{1}\right)\right], \tag{23.33}$$

where the summation over internal Keldysh and time (or energy) indices is assumed. The diagonalization of $\{\check{G}, \check{G}_c\}/2 - \check{1}$ is performed along the lines of § 22. First we

rewrite $\{\check{G},\check{G}_c\}/2-\check{1}=\check{\mathcal{A}}+\check{\mathcal{B}}$ where

$$\check{\mathcal{A}}=\begin{pmatrix}1 & b\\ 0 & 0\end{pmatrix}\otimes A,\qquad \check{\mathcal{B}}=\begin{pmatrix}0 & -b\\ 0 & 1\end{pmatrix}\otimes B, \tag{23.34}$$

$A=(1-\tilde{h}h)(c-1)+i(h-\tilde{h})s$, $B=(1-h\tilde{h})(c-1)+i(h-\tilde{h})s$, and $b=is/(c-1)$. Because $\check{\mathcal{A}}\check{\mathcal{B}}=\check{\mathcal{B}}\check{\mathcal{A}}=0$, the operators $\check{\mathcal{A}}$ and $\check{\mathcal{B}}$ commute and satisfy for integer n:

$$(\check{\mathcal{A}}+\check{\mathcal{B}})^n=\begin{pmatrix}1 & b\\ 0 & 0\end{pmatrix}\otimes A^n+\begin{pmatrix}0 & -b\\ 0 & 1\end{pmatrix}\otimes B^n. \tag{23.35}$$

The cumulant generating function given by Eq. (23.33) reduces to

$$\mathcal{S}=\sum_n \mathrm{Tr}\ln\left(1+\frac{T_n}{2}A\right)+\sum_n \mathrm{Tr}\ln\left(1+\frac{T_n}{2}B\right). \tag{23.36}$$

The operators A and B can be diagonalized in the eigensubspaces of $\{h,\tilde{h}\}$ which are invariant with respect to h, $\tilde{h}$, A, and B. By repeating the procedure of § 22 we obtain the cumulant generating function in the form

$$\mathcal{S}(\{\chi\})=\mathcal{S}_{1L}+\mathcal{S}_{1R}+\mathcal{S}_2. \tag{23.37}$$

Here $\mathcal{S}_{1L,R}$ are the contributions of bidirectional processes and $\mathcal{S}_2$ is the contribution of the unidirectional ones. The unidirectional processes are described by

$$\mathcal{S}_2(\{\chi\})=\frac{t_0e\bar{V}}{\pi}\sum_n \ln\left(1+T_n\sum_i \tilde{g}_i(e^{i\chi_i}-1)\right), \tag{23.38}$$

where t_0 is the measurement time and $\bar{V}$ is the dc voltage offset. Here we assume that $e\bar{V}>0$. The bidirectional processes are described by

$$\mathcal{S}_{1\alpha}(\{\chi\})=M_\alpha\sum_k\sum_n \ln\left[1+p_{k\alpha}T_nR_n\left(\sum_i \tilde{g}_i(e^{i\chi_i}+e^{-i\chi_i}-2)\right)\right.$$
$$\left.+p_{k\alpha}T_n^2\left(\sum_{i<j}\tilde{g}_i\tilde{g}_j(e^{i\chi_i}e^{-i\chi_j}+e^{-i\chi_i}e^{i\chi_j}-2)\right)\right]. \tag{23.39}$$

Here k labels the bidirectional processes, n labels transport channels, i and j label the outgoing terminals, and $\alpha=L,R$. The number of attempts $M_{L,R}$ and the probabilities $p_{k\alpha}$ are the same as in § 22.

Equations (23.37) – (23.39) give the statistics of the charge transfer in a multiterminal beam splitter at low temperatures in the presence of a periodic time-dependent drive at the source terminal. Equations (23.38) and (23.39) have a direct physical interpretation. The unidirectional events, which are described by $\mathcal{S}_2$, are the single-electron transfers across the structure due to the dc offset voltage $\bar{V}$ applied to the source terminal. The term $T_n\tilde{g}_ie^{i\chi_i}$ in Eq. (23.38) represents the process in which an electron in the nth transport channel traverses the conductor with probability T_n and enters the outgoing terminal i with probability $\tilde{g}_i=g_i/g$.

On the other hand, the bidirectional processes represent the electron-hole *pairs* which are created in the source terminal and are injected towards the conductor. The probabilities of such excitations are given by $p_{k\alpha}$. The interpretation of the cumulant generating function given by Eq. (23.39) can be obtained from a simple counting argument as in § 8. The term $p_kT_nR_n\tilde{g}_ie^{i\chi_i}$ in (23.39) represents the process

in which electron-hole excitation is created, hole is reflected, and electron is transmitted into the outgoing terminal i. Similarly, the term $p_k T_n R_n \tilde{g}_i e^{-i\chi_i}$ represents the process in which the electron is reflected and the hole is transmitted. Finally, the term $p_k T_n^2 \tilde{g}_i \tilde{g}_j e^{i\chi_i} e^{-i\chi_j}$ $(i \neq j)$ represents the process in which both particles are transmitted with electron entering terminal i and hole entering terminal j.

Charge transfer statistics and current correlations can be obtained using the cumulant generating function $\mathcal{S}(\{\chi\})$. For example, the current cross correlation between *different* terminals i and j is given by $S_{ij} = (e^2/t_0)\partial^2_{i\chi_i, i\chi_j}\mathcal{S}|_{\chi=0}$:

$$S_{ij} = -\frac{2e^2}{\pi}\left(\sum_n T_n^2\right)\tilde{g}_i\tilde{g}_j\left(\omega_1\sum_k p_{kL} + (\omega-\omega_1)\sum_k p_{kR}\right). \tag{23.40}$$

We find that only bidirectional processes in which both particles are transferred (one into the terminal i and another into the terminal j) give the contributions to the cross correlation S_{ij}. This result has been obtained previously by Rychkov *et al.* [96] in the limit of small driving amplitudes ($\bar{V} = 0$ and $eV_0/\omega \ll 1$).

The cross correlation S_{ij} depends on bidirectional processes and is proportional to the excess noise $S_I - S_{\rm dc}$ in a 2-terminal junction [Eq. (23.28)]. The excess noise is just a small correction to the $S_{\rm dc}$ generated by unidirectional processes for a bias voltage with $\bar{V} \simeq V_0$ (Fig. 39). The contribution of the $S_{\rm dc}$ component can be reduced by measuring current cross correlations between different outgoing terminals in the beam splitter geometry with negligible backscattering [152]. This is achieved for the total conductance of the outgoing contacts much larger than the conductance of the source contact.

§ 24. Summary

In this Chapter, we have studied the statistics of the charge transfer in a quantum point contact driven by a time-dependent voltage. We have deduced the elementary transport processes at zero temperature from an analytical result for the cumulant generating function. The transport consists of unidirectional and bidirectional charge transfer events. The unidirectional events represent electrons which emerge from the source terminal because of excess dc bias voltage. The bidirectional events represent electron-hole *pairs* which are created in the source terminal by the ac voltage and are injected towards the contact. This interpretation is further supported by the charge transfer statistics of a multiterminal beam splitter, in which case the injected particles can be partitioned into different outgoing terminals.

The unidirectional events are described by binomial cumulant generating function. The number of attempts is proportional to the dc voltage offset. For an ac voltage bias without dc offset, only bidirectional events remain. A bidirectional event is characterized by the probability of a pair creation which is related to the time-dependence of the ac voltage bias. In general, in the presence of both dc and ac potentials, the statistics of charge transfer is the simplest for a dc potential which corresponds to an integer number of attempts per period per spin. For Lorentzian-shaped voltage pulses with amplitudes quantized in integer multiples of the drive frequency the electron-hole pairs are not created. In this case the charge transfer statistics is the same as the one of the effective dc voltage bias.

Unidirectional events account for the net charge transfer. Bidirectional events contribute only to even cumulants of charge transfer at zero temperature and can be

probed by noise measurements. For an ac voltage bias and no dc offset, the differential photon assisted noise $\partial S_I/\partial V_0$ oscillates as a function of the drive amplitude V_0 due to new bidirectional events which are created as V_0 is increased. The bidirectional events can be probed also in the presence of both dc and ac potentials by current cross correlations in a multiterminal beam splitter geometry with negligible backscattering.

CHAPTER VIII

Conclusion and outlook

In this Thesis we have presented the circuit theory of mesoscopic transport. The theory provides an efficient description of transport in mesoscopic structures with conductances much larger than the conductance quantum, $G \gg G_Q$. We have focused on the noninteracting case which is a valid approximation at energies and temperatures smaller than the inverse dwell time needed for an electron to traverse the junction and the inverse RC time of the charge relaxation. A comprehensive list of references on developments of the circuit theory, including those which take into account interaction effects, is given in [113]. The G_Q-corrections to various transport characteristics (e.g., weak localization effect on conductance and universal conductance fluctuations) have been incorporated into the circuit-theory formalism in [197].

In the following we summarize the structure of the circuit theory. The mesoscopic circuit theory is applicable for multiterminal mesoscopic junctions of arbitrary complex geometry and different types of contacts and terminals, including superconductors and ferromagnets. The method of calculation is as follows. The junction is first divided into a discrete set of *nodes* and *connectors*. The nodes are usually cavities or diffusive parts of the system which provide the isotropization of the electronic distribution function. Interfaces, barriers, and regions in which the transport is not diffusive are modelled as connectors with the corresponding scattering properties. Usually very complex mesoscopic structures can be represented by using only a few discrete circuit elements. The states of internal nodes are determined from current conservation equations, with the properties of the terminals supplied as boundary conditions. In this sense the mesoscopic circuit theory resembles the traditional circuit theory of macroscopic conductors (Kirchhoff's laws). However, in the mesoscopic case, the currents and the states of terminals and nodes are described by matrices instead of scalars.

Since the mesoscopic circuit theory is a finite-element method, the set of matrix equations can be solved numerically by simple iteration. The accuracy of the method can be improved, if necessary, by increasing the number of discrete elements. In some cases, including 2-terminal junctions with arbitrary contacts and multiterminal structures with tunnel couplings, the set of circuit theory matrix equations simplifies considerably, and analytical results can be obtained.

The circuit theory describes a variety of different physical systems within the same formalism. For example, the conductance in coherent normal conductors, the Andreev conductance in normal-superconductor heterojunctions, and various Josephson current-phase relations for the supercurrent between superconductors are all obtained from the same circuit-theory formula supplied with different boundary conditions. The appropriate coupling between electron and hole states within the system is automatically taken into account by the matrix structure of the theory.

Effects such as dephasing and inelastic scattering can be taken into account by introducing fictitious dephasing and voltage probes. Furthermore, the theory can be generalized to access not only the current but the complete statistics of charge transfer in a multiterminal setup. Remarkably, the structure of the theory remains the same, with the only change being the simple modification of the boundary conditions at the terminals. This modification consists of a gauge-like transformation of the quasiclassical Keldysh-Green's functions of the terminals to incorporate the so-called counting fields. For the cases in which the system of the circuit-theory equations can be solved analytically, this results in the complete charge transfer statistics. If an analytical solution is not possible, the higher-order current correlations can be obtained in a systematic way by expansion of the circuit-theory equations in the counting fields. In general, the results are obtained much simpler than using the standard Keldysh-Green's functions theory of nonequilibrium and nonhomogeneous systems. The circuit theory uses the advantage of the discretization of the system into nodes and connectors and captures the relevant physics in the limit $G \gg G_Q$ with the minimal computational overhead.

Although the circuit-theory rules are simple to formulate and apply, the underlying theory is quite complex. The central equation for the matrix current between 2 terminals (§ 12) is obtained by combining the scattering formalism and the nonequilibrium Keldysh-Green's functions technique [113, 150]. The charge transfer statistics is introduced by modelling the charge detector which interacts with the system. After tracing out the detector degrees of freedom, an effective action (influence functional) is obtained which determines the charge transfer statistics [103, 143, 159]. This action can be included in the circuit theory by extending the concept of time evolution on the Keldysh contour: In the extended formulation, the forward and the backward evolutions are governed by different hamiltonians (§ 13). Remarkably, this change can be incorporated in the boundary conditions of the quasiclassical Keldysh-Green's functions of terminals, without altering the structure of the circuit theory. Furthermore, the generalization to multiterminal circuits is straightforward (§ 13.3).

In § 13.4, we have shown that the general template of the circuit theory simplifies considerably in the case of coherent 2-terminal junctions with several contacts in series. The circuit-theory matrix equations can be treated, effectively, as scalar ones. The transmission distribution of the composite system can be obtained in a simple way from the scattering properties of individual contacts [66, 113].

In § 13.5, we provided an example of a full circuit-theory calculation. We have studied a beam splitter geometry which consists of a cavity coupled to a superconductor and two normal terminals. The current cross correlations in the normal terminals are studied as a function of dephasing between electrons and holes due to the finite dwell time through the cavity. In the incoherent case, the current cross correlations in normal terminals are negative irrespective of the conductance of the contacts. In the coherent case, the cross correlations are positive (negative) for the cavity strongly coupled to the superconductor (normal terminals). The presence of normal backscattering at the cavity-superconductor contact shifts the cross correlations in the normal terminals towards positive values [165, 166].

In Chapter V, we have studied the charge transfer statistics for an open cavity between a superconductor and a normal metal at temperatures and bias voltages below the superconducting gap. At finite temperatures, the charge is transferred in pairs in both directions. The probability of pair transfer through the cavity is given

by the distribution of Andreev reflection eigenvalues. The form of the cumulant generating function manifestly reveals how the subgap transport in superconductor-normal metal structures is affected both by the effective charge doubling due to the Andreev process and by the modification of the transmission properties due to electron-hole correlations introduced by the superconductor. In an open cavity, the Fano factor is enhanced with respect to the corresponding normal-state junction in agreement with experimental results [89]. In comparison to the tunnel coupling, the conductance and Fano factor exhibit opposite trends as a function of the junction asymmetry, which can be used to experimentally probe the quality of the contacts. The third cumulant is also affected by the presence of a superconductor. It probes the asymmetry of the Andreev reflection distribution function.

In Chapter VI, we have studied quasiparticle transport in arrays of chaotic cavities focusing on the crossover from a single cavity to the universal limit of a diffusive wire as the number of inner contacts is increased. We have obtained the distribution of transmission eigenvalues, the cumulant generating function, and the first three cumulants both in the normal and in the superconducting state, generalizing the previous results on noise [68, 69] in such a system to all higher-order correlations.

In Chapter VII, we have studied a generic mesoscopic contact driven by a time-dependent voltage. The cumulant generating function of the charge transfer statistics is obtained analytically at zero temperature. The elementary charge transfer events consist of single-particle and two-particle processes. The single-particle processes represent electrons which are injected from the source terminal due to excess dc bias voltage. The two-particle processes represent electron-hole pairs which are created by the time-dependent voltage bias and are injected towards the contact. The probabilities of these electron-hole pair creations are obtained in terms of the properties of the driving voltage.

Two-particle processes do not contribute to the average current and higher-order odd cumulants of the charge transferred at low temperature. However, they do contribute to the noise and higher-order even cumulants. We have calculated the noise generated by different time-dependent driving signals. For an ac potential applied, the noise is entirely due to two-particle processes. The individual processes can be identified from the oscillations of the differential noise $\partial S_I/\partial V_0$ as the amplitude V_0 of the drive is increased. For both dc and ac potentials present, the two-particle processes give rise to the excess noise $S_I - S_{\rm dc}$ with respect to the dc level $S_{\rm dc}$. For a voltage drive with ac amplitude comparable to dc voltage offset, the excess noise is just a small correction with respect to $S_{\rm dc}$. The contribution of the $S_{\rm dc}$ component can be reduced by measuring current cross correlations between different outgoing terminals in the beam splitter geometry with negligible backscattering [152]. In this case the cross correlations are only due to two-particle processes in which the incoming electron-hole pair is split and the particles enter different terminals.

Several open questions remain to be addressed concerning the charge transfer statistics in the presence of time-dependent driving. One question concerns the many-body electronic state incident to the contact. This state has been obtained for Lorentzian voltage pulses which correspond to integer charge transfers [189]. For an ac voltage drive with the amplitude much smaller than the driving frequency, the incident many-body state has been obtained in [96]. The structure of such states is not known for a time-dependent dive of arbitrary amplitude. It would be interesting to extend the theory to include nonperiodic driving signals and to analyze

the structure of elementary processes in the case in which the driving signal itself is a random process.

Another question concerns the charge transfer statistics at finite temperatures. For a dc bias voltage, the elementary transport processes can be obtained in the full temperature range: from unidirectional binomial charge transport processes at low temperatures to bidirectional transport processes due to thermal fluctuations at high temperatures. The elementary transport processes at finite temperatures in the presence of a time-dependent voltage drive have not been identified so far.

CHAPTER IX

Appendix

§ 25. Fluctuation-dissipation theorem

Here we give a short account of equilibrium fluctuations and their relation to the dissipative response of the system in the presence of external time-dependent perturbation. This important result is known as fluctuation-dissipation theorem [14]. First we formulate the theorem in a more general form which is common in the literature [1, 129], and then apply it to the particular two-terminal mesoscopic junction. As a result we obtain Eq. (10.35) which relates thermal current fluctuations and conductance of the system. Although the same formula follows from the scattering formalism, it is actually just a manifestation of the much more general relationship between equilibrium fluctuations and the corresponding response to external driving, valid for any system.

Let us consider an isolated quantum system described by the unperturbed hamiltonian $\hat{H}$. We are interested in equilibrium fluctuations of an observable $\hat{A}$ which characterizes the system and does not depend on time in the Schrödinger picture. The fluctuations are characterized by the correlation function

$$S_A(t'-t'') = \frac{1}{2}\left\langle \{\Delta\hat{A}_H(t'), \Delta\hat{A}_H(t'')\} \right\rangle_H, \tag{25.1}$$

where $\hat{A}_H(t)$ are operators in the Heisenberg picture, $\Delta\hat{A}_H(t) = \hat{A}_H(t) - \langle\hat{A}\rangle_H$ is the deviation from the average value, and the average $\langle\cdots\rangle_H$ is taken with respect to the equilibrium state $\hat{\rho}_H = e^{-\hat{H}/T_e}/\operatorname{Tr}(e^{-\hat{H}/T_e})$. Because $\hat{H}$ does not depend on time, the correlator S_A depends only on time difference $t'-t''$. Taking the Fourier transformation we obtain

$$S_A(t'-t'') = \int \frac{d\Omega}{2\pi}\, S_A(\Omega)\, e^{-i\Omega(t'-t'')}, \tag{25.2}$$

where $S_A(\Omega)$ is the spectral weight of fluctuations given by

$$\left\langle [\Delta\hat{A}_H(t)]^2 \right\rangle_H = \int \frac{d\Omega}{2\pi}\, S_A(\Omega). \tag{25.3}$$

Note that the left hand side of Eq. (25.3) actually does not depend on time. Sometimes it is more convenient to deal with the correlation of the observable $\hat{A}$ alone, defined by

$$\tilde{S}_A(t'-t'') = \frac{1}{2}\left\langle \{\hat{A}_H(t'), \hat{A}_H(t'')\} \right\rangle_H. \tag{25.4}$$

In this case the correlation of fluctuations and the spectral weight are given by $S_A(t'-t'') = \tilde{S}_A(t'-t'') - \langle\hat{A}\rangle_H^2$ and $S_A(\Omega) = \tilde{S}_A(\Omega) - 2\pi\delta(\Omega)\,\langle\hat{A}\rangle_H^2$, respectively.

Now let us consider the response of the system to a time-dependent perturbation given by

$$\hat{H}'(t) = -\hat{A}\, f(t), \tag{25.5}$$

where $f(t)$ is some external force which is adiabatically switched on at $t = -\infty$. Due to the time-dependent perturbation, the average of $\hat{A}$ changes with time and differs from its equilibrium value by $\delta A(t) \equiv \langle \hat{A}_{\mathcal{H}}(t) \rangle_H - \langle \hat{A} \rangle_H$, where $\hat{\mathcal{H}} = \hat{H} + \hat{H}'(t)$. For sufficiently weak perturbations, $\delta A(t)$ can be expressed in terms of f up to linear order:

$$\delta A(t) = \int_0^\infty d\tau \; \alpha(\tau) f(t-\tau). \tag{25.6}$$

Here we have introduced the generalized susceptibility $\alpha(\tau)$ which describes the response of the system at time t due to external force acting at previous times $t-\tau$. The causality condition $\alpha(\tau) = 0$ for $\tau < 0$ is taken into account in Eq. (25.6) explicitly. Taking the Fourier transform we obtain

$$\delta A(\Omega) = \alpha(\Omega) \; f(\Omega), \tag{25.7}$$

where

$$\alpha(\Omega) = \int_0^\infty d\tau \; \alpha(\tau) \; e^{i\Omega\tau}. \tag{25.8}$$

Because $\alpha(\tau)$ is real, the Fourier components satisfy

$$\alpha'(-\Omega) = \alpha'(\Omega), \qquad \alpha''(-\Omega) = -\alpha''(\Omega), \tag{25.9}$$

where α' and α'' denote real and imaginary parts, respectively. Relations analogous to Eq. (25.9) hold for $f(\Omega)$.

In the following we show that the imaginary part $\alpha''(\Omega)$ of the generalized susceptibility is related to dissipation. The system changes its state by absorbtion of energy from an external driving force f. After absorption, the energy is dissipated in the system, i.e., converted into heat distributed over many degrees of freedom. The rate of energy change due to time-dependent perturbation is given by

$$\frac{dE}{dt} = \frac{d}{dt} \langle \hat{\mathcal{H}} \rangle_{\mathcal{H}(t)} = \left\langle \frac{\partial \hat{\mathcal{H}}(t)}{\partial t} \right\rangle_{\mathcal{H}(t)} = -\langle \hat{A}_{\mathcal{H}}(t) \rangle_H \; \frac{df}{dt}. \tag{25.10}$$

If the expression for dE/dt is known, then by comparison with Eq. (25.10) it is possible to identify the generalized force f which corresponds to the observable $\hat{A}$ of interest. From Eqs. (25.6) – (25.10) we obtain the total energy dissipated over time of perturbation [$f(t) = 0$ for $t \to \pm\infty$]:

$$Q = \int_{-\infty}^{\infty} dt \; \frac{dE}{dt} = \int_0^\infty \frac{d\Omega}{2\pi} \; 2\alpha''(\Omega) \; |f(\Omega)|^2. \tag{25.11}$$

Since any realistic process is accompanied with some dissipation, we conclude that $\alpha''(\Omega) > 0$ for $\Omega > 0$.

The generalized susceptibility $\alpha(\Omega)$ possesses a number of properties which follow from causality and hold independently of the system under consideration. To obtain these properties we generalize Eq. (25.8) by allowing Ω to be complex, $\Omega = \Omega' + i\Omega''$. In the upper half plane the integral in Eq. (25.8) converges, while in the lower half plane we define $\alpha(\Omega)$ by analytic continuation. In the following we list some of the properties of $\alpha(\Omega)$ without proof, and refer to [1] for a more discussion. First, $\alpha(\Omega)$ is single-valued and nonsingular in the upper half plane. On the real axis, $\alpha(\Omega)$ is also nonsingular, except possibly at $\Omega = 0$. From Eq. (25.8) we obtain that $\alpha(-\Omega^*) = \alpha^*(\Omega)$. Therefore, $\alpha(\Omega)$ is real on the upper imaginary semiaxis. It monotonically decays from some positive value $\alpha(+i0)$ to 0 as $\Omega \to +i\infty$. In

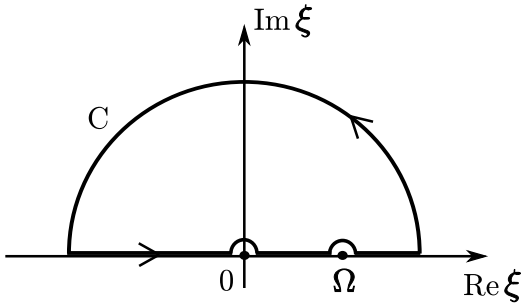

Fig. 44: *Contour of integration used in the derivation of the Kramers-Kronig relations. The radius of the semicircle is taken in the limit $|\xi| \to \infty$. The generalized susceptibility $\alpha(\xi)$ is analytic in the upper half plane and on the real axis, with the possible singularity at the coordinate origin. The function $\alpha(\xi)/(\xi - \Omega)$ is analytic inside the contour C.*

the upper half plane, away from the imaginary semiaxis, $\alpha(\Omega)$ is purely imaginary. Therefore, $\alpha(\Omega)$ has no zeros in the upper half plane.

The properties listed above enable us to relate real and imaginary parts of $\alpha(\Omega)$. Let us consider the function $\alpha(\xi)/(\xi - \Omega)$, with Ω real. This function is analytic inside the contour C depicted on Fig. 44 and satisfies $\oint_C d\xi\, \alpha(\xi)/(\xi - \Omega) = 0$. Using $(\xi - \Omega + i0)^{-1} = \text{p.v.}(\xi - \Omega)^{-1} - i\pi\delta(\xi - \Omega)$ we obtain

$$i\alpha(\Omega) = \frac{1}{\pi}\!\!\int\!\!\!\!\!\!-_{-\infty}^{\infty} \frac{\alpha(\xi)}{\xi - \Omega}\, d\xi - \frac{C}{\Omega}. \tag{25.12}$$

Therefore, the real and imaginary parts of $\alpha(\Omega)$ are related by

$$\alpha'(\Omega) = \frac{1}{\pi}\!\!\int\!\!\!\!\!\!-_{-\infty}^{\infty} \frac{\alpha''(\xi)}{\xi - \Omega}\, d\xi, \tag{25.13a}$$

$$\alpha''(\Omega) = -\frac{1}{\pi}\!\!\int\!\!\!\!\!\!-_{-\infty}^{\infty} \frac{\alpha'(\xi)}{\xi - \Omega}\, d\xi + \frac{C}{\Omega}. \tag{25.13b}$$

The integration in Eqs. (25.12) and (25.13) is taken in the sense of a principal value, avoiding the singularity at $\xi = \Omega$ and the one which may be present at $\xi = 0$. The later (if present) is taken into account by the term C/Ω, where $\alpha(\xi) = iC/\xi$ in the vicinity $\xi = 0$. Equations (25.12) and (25.13) are the famous Kramers-Kronig relations. They follow from the casuality of $\alpha(\tau)$ and hold quite generally, independent of the system under consideration.

Another useful relation can be derived between $\alpha(i\Omega)$ on the upper imaginary semiaxis and $\alpha''(\Omega)$ on the real axis. Let us integrate the function $\xi\alpha(\xi)/(\xi^2 + \Omega^2)$ over ξ at the semicircle of large radius in the upper half plane. Using that $\alpha'(\xi)$ is an even function for real ξ, we find

$$\alpha(i\Omega) = \frac{2}{\pi}\int_0^{\infty} \frac{\xi\, \alpha''(\xi)}{\Omega^2 + \xi^2}\, d\xi, \tag{25.14}$$

where $\Omega > 0$. After integration of both sides over Ω we obtain

$$\int_0^{\infty} \alpha(i\Omega)\, d\Omega = \int_0^{\infty} \alpha''(\Omega)\, d\Omega. \tag{25.15}$$

The generalized susceptibility has been introduced in Eq. (25.6) phenomenologically. To relate $\alpha(\tau)$ to the microscopic properties of the system we calculate $\delta A(t)$

using the Kubo linear response formula [198]

$$\delta A(t) = -i \int_{t_0}^{t} dt' \ \left\langle [\hat{A}_H(t), \hat{H}'_H(t')] \right\rangle_H , \tag{25.16}$$

where the perturbation is switched on at time t_0. Comparing Eqs. (25.6) and (25.16) we obtain

$$\alpha(t' - t'') = i\theta(t' - t'') \left\langle [\hat{A}_H(t'), \hat{A}_H(t'')] \right\rangle_H . \tag{25.17}$$

Equations (25.16) and (25.17) express the linear response of the system in a non-equilibrium state in terms of its equilibrium properties. From Eq. (25.17) we obtain

$$\begin{aligned} \alpha''(\Omega) = \frac{\alpha(\Omega) - \alpha^*(\Omega)}{2i} &= \frac{1}{2} \int_{-\infty}^{\infty} d\tau \ e^{i\Omega\tau} \left\langle [\hat{A}_H(\tau), \hat{A}_H(0)] \right\rangle_H \\ &= \frac{e^{\Omega/T_e} - 1}{2} \int_{-\infty}^{\infty} d\tau \ e^{i\Omega\tau} \langle \hat{A}_H(0) \hat{A}_H(\tau) \rangle_H , \end{aligned} \tag{25.18}$$

where in the last step we used $\langle \hat{A}_H(t') \hat{A}_H(t'') \rangle_H = \langle \hat{A}_H(t'') \hat{A}_H(t' + iT_e^{-1}) \rangle_H$. Similarly, from Eq. (25.4) we obtain

$$\tilde{S}_A(\Omega) = \frac{e^{\Omega/T_e} + 1}{2} \int_{-\infty}^{\infty} d\tau \ e^{i\Omega\tau} \langle \hat{A}_H(0) \hat{A}_H(\tau) \rangle_H . \tag{25.19}$$

From Eqs. (25.18) and (25.19) we obtain the result known as a fluctuation-dissipation theorem [14]

$$\tilde{S}_A(\Omega) = \alpha''(\Omega) \ \coth \left(\frac{\Omega}{2T_e} \right) , \tag{25.20}$$

which relates the equilibrium fluctuations of the observable $\hat{A}$ and the dissipative response of the system upon time-dependent perturbation $\hat{H}' = -\hat{A} f(t)$. This result has been obtained in the linear response regime, i.e., for sufficiently weak perturbations f. However, the size of perturbation does not appear in Eq. (25.20) and therefore makes no restriction on the possible values of the equilibrium fluctuations. The properties of equilibrium fluctuations are completely determined by the linear response of the system to an external drive, no matter how weak it is.

In the classical limit $\Omega \ll T_e$, Eq. (25.20) reduces to

$$\tilde{S}_A(\Omega) = 2T_e \alpha''(\Omega)/\Omega . \tag{25.21}$$

If $\Omega \ll T_e$ for all frequencies Ω for which $\alpha''(\Omega)$ is nonvanishing, we have

$$\left\langle \hat{A}_H(t)^2 \right\rangle_H = \int_{-\infty}^{\infty} \frac{d\Omega}{2\pi} \ \tilde{S}_A(\Omega) = T_e \alpha(0), \tag{25.22}$$

where in the last step we used Eq. (25.14). In this case the equilibrium fluctuations are determined by the static response $\alpha(\Omega = 0)$.

In the following we apply the general formalism of the fluctuation-dissipation theorem to the mesoscopic two-terminal junction described in § 10.5. The rate of energy dissipation for the applied voltage $V(t)$ is given by $dE/dt = V(t) \langle \hat{I}(t) \rangle$. By comparing with Eq. (25.10) we obtain $\hat{A} = \hat{I}$ and identify the generalized force $\dot{f} = -V(t)$ which is related to the current fluctuations. Equation (25.7) reduces to

$I(\Omega) = V(\Omega)/Z(\Omega)$, where we introduced the impedance $Z(\Omega) = i\Omega/\alpha(\Omega)$ and used that $\langle \hat{I} \rangle = 0$ in equilibrium. From the fluctuation-dissipation theorem we obtain

$$S_I(\Omega) = G(\Omega)\, \Omega \coth\left(\frac{\Omega}{2T_e}\right) = 2G(\Omega)\left(\frac{\Omega}{2} + \frac{\Omega}{e^{\Omega/T_e} - 1}\right), \tag{25.23}$$

with the conductance defined by $G(\Omega) = \mathrm{Re}[1/Z(\Omega)]$. At large temperatures we recover the result for the thermal current noise power given by Eq. (10.35) which has been obtained from the scattering formalism.

§ 26. Moment problem

The formulation of the moment problem in one dimension is the following: Given a sequence $\mathcal{M}_0, \mathcal{M}_1, \ldots$ of real numbers, find necessary and sufficient conditions for the existence of a measure f on support[29] S such that

$$\mathcal{M}_n = \int_S x^n \, df(x), \qquad \text{for } n = 0, 1, \ldots. \tag{26.1}$$

Depending on the choice of support, there are three types of moment problems: the Hamburger [199] moment problem in which the support is the whole real axis $S = (-\infty, +\infty)$, the Stieltjes [200] moment problem in which the support is the positive semiaxis $S = [0, +\infty)$, and the Hausdorff [201] moment problem in which the support is a finite interval (which can be taken as $S = [0, 1]$ without loss of generality). In general, the sequence of moments does not determine the probability measure uniquely. For example, Stieltjes showed that

$$\int_0^\infty x^{n - \ln x} \sin(2\pi \ln x) \, dx = 0 \tag{26.2}$$

for $n = 0, 1, \ldots$, which implies that all probability densities on the half-line of the form $f_\lambda(x) = x^{-\ln x}[1 + \lambda \sin(2\pi \ln x)]$ with $\lambda \in [0, 1]$ have the same sequence of moments $\mathcal{M}_n = \exp[(n+1)^2/4]\sqrt{\pi}$ (Fig. 45). Therefore, the conditions of uniqueness are also nontrivial.

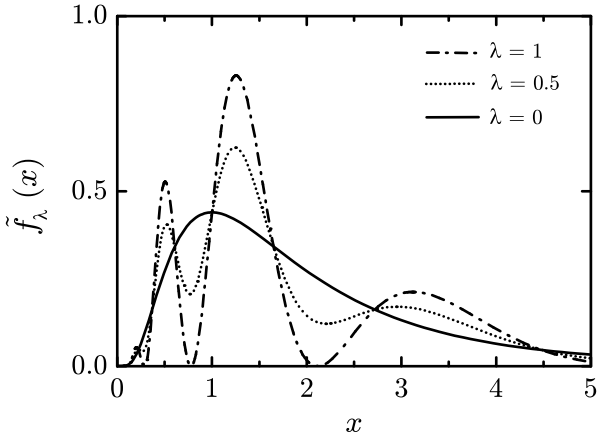

Fig. 45: *The normalized Stieltjes probability density* $\tilde{f}_\lambda(x) = (\pi\sqrt{e})^{-1/2} f_\lambda(x)$ *for different values of the parameter* λ. *All probability densities* $\tilde{f}_\lambda$ *have the same moments* $\langle x^n \rangle = e^{n(n+2)/4}$ *independent of* λ.

First we give the results on the existence of a solution [202–204]. Let $\{\mathcal{M}_n\}$ be a sequence of real numbers and let us define the determinants $h_n = \det \boldsymbol{h}_n$ and $s_n = \det \boldsymbol{s}_n$, where $(\boldsymbol{h}_n)_{ij} = \mathcal{M}_{i+j-2}$ and $(\boldsymbol{s}_n)_{ij} = \mathcal{M}_{i+j-1}$, with $i, j = 1, \ldots, n$. A necessary and sufficient condition for the existence of a measure f on the support $S = (-\infty, \infty)$ obeying Eq. (26.1) is that $h_n > 0$ for all $n = 1, 2, \ldots$. A necessary and sufficient condition for the existence of a measure f supported on $S = [0, +\infty)$ is that both $h_n > 0$ and $s_n > 0$ for all $n = 1, 2, \ldots$. In the case of the Hausdorff moment problem with finite support $S = [0, 1]$, the probability measure exists if and only if

[29] The support S of a measure $f : X \to \mathbb{R}$ is the set of all points $x \in X$ for which every open neighborhood of x has a positive measure.

all finite differences are nonnegative, $\Delta^k \mathcal{M}_n \geq 0$, where $\Delta \mathcal{M}_n = \mathcal{M}_n - \mathcal{M}_{n+1}$. The probability measure in the Hausdorff case, if it exists, is always unique.

In the following we give the results on the uniqueness of the measure in the Hamburger and Stieltjes moment problem. Let $\{\mathcal{M}_n\}$ be a set of Hamburger (Stieltjes) moments for which the probability measure exists. If the moments fulfill $|\mathcal{M}_n| \leq CR^n n!$ $[|\mathcal{M}_n| \leq CR^n (2n)!]$ for some $C, R > 0$, then the measure in the Hamburger (Stieltjes) problem is unique. The following Carleman's criterion is also useful: If $\sum_{n=1}^{\infty} \mathcal{M}_{2n}^{-1/2n} = +\infty$ $[\sum_{n=1}^{\infty} \mathcal{M}_n^{-1/2n} = +\infty]$ then the Hamburger (Stieltjes) probability measure is unique [204]. The above criteria state that a not too rapid growth of moments implies the uniqueness of the probability measure. The drawback is that they represent sufficient conditions for uniqueness only, i.e., we cannot conclude that the moment problem has multiple solutions just because the moment sequence increases very rapidly. In fact, there are sequences of moments of arbitrary rapid growth with unique probability measures [202].

A necessary and sufficient condition for uniqueness in the Hamburger moment problem can be formulated in terms of the determinants h_n and $t_n = \det \boldsymbol{t}_n$, with $(\boldsymbol{t}_n)_{ij} = \mathcal{M}_{i+j+2}$ $(i, j = 1, \ldots, n)$. The probability measure in the Hamburger problem is unique if and only if $\lim_{n\to\infty}(h_n/t_{n-2}) = 0$. An alternative necessary and sufficient condition is that the smallest eigenvalue of $\boldsymbol{h}_n$ tends to 0 as $n \to \infty$.

In this paragraph we summarized some results on the moment problem in one dimension which illustrate that recovering the probability measure from a given sequence of moments is, in general, a nontrivial mathematical task. In the multidimensional case, the moment problem becomes even more involved [203].

§ 27. Quasiclassical Green's functions

The method of quasiclassical Green's functions is explained in detail in [125] in the context of the Bardeen-Cooper-Schrieffer theory of superconductivity [155] (see also [130, 133]). In this paragraph we give a general definition of the quasiclassical Green's functions and provide results for homogeneous normal and superconducting states. These quasiclassical Green's functions characterize the terminals of a multiterminal mesoscopic junction and are used as boundary conditions in the circuit theory (Chapter IV).

The quasiclassical Green's functions are introduced as follows. First we recall that single-particle averages are expressed in terms of an exact Green's function $G(\boldsymbol{r}', \boldsymbol{r}'')$ by taking the limit $\boldsymbol{r}' \to \boldsymbol{r}''$ [Eq. (11.18)]. In the momentum representation, the limit $\boldsymbol{r}' \to \boldsymbol{r}''$ reduces to an integration over momentum. Therefore, physical quantities are given by products of functions of momentum and exact Green's functions, integrated over momentum. The properties of the system are determined by quasiparticles in the vicinity of the Fermi surface and we can put $\boldsymbol{p} \approx \boldsymbol{p}_F$ in all prefactors of the Green's functions. Here $\boldsymbol{p}_F = p_F \boldsymbol{p}/|\boldsymbol{p}|$ is the Fermi momentum in direction of propagation. The integration over momentum $(2\pi)^{-3} \int d\boldsymbol{p}$ can be parametrized using the Fermi surface in the normal state, $d\boldsymbol{p}/(2\pi)^3 = (d\xi_{\boldsymbol{p}}/v_F)\, dS_F/(2\pi)^3$. Here $d\xi_{\boldsymbol{p}}/v_F$ is the increase of momentum in the direction perpendicular to the Fermi surface and dS_F is the element of the Fermi surface. For a spherical Fermi surface with $\xi_{\boldsymbol{p}} = \boldsymbol{p}^2/2m - \mu$ and $dS_F = p_F^2 d\Omega_{\boldsymbol{p}}$ we obtain

$$\int \frac{d\boldsymbol{p}}{(2\pi)^3} \cdots = \mathcal{V}(0) \int d\xi_{\boldsymbol{p}} \int \frac{d\Omega_{\boldsymbol{p}}}{4\pi} \cdots . \tag{27.1}$$

Here $\mathcal{V}(0) = mp_F/(2\pi^2)$ is the density of states per spin at the Fermi energy. Since we take $\boldsymbol{p} \approx \boldsymbol{p}_F$ in the prefactors of the Green's functions, the integration $\int d\xi_{\boldsymbol{p}}$ acts only on the Green's functions and can be included into the definition of the quasiclassical Green's functions. The quasiclassical counterparts of the exact Green's functions $G^{\pm\pm}$ and $G^{R,A,K}$ are defined by

$$G_{\mathcal{E}',\mathcal{E}''}(\boldsymbol{p}_F, \boldsymbol{k}) = \oint \frac{d\xi_{\boldsymbol{p}}}{\pi}\, iG_{\mathcal{E}',\mathcal{E}''}\left(\boldsymbol{p} + \frac{\boldsymbol{k}}{2}, \boldsymbol{p} - \frac{\boldsymbol{k}}{2}\right). \tag{27.2a}$$

Here $G_{\mathcal{E}',\mathcal{E}''}(\boldsymbol{p} + \boldsymbol{k}/2, \boldsymbol{p} - \boldsymbol{k}/2)$ is an exact Green's function in the momentum representation and $\oint d\xi_{\boldsymbol{p}}$ denotes the contour integration as shown in Fig. 46. The quasiclassical Green's functions in the coordinate representation are given by

$$G_{\mathcal{E}',\mathcal{E}''}(\boldsymbol{p}_F, \boldsymbol{r}) = \int \frac{d\boldsymbol{k}}{(2\pi)^3}\, G_{\mathcal{E}',\mathcal{E}''}(\boldsymbol{p}_F, \boldsymbol{k})\, e^{i\boldsymbol{k}\boldsymbol{r}}. \tag{27.2b}$$

Fast oscillations on the scale of λ_F with respect to the relative coordinate $\boldsymbol{r}' - \boldsymbol{r}''$ are integrated out in the quasiclassical Green's functions. A dependence on the center of mass coordinate $\boldsymbol{r} = (\boldsymbol{r}' + \boldsymbol{r}'')/2$ is preserved because of the much larger characteristic length scale. In the superconducting state this length scale is of the order of the coherence length $\xi \sim v_F/|\Delta| \gg \lambda_F$. Fast oscillations on the scale λ_F are not relevant for the superconducting properties. The accuracy of the quasiclassical approximation is of the order of $\Delta_0/\mathcal{E}_F \sim 10^{-3}$ for conventional superconductors and $\Delta_0/\mathcal{E}_F \sim 10^{-1} - 10^{-2}$ for the high-temperature ones.

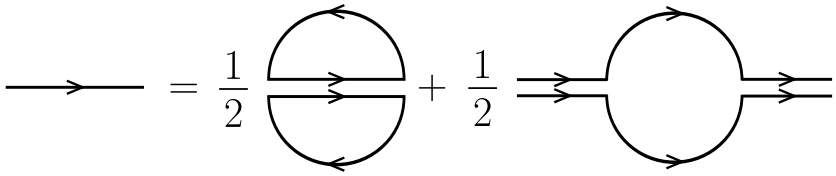

Fig. 46: *The integration $\int_{-\infty}^{\infty} d\xi_{\boldsymbol{p}}$ is decomposed into 4 contour integrals in the complex $\xi_{\boldsymbol{p}}$ plane. The integral $\oint d\xi_{\boldsymbol{p}}$ which appears in the definition of the quasiclassical Green's functions corresponds to the first term on the right hand side of the figure, i.e., it denotes the average of the integrals taken over the closed semicircles in the upper and the lower half planes. The radius of the contour is taken to be finite but much larger than any characteristic energy scale of the system. This cutoff at large energies is needed to ensure the convergence of the diagonal components in $\bar{G}^{R,A}$* [125].

In the following we provide expressions for the quasiclassical Keldysh-Green's functions of normal and superconducting terminals. The quasiclassical Keldysh-Green's function $\check{G}_{\mathcal{E}',\mathcal{E}''}(\boldsymbol{p}_F, \boldsymbol{r})$ in a homogeneous state does not depend on the direction of propagation and the coordinate, $\check{G}_{\mathcal{E}',\mathcal{E}''}(\boldsymbol{p}_F, \boldsymbol{r}) = \check{G}(\mathcal{E}', \mathcal{E}'')$. In equilibrium, $\check{G}(\mathcal{E}', \mathcal{E}'')$ is diagonal in energy:

$$\check{G}(\mathcal{E}', \mathcal{E}'') = 2\pi\delta(\mathcal{E}' - \mathcal{E}'')\, \check{G}(\mathcal{E}'). \tag{27.3}$$

In the normal state $\check{G}(\mathcal{E})$ is given by

$$\check{G}(\mathcal{E}) = \begin{pmatrix} 1 & 2h \\ 0 & -1 \end{pmatrix}, \tag{27.4}$$

where $h(\mathcal{E}) = 1 - 2n(\mathcal{E})$ and $n(\mathcal{E}) = (e^{\beta(\mathcal{E}-eV)} + 1)^{-1}$. Here eV takes into account the shift of the chemical potential by an external dc voltage applied. In the Keldysh($\check{}$)-Nambu($\bar{}$) space, the normal terminals are described by

$$\check{G}(\mathcal{E}) = \begin{pmatrix} \bar{G}^R & \bar{G}^K \\ 0 & \bar{G}^A \end{pmatrix}, \tag{27.5}$$

where $\bar{G}^R = -\bar{G}_A = \bar{\tau}_3$ and

$$\bar{G}^K(\mathcal{E}) = \begin{pmatrix} 2h(\mathcal{E}) & 0 \\ 0 & 2h(-\mathcal{E}) \end{pmatrix}. \tag{27.6}$$

Here $h(\pm\mathcal{E}) = 1 - 2n(\pm\mathcal{E})$ with $n(\mathcal{E}) = (e^{\beta(\mathcal{E}-eV)} + 1)^{-1}$ and $1 - n(-\mathcal{E}) = (e^{\beta(\mathcal{E}+eV)} + 1)^{-1}$ being the electron and the hole state occupation numbers [164].

The quasiclassical Keldysh-Green's function of a superconducting terminal in equilibrium is given by Eqs. (27.3) and (27.5), with $\bar{G}^{R,A}$ given by

$$\begin{aligned} \bar{G}^{R,A}(\mathcal{E}) &= \begin{pmatrix} g^{R,A} & f^{R,A} \\ -f^{\dagger R,A} & -g^{R,A} \end{pmatrix} \\ &= \frac{\pm 1}{(\mathcal{E} \pm i\delta + |\Delta|)^{1/2} (\mathcal{E} \pm i\delta - |\Delta|)^{1/2}} \begin{pmatrix} \mathcal{E} \pm i\delta & \Delta \\ -\Delta^* & -(\mathcal{E} \pm i\delta) \end{pmatrix}, \end{aligned} \tag{27.7}$$

where $\delta \to 0+$. Taking into account that the branch cut of $z^{1/2}$ is along the negative real axis, we obtain

$$g^R(\mathcal{E}) = -g^A(\mathcal{E}) = \frac{|\mathcal{E}|}{\sqrt{\mathcal{E}^2 - |\Delta|^2}}, \quad f^R(\mathcal{E}) = -f^A(\mathcal{E}) = \frac{\Delta\, \mathrm{sgn}(\mathcal{E})}{\sqrt{\mathcal{E}^2 - |\Delta|^2}}, \tag{27.8}$$

for $|\mathcal{E}| > |\Delta|$ and

$$g^R(\mathcal{E}) = g^A(\mathcal{E}) = \frac{-i\mathcal{E}}{\sqrt{|\Delta|^2 - \mathcal{E}^2}}, \quad f^R(\mathcal{E}) = f^A(\mathcal{E}) = \frac{-i\Delta}{\sqrt{|\Delta|^2 - \mathcal{E}^2}} \tag{27.9}$$

for $|\mathcal{E}| < |\Delta|$. The components $f^{\dagger R,A}$ are given by normalization $(\bar{G}^{R,A})^2 = 1$. In the equilibrium state, the Keldysh component $\bar{G}^K$ is given by $\bar{G}^K = (\bar{G}^R - \bar{G}^A)\tanh(\mathcal{E}/2T_e)$. Here we assume that no external voltage is applied to the superconducting terminal, $eV = 0$.

In the presence of a time-dependent voltage drive, the Keldysh-Green's functions of the corresponding terminals are no longer diagonal in energy. In the following we use the quasiclassical Green's functions in the time domain $\check{G}(t', t'')$ and suppress time indices for brevity. The products are interpreted in terms of a convolution over internal indices, e.g., $(\check{G}_1\check{G}_2)(t', t'') = \int dt_1 \check{G}_1(t', t_1)\check{G}_2(t_1, t'')$. The time-dependent voltage drive $V(t)$ applied to a normal terminal is taken into account by the gauge transformation [160, 196]

$$\check{G} = \begin{pmatrix} 1 & 2UhU^\dagger \\ 0 & -1 \end{pmatrix}. \tag{27.10}$$

Here U is an unitary operator which is given by $U(t', t'') = \exp[-i\int_0^{t'} eV(t)dt]\ \delta(t' - t'')$ in time representation and $h(\mathcal{E}', \mathcal{E}'') = \tanh(\mathcal{E}'/2T_e)2\pi\delta(\mathcal{E}' - \mathcal{E}'')$ in energy representation. In the Keldysh($\check{}$)-Nambu($\bar{}$) space, the normal terminals in the presence of a time dependent voltage drive are described by

$$\check{G} = \begin{pmatrix} \bar{\tau}_3 & \bar{G}^K \\ 0 & -\bar{\tau}_3 \end{pmatrix}, \tag{27.11}$$

where

$$\bar{G}^K = \begin{pmatrix} 2UhU^\dagger & 0 \\ 0 & -2U^\dagger hU \end{pmatrix}. \tag{27.12}$$

For a dc voltage applied $V(t) = \text{const}$, Eqs. (27.10) and (27.11) reduce to Eqs. (27.4) and (27.5), respectively.

§ 28. Determinants of block matrices

Let $\boldsymbol{A}$, $\boldsymbol{B}$, $\boldsymbol{C}$, and $\boldsymbol{D}$ be the quadratic matrices of the same size. Then the following equalities hold:

$$\det\begin{pmatrix}\boldsymbol{A} & \boldsymbol{B}\\ \boldsymbol{C} & \boldsymbol{D}\end{pmatrix} = \begin{cases}\det(\boldsymbol{A}\boldsymbol{D}-\boldsymbol{B}\boldsymbol{C}), & [\boldsymbol{C},\boldsymbol{D}]=0,\\ \det(\boldsymbol{D}\boldsymbol{A}-\boldsymbol{B}\boldsymbol{C}), & [\boldsymbol{B},\boldsymbol{D}]=0,\\ \det(\boldsymbol{D}\boldsymbol{A}-\boldsymbol{C}\boldsymbol{B}), & [\boldsymbol{A},\boldsymbol{B}]=0,\\ \det(\boldsymbol{A}\boldsymbol{D}-\boldsymbol{C}\boldsymbol{B}), & [\boldsymbol{A},\boldsymbol{C}]=0.\end{cases} \tag{28.1}$$

In the case in which more than two blocks commute with each other, the corresponding determinants on the right hand side of Eq. (28.1) coincide.

In the literature, usually a special case of Eq. (28.1) is given in which one of the blocks is equal to zero, e.g.,

$$\det\begin{pmatrix}\boldsymbol{A} & \boldsymbol{B}\\ \boldsymbol{0} & \boldsymbol{D}\end{pmatrix} = \det\begin{pmatrix}\boldsymbol{A} & \boldsymbol{0}\\ \boldsymbol{C} & \boldsymbol{D}\end{pmatrix} = \det(\boldsymbol{A})\det(\boldsymbol{D}), \tag{28.2}$$

and similar when one of the diagonal blocks is zero [205]. Here we prove the more general statement given by Eq. (28.1), following Ref. [206].

Suppose that $[\boldsymbol{C},\boldsymbol{D}]=0$. In this case we have

$$\begin{pmatrix}\boldsymbol{A} & \boldsymbol{B}\\ \boldsymbol{C} & \boldsymbol{D}\end{pmatrix}\begin{pmatrix}\boldsymbol{D} & \boldsymbol{0}\\ -\boldsymbol{C} & \boldsymbol{1}\end{pmatrix} = \begin{pmatrix}\boldsymbol{A}\boldsymbol{D}-\boldsymbol{B}\boldsymbol{C} & \boldsymbol{B}\\ \boldsymbol{0} & \boldsymbol{D}\end{pmatrix}. \tag{28.3}$$

Taking the determinant of the left and right hand side and using Eq. (28.2) we find

$$(\det\boldsymbol{D})\left[\det\begin{pmatrix}\boldsymbol{A} & \boldsymbol{B}\\ \boldsymbol{C} & \boldsymbol{D}\end{pmatrix} - \det(\boldsymbol{A}\boldsymbol{D}-\boldsymbol{B}\boldsymbol{C})\right] = 0. \tag{28.4}$$

For a nonsingular $\boldsymbol{D}$ we obtain the first equality given by Eq. (28.1). From continuity, the equality holds even if $\boldsymbol{D}$ is singular. To see this more formally, let us substitute $\boldsymbol{D} \to \boldsymbol{D}_x = \boldsymbol{D} + x\boldsymbol{1}$ in Eq. (28.3) ($[\boldsymbol{C},\boldsymbol{D}_x]=0$ still holds). Equation (28.4) becomes the product of two polynomials equal to the zero polynomial. The first factor, $\det\boldsymbol{D}_x$, is not a zero polynomial, which means that the second factor must be the zero polynomial:

$$\det\begin{pmatrix}\boldsymbol{A} & \boldsymbol{B}\\ \boldsymbol{C} & \boldsymbol{D}_x\end{pmatrix} - \det(\boldsymbol{A}\boldsymbol{D}_x-\boldsymbol{B}\boldsymbol{C}) = 0. \tag{28.5}$$

Taking $x=0$ we obtain the first equality in Eq. (28.1). The proof of other equalities is analogous.

§ 29. Notation

Physical constants:

$e = -\|e\| = -1.602 \times 10^{-19}$ C	electron charge
$k_B = 1.381 \times 10^{-23}$ J/K$= 0.0862$ meV/K	Boltzmann constant
$\hbar = h/(2\pi) = 1.054 \times 10^{-34}$ Js	reduced Planck's constant
$G_Q = 2_s e^2/h \approx (13\ \mathrm{k\Omega})^{-1}$	conductance quantum

We put $\hbar = k_B = 1$ for brevity in all chapters except in the introductory Chapter I.

List of frequently used symbols:

$\boldsymbol{A}$	vector potential
$\boldsymbol{B}$	magnetic field
$D = v_F l/3$	diffusion coefficient
$E_{\mathrm{Th}} = \hbar D/L^2$	Thouless energy (p.71, § 13.5)
$\mathcal{E}$	single particle energy
$\mathcal{E}_F$	Fermi energy
$F = S_I^{\mathrm{shot}}/\|e\langle I\rangle\|$	Fano factor
G	conductance
$\check{G}(x', x'')$, $\check{G}(x', x'')$	Keldysh-Green's functions, where $x = (t, \boldsymbol{r})$ (p.63, p.73)
$\check{G}(\chi)$	extended Keldysh-Green's function
I	current
$\check{I}$	matrix current
L	system size (length)
l	elastic mean free path
l_ϕ	phase coherence length
l_{ee}	electron-electron scattering length
$l_{e-\mathrm{ph}}$	electron-phonon scattering length
λ_F	Fermi wavelength
p_F	Fermi momentum
$\mathcal{P}(N)$	probability distribution function of the number of charges transferred
$R_n^A = T_n^2/(2 - T_n)^2$	probability of the Andreev reflection
$\rho(T)$	distribution of transmission eigenvalues (p.43, p.47, § 13.4)
$S_I(t', t'') = (1/2)\langle\{\Delta\hat{I}(t'), \Delta\hat{I}(t'')\}\rangle$	current correlation function (p.41, p.131)
$S_I(\Omega)$	spectral weight of current fluctuations; Ω can take both positive and negative values

$S_I \equiv S_I(\Omega = 0)$	current noise power
$S_I^{\rm shot}$	shot noise power
$\mathcal{S}(\chi)$	cumulant generating function
T_e	temperature
T_n	transmission eigenvalues
$\check{\tau}_i$	Pauli matrices in the Keldysh space, $\check{\tau}_1 = \left(\begin{smallmatrix} 0 & 1 \\ 1 & 0 \end{smallmatrix}\right)$, $\check{\tau}_2 = \left(\begin{smallmatrix} 0 & -i \\ i & 0 \end{smallmatrix}\right)$, $\check{\tau}_3 = \left(\begin{smallmatrix} 1 & 0 \\ 0 & -1 \end{smallmatrix}\right)$
V	voltage
v_F	Fermi velocity
W	system size (width)
χ	counting field

Throughout this Thesis we use the following conventions for the Fourier transformation of functions of space-time arguments:

$$\varphi(t, \boldsymbol{r}) = \int \frac{d\mathcal{E}}{2\pi} \int \frac{d\boldsymbol{p}}{(2\pi)^3}\, \varphi(\mathcal{E}, \boldsymbol{p})\, e^{i(\boldsymbol{p}\boldsymbol{r} - \mathcal{E}t)}, \tag{29.1a}$$

$$\varphi(\mathcal{E}, \boldsymbol{p}) = \int dt \int d\boldsymbol{r}\, \varphi(t, \boldsymbol{r})\, e^{-i(\boldsymbol{p}\boldsymbol{r} - \mathcal{E}t)}. \tag{29.1b}$$

By putting $\varphi(\boldsymbol{r}) = \langle \boldsymbol{r}|\boldsymbol{p}\rangle$ we obtain the following relations between the single-particle coordinate and momentum eigenvectors:

$$\langle \boldsymbol{r}|\boldsymbol{p}\rangle = e^{i\boldsymbol{p}\boldsymbol{r}}, \tag{29.2a}$$

$$\langle \boldsymbol{r}'|\boldsymbol{r}\rangle = \delta(\boldsymbol{r} - \boldsymbol{r}'), \tag{29.2b}$$

$$\langle \boldsymbol{p}'|\boldsymbol{p}\rangle = (2\pi)^3 \delta(\boldsymbol{p} - \boldsymbol{p}'), \tag{29.2c}$$

$$\int d\boldsymbol{r}\, |\boldsymbol{r}\rangle\langle \boldsymbol{r}| = \int \frac{d\boldsymbol{p}}{(2\pi)^3}\, |\boldsymbol{p}\rangle\langle \boldsymbol{p}| = 1. \tag{29.2d}$$

The field operators can be expressed in terms of creation and annihilation operators by

$$\hat{\psi}(\boldsymbol{r}) = \sum_f \langle \boldsymbol{r}|f\rangle\, \hat{a}_f, \qquad \hat{\psi}^\dagger(\boldsymbol{r}) = \sum_f \langle f|\boldsymbol{r}\rangle\, \hat{a}_f^\dagger, \tag{29.3a,b}$$

where the quantum numbers f label states in the single-particle basis $\{|f\rangle\}$. From Eqs. (11.6) and (29.3) we obtain the transformation rules between the Green's functions in space-time and energy-momentum representations:

$$G(t_1, \boldsymbol{r}_1; t_2, \boldsymbol{r}_2) = \int \frac{d\mathcal{E}_1 d\mathcal{E}_2}{(2\pi)^2} \int \frac{d\boldsymbol{p}_1 d\boldsymbol{p}_2}{(2\pi)^6}\, G(\mathcal{E}_1, \boldsymbol{p}_1; \mathcal{E}_2, \boldsymbol{p}_2)\, e^{i(\boldsymbol{p}_1\boldsymbol{r}_1 - \mathcal{E}_1 t_1)}\, e^{-i(\boldsymbol{p}_2\boldsymbol{r}_2 - \mathcal{E}_2 t_2)}, \tag{29.4a}$$

$$G(\mathcal{E}_1, \boldsymbol{p}_1; \mathcal{E}_2, \boldsymbol{p}_2) = \int dt_1 dt_2 \int d\boldsymbol{r}_1 d\boldsymbol{r}_2\, G(t_1, \boldsymbol{r}_1; t_2, \boldsymbol{r}_2)\, e^{-i(\boldsymbol{p}_1\boldsymbol{r}_1 - \mathcal{E}_1 t_1)}\, e^{i(\boldsymbol{p}_2\boldsymbol{r}_2 - \mathcal{E}_2 t_2)}. \tag{29.4b}$$

The same transformation rules hold for all Green's functions defined by Eqs. (11.7) and (11.8).

Bibliography

[1] L. D. Landau and E. M. Lifshitz, *Statistical Physics, Part 1*, Vol. 5 of *Course of Theoretical Physics* (Pergamon Press, Oxford, 1980).
[2] W. Schottky, Ann. Phys. (Leipzig) **362**, 541 (1918).
[3] R. A. Millikan, Phys. Rev. **2**, 109 (1913).
[4] C. A. Hartmann, Ann. Phys. **65**, 51 (1921).
[5] J. B. Johnson, Phys. Rev. **26**, 71 (1925).
[6] A. W. Hull and N. H. Wiliams, Science **60**, 100 (1924).
[7] A. W. Hull and N. H. Williams, Phys. Rev. **25**, 147 (1925).
[8] N. H. Wiliams and H. B. Vincent, Phys. Rev. **28**, 1250 (1926).
[9] N. H. Williams and W. S. Huxford, Phys. Rev. **33**, 773 (1929).
[10] P. Dutta and P. M. Horn, Rev. Mod. Phys. **53**, 497 (1981).
[11] J. B. Johnson, Phys. Rev. **32**, 97 (1928).
[12] H. Nyquist, Phys. Rev. **32**, 110 (1928).
[13] C. D. Motchenbacher and J. A. Connelly, *Low-Noise Electronic System Design* (John Wiley & Sons, New York, 1993).
[14] H. B. Callen and T. A. Welton, Phys. Rev. **83**, 34 (1951).
[15] S. Datta, *Electronic Transport in Mesoscopic Systems* (Cambridge University Press, Cambridge, 1997).
[16] Y. Imry, *Introduction to Mesoscopic Physics* (Oxford University Press, New York, 1997).
[17] B. J. van Wees *et al.*, Phys. Rev. Lett. **60**, 848 (1988).
[18] D. A. Wharam *et al.*, J. Phys. C **21**, L209 (1988).
[19] L. I. Glazman, G. B. Lesovik, D. E. Khmel'nitskii, and R. I. Shekhter, JETP Lett. **48**, 238 (1988).
[20] A. Yacoby and Y. Imry, Europhys. Lett. **11**, 663 (1990).
[21] Y. Aharonov and D. Bohm, Phys. Rev. **115**, 485 (1959), **123**, 1511 (1961).
[22] R. A. Webb, S. Washburn, C. P. Umbach, and R. B. Laibowitz, Phys. Rev. Lett. **54**, 2696 (1985).
[23] G. Timp *et al.*, Phys. Rev. Lett. **58**, 2814 (1987).
[24] B. L. Altshuler, JETP Lett. **41**, 648 (1985).
[25] P. A. Lee and A. D. Stone, Phys. Rev. Lett. **55**, 1622 (1985).
[26] Y. M. Blanter and M. Büttiker, Phys. Rep. **336**, 1 (2000).
[27] Y. M. Blanter, cond-mat/0511478 (unpublished).
[28] M. J. M. de Jong and C. W. J. Beenakker, in *Mesoscopic Electron Transport*, Vol. 345 of *NATO ASI Series*, edited by L. P. Kouwenhoven, G. Schön, and L. L. Sohn (Kluwer Academic Publishers, Dordrecht, 1997), pp. 225–258, cond-mat/9611140.
[29] M. Reznikov *et al.*, Superlatt. Microstruct. **23**, 901 (1998).

[30] T. Martin, in *Nanophysics: Coherence and Transport*, Vol. 81 of *Lecture Notes of the Les Houches Summer School 2004*, edited by H. Bouchiat *et al.* (Elsevier Science, Amsterdam, 2005), cond-mat/0501208.
[31] S. M. Kogan, *Electronic Noise and Fluctuations in Solids* (Cambridge University Press, Cambridge, 1996).
[32] B. Reulet, in *Nanophysics: Coherence and Transport*, Vol. 81 of *Lecture Notes of the Les Houches Summer School 2004*, edited by H. Bouchiat *et al.* (Elsevier Science, Amsterdam, 2005), cond-mat/0502077.
[33] M. Büttiker, Phys. Rev. Lett. **65**, 2901 (1990).
[34] M. Büttiker, Phys. Rev. B **46**, 12485 (1992).
[35] T. Martin and R. Landauer, Phys. Rev. B **45**, 1742 (1992).
[36] V. A. Khlus, Zh. Eksp. Teor. Fiz. **93**, 2179 (1987), [Sov. Phys. JETP **66**, 1243 (1987)].
[37] G. B. Lesovik, JETP Lett. **49**, 592 (1989).
[38] B. Yurke and G. P. Kochanski, Phys. Rev. B **41**, 8184 (1990).
[39] U. Fano, Phys. Rev. **72**, 26 (1947).
[40] M. Reznikov, M. Heiblum, H. Shtrikman, and D. Mahalu, Phys. Rev. Lett. **75**, 3340 (1995).
[41] A. Kumar *et al.*, Phys. Rev. Lett. **76**, 2778 (1996).
[42] L.-H. Reydellet *et al.*, Phys. Rev. Lett. **90**, 176803 (2003).
[43] Y. V. Nazarov, Phys. Rev. Lett. **73**, 134 (1994).
[44] E. V. Sukhorukov and D. Loss, Phys. Rev. Lett. **80**, 4959 (1998).
[45] E. V. Sukhorukov and D. Loss, Phys. Rev. B **59**, 13054 (1999).
[46] C. W. J. Beenakker, Rev. Mod. Phys. **69**, 731 (1997).
[47] O. N. Dorokhov, Solid State Commun. **51**, 381 (1984).
[48] O. N. Dorokhov, JETP Lett. **36**, 318 (1982).
[49] P. A. Mello and J.-L. Pichard, Phys. Rev. B **40**, 5276 (1989).
[50] C. W. J. Beenakker and M. Büttiker, Phys. Rev. B **46**, R1889 (1992).
[51] K. E. Nagaev, Phys. Lett. A **169**, 103 (1992).
[52] M. J. M. de Jong and C. W. J. Beenakker, Phys. Rev. B **51**, 16867 (1995).
[53] M. J. M. de Jong and C. W. J. Beenakker, Physica A **230**, 219 (1996).
[54] M. Vanevic and W. Belzig, Europhys. Lett. **75**, 604 (2006).
[55] V. I. Kozub and A. M. Rudin, JETP Lett. **62**, 49 (1995).
[56] V. I. Kozub and A. M. Rudin, Phys. Rev. B **52**, 7853 (1995).
[57] K. E. Nagaev, Phys. Rev. B **52**, 4740 (1995).
[58] F. Liefrink *et al.*, Phys. Rev. B **49**, R14066 (1994).
[59] A. H. Steinbach, J. M. Martinis, and M. H. Devoret, Phys. Rev. Lett. **76**, 3806 (1996).
[60] M. Henny, S. Oberholzer, C. Strunk, and C. Schönenberger, Phys. Rev. B **59**, 2871 (1999).
[61] A. Shimizu and M. Ueda, Phys. Rev. Lett. **69**, 1403 (1992), erratum **86**, 3694 (2001).
[62] C. W. J. Beenakker and H. van Houten, Phys. Rev. B **43**, 12066 (1991).
[63] M. J. M. de Jong and C. W. J. Beenakker, Phys. Rev. B **46**, 13400 (1992).
[64] H. U. Baranger and P. A. Mello, Phys. Rev. Lett. **73**, 142 (1994).
[65] R. A. Jalabert, J.-L. Pichard, and C. W. J. Beenakker, Europhys. Lett. **27**, 255 (1994).
[66] Y. V. Nazarov, in *Quantum Dynamics of Submicron Structures*, edited by H. A. Cerdeira, B. Kramer, and G. Schön (Kluwer, Dordrecht, 1995).

[67] Y. M. Blanter and E. V. Sukhorukov, Phys. Rev. Lett. **84**, 1280 (2000).
[68] S. Oberholzer *et al.*, Phys. Rev. Lett. **86**, 2114 (2001).
[69] S. Oberholzer, E. V. Sukhorukov, C. Strunk, and C. Schönenberger, Phys. Rev. B **66**, 233304 (2002).
[70] K. M. Schep and G. E. W. Bauer, Phys. Rev. Lett. **78**, 3015 (1997).
[71] J. A. Melsen and C. W. J. Beenakker, Physica B **203**, 219 (1994).
[72] O. Agam, I. Aleiner, and A. Larkin, Phys. Rev. Lett. **85**, 3153 (2000).
[73] P. G. Silvestrov, M. C. Goorden, and C. W. J. Beenakker, Phys. Rev. B **67**, R241301 (2003).
[74] J. Tworzydlo, A. Tajic, H. Schomerus, and C. W. J. Beenakker, Phys. Rev. B **68**, 115313 (2003).
[75] S. Oberholzer, E. V. Sukhorukov, and C. Schönenberger, Nature (London) **415**, 765 (2002).
[76] E. V. Sukhorukov and O. M. Bulashenko, Phys. Rev. Lett. **94**, 116803 (2005).
[77] R. de Picciotto *et al.*, Nature (London) **389**, 162 (1997).
[78] L. Saminadayar, D. C. Glattli, Y. Jin, and B. Etienne, Phys. Rev. Lett. **79**, 2526 (1997).
[79] M. Reznikov *et al.*, Nature (London) **399**, 238 (1999).
[80] R. B. Laughlin, Phys. Rev. Lett. **50**, 1395 (1983).
[81] C. L. Kane and M. P. A. Fisher, Phys. Rev. Lett. **72**, 724 (1994).
[82] A. F. Andreev, Zh. Eksp. Teor. Fiz. **46**, 1823 (1964), [Sov. J. Low Temp. Phys. **19**, 1228 (1964)].
[83] C. W. J. Beenakker, Phys. Rev. B **46**, R12841 (1992).
[84] M. J. M. de Jong and C. W. J. Beenakker, Phys. Rev. B **49**, R16070 (1994).
[85] X. Jehl, M. Sanquer, R. Calemczuk, and D. Mailly, Nature **405**, 50 (2000).
[86] X. Jehl and M. Sanquer, Phys. Rev. B **63**, 052511 (2001).
[87] K. E. Nagaev and M. Büttiker, Phys. Rev. B **63**, R081301 (2001).
[88] F. Lefloch, C. Hoffmann, M. Sanquer, and D. Quirion, Phys. Rev. Lett. **90**, 067002 (2003).
[89] B.-R. Choi *et al.*, Phys. Rev. B **72**, 024501 (2005).
[90] Y. V. Nazarov and T. H. Stoof, Phys. Rev. Lett. **76**, 823 (1996).
[91] W. Belzig and Y. V. Nazarov, Phys. Rev. Lett. **87**, 067006 (2001).
[92] P. Samuelsson, W. Belzig, and Y. V. Nazarov, Phys. Rev. Lett. **92**, 196807 (2004).
[93] P. Samuelsson, Phys. Rev. B **67**, 054508 (2003).
[94] G. B. Lesovik and L. S. Levitov, Phys. Rev. Lett. **72**, 538 (1994).
[95] M. H. Pedersen and M. Büttiker, Phys. Rev. B **58**, 12993 (1998).
[96] V. S. Rychkov, M. L. Polianski, and M. Büttiker, Phys. Rev. B **72**, 155326 (2005).
[97] M. Vanevic, Y. V. Nazarov, and W. Belzig, Phys. Rev. Lett. **99**, 076601 (2007).
[98] R. J. Schoelkopf, A. A. Kozhevnikov, D. E. Prober, and M. J. Rooks, Phys. Rev. Lett. **80**, 2437 (1998).
[99] A. A. Kozhevnikov, R. J. Schoelkopf, and D. E. Prober, Phys. Rev. Lett. **84**, 3398 (2000).
[100] B. Reulet, J. Senzier, and D. E. Prober, Phys. Rev. Lett. **91**, 196601 (2003).
[101] M. Kindermann, Y. Nazarov, and C. W. J. Beenakker, Phys. Rev. Lett. **90**, 246805 (2003).
[102] M. Kindermann, Y. V. Nazarov, and C. W. J. Beenakker, Phys. Rev. B **69**, 035336 (2004).

[103] M. Kindermann and Y. V. Nazarov, in *Quantum Noise in Mesoscopic Physics*, Vol. 97 of *NATO ASI Series II*, edited by Y. V. Nazarov (Kluwer, Dordrecht, 2003), cond-mat/0303590.
[104] Y. Bomze *et al.*, Phys. Rev. Lett. **95**, 176601 (2005).
[105] *Handbook of Mathematical Functions*, edited by M. Abramowitz and I. A. Stegun (Dover Publications, New York, 1964).
[106] K. Huang, *Statistical mechanics* (John Wiley and Sons, Chichester, 1988).
[107] W. Belzig, C. Schroll, and C. Bruder, Phys. Rev. A **75**, 063611 (2007).
[108] R. Landauer, IBM J. Res. Dev. **1**, 223 (1957).
[109] R. Landauer, IBM J. Res. Dev. **32**, 306 (1988).
[110] Y. Imry, in *Directions in Condensed Matter Physics*, edited by G. Grinstein and G. Mazenko (World Scientific, Singapore, 1986).
[111] M. Büttiker, IBM J. Res. Dev. **32**, 317 (1988).
[112] M. Büttiker, Y. Imry, R. Landauer, and S. Pinhas, Phys. Rev. B **31**, 6207 (1985).
[113] Y. V. Nazarov, in *Handbook of Theoretical and Computational Nanotechnology*, edited by M. Rieth and W. Schommers (American Scientific Publishers, Valencia, 2006).
[114] L. D. Landau and E. M. Lifshitz, *Quantum Mechanics*, Vol. 3 of *Course of Theoretical Physics* (Pergamon Press, Oxford, 1991), section 25.
[115] J. J. Sakurai, *Modern Quantum Mechanics* (Addison-Wesley Publishing Company, New York, 1994).
[116] M. Büttiker, Phys. Rev. Lett. **57**, 1761 (1986).
[117] C. W. J. Beenakker, in *Mesoscopic Quantum Physics*, edited by E. Akkermans, G. Montambaux, J.-L. Pichard, and J. Zinn-Justin (North-Holland, Amsterdam, 1995), cond-mat/9406083.
[118] B. J. van Wees, Superlatt. Microstruct. **23**, 917 (1998).
[119] M. Büttiker, Phys. Rev. B **33**, 3020 (1986).
[120] M. Büttiker, IBM J. Res. Dev. **32**, 63 (1988).
[121] C. W. J. Beenakker and B. Michaelis, J. Phys. A: Math. Gen. **38**, 10639 (2005).
[122] B. J. van Wees *et al.*, Phys. Rev. B **43**, 12431 (1991).
[123] R. L. Stratonovich, *Nonlinear Nonequilibrium Thermodynamics I: Linear and Nonlinear Fluctuation-Dissipation Theorems* (Springer, Berlin, 1993).
[124] J. J. Riquelme *et al.*, Europhys. Lett. **70**, 663 (2005).
[125] N. B. Kopnin, *Theory of Nonequilibrium Superconductivity* (Clarendon Press, Oxford, 2001).
[126] A. A. Abrikosov, L. P. Gorkov, and I. E. Dzyaloshinski, *Quantum Field Theoretical Methods in Statistical Physics* (Pergamon Press, Oxford, 1965).
[127] E. M. Lifshitz and L. P. Pitaevskii, *Statistical Physics, Part 2*, Vol. 9 of *Course of Theoretical Physics* (Butterworth-Heinemann, Oxford, 2001).
[128] E. M. Lifshitz and L. P. Pitaevskii, *Physical Kinetics*, Vol. 10 of *Course of Theoretical Physics* (Butterworth-Heinemann, Oxford, 1981).
[129] H. Bruus and K. Flensberg, *Many-Body Quantum Theory in Condensed Matter Physics: An Introduction* (Oxford University Press, New York, 2004).
[130] J. Rammer, *Quantum Field Theory of Non-equilibrium States* (Cambridge University Press, New York, 2007).
[131] A. L. Fetter and J. D. Walecka, *Quantum Theory of Many-Particle Systems* (Dover Publications, New York, 2003).

[132] G. Rickayzen, *Green's Functions and Condensed Matter* (Academic Press, London, 1980).
[133] J. Rammer and H. Smith, Rev. Mod. Phys. **58**, 323 (1986).
[134] W. Belzig *et al.*, Superlatt. Microstruct. **25**, 1251 (1999).
[135] L. P. Keldysh, Sov. Phys. JETP **20**, 1018 (1965).
[136] P. Danielewicz, Ann. Phys. (NY) **152**, 239 (1984).
[137] Y. Yacoby, Phys. Rev. **169**, 610 (1968).
[138] A. P. Jauho and K. Johnsen, Phys. Rev. Lett. **76**, 4576 (1996).
[139] K. B. Nordstrom *et al.*, Phys. Status Solidi B **204**, 52 (1997).
[140] T. Brandes, Phys. Rev. B **56**, 1213 (1997).
[141] L. S. Levitov and G. B. Lesovik, JETP Lett. **58**, 230 (1993).
[142] D. A. Ivanov and L. S. Levitov, JETP Lett. **58**, 461 (1993).
[143] L. S. Levitov, H.-W. Lee, and G. B. Lesovik, J. Math. Phys. **37**, 4845 (1996).
[144] K. E. Nagaev, Phys. Rev. B **66**, 075334 (2002).
[145] K. E. Nagaev, P. Samuelsson, and S. Pilgram, Phys. Rev. B **66**, 195318 (2002).
[146] S. Pilgram, A. N. Jordan, E. V. Sukhorukov, and M. Büttiker, Phys. Rev. Lett. **90**, 206801 (2003).
[147] A. N. Jordan, E. V. Sukhorukov, and S. Pilgram, J. Math. Phys. **45**, 4386 (2004).
[148] Y. V. Nazarov, Ann. Phys. (Leipzig) **8**, SI193 (1999), cond-mat/9908143.
[149] W. Belzig and Y. V. Nazarov, Phys. Rev. Lett. **87**, 197006 (2001).
[150] Y. V. Nazarov, Superlatt. Microstruct. **25**, 1221 (1999).
[151] Y. V. Nazarov and D. A. Bagrets, Phys. Rev. Lett. **88**, 196801 (2002).
[152] W. Belzig, in *Quantum Noise in Mesoscopic Physics*, Vol. 97 of *NATO ASI Series II*, edited by Y. V. Nazarov (Kluwer, Dordrecht, 2003), cond-mat/0210125.
[153] G. E. Blonder, M. Tinkham, and T. M. Klapwijk, Phys. Rev. B **25**, 4515 (1982).
[154] C. W. J. Beenakker, Phys. Rev. Lett. **67**, 3836 (1991), erratum **68**, 1442 (1992).
[155] M. Tinkham, *Introduction to Superconductivity* (McGraw-Hill, New York, 1996).
[156] V. Ambegaokar and A. Baratoff, Phys. Rev. Lett. **10**, 486 (1963), erratum **11**, 104 (1963).
[157] I. O. Kulik and A. N. Omelyanchuk, Fiz. Nizk. Temp. **3**, 945 (1977), [Sov. J. Low Temp. Phys. **3**, 459 (1977)].
[158] I. O. Kulik and A. N. Omelyanchuk, JETP Lett. **21**, 96 (1975).
[159] Y. V. Nazarov and M. Kindermann, Eur. Phys. J. B **35**, 413 (2003).
[160] D. A. Ivanov, H. W. Lee, and L. S. Levitov, Phys. Rev. B **56**, 6839 (1997).
[161] I. Klich, in *Quantum Noise in Mesoscopic Physics*, Vol. 97 of *NATO ASI Series II*, edited by Y. V. Nazarov (Kluwer, Dordrecht, 2003), cond-mat/0209642.
[162] J. E. Avron, S. Bachmann, G. Graf, and I. Klich, arXiv:0705.0099 (unpublished).
[163] D. A. Bagrets and Y. V. Nazarov, Phys. Rev. Lett. **94**, 056801 (2005).
[164] M. P. Anantram and S. Datta, Phys. Rev. B **53**, 16390 (1996).
[165] P. Samuelsson and M. Büttiker, Phys. Rev. Lett. **89**, 046601 (2002).
[166] P. Samuelsson and M. Büttiker, Phys. Rev. B **66**, R201306 (2002).
[167] J. Börlin, W. Belzig, and C. Bruder, Phys. Rev. Lett. **88**, 197001 (2002).
[168] W. Belzig and P. Samuelsson, Europhys. Lett. **64**, 253 (2003).
[169] G. Bignon, F. Pistolesi, and M. Houzet, Eur. Phys. J. B **50**, 465 (2006).

[170] O. M. Bulashenko, J. Stat. Mech. P08013 (2005), cond-mat/0403388.
[171] B. A. Muzykantskii and D. E. Khmelnitskii, Phys. Rev. B **50**, 3982 (1994).
[172] *Quantum Noise in Mesoscopic Physics*, Vol. 97 of *NATO ASI Series II*, edited by Y. V. Nazarov (Kluwer, Dordrecht, 2003).
[173] *Nanophysics: Coherence and Transport*, Vol. 81 of *Lecture Notes of the Les Houches Summer School 2004*, edited by H. Bouchiat *et al.* (Elsevier Science, Amsterdam, 2005).
[174] R. J. Schoelkopf *et al.*, Phys. Rev. Lett. **78**, 3370 (1997).
[175] W. Song, A. K. M. Newaz, J. K. Son, and E. E. Mendez, Phys. Rev. Lett. **96**, 126803 (2006).
[176] L. DiCarlo *et al.*, Rev. Sci. Instru. **77**, 073906 (2006), cond-mat/0604018.
[177] C. W. J. Beenakker, in *Quantum Computers, Algorithms and Chaos*, Vol. 162 of *Proc. Int. School Phys. E. Fermi*, edited by G. Casati, D. Shepelyansky, P. Zoller, and G. Benenti (IOS Press, Amsterdam, 2006), cond-mat/0508488.
[178] L. S. Levitov and M. Reznikov, Phys. Rev. B **70**, 115305 (2004), see also cond-mat/0111057.
[179] L. S. Levitov, in *Quantum Noise in Mesoscopic Physics*, Vol. 97 of *NATO ASI Series II*, edited by Y. V. Nazarov (Kluwer, Dordrecht, 2003), cond-mat/0210284.
[180] H.-W. Lee, L. S. Levitov, and A. Y. Yakovets, Phys. Rev. B **51**, 4075 (1995).
[181] P.-E. Roche and B. Douçot, Eur. Phys. J. B **27**, 393 (2002).
[182] A. M. S. Macêdo, Phys. Rev. B **66**, 033306 (2002).
[183] A. L. R. Barbosa and A. M. S. Macêdo, Phys. Rev. B **71**, 235307 (2005).
[184] D. S. Golubev and A. D. Zaikin, Phys. Rev. B **70**, 165423 (2004).
[185] D. S. Golubev and A. D. Zaikin, Phys. Rev. B **69**, 075318 (2004).
[186] D. S. Golubev, A. V. Galaktionov, and A. D. Zaikin, Phys. Rev. B **72**, 205417 (2005).
[187] M. Vanevic and W. Belzig, Phys. Rev. B **72**, 134522 (2005).
[188] H.-W. Lee and L. S. Levitov, cond-mat/9507011 (unpublished).
[189] J. Keeling, I. Klich, and L. S. Levitov, Phys. Rev. Lett. **97**, 116403 (2006).
[190] N. d'Ambrumenil and B. Muzykantskii, Phys. Rev. B **71**, 045326 (2005).
[191] M. L. Polianski, P. Samuelsson, and M. Büttiker, Phys. Rev. B **72**, R161302 (2005).
[192] A. G. Abanov and D. A. Ivanov, arXiv:0709.2898 (unpublished).
[193] J. Tobiska and Y. V. Nazarov, Phys. Rev. B **72**, 235328 (2005).
[194] A. Di Lorenzo and Y. V. Nazarov, Phys. Rev. Lett. **94**, 210601 (2005).
[195] L. Faoro, F. Taddei, and R. Fazio, Phys. Rev. B **69**, 125326 (2004).
[196] D. Bagrets and F. Pistolesi, Phys. Rev. B **75**, 165315 (2007), see also cond-mat/0606775v1.
[197] G. Campagnano and Y. V. Nazarov, Phys. Rev. B **74**, 125307 (2006).
[198] R. Kubo, J. Phys. Soc. Jpn. **12**, 570 (1957).
[199] H. Hamburger, Math. Ann. **81**, 235 (1920), **82**, 120 (1920); **82**, 168 (1921).
[200] T. J. Stieltjes, Annales de la Faculté des Sciences de Toulouse **8**, J1 (1894), **9**, A5 (1895).
[201] F. Hausdorff, Mathematische Zeitschrift **9**, 74 (1921), **9**, 280 (1921).
[202] B. Simon, Adv. Math. **137**, 82 (1998).
[203] C. Berg, in *Probability Measures on Groups and Related Structures, XI Proceedings Oberwolfach*, edited by H. Heyer (World Scientific, Singapore, 1995).

[204] J. S. Christiansen, The moment problem, an introduction (unpublished). Available at the web page http://www.its.caltech.edu/~stordal.
[205] H. Lütkepohl, *Handbook of Matrices* (John Wiley and Sons, New York, 1996).
[206] J. R. Silvester, Math. Gazette **84**, 460 (2000).

List of Publications

M. Vanevic, Yu. V. Nazarov, and W. Belzig,
Elementary Events of Electron Transfer in a Voltage-Driven Quantum Point Contact,
Phys. Rev. Lett. **99**, 076601 (2007).
(the accompanying Phys. Rev. B paper is in preparation)

M. Vanevic and W. Belzig,
Quasiparticle Transport in Arrays of Chaotic Cavities,
Europhys. Lett. **75**, 604 (2006).

M. Vanevic and W. Belzig,
Full Counting Statistics of Andreev Scattering in an Asymmetric Chaotic Cavity,
Phys. Rev. B **72**, 134522 (2005).

M. Vanevic and Z. Radovic,
Quasiparticle States in Superconducting Superlattices,
Eur. Phys. J. B **46**, 419 (2005).